# Sigma Delta Modulation Of A Chaotic Signal

*Gary Ushaw*


*A thesis submitted for the degree of Doctor of Philosophy.*

**The University of Edinburgh.**

- October 1996 -

## Abstract

Sigma delta modulation ($\Sigma\Delta$M) has become a widespread method of analogue to digital conversion, however its operation has not been completely defined. The majority of the analysis carried out on the circuit has been from a linear standpoint, with non-linear analysis hinting at hidden complexities in the modulator's operation. The sigma delta modulator itself is a non-linear system consisting, as it does, of a number of integrators and a one bit quantiser in a feedback loop. This configuration can be generalised as a non-linearity within a feedback path, which is a classic route to chaotic behaviour.

This initially raises the prospect that a sigma delta modulator may be capable of chaotic modes of operation with a non-chaotic input. In fact, the problem does not arise and we show why not. To facilitate this investigation, a set of differential equations is formulated to represent $\Sigma\Delta$M; these equations are subsequently utilised in a stability study of the sigma delta modulator.

Of more interest, and more uncertainty, is the effect sigma delta modulation may have on a chaotic signal. If $\Sigma\Delta$M makes a chaotic signal more chaotic then this will have serious repercussions on the predictability of that signal. In the past, analysis of the circuit has tended to be based around a steady state input or a slowly moving non-chaotic input such as a low frequency sine wave. This has greatly eased the complexity of such analyses, but it does not address the problem at hand.

In this thesis we present the results of comparing the sigma delta modulation of a chaotic signal to a direct quantisation of the same signal. The tool we use to investigate this is the Lyapunov spectrum of the time series, measured using an algorithm developed at Edinburgh University. The Lyapunov exponents of a chaotic signal are presented before and after both $\Sigma\Delta$M and direct quantisation, and it is shown that $\Sigma\Delta$M does not increase the chaos of the signal. Indeed, it is shown that $\Sigma\Delta$M has no more effect on the predictability of the signal, as measured by the Lyapunov spectrum, than direct quantisation.

As such, we conclude that sigma delta modulation provides a reliable method for analogue to digital conversion of chaotic signals.

It should be pointed out that, due to the incompleteness of rigorous analysis of $\Sigma\Delta$M and the complex processes involved in applying such analysis to a chaotic signal, the results of this thesis are largely based upon experimentation and observation from a simulation of a sigma delta modulator.

# Declaration of originality

I hereby declare that this thesis and the work reported herein was composed and originated entirely by myself, in the Department of Electrical Engineering at the University of Edinburgh, except for the development of the Lyapunov extraction algorithm described in chapter 6 which was carried out in collaboration with Mike Banbrook.

Gary Ushaw

# Acknowledgements

I would like to thank the following people for their invaluable assistance during the course of this PhD:

- Steve McLaughlin, my supervisor, for his continuous support and guidance. Also for reading and checking this thesis.
- Dave Broomhead, Jerry Huke, David Hughes and Robin Jones of the Defence Research Agency, Malvern for useful discussions and advice.
- Mike Banbrook with whom I collaborated on the Lyapunov exponent extraction algorithm described in chapter 6, and without whom etc. etc.
- The other members of the Signal Processing Group for their support throughout my PhD.
- DRA Malvern, CASE and EPSRC for providing financial support.

# Contents

# List of Figures

# Abbreviations

| | |
|---|---|
| **ΣΔM** | Sigma delta modulation |
| **ADC** | Analogue to digital converter |
| **DAC** | Digital to analogue converter |
| *svd* | Singular value decomposition |

# List of principal symbols

| | |
|---|---|
| $u(t)$ | the input to a sigma delta modulator. |
| $x_n(t)$ | the output of the $n^{th}$ integrator in a sigma delta modulator. |
| $y(t)$ | the output of a sigma delta modulator. |
| $e(t)$ | the output of the comparator in a sigma delta modulator. |
| $k_n$ | the leakage of the $n^{th}$ integrator in a sigma delta modulator. |
| $a_n$ | the feedback factor in the $n^{th}$ loop of a sigma delta modulator. |
| $M$ | the saturation level of the tanh function. |
| $p$ | the slope of the tanh function. |
| $\tau$ | the delay introduced in the tanh function. |
| $\rho$ | the leakage factor in a discrete integrator |
| $\lambda$ | a constant input to the sigma delta modulator, i.e. $u(t) = \lambda$. |
| $\nu(t)$ | a small change in $x(t)$. |
| $\lambda_n$ | the $n^{th}$ Lyapunov exponent of a system. |
| $\mathbf{X}$ | the trajectory matrix of some time series $x(t)$. |
| $\mathbf{\Theta}$ | the structure matrix $\theta = \mathbf{X}\mathbf{X}^T$. |
| $\mathbf{\Xi}$ | the covariance matrix $\mathbf{\Xi} = \mathbf{X}^T\mathbf{X}$. |
| $\mathbf{S}$ | the eigenvectors of the stricture matrix |
| $\mathbf{C}$ | the eigenvectors of the covariance matrix. |
| $\mathbf{\Sigma}$ | matrix of singular values. |
| $\sigma_n$ | the $n^{th}$ singular value. |
| $N$ | the number of points on the embedded attractor. |
| $w$ | the dimension of the initial embedding. |
| $d$ | the estimated actual dimension of the system. |
| $\hat{\mathbf{X}}$ | the reduced trajectory matrix. |
| $\epsilon$ | the radius of the neighbourhood. |
| $\mathbf{\Gamma_0}(\underline{\mathbf{x_0}}, \epsilon)$ | the neighbourhood set centred on $\underline{\mathbf{x_0}}$ with radius $\epsilon$. |
| $\mathbf{B_n}$ | the neighbourhood matrix at point $n$ on the attractor. |
| $\mathbf{T_n}$ | the transformation at point $n$ on the attractor. |

# Chapter 1

# INTRODUCTION

## 1.1 MOTIVATION

In recent years the sigma delta modulator has become the analogue to digital converter *du jour*, particularly in low frequency and audio applications. In parallel with this, the emergent science of chaos theory has grown into a hot topic in many areas of research. Increasingly, real-world systems which are either known or thought to be chaotic are being measured for analysis, prediction or processing. However, little work has been published on how the method of measuring a chaotic system affects the observed dynamics of that system. It is eminently possible that a non-linear method of measuring a signal derived from such a chaotic system may adversely affect the measurable dynamical properties of that system, perhaps even making the measured system more chaotic than the actual system. If this does, in fact, occur then it will have a serious detrimental effect on the predictability of such a signal.

Of particular interest here is the aforementioned sigma delta modulator, which consists of a non-linear element within a feedback path. This is a classic route to chaos in itself: many known chaotic systems can be described by this generalisation, involving a non-linearity which is somehow folded back on itself. Clearly, it is possible that the use of a sigma delta modulator to measure a chaotic signal may cause that measured signal to be more chaotic than the actual signal under scrutiny. It is also possible that such a structure may be capable of chaotic modes of operation with a non-chaotic input. These questions are addressed in this thesis.

The work of Badii and Politi [1] first broached the subject of the effects of linear filtering of a signal on the measurable dynamical properties of the system from which the signal originates. Several further papers [2–4] went on to show that linear filtering can affect the dynamical properties of a signal, by considering an invariant geometric property of the system attractor such as the correlation dimension. In [5], it was shown that this is not the case for all linear filters. However, if a linear filter can be shown to affect the dynamics of a signal, then it is likely that a non-linear filter, such as a sigma delta modulator, is capable of similar, or greater, corruption of the system's dynamical properties.

There is also evidence that structures similar to the sigma delta modulator may be capable of chaotic modes of operation with a non-chaotic input. In [6], an adaptive autoregressive moving average (ARMA) predictor is considered. As with the sigma delta modulator, the predictor

contains a non-linearity (a quantiser) within a feedback loop, and it is shown that, for certain coefficients and input levels, it is possible for chaotic modes of operation to arise. Similarly, the stability of the differential pulse code modulation (DPCM) transmission system is described in [7], and again the possibility of chaotic modes of operation is mooted.

Since beginning the work contained in this thesis, a number of papers have been published (e.g. [8,9]) dealing with a method of suppressing tones in sigma delta modulation, whereby the coefficients of the circuit are purposefully designed to make the modulator chaotic. This would seem to support our supposition that the sigma delta modulator may be capable of chaotic modes of operation with a non-chaotic input.

When considered as a whole, this body of research, i.e. the indications that structures similar to that of the sigma delta modulator are capable of chaotic modes of operation, and that even linear filtering of signals can affect their measurable dynamics, implies that there may be problems when using $\Sigma\Delta$M to measure a chaotic signal.

Figure 1.1 shows the situation schematically: a chaotic signal, in this case represented by a two dimensional phase plot of the Lorenz system (the meaning of a phase plot is discussed in the next chapter), is sampled by a first order sigma delta modulator. The dynamics of the modulator output must then be compared to those of the input to assess what effect has been introduced by this non-linear filtering of a non-linear signal.

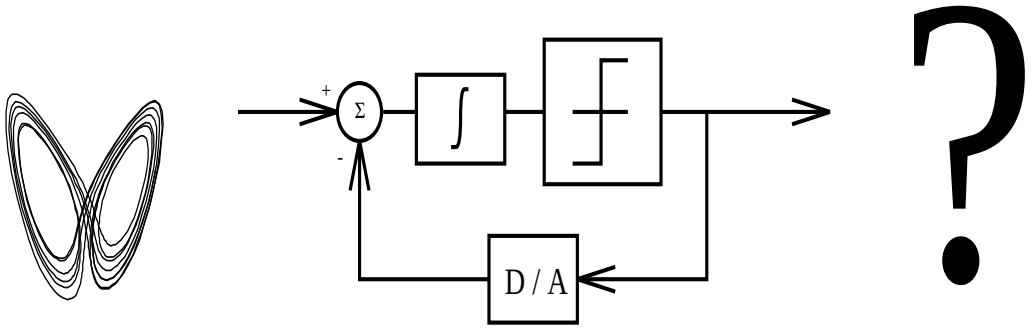


**Figure 1.1**: *Sigma delta modulation of a chaotic signal: what happens?*

As the sigma delta modulator is used in an increasingly varied range of applications, this question becomes more pertinent. In recent years it has been suggested that a large variety of signals may be chaotic in nature: speech [10, 11], radar clutter [12] and medical signals [13, 14] have all been tarred with this brush and, in all these cases, the sigma delta modulator is regularly in use as an analogue to digital conversion process. Also, increasingly, the method of achieving

an analogue to digital conversion on digital signal processing (DSP) cards in personal computers is that of ΣΔM; consequently, many scientists studying 'real-world' chaotic phenomena may be using a sigma delta modulator to obtain data from the system under study. It should be noted from the outset that the types of sigma delta modulator considered throughout this thesis involve analogue integrators, rather than the more commonly used discrete ones, since the Defence Research Agency at Malvern were primarily interested in higher frequency and power signals than are commonly associated with these devices.

This thesis will set out to investigate whether a sigma delta modulator is capable of chaotic modes of operation with a non-chaotic input, and how the non-linear filtering of ΣΔM affects the measurable dynamics of a modulated chaotic signal.

## 1.2 STRUCTURE OF THE THESIS

The thesis is divided into a number of chapters, as described in this section.

The following two chapters provide a background to the problem under discussion. In chapter two, we consider the science of chaos theory, with particular emphasis on its relevance to signal processing and its application to real-world measured signals. It is shown that, in this respect, the science is still very much in its infancy, and it is established that a rather empirical approach must be resorted to for the purposes of this thesis. The third chapter provides a description of ΣΔM, outlining its development and its operation. A summary of the existing work that is relevant to the study of the ΣΔM of a chaotic signal is included. It is indicated that a full analytical description of ΣΔM has not been attained in the field, and some more complex architectures are described.

Chapter four deals with an attempt to algebraically analyse the sigma delta modulator in order to measure the system's Lyapunov exponents, and hence investigate its dynamics. To this end, a set of differential equations are constructed to represent a continuous model of the sigma delta modulator. These equations are subsequently utilised in a stability study of ΣΔM in chapter five. The reasoning for this is that a mathematical study of the differential equations ought to reveal information about the system they represent. The results from this study are compared to those attained from a software simulation of an equivalent modulator.

In chapter six, we present an algorithm for the extraction of Lyapunov exponents from a time series. The algorithm is described in detail, the application and the interpretation of the results are discussed, and some examples are given. The seventh chapter reports on the application of this Lyapunov exponent extraction algorithm to time series produced by the ΣΔM of chaotic signals. The results are compared to those produced by a direct quantisation of the same data. A range of artificially generated chaotic signals are considered and we also investigate the tone-suppressing architecture of ΣΔM that has been labelled as chaotic.

The eighth and final chapter contains the conclusions, a summary of the work, and discussion

of further work which suggests itself.

# Chapter 2

# CHAOS : THE BACKGROUND

## 2.1 INTRODUCTION

The word *chaos* has been invoked with gay abandon across a broad range of fields in recent years. The new science of *chaos theory* has provoked reactions ranging from a belief that it will solve all problems of non-linear dynamics and help us understand the underlying nature of the universe itself, to a disdainful sneer at the latest flash-in-the-pan idea which will ultimately prove to be a red herring. Opinions vary and it is still a somewhat controversial topic, with little consensus existing even on a rigorous definition of chaos itself.

What is clear is that a new way of describing complex non-linear processes has emerged, and it is an ongoing project to provide this mostly qualitative analysis with a quantitative basis. In particular, there has been very little success in applying the theories of chaotic systems to a real-world situation in any meaningful way. In general, chaos has most successfully met the physical plane as an application to fields such as secure coding or image representation (i.e. by adding chaos to a non-chaotic system to some advantage). When it comes to measuring chaos in a real-world environment, and making useful conclusions from those measurements, the science is still very much in its infancy.

This chapter sets out the background of chaos theory and discusses some of the measures of chaos that have been developed. As mentioned, there are many different ways of describing this field, and our own approach is from a signal processing point of view, with our ultimate goal being to consider the measurement and analysis of a real-world chaotic signal.

## 2.2 HISTORY

Any history of the emergent science that is chaos theory must have a rather murky beginning. Perhaps more so than any other field, the observations and theories that now form the cornerstone of chaos theory, sprang up across a broad range of subjects and were discussed by researchers from a variety of different backgrounds, to such an extent that it is impossible to pin-point exactly where or when these ideas originated. Indeed, one of the fundamental aspects of chaos is that it is observable almost anywhere, so it is little surprise that such a widely differing set of people began noticing it at around the same time. It was, if you'll excuse the cliche, an idea whose time had come.

For many years prior to the coining of the term *chaos theory*, the phenomena which would later become describable in this manner had on occasion been observed. Most famously, in the early sixties Edward Lorenz was investigating models for weather forecasting [15] when it became apparent to him that the unpredictability of the weather would need to be included in his model. To his surprise he found that an apparently simple set of differential equations could exhibit this unpredictability, and a description of the *sensitive dependence on initial conditions*, which is at the very heart of what was to become chaos theory, was achieved. It should be pointed out that his model, whilst not being capable of predicting the behaviour of weather patterns, did tell us a lot about the nature of the dynamical processes at work in the weather. Specifically, that the system can not be reliably predicted without 100% accurate measurements of its state, and those 100% accurate measurements can never be attained.

Of course, any piece of research has antecedents, and Lorenz points toward the work of Poincare in the 1900s, who established the beginnings of a theory of dynamical systems. Poincare showed that, while the majority of differential equations have a general solution, that general solution can not be found. Hence, he opened up the field of numerical, rather than analytical, solutions of differential equations. This work was utilised and continued by Shannon and also Van der Pohl in the 1930s, who also observed chaotic systems without naming them as such.

At much the same time as Lorenz was beginning to notice the hidden complexities of his weather prediction model, other researchers in other fields were becoming aware of the problem. Notably, Benoit Mandelbrot who was investigating error clusters in communications systems. Chaos theory evolved from an increasing awareness that apparently simple systems could behave in an extremely complicated fashion. In the mid-70s, Mitchell Feigenbaum was working on non-linear dynamics at the Los Alamos Research Centre, specifically the iterative solutions of simple non-linear equations, and was perhaps the first worker to actually lay down some of the basic tenets of chaos theory in a generally applicable fashion [16, 17]. At much the same time, however, an amount of related work was going on: Robert May and James Yorke of Princeton had defined the concept of period doubling leading to chaos (indeed, it was Yorke who first coined the term *chaos*) [18]; May also published a ground-breaking paper in Nature which was effectively a plea for researchers across all disciplines to consider these non-linear systems [19]; Benoit Mandelbrot at IBM had come up with the word *fractal* to describe a new breed of geometric shape [20]; Ruelle and Takens talked about *strange attractors* representing non-linear systems in phase space [21, 22].

It should perhaps be noted that the word *chaos* was chosen by Yorke to describe these phenomena, as he felt it would be rather attention-grabbing. Unfortunately, he was correct in this assumption, and the name has stuck. As has happened so many times before, a new phenomenon needed naming and, rather than coming up with a neologism to describe it, a perfectly innocent existent word was hi-jacked and forced to take on a very specific meaning within the context of science.

The terms and theories for describing chaos were falling into place, and, within a decade, chaos theory was one of the biggest growth areas in academic research. A full history of the emergence of chaos theory can be found in Gleick's populist book [23], or Lorenz' work [15] and more detailed bibliographies can be found therein; for the purposes of this thesis we shall only consider those areas which are relevant to the problem at hand.

## 2.3 WHAT IS CHAOS?

Providing a rigorous definition of *chaos* is a can of worms we'd rather not open here, however there are a number of features which a chaotic system will tend to exhibit:

- *sensitive dependence on initial conditions.* A very small perturbation to a system in a chaotic mode will radically change the state of that system over time. This is perhaps best visualised by considering two identical systems, without worrying too much about exactly what these hypothetical systems represent. If these systems are in an identical state at a certain time, then one would expect them to have each moved to a new identical state after a particular period of time. Conventionally, if their initial states were not 100% identical one would still expect some similarity in their states at the second observation time. However, if our hypothetical systems are chaotic in nature, then any initial discrepancy between their states will quickly result in large differences in the states of the two systems and, at the second observation point, they will be in completely different states with no correlation between the two. This sensitive dependence on initial conditions is most popularly, and not entirely apocryphally, illustrated by the *butterfly effect* [15], whereby it is said that a butterfly flapping its wings in the Brazilian rainforest can cause a hurricane to strike Hong Kong harbour; a slight change in conditions leading to a vastly different outcome.

- *long term prediction is impossible.* This is a direct result of a chaotic system's sensitive dependence on initial conditions. An error, however small, in measuring an instantaneous output of a system is equivalent to a slight perturbation to the model of that system. Of course, it is inevitable that any measurement of the states of a system must contain an error. It follows that an actual chaotic system and the predicted system based upon the measured instant, will rapidly diverge to different parts of the phase space, making long term prediction impossible.

- *non-periodic but bounded.* A chaotic system is not periodic, in that it will never repeat a particular variable state. However, the system is bounded, if the initial values fall within the basin of attraction, which means that the variables of the system remain within certain limits as the system evolves. It should be noted that the trajectory derived from a chaotic system can diverge to infinity (i.e. be unbounded) for initial conditions outside the basin of attraction.

- *expansion and contraction of the phase space.* As a result of this non-periodic boundedness, both expansion and contraction of the phase space must occur. This is in direct contrast to, for example, an unstable system, in which the phase space expands to infinity, or a damped system, in which the phase space contracts to a point. This presence of both expansion and contraction of the phase space implies that the system exhibits both positive and negative entropy, which leads to positive and negative Lyapunov exponents describing the system's dynamics, as we shall see in a later section of this chapter.

An important tool in the study of chaotic dynamics is the phase space plot. The state of the system is represented as a $\mathrm{d}$-dimensional vector, containing the instantaneous values of each of the $\mathrm{d}$ variables defining the system. As the system evolves, this vector is used to plot a point moving in a $\mathrm{d}$-dimensional space to create a trajectory. The resulting geometrical structure, after the trajectory has been evolved for an infinite period of time or number of iterations, is termed an *attractor*. This label reflects the fact that since, in a periodic system, for example, a slight perturbation to the instantaneous values will disappear over time as the flow is 'attracted' back onto the periodic orbit. Figure 2.1 shows a series of attractors for a simple periodic system, a fixed point system, and a more complex periodic system. In fact the second plot does not show the attractor but the plot of a typical point's progress onto the attractor, which is the origin.

Figure2.1a Figure2.1b Figure2.1c

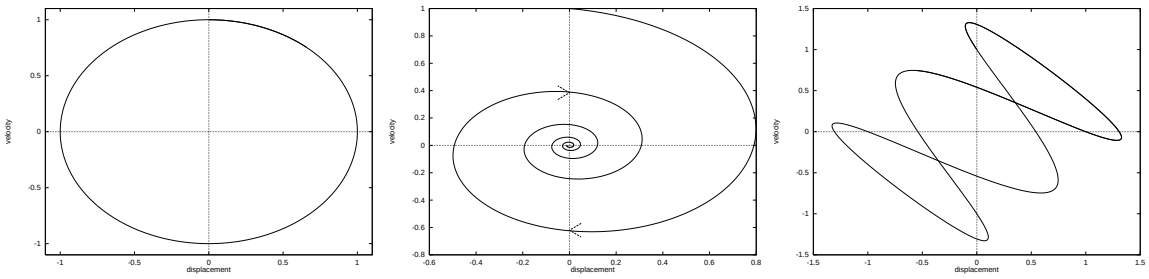


**Figure 2.1**: *Examples of attractors generated by a pendulum, with angular velocity plotted against angular displacement: a) a simple un-damped pendulum (i.e. periodic), b) a damped pendulum and c) a driven pendulum involving a more complicated period*

In the case of the plots shown in Figures 2.1a and 2.1c, a slight perturbation to the system is quickly recovered from, as the phase plot returns to the periodic attractor. For a system in a chaotic mode, however, a slight perturbation to the instantaneous conditions causes the flow to diverge radically from its un-perturbed path. Hence a different kind of attractor must be produced in phase space by a chaotic system; this type of attractor is referred to as a *strange attractor*.

In order to illustrate more intuitively what is meant by a chaotic system and a strange attractor, we present two examples: the Henon map, a chaotic discrete mapping, and the Lorenz attractor,

a chaotic flow.

### 2.3.1 The Henon Map

The Henon map [24] is described by the discrete equations

$$x_{n+1} = y_n + 1 - 1.4x_n^2 \qquad y_{n+1} = 0.3x_n \tag{2.1}$$

and is plotted in Figure 2.2.

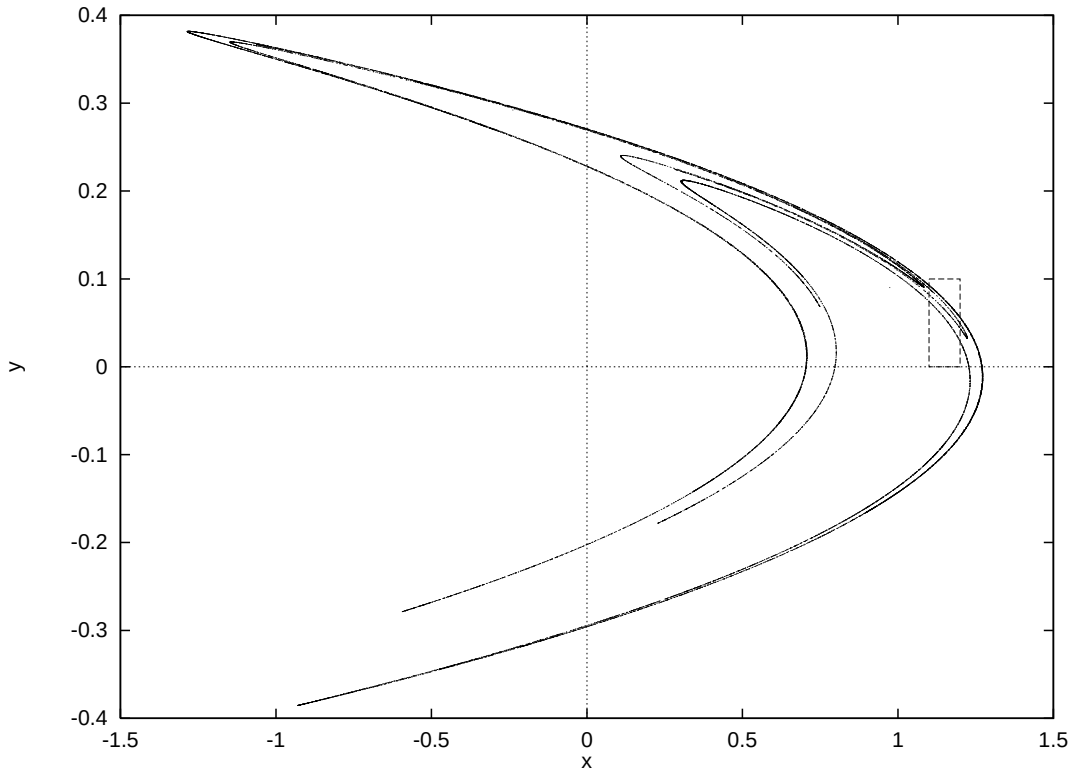


**Figure 2.2**: *The Henon attractor: a chaotic discrete mapping.*

The complexity of this phase plot becomes apparent by "zooming in" on part of the attractor. Figure 2.3a shows an enlargement of the area in the box in Figure 2.2, and again Figure 2.3b shows an enlargement of the area indicated in Figure 2.3a. If this process is repeated, further levels of complexity continually become apparent.

This is a common, but not necessary, feature in chaotic attractors, whereby closer examination of any section of the phase space will reveal more complexity. It is this phenomenon that Mandelbrot famously labelled *fractal*, and leads to the non-integer dimensions that are used to describe chaotic phenomena. It is also apparent from the Henon map that an apparently simple system (in this case, the two discrete equations of 2.1) can lead to surprisingly complex

Figure 2.3a Figure 2.3b

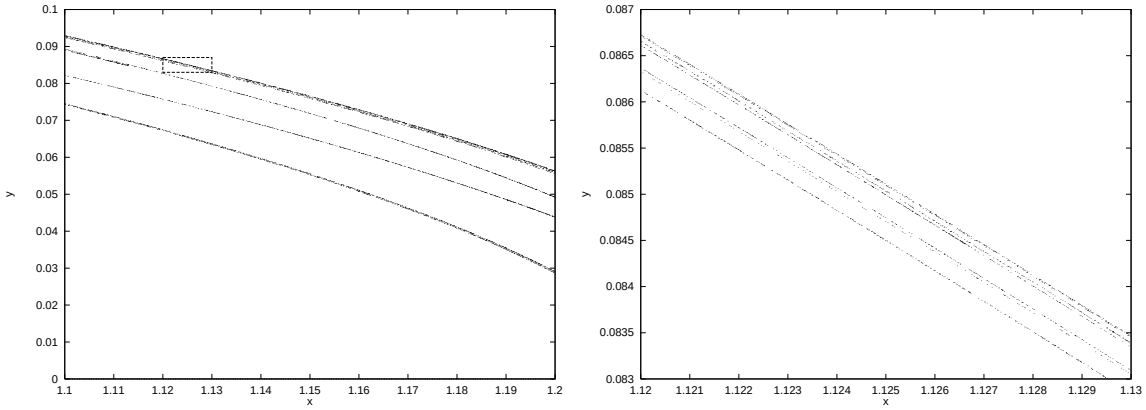


**Figure 2.3**: *Detail of sections of the Henon attractor*

behaviour; and equally, that an apparently complex system can be described in a surprisingly simple fashion.

### 2.3.2 The Lorenz Attractor

The Lorenz system [25] was originally constructed in an attempt to develop models of weather patterns. Although it was unsuccessful in this respect, it has become recognised as one of the first chaotic systems formulated. It is described by the differential equations

$$\dot{X} = \sigma(Y - X) \qquad \dot{Y} = rX - Y - XZ \qquad \dot{Z} = -bZ + XY \tag{2.2}$$

where different values of the coefficients $\sigma$, $r$ and $b$ can induce a range of behaviour in the system including periodic and, of interest here, chaotic modes of operation. Figure 2.4 shows the Lorenz attractor with $\sigma = 16.0$, $r = 40.0$ and $b = 4.0$ constructed by plotting the values of $X$, $Y$ and $Z$ in a three dimensional phase space as the differential equations are numerically solved.

Although not readily apparent when studying this three dimensional phase space in the necessary two dimensions of the print medium, the evolved trajectory of this attractor never returns to a point it has previously passed through, or, to put it another way, there are no self-crossings on the attractor. As with the Henon map, "zooming in" on a strand of the attractor would reveal more and more lines of the trajectory, none of which cross over. This illustrates the non-periodic boundedness of a chaotic attractor. It is also possible to see the sensitive dependence on initial conditions that is at the very heart of chaos theory; two points on neighbouring trajectories on the attractor very quickly move to different parts of the phase space as the system evolves.

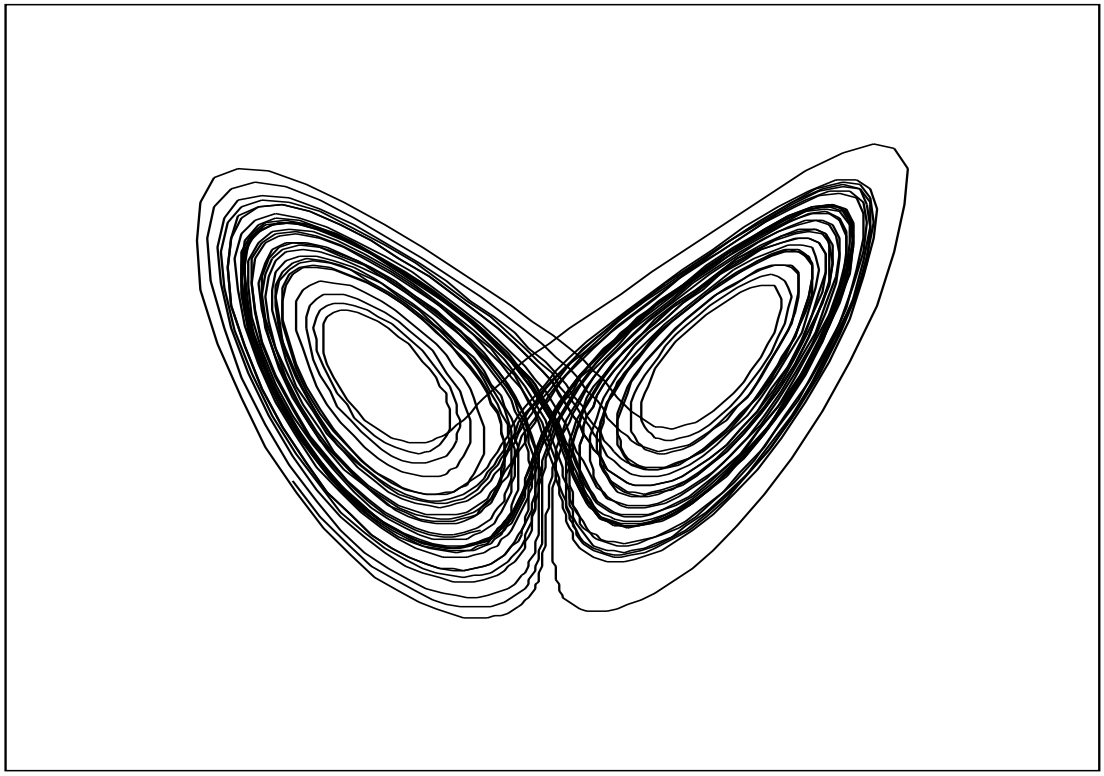

**Figure 2.4**: *The Lorenz Attractor: a chaotic flow.*

The fact that the lack of self-crossings is not clear from considering the two-dimensional plot of the Lorenz attractor in Figure 2.4 leads us to the first of the measures employed in the study of chaos: *dimension*.

## 2.4 DIMENSION

In discussing the Henon map, mention was made of the term *fractal*, whereby the complex structure of the map is described by a non-integer dimension; also in the section on Lorenz' equations it is hinted that the number of dimensions in which an attractor is considered has far-reaching effects on the researcher's ability to adequately analyse the data. The *dimension* of an attractor is an important aspect of chaos theory and is discussed in detail in this section.

Consider first the dimension of some objects with which we are familiar. The maxim goes that a line should have length but no breadth, it is a one dimensional structure; a two dimensional plane is just as easy to imagine, a sheet of paper can be thought of in this way; three dimensional objects are all around us. However, reconsider that two dimensional sheet of paper, and then crumple it up in your hand. Is the resulting scrunched up ball now a three dimensional object? Yet it is still composed entirely of a two dimensional sheet of paper. It is this hazy area between integer dimensions in which fractals and chaotic attractors are found.

Before carrying out any analysis of a chaotic system, the number of dimensions in which the analysis is to take place must be determined. Consider the plot of the Lorenz attractor shown

in Figure 2.4; this is a two dimensional projection of a three dimensional figure. It is not clear from this projection that no self-crossings occur around the trajectory of the attractor, with what appears to be an area of cross-overs occurring in the central portion. It is only when the attractor is viewed in three dimensions that its true shape becomes apparent. Figure 2.5 attempts to demonstrate this by presenting a number of views of the attractor as it is rotated through a three-dimensional space.

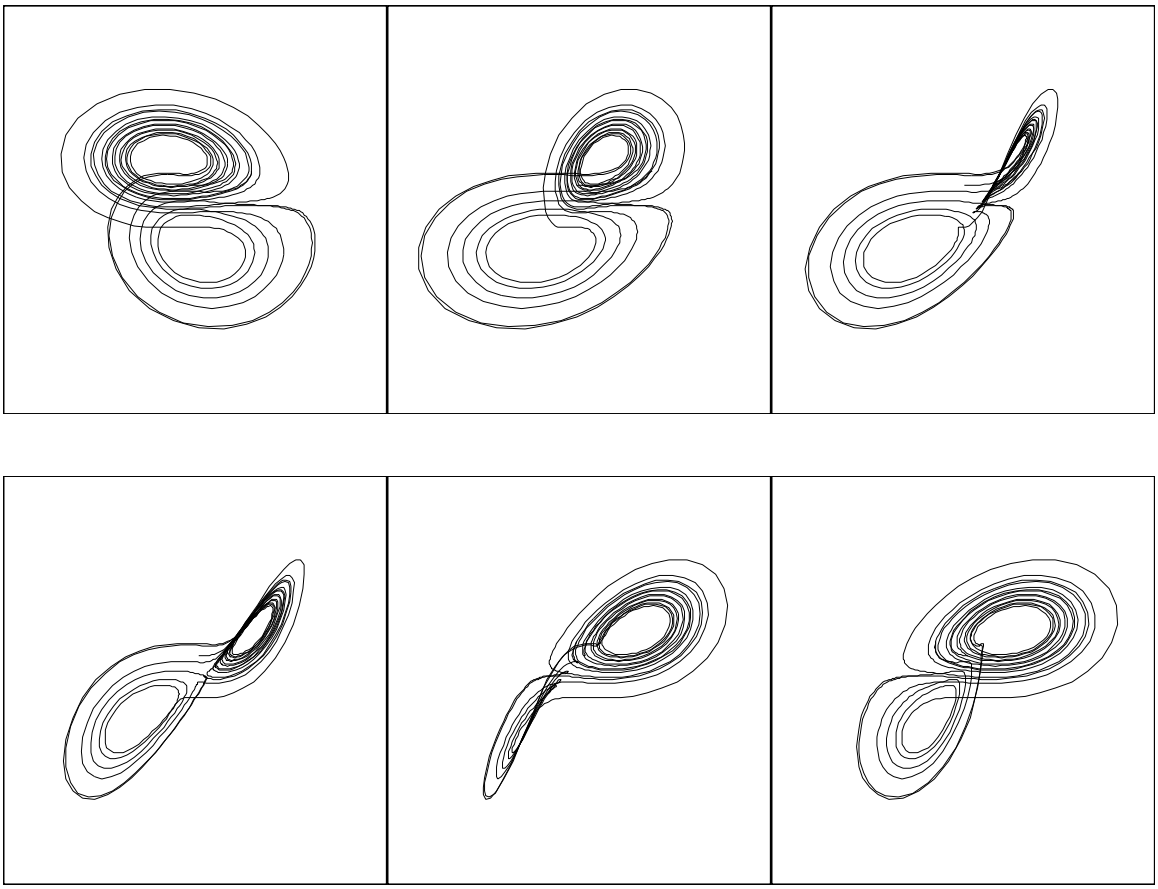

**Figure 2.5**: *Lorenz attractor viewed as it rotates about the Y-axis*

To be honest, the true shape of the attractor is still not readily apparent from this series of snap-shots, and can only be appreciated fully with the use of an animated 3D-plotter: a facility clearly not available within the pages of a thesis. However, this does demonstrate the problems inherent in choosing too low a dimension in which to model a chaotic system. Trajectories which appear to be close together in a two-dimensional projection actually turn out to be on different parts of the attractor, and removed from one another, in the three dimensional space. Over-estimating the dimension of the attractor also causes problems, but these are rather more subtle and shall be returned to in due course.

However, the number of dimensions necessary to fully 'see' the attractor in question, i.e. the number of dimensions required for no self-crossings in the phase space, is not, strictly speaking, the *dimension* of the attractor. The *dimension* of an attractor is equal to the number of degrees

of freedom within that attractor, which leads to, for example, the number of Lyapunov exponents (see later in this chapter) required to describe the dynamical properties of the particular mode of the system. The attribute of *dimension*, for the remainder of this thesis, will refer to this dynamical dimension of the system. Any other meanings attributed to the word *dimension* will be clarified by a suitable adjective (e.g. correlation dimension, Lyapunov dimension, etc.). In particular, the number of dimensions in which the attractor is plotted will be referred to as the *embedding dimension* for reasons which will become apparent.

This section is now split into two subsections; the first considering this dynamical dimension with particular reference to systems fully defined by a set of characteristic equations, the second considering the problem of embedding a time series in a suitable number of dimensions for reliable analysis.

### 2.4.1 Dimension As Order Of The System

Finding the order of a system is, essentially, a case of solving the initial value problem for that system: i.e. what is the minimum number of initial values required to fully define the state of the system at $t = 0$? This figure is termed the order of the system.

If the characteristic equations describing the system are known, then finding the number of initial values required is, in general, a trivial process. A system described by, for example, three first order differential equations requires three initial conditions to fully describe its state and the system has an order of three. Similarly a system described by, for example, a single third order differential equation also has an order of three, since initial values must be placed on the variable of concern as well as its first two derivatives.

Consequently when considering the Lorenz equations 2.2 we immediately see that there are three first order differential equations defining the system and an order of three is apparent. An example of a system defined by a single third order differential equation is Duffing's equation:

$$\frac{d^2x}{dt^2} = x - x^3 - \delta\frac{dx}{dt} - \gamma\cos\omega t \tag{2.3}$$

and again an order of three is apparent, since initial values must be placed on $x$, $\frac{dx}{dt}$ and $\frac{d^2x}{dt^2}$.

Of more interest is the Mackey Glass [26] equation

$$\frac{dx}{dt} = \frac{ax(t-\tau)}{1 + x(t-\tau)^{10}} - bx(t) \tag{2.4}$$

which appears fairly innocuous at first sight. However, the delay term $x(t-\tau)$ has serious repercussions on the dimension of the system. This delay can only be fully described by either a function, or an infinite set of parameters, due to the continuous nature of the system. In effect,

this means that an infinite number of components are necessary to define the state of the system, which leads to an order of infinity, an infinite dimensional system, and an infinite dimensional phase space, and the problem is apparent. In practice, to address this issue, analysis of the Mackey Glass equation tends to involve an approximation of the delay to a number of discrete measurements, and hence a finite dimensional calculation [27]. The implications of a delay in the differential equations defining a dynamical system are considered in more detail in chapter 4, when the problem becomes pertinent to the work in hand.

It will be noted that, rather than talking about the number of initial conditions, or number of degrees of freedom, leading directly to a value of the dimension in the above examples, only the order of the systems have been mentioned. This is because all three of the examples given are chaotic systems, which means that the attractor described by them does not fully cover the $n$-dimensional manifold implied by the order of the systems. In general, such attractors will have a lower dimension than the order, a *fractal* dimension.

A number of methods exist for estimating this fractal dimension of an attractor; indeed there are a number of different *types* of dimension that can be calculated. The *capacity*, the *information* dimension, the *correlation* dimension and the *Lyapunov* dimension all provide information about this aspect of an attractor. Unfortunately they also each provide a slightly different result for any particular attractor, which only adds to the confusion for the novice. These four types of dimension measurement are now briefly considered in turn. It should be noted that our intention here is not to give a full implementation of each of these measures, but to provide a feel for what each measure achieves. The interested reader is directed toward the works indicated for full descriptions of the dimension measures, or to [28, 29] for more extensive summaries than those contained herein.

- *Capacity.* This is the simplest type of dimension, and is sometimes referred to as *fractal dimension*. In calculating the capacity $D_{cap}$ of some attractor $A$, the attractor is covered with volume elements (typically cubes, or hyper-cubes) of width $\epsilon$, with $N(\epsilon)$ being the number of volume elements needed to cover $A$. As $\epsilon$ is reduced, the sum of these volume elements approaches the volume of $A$. If $A$ is a $D$-dimensional manifold ($D$ being an integer), then , for small $\epsilon$, the number of volume elements needed to cover $A$ is inversely proportional to $\epsilon^D$, i.e.

$$N(\epsilon) = k\epsilon^{-D} \tag{2.5}$$

  where $k$ is some constant. The capacity is calculated from

$$D_{cap} = \lim_{\epsilon \to 0} \frac{\ln N(\epsilon)}{\ln \frac{1}{\epsilon}} \tag{2.6}$$

  as described in [29]. If $A$ is a piece of a $D$-dimensional manifold $D_{cap}$ is equal to the dimension of the manifold which is an integer, however for objects that are not manifolds $D_{cap}$ is usually non-integer. For an accurate result, however, this measure of dimension

requires complete knowledge of the attractor, rather than only a temporal section of it, as is available with measured or calculated attractors. Consequently the following two dimension measures, each involving a probabilistic term, are regarded as being of more use.

- *Information dimension.* This measure is defined in terms of how often a trajectory is found in a particular volume of the phase space. Information dimension is again based upon $N(\epsilon)$ volume elements, each of diameter $\epsilon$, but in this case a measure of entropy $S(\epsilon)$ is utilised, i.e.

$$S(\epsilon) = -\sum_{i=1}^{N(\epsilon)} P_i \ln P_i \tag{2.7}$$

where $P_i$ is the relative frequency with which a typical trajectory enters the $i^{th}$ element of the covering. The information dimension is then calculated from

$$D_i = \lim_{\epsilon \to 0} \frac{\ln S(\epsilon)}{\ln \frac{1}{\epsilon}} \tag{2.8}$$

and it is apparent that this dimension measure is more affected by those volumes that contain lots of trajectories than those that contain few. Also, it is possible to generate a value of information dimension with some confidence from the partial attractor inevitably generated experimentally or numerically. .

- *Correlation dimension.* This measurement is also probabilistic in nature, and is derived from

$$D_c = \lim_{\epsilon \to 0} \frac{\ln \sum_{i=1}^{N(\epsilon)} P_i^2}{\ln \epsilon} \tag{2.9}$$

with $P_i$ again being a measure of the relative frequency with which a trajectory enters the $i^{th}$ volume element. In practice, it is the most efficient of the measurements to implement, in terms of computing time, and, as such, is the measure of dimension most frequently used. Grassberger provides a full implementation of correlation dimension [30].

- Lyapunov dimension. The Lyapunov dimension was defined by Kaplan and Yorke [31] as a measure based on the Lyapunov exponents of an attractor,

$$D_L = j + \frac{\sum_{i=1}^{j} \lambda_i}{|\lambda_{i+1}|} \tag{2.10}$$

where $j$ is the largest integer such that $\sum_{i=1}^{j} \lambda_i \geq 0$ and $\lambda_i$ is the $i^{th}$ largest Lyapunov exponent. The Lyapunov exponents of an attractor are a measure of its predictability and are discussed in detail later in this chapter. It is clear that the Lyapunov dimension is a completely different type of measure to the previous three, and it may not strictly be a measure of dimension at all. In [31], it is pointed out that the Lyapunov dimension may provide an upper limit on the measured dimension of the attractor under consideration. What the Lyapunov dimension achieves is a running total of the Lyapunov exponents

of an attractor; when that running total becomes negative, it is an indication that the Lyapunov exponent which was most recently added is the last Lyapunov exponent with meaning. Since a $n$-dimensional attractor has $n$ meaningful Lyapunov exponents, the Lyapunov dimension is found by finding the fractional number of Lyapunov exponents which would put the running total on the zero axis. This measure will have some relevance to the results in the penultimate chapter of this thesis.

It should be noted that these four types of dimension are each distinct invariant measures of an attractor in their own right. In general, for a particular attractor, each produces a figure between the same two integers, implying that, in order to fully represent the dynamics of the attractor, the rounded-up integer number of dimensions are required. For example, the Lorenz attractor described earlier is said to have a correlation dimension of 2.07 [32], which implies that the data must be considered as 3-dimensional for a successful analysis.

For many artificially generated attractors, the application of these measures for a range of embedding dimensions will lead to some convergence of the results to give an indication of the value of the dimension calculated. However, when applied to real-world, noisy time series, it has been noted [33, 34] that such convergence does not always occur. This calls into question the practical usefulness of all four of these measures and, for the purposes of this thesis at least, they will not be considered further. They have, however, served as an indication of some of the complexities involved in the study of chaotic systems, and of the pit-falls hidden in applying much of the literature on analysis of chaotic systems to a "real-world" signal.

### 2.4.2 Embedding A Time Series

If chaos theory is to have some long-term consequence on science as a whole, it must be possible to apply it to a "real-world" situation. In general, when considering a system, the differential equations defining that system are not known and all information about the system must be gleaned from one or more time series measured from the system. As such, some method of embedding a time series so that it is dynamically identical to the system as a whole is required.

This is achieved by Takens' method of delays [35]. Takens provided a remarkable theorem showing that a single time series of a system can be embedded in such a way as to exhibit the dynamics of the generating system attractor. The actual proof of the theorem is beyond the scope of this thesis and, as such, it's not really worth stating the theorem in all its glory. Instead, we only consider the method of applying Takens' theorem, and the implications it has on the subject of our work.

Consider a time series $x(t)$

$$x(t) = (x_0, x_1, x_2, x_3, x_4 \ldots x_n) \tag{2.11}$$

consisting of a series of instantaneous values of $x$ taken at some sampling time $\Delta t$. If a matrix $X$ is constructed by running a $d$-length window through this series

$$\mathbf{X} = \begin{pmatrix} x_0 & x_1 & x_2 & \dots & x_{d-1} \\ x_1 & x_2 & x_3 & \dots & x_d \\ x_2 & x_3 & x_4 & \dots & x_{d+1} \\ \vdots & & & & \\ x_{n-d+1} & x_{n-d+2} & x_{n-d+3} & \dots & x_n \end{pmatrix} \tag{2.12}$$

then this matrix exhibits the same dynamical characteristics as the system from which the time series was measured. Plotting each column of $X$ as an axis of a $d$-dimensional phase space will produce the attractor of the system. Of course, $d$ must be chosen to be at least as great as the dimension of the generating system attractor, and $\Delta t$ must also be chosen with some care. If $\Delta t$ is too small, then there will be little change in the values contained in a single horizontal vector of the matrix and the attractor will be squashed up and indistinguishable from a straight line; if $\Delta t$ is too big, then higher frequency dynamics will be ignored and a full representation will not be achieved. As a rule of thumb, the reciprocal of the Nyquist frequency of the signal is used for $\Delta t$. It has been suggested that a measure of the signal labelled the *mutual information* can be of use here [36]. The mutual information provides a measure of the general (as opposed to linear) dependence of two variables; hence, by calculating this measure for two points at increasing separations along the the time series, an indication of the necessary time delay for completely uncorrelated samples is provided. As with many of the measures detailed in this chapter, the results from such analysis should not be taken as written in stone, but should be taken into consideration alongside results indicated by other methods.

The implications of Takens' theorem are immediate and far-reaching. It provides a framework for the analysis of a multi-dimensional system when as little as a single time series from that system is available for measurement. Without this, it is safe to say that any attempt at considering a "real-world" chaotic system would be stymied almost from the outset.

The first problem is, however, choosing the number of dimensions in which to embed an attractor, when the differential equations defining the system are not known. Unfortunately, we have found during the course of this work, that the most reliable approach is to fall back on a trial and error approach. A cursory glance at the literature in the area may call this claim into question, with a number of methods having been suggested, including a singular value decomposition [37] as well as the various dimension measures outlined previously. A closer investigation of such work, and, more importantly, an attempt to apply it to actual time series, reveals that invariably the algorithms under consideration are "tweaked" to nudge the results toward the answers that are already known from analysis of the differential equations producing the time series. This is, of course, not possible when considering a time series from a system which has not been defined by differential equations; and any results derived from such a signal have been found to be of dubious merit with some ambiguity involved in deciding exactly what

dimension is indicated.

This brings us back to our trial and error approach, but the key phrase here is *an educated guess*. A combination of the methods suggested needs to be utilised, in particular it is worth embedding a series in a range of dimensions and considering the results from each. It will often be apparent from this what dimension the attractor should be embedded in. This all sounds very vague and hit or miss, but it must be borne in mind that, as already mentioned, chaos theory is a science still very much in its infancy, particularly when it comes to the study of non-artificial signals and systems. The work described in this entire chapter is intended to represent the first steps toward achieving a reliable frame-work in which to discuss chaos in the real world.

Once the dimension of the attractor is decided, the number of dimensions in which the time series must be embedded for successful analysis must be chosen. In general a rule of thumb of $2d + 1$, where $d$ is the integer dimension, is recommended by Takens [35]. However it is often possible to fully represent and successfully analyse an attractor in an embedding dimension of less than $2d + 1$.

Consider a 2-torus which, in phase space, looks like a dough-nut. The equation (2.13) for generating the time series of a 2-torus is simply the sum of two incommensurate sine waves.

$$x(t) = A\sin(\omega t) + B\sin(\theta t) \tag{2.13}$$

Figure 2.6a

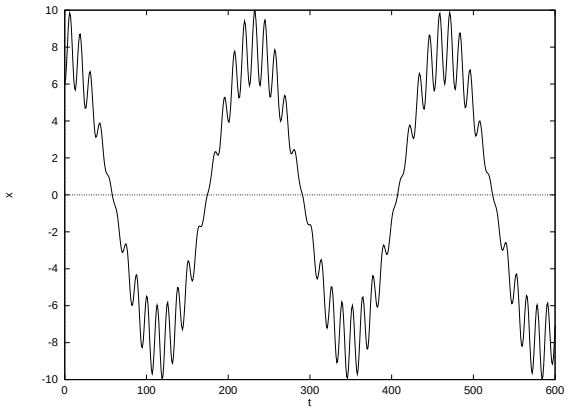


Figure 2.6b

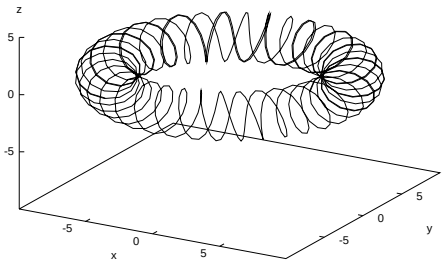


**Figure 2.6**: *A 2-torus showing a) a section of the time series and b) the phase space plot*

A portion of such a time series is shown in Figure 2.6a, with a 3-dimensional phase space plot shown in Figure 2.6b. The dimension, i.e. the number of degrees of freedom, of an incommensurate 2-torus is two, which is easily apparent from the equation. However, in order to fully 'see' the dough-nut shape of the 2-torus, a phase space of at least 3 dimensions must be used. Indeed, three dimensions are only sufficient if the higher frequency sine wave is of less amplitude than the lower frequency one, higher values leading to a cross-over region in the

centre of the 3D plot, and in general an embedding dimension of 4 is needed to see the 2-torus with no self crossings. It is immediately apparent that this is less than the figure of $2d + 1$ recommended by Takens (which would be 5 in this case).

Now we consider a chaotic attractor from a system which can also be adequately represented in less than the $2d + 1$ dimensions which are, in general, recommended. That system is the Lorenz system: we have already seen that the attractor can be plotted in three dimensions with no self-crossings, and, although it is beyond the scope of this thesis to prove this, the Lorenz attractor can be successfully analysed when embedded in three dimensions (considerably less than $2d + 1$). It should be remembered however that the fact that the Lorenz attractor can be plotted with no self-crossings and successfully analysed in three dimensions, and has three degrees of freedom (i.e. its order), is unusual [38], although generally known within the field. Most attractors must be embedded in a higher dimensional phase space than the number of degrees of freedom would suggest, i.e. for most attractors, embedding dimension > dimension. Takens' theorem [35] states that, in general, embedding dimension = 2×dimension+1 for a good phase space representation. It is worth noting that an increasing amount of noise on a system may require an increase in the embedding dimension required to analyse the attractor of the system reliably with no self-crossings.

## 2.5 LYAPUNOV EXPONENTS

The Lyapunov exponents, or Lyapunov spectrum, of an attractor provide dynamical information about the system's behaviour in an intuitive way. Put simply, the Lyapunov exponents of an attractor describe the average exponential expansion or contraction of the attractor in a set of orthogonal directions in phase space as it evolves. Consequently an attractor which is $d$-dimensional has $d$ Lyapunov exponents.

Strictly speaking, an attractor of dimension $d$ has $d$ Lyapunov exponents. However, since we are considering the analysis of real-world noisy signals and systems in this thesis, we must consider the embedding dimension of the attractor under investigation. If the differential equations defining a system are known, then a number of Lyapunov exponents equal to the order of the system can be calculated. If the equations are not known, however, then we must rely on an embedded attractor in a number of dimensions possibly higher than the system's order, which will inevitably lead to the calculation of an equal number of Lyapunov exponents. Some of these exponents are spurious, in terms of the system, but they do communicate information about how the noise on the measured system affects its measurable dynamics.

The quickest way to appreciate the information conveyed by an attractor's Lyapunov spectrum is to consider a number of simple examples:

- *a stable equilibrium point.* All Lyapunov exponents are negative since the phase space contracts toward the final steady state.

- *A stable limit cycle.* The attractor is a periodic orbit, as in Figure 2.1a, and again the trajectories contract onto this orbit. Consequently only negative Lyapunov exponents result, except for the highest which is exactly zero. A zero exponent indicates a flow and results from the temporally invariant nature of the continuous evolution of the system in the direction of the attractor trajectory.

- *An unstable unbounded system.* Such a system has only positive components since it is expanding to infinity.

- *Chaos.* As we have already seen, a chaotic attractor exhibits both contraction and expansion, resulting in the non-periodic yet bounded nature that we are familiar with. This behaviour leads to both positive and negative exponents in the attractor's Lyapunov spectrum, and this phenomenon is a popular test for chaos, indeed it is even mooted as a definition of chaos. Chaotic attractors with more than one positive Lyapunov exponent have been labelled *hyper-chaotic* by some workers [32,39]. The presence of a zero exponent in a chaotic attractor's Lyapunov spectrum indicates a flow, such as the Lorenz system; the absence of a zero implies a discrete map such as the Henon equations.

Mathematically the Lyapunov exponents $\lambda_{i=1\ldots k}$ of a k-dimensional attractor can be defined by

$$\lambda_i = \lim_{n\to\infty}(\frac{1}{n}\ln(\mathrm{eig}\prod_{q=0}^{n} T(q)) \tag{2.14}$$

where $T$ is the local tangent map as $q$ moves around the attractor [40,41]. It can be seen that the exponents define an average rate of exponential growth in a set of orthonormal directions in the embedding space.

Consequently, if the differential equations defining the system are known, the Lyapunov exponents are calculated by iterating those equations numerically and substituting each of these calculated values into the Jacobian of the system (which is exponentially related to the tangent map). For example, consider the Lorenz system,

$$\dot{X} = \sigma(Y - X) \qquad \dot{Y} = rX - Y - XZ \qquad \dot{Z} = -bZ + XY \tag{2.15}$$

the Jacobian of this system is

$$\mathbf{J} = \begin{pmatrix} -\sigma & \sigma & 0 \\ r - Z & -1 & -X \\ Y & X & -b \end{pmatrix} \tag{2.16}$$

formed from the partial derivatives of each expression with respect to $X$, $Y$ and $Z$. As Lorenz' equations are iterated, the values of the three components are used to calculate the Jacobian

at each step on the attractor, which is then included in the running product for calculation of the Lyapunov exponents.

This method of calculating the Lyapunov spectrum of a system in a particular mode from the differential equations is detailed in [32, 42], and has produced exponent values for a range of chaotic systems which have become accepted within the community as the definitive values. The Lorenz system, for example, is said to have Lyapunov exponents of $+1.37$, $0$ and $-22.37$ for coefficient values of $\sigma = 16$, $r = 40$ and $b = 4$; these values are referred to in later chapters as a yardstick for comparison of our own results. A simple check on these values is provided by comparing the sum of the Lyapunov exponents to the trace of the Jacobian (i.e. the sum of the diagonal elements). These values ought to be equal since the sum of a matrix's eigenvalues is equal to its trace. In this case, with the values of coefficients indicated, both sums come to $-21.0$.

However, if the science of chaos theory is to come of age, then it must be possible to apply its tools to actual physical systems. In general, the differential equations defining a system's dynamics are not known, and are not easily formulated. This means that some other method of extracting a system's Lyapunov spectrum must be developed.

A number of algorithms have been published which address this very problem [40, 43–46]. Each of them makes use of the aforementioned Takens' theorem [35] to take advantage of the fact that a suitable time series measured from a multi-dimensional system contains the full dynamical information of the behaviour of that system. They achieve this by constructing the attractor, using the method of delays or otherwise, from the sampled data, and considering the transformation of a set of points as it evolves around the observed attractor. By comparing an evolved set of vector differences between points in a neighbourhood to those same vector differences prior to the evolve step, an approximation of the transformation occurring can be constructed. This is, in effect, the tangent map at that point, in the limit of an infinitely small evolve step and an infinitely small volume neighbourhood, and the Lyapunov exponents can be calculated from a string of such tangent maps as before.

However, each of the published algorithms for implementing such an approach that are known to the author, have proven to be both unwieldy and ambiguous when applied to time series with added noise. It was decided to develop our own algorithm to address the time series that we intend to analyse. This algorithm for extracting the Lyapunov exponents of an attractor from a single time series derived from that attractor's generating system is described in detail in chapter 6.

## 2.6 CHAOS AND SIGNAL PROCESSING

Clearly this new science of chaos theory is not something which can be ignored by the signal processing community. As was intimated in the introductory chapter, a wide range of both

signals and systems in the field have been suggested to be chaotic in nature, or capable of chaotic modes of operation.

Much of signal processing relies on constructing some form of model of the system under study, whether for predictive purposes or some other form of analysis. The problem with a chaotic system, however, is that, even if that model were a 100% perfect representation of the system under study (unlikely in itself), it is still limited in its application due to the sensitive dependence on initial conditions inherent in a chaotic system. Any measured instantaneous value obtained from the system, must contain some error, whether due to quantisation or some other effect and, for a chaotic system, that error will quickly escalate until the modelled signal bears no similarity to the actual signal under study, and is completely uncorrelated to it.

Consequently, the method of measuring a chaotic signal must be considered in detail, and the effects of applying that measurement taken into account in subsequent analysis.

This chapter has served as an introduction to the basic philosophy and tools of chaos theory, with regard to the problem to be considered in this thesis. Particular reference has been made to the complexities involved in analysing chaotic signals from physical systems, and to the pitfalls and ambiguities involved in applying much of the existing literature to such a signal. The problem essentially is that very little successful research has been conducted into studying and measuring chaos from a physical, or "real-world", source. Consequently, we hope to have made it clear that extreme care must be utilised in approaching such a goal.

Chapter 3

# SIGMA DELTA MODULATION: A RETROSPECTIVE

## 3.1 INTRODUCTION

Sigma delta modulation is a technique for analogue to digital conversion (ADC) that is used throughout the signal processing community. It has rapidly become the most popular form of ADC for lower frequency applications due to its cheaper price and reduced complexity in comparison to other solutions. Indeed, it is almost impossible to purchase a modern compact disc player which does not utilise this over-sampling, or bit-streaming, architecture. As knowledge of, and faith in, the technology increases, the range of available sigma delta modulators is widening, with higher frequency modulators of precisions as great as 16-bits now available.

The sigma delta modulator is an oversampling device in that, in order to achieve a precise digital conversion, it averages a number of coarser conversions at a higher sampling rate. How this is achieved is addressed in this chapter, but first we present an introduction to the concept of analogue to digital conversion, and a brief history of the development of sigma delta modulation. We then consider the existing work on the analysis of $\Sigma\Delta$M, showing that such work is thus far incomplete, particularly when it comes to the understanding of higher order modulators, and to the study of the effects of $\Sigma\Delta$M on moving signals.

It is worth noting that this chapter is not intended as a definitive history of analysis of the sigma delta modulator, as such a project would rapidly degenerate into a long list of paper titles. Instead, we discuss that portion of the analysis which is pertinent to understanding the problem at hand: i.e. the effect of $\Sigma\Delta$M on a chaotic signal.

## 3.2 ANALOGUE TO DIGITAL CONVERSION TECHNIQUES

Sigma delta modulation is a form of analogue to digital conversion; in this section a brief introduction to ADC is given. The overall performance of any system involving digital processing, or digital representation, of an analogue quantity is largely determined by the precision of the analogue to digital technique used. The precision of an analogue to digital converter can be seen as having two factors defining it – the accuracy of the digital approximation to the analogue input at a sampling instant, and the rate at which those samples are taken. Unfortunately, as

is so often the case, these two desirability factors are mutually conflicting – i.e. the more often a sample is taken, the less time there is available and the less precise it tends to be; conversely, the more precise a sample, the longer it takes to be made so the lower the sampling rate must be. Any analogue to digital converter involves some sort of trade off between the sampling speed and the accuracy of each sample.

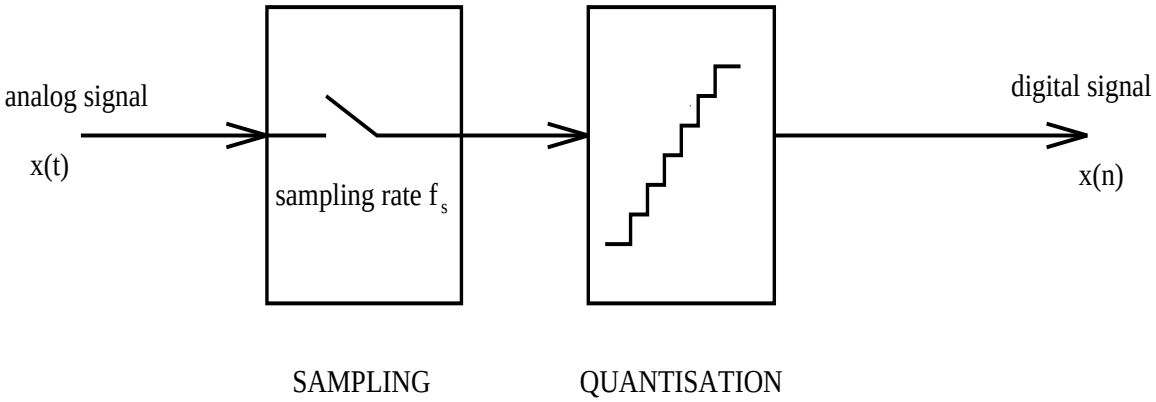


**Figure 3.1**: *Generic Analogue to Digital Converter*

A generalised A-D conversion process is shown in Figure 3.1. A continuous signal, x(t), is transformed into a series of discrete samples at regular time intervals, each of which has a continuous range of values. Typically the sampler is actually a sample and hold circuit, maintaining the sampled value for the period of time until the next sample is taken, so that it can be reliably quantised to give a fully digital output x(n). This quantisation is usually achieved by comparing the sampled value to a range of reference levels generated internally by the quantiser. The resolution of such a converter is determined by the number and spacing of these reference levels. If very high precision is required then the spacing of these levels may be in the order of microvolts, putting great strain on component matching tolerances and VLSI manufacturing techniques. However, processes such as laser-trimming or self-calibration can be utilised, but this increases the complexity of the fabrication process, the device size and the component cost.

Analogue to digital converters can be grouped according to the sampling rate used. In Nyquist rate converters the sample rate is at least twice the maximum frequency of the signal to be sampled. This type of conversion is used in double integration, successive approximation register and flash type converters. In over-sampling converters, such as sigma delta modulators, the sampling rate is much higher than the maximum frequency of the signal.

If a signal to be sampled has frequencies higher than the Nyquist frequency of the sampler, it will not be correctly converted and extra components will be produced at lower frequencies in the digital output. This phenomenon is known as aliasing. To prevent it, the input signal to the converter must be low pass filtered to the Nyquist frequency. This leads to an advantage of using sigma delta modulation whereby the aliasing filter can be far less steep than in conventional ADCs due to the oversampling nature of the device.

### 3.3 DELTA MODULATION

The sigma delta modulator was first developed as a variant on the more simple *delta modulator* [47]. A schematic of a delta modulator is shown in Figure 3.2. It operates by quantising

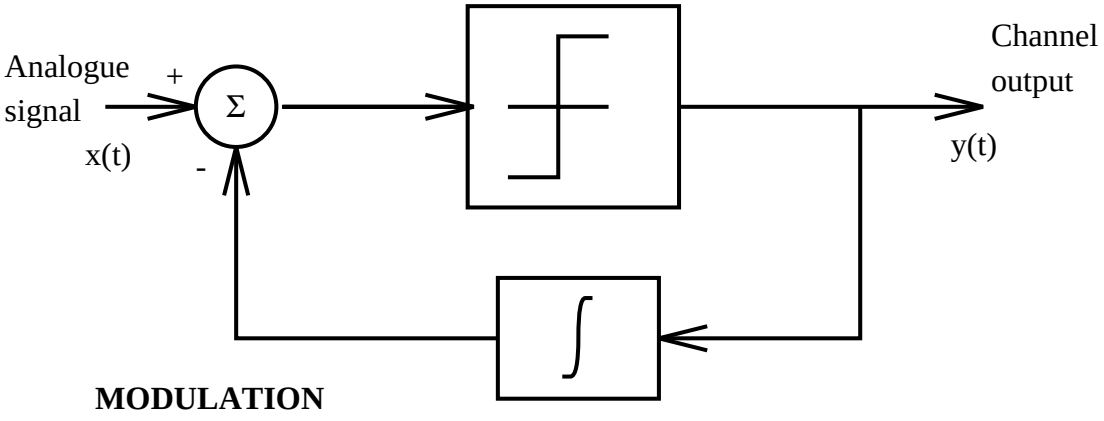


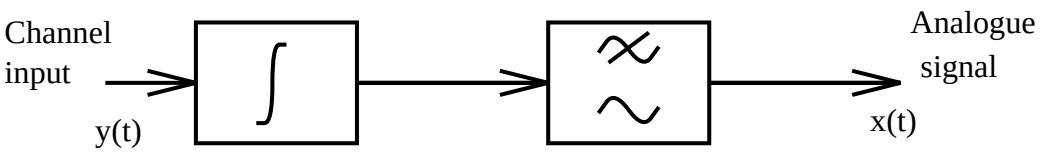


**Figure 3.2**: *Delta modulation and demodulation.*

the difference between the analogue input and the integral of the one bit quantised output. Consequently, this integral of the quantised output is an approximation to the value of the input at the previous sampling instant. When demodulating the bit-stream output of this modulator, therefore, it is necessary to integrate it before low-pass filtering it. The name *delta* modulation comes from this differencing of the input with the integrated output.

To form a sigma delta modulator from this structure, the two integrators (i.e. the one in the feedback path, and the one in the demodulator) were combined to produce a single integrator in the feedforward path [48]. Figure 3.4 shows this structure. Hence, the circuit now includes a difference at the comparator (delta) and a sum at the integrator (sigma) and was labelled either delta sigma modulation or sigma delta modulation. It should be noted that the demodulator now consists only of a low-pass filter, and the output of the modulator is a binary sequence.

### 3.4 SIGMA DELTA MODULATION

Before discussing the architecture of the sigma delta modulator, it is worth considering exactly what it does, in a black box sense. Figure 3.3 represents an input and a corresponding output of a sigma delta modulator. The input is a continuous, analogue signal, indicated by the curved line. The output has but two states, high and low, which provides us with a sequence of 1s and $-1$s in response to the input. In fact, Figure 3.3 shows an over-simplified version of the

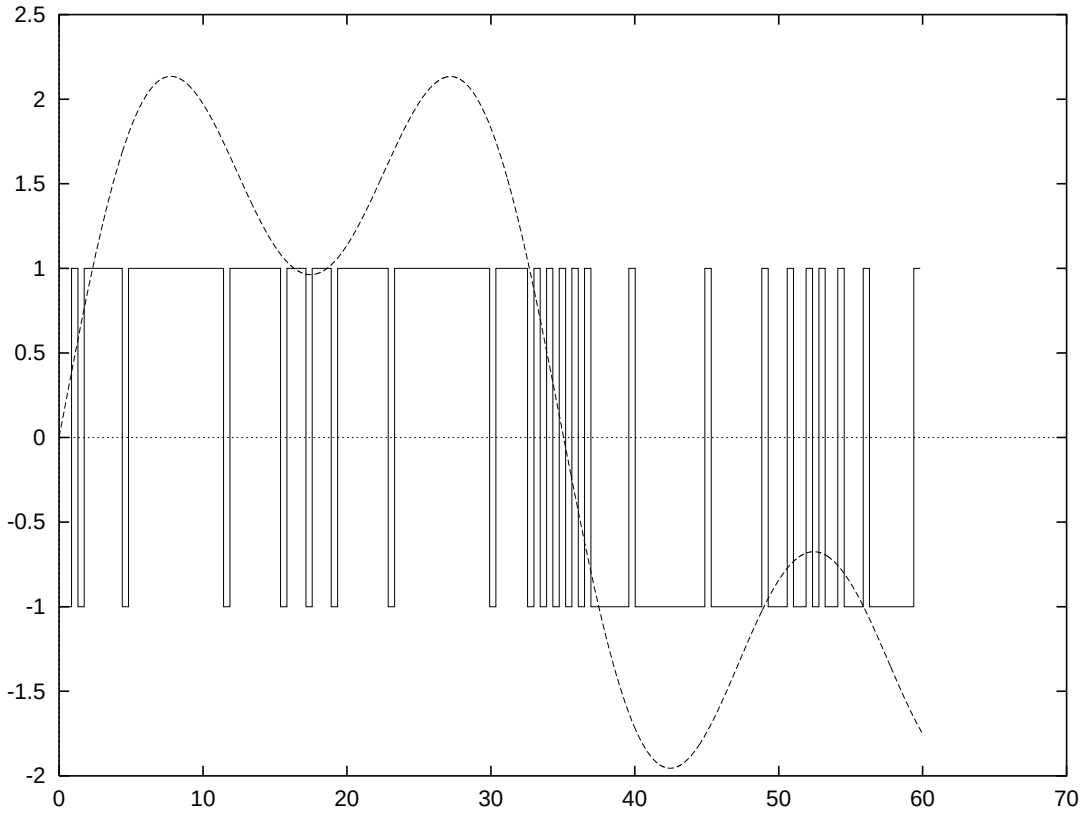


**Figure 3.3**: *Input and output of sigma delta modulator.*

output, in order to better show the performance of $\Sigma\Delta$M, in that the over-sampling rate has been greatly reduced. It can be seen from the figure that, while the input has a high positive amplitude, the output consists mostly of 1s; similarly when the input has a high negative amplitude, the output consists mostly of $-1$s; when the input is near zero, the output oscillates between 1 and $-1$. It is clear from this behaviour that, as the over-sampling rate is increased, an average value of the output approximates toward the input.

A first order sigma delta converter is shown in Figure 3.4. It consists of an analogue comparator, an analogue integrator and a one-bit quantiser in a feedback loop. The difference between the input signal and the quantised output value (i.e. the quantisation error between the current input and the previous sampled output) is integrated. The output of the integrator is then quantised to one bit to give the output value, which is fed back for comparison to the input during the subsequent sampling period. The digital to analogue converter in the feedback path reconverts the output to an analogue signal for comparison to the analogue input, it also

introduces a delay so that the previous output is compared to the current input. Although the quantisation error at any particular instance is high due to the coarse nature of the two-level quantiser, the repeated action of the feedback loop produces a string of $+1$ or $-1$ outputs which can be averaged over many sampling periods to give a very precise result. This averaging is achieved with a decimation filter. It is this decimation process which necessitates the over-

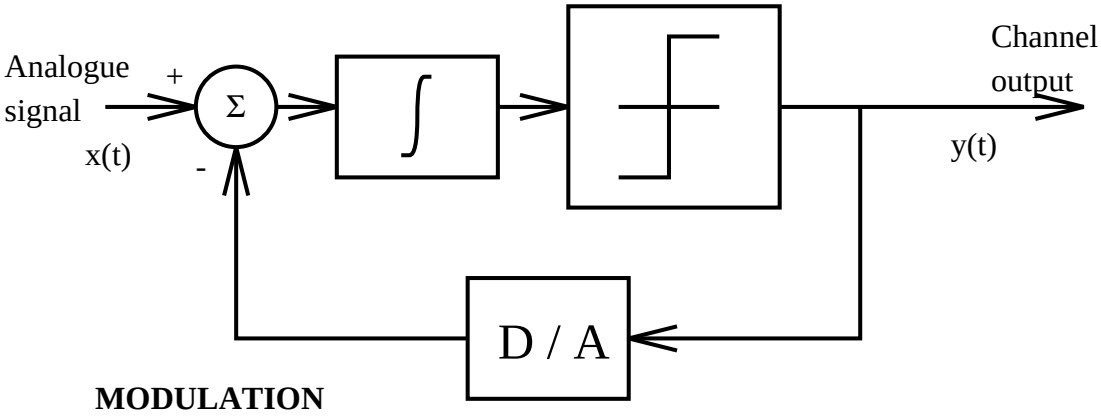


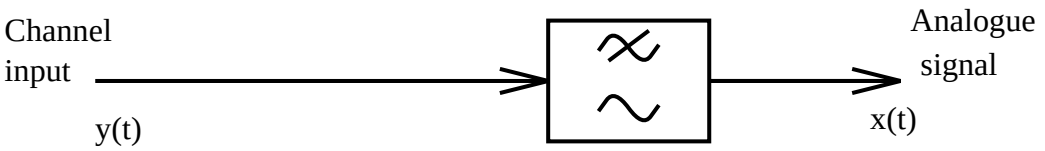


**DEMODULATION**

**Figure 3.4**: *First order sigma delta converter*

sampling of the input signal, as a number of samples must be taken without too much fluctuation in the signal in order to achieve a reliable average. Hence, a trade-off occurs between the resolution of the converter and the over-sampling rate.

Figure 3.5 further clarifies the operation of a sigma delta converter by presenting a series of waveforms taken from such a modulator with a sinusoidal input. The waveforms are taken from a computer simulation of a first order sigma delta modulator. The input is shown in Figure 3.5a. Figure 3.5c shows the output of the one bit quantiser and the operation of the modulator is clear from the high incidence of $+1$s when the input is high, etc. Figure 3.5d shows the output after decimation, wherein the bit-stream has been averaged over a window equal to the over-sampling ratio. Figure 3.5b shows the time series at the input to the quantiser, i.e. the output from the integrator. It is clear that this is a complex signal, and it is this time series which will be the main focus of the continuous analysis of chapter 4.

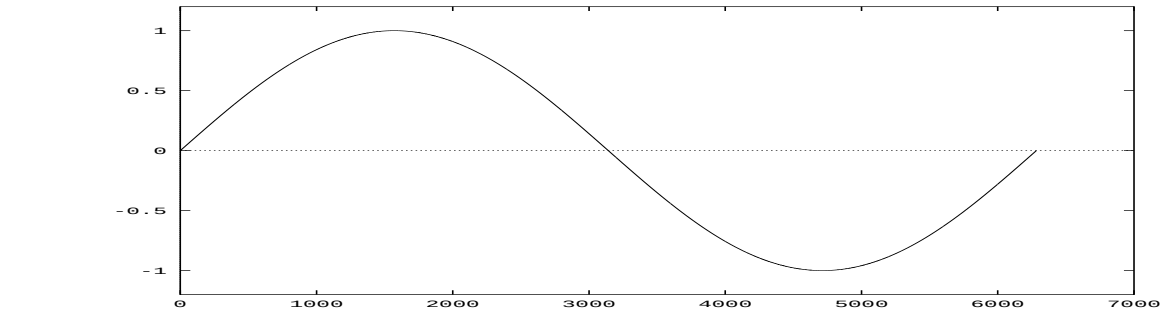


a

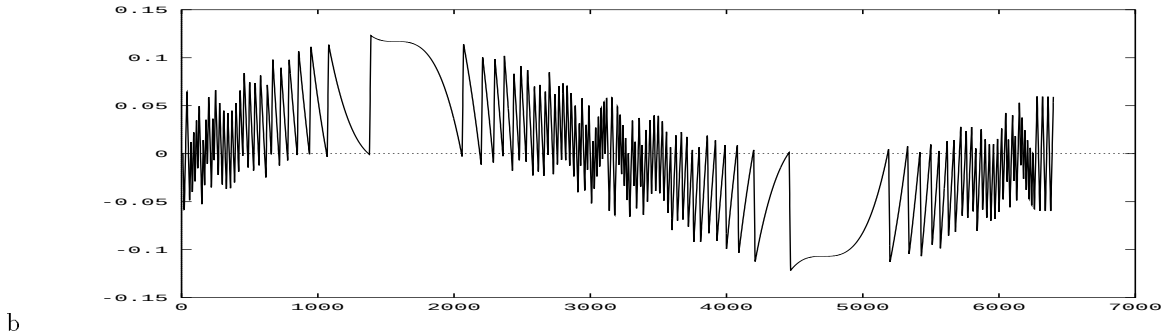


b

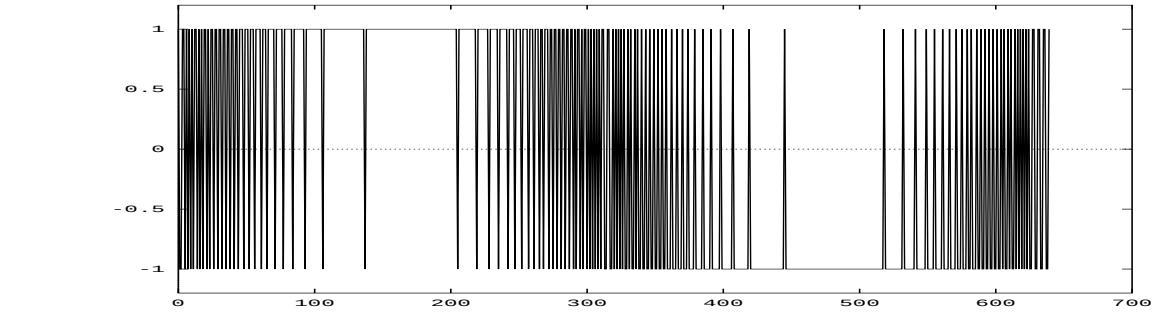


c

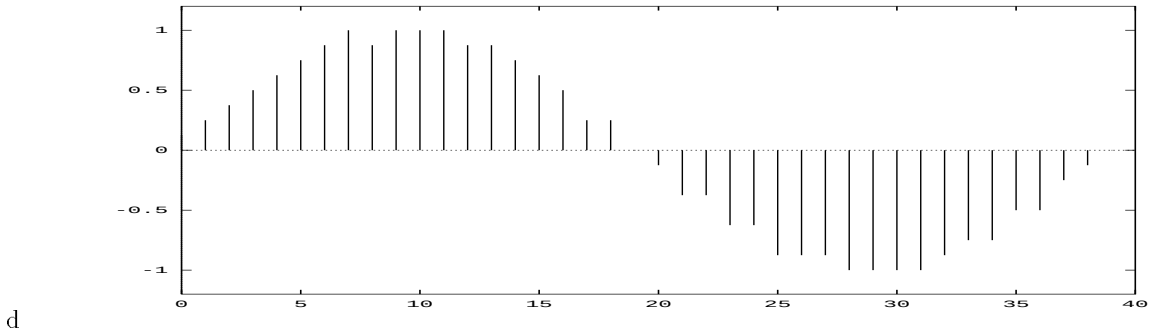


d

**Figure 3.5**: *Time series for sinusoidal input to first order sigma delta converter showing a) the analogue input to the modulator, b) the output of the integrator, c) the output from the quantiser (and from the modulator as a whole), and d) the output from the modulator after decimation.*

The values on the abscissae of these plots are also informative, since they show the number of points in the data produced by the computer simulation at each step of the conversion process. We start with a highly sampled sine wave (Figure 3.5a) to provide a reliable integration of the signal (Figure 3.5b). The abscissa of Figure 3.5c shows the number of one bit samples taken – i.e. at the oversampling rate, which is then decimated to smaller values on the abscissa of Figure 3.5d, giving the final sample rate of the converter as a whole.

So far, only first order sigma delta converters have been considered, but higher order converters do exist, and are regularly in use. Figure 3.6 shows a general diagram for higher order sigma delta modulation.

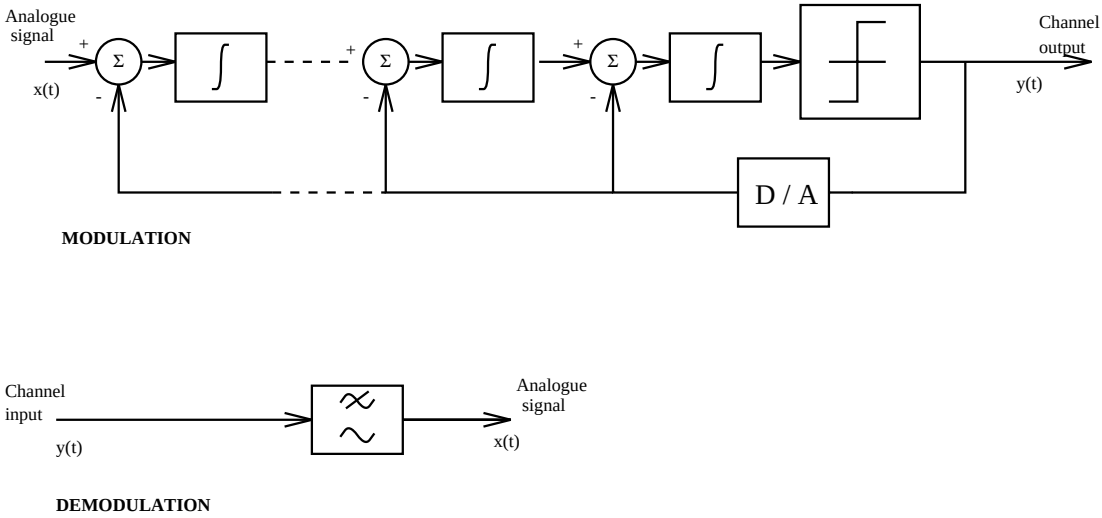


**Figure 3.6**: *Higher order sigma delta modulation and demodulation*

For example, a second order modulator has one extra integrator and comparator on the front of a first order modulator. In practice these higher order converters become increasingly unstable and are rarely used above about fourth order. In this thesis, analysis will only be given of sigma delta modulators up to third order.

Sigma delta modulators are sometimes referred to as *noise-shaping converters*, due to the way they push noise out of the low frequency band, a feature which is utilised in the demodulation process. This will be shown more specifically in the next section.

It has been demonstrated in this section that the sigma delta modulator is an over-sampling analogue to digital converter, offering only a two-level quantisation but at a sufficiently high rate for the output to be averaged to an acceptable resolution.

## 3.5 EXISTING ANALYSIS OF SIGMA DELTA MODULATION

As has been intimated, the operation of the sigma delta modulator has not been fully defined, particularly with regard to higher order modulators, or to the modulation of moving signals.

This section lays out some of the approaches which have been considered, and sums up the knowledge which has been achieved. First, we consider a very basic analysis of the circuit. Again it should be stressed that we are only considering that portion of the work known to the author which has relevance to the central problem of this thesis.

### 3.5.1 Basic analysis

Initially, we shall consider a very basic approach to the analysis of $\Sigma\Delta$M. It is based on the notion of representing the one bit quantiser as an additive noise source. Since the sigma delta modulator is an analogue to digital converter it straddles the interface between the continuous and the discrete, i.e. it has both analogue and digital components in its architecture. Consequently, we shall analyse it here in both the discrete and the continuous domain.

First, consider a continuous representation. Figure 3.7 shows a schematic of the Laplace transform equivalent of a first order modulator.

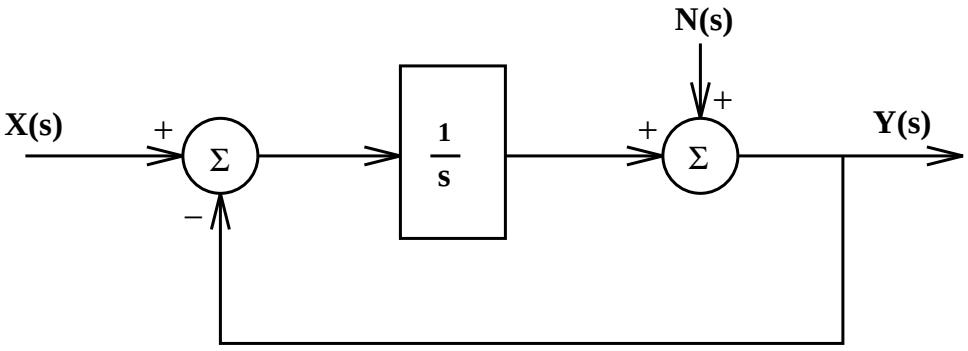


**Figure 3.7**: *Laplace transform of first order sigma delta modulator*

The one bit quantiser has been replaced by an additive noise source $N(s)$. It should also be noted that this basic approach completely ignores the delay element in the circuit.

The signal transfer function can be written by setting the noise $N(s)$ to zero.

$$Y(s) = \frac{X(s) - Y(s)}{s} \tag{3.1}$$

$$\frac{Y(s)}{X(s)} = \frac{1}{s+1} \tag{3.2}$$

This is the general form of a low pass filter.

Similarly, the noise transfer function can be written by setting the input $X(s)$ to zero.

$$Y(s) = -\frac{Y(s)}{s} + N(s) \tag{3.3}$$

$$\frac{Y(s)}{N(s)} = \frac{s}{s+1} \tag{3.4}$$

This is the general form of a high pass filter. The noise shaping behaviour of the sigma delta

modulator is thus apparent, with the noise being limited to the higher frequency band, and the signal to the lower frequency band.

Alternatively, consider Figure 3.8 which shows the Z transform equivalent to the first order modulator.

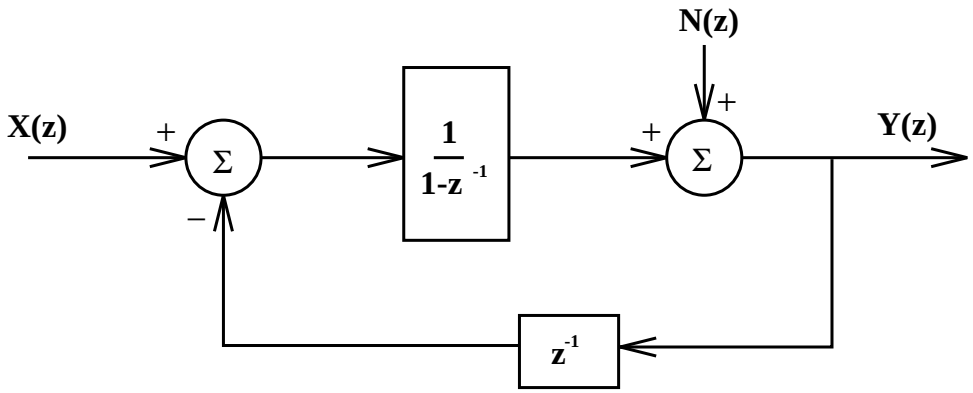


**Figure 3.8**: *Z transform of first order sigma delta modulator*

An expression for the output $Y(z)$ can be written in terms of the input $X(z)$ and the additive noise $N(z)$.

$$Y(z) = \frac{X(z) - Y(z)z^{-1}}{1 - z^{-1}} + N(z) \tag{3.5}$$

$$Y(z) = X(z) + (1 - z^{-1})N(z) \tag{3.6}$$

Again, it can be seen that the noise term $N(z)$ is pushed up the frequency spectrum, since the term $(1 - z^{-1})$ is equivalent to a differentiation.

Although basic analyses, based on a very crude representation of the one bit quantiser, both of these expressions show the noise-shaping nature of $\Sigma\Delta$M, and demonstrate why the output must be low pass filtered to return it to an approximation of the input.

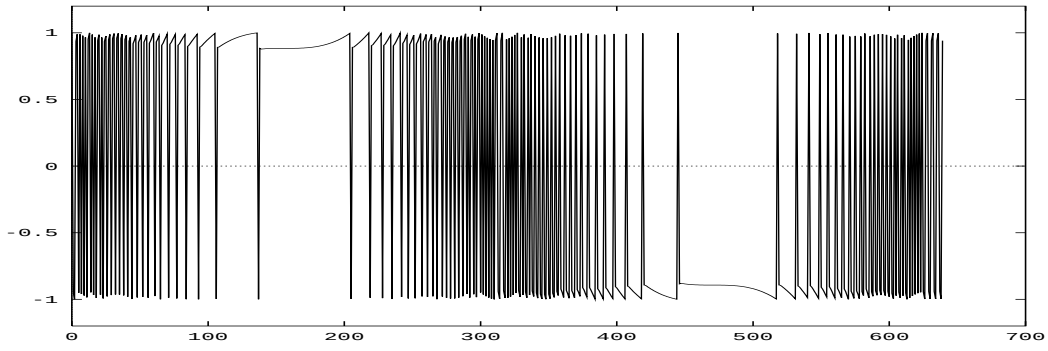


**Figure 3.9**: *Noise added by one bit quantiser for sinusoidal input*

The problem with utilising this technique to glean any further knowledge about the operation of the modulator stems from the implicit assumption that the noise added by the quantiser is

uncorrelated to the input signal. A plot of this added noise for the input sinusoid previously presented is shown in Figure 3.9 and reveals that this assumption does not hold true, since the structure of the sinusoid is readily apparent in the noise waveform.

Clearly, a more accurate form of analysis is required.

### 3.5.2 Existing work

A wide range of approaches to analysing the behaviour of sigma delta modulators has been brought to bear on the problem. These analyses can be split into four sub-groups, depending on whether a continuous or a discrete representation of the circuit is used, and on whether a linear or non-linear technique is implemented. In general, a linearisation of the circuit makes for a less accurate model, but also a simpler one. The distinction between the efficacy of a continuous and discrete approach is less clear-cut, however, since the sigma delta modulator consists of both analogue and digital elements. To date, the majority of published work in the field has involved a discrete approximation of the circuit.

The work presented in [49] was perhaps the first to attempt to describe the non-linearity of sigma delta modulation. In that paper, the influence of non-linear phenomena on the circuit's behaviour is demonstrated for first order modulators with a d.c. input. A paper by Iwersen [50] is also referred to, wherein the additive noise spectrum of delta modulation is shown to be dependent on the modulator input signal, as was demonstrated in the previous section.

Since then, various non-linear techniques have been applied to the analysis of the sigma delta modulator. Ardalan and Paulos [51] modeled the quantiser with a linearised gain, obtained by minimising a mean-square-error criterion, followed by an additive noise source representing distortion components. The analysis was based on d.c. and sinusoidal inputs; however the input to the non-linearity was still modelled as the modulator input plus additive Gaussian noise. They used this method to show that the stability of the modulators, particularly higher order modulators, is dependent on the input signal.

Gray, with various authors, has constructed non-linear difference equations to represent $\Sigma\Delta$M in the discrete domain. He showed that the conditions required by the white noise model of quantisation noise are violated in a fundamental manner in sigma delta modulators [52]. In [53], the difference equations are utilised to derive the sample moments and power spectrum of a first order sigma delta modulator, with a sinusoidal input, as had been achieved for a d.c. input in [52]. However, as he noted, the method is very mathematically complex, which would probably preclude its application to more complicated modulator architectures. The analysis was successfully applied to a two-stage sigma delta modulator in [54] (note that a two stage sigma delta modulator is distinct from a second order device; the multi-stage or MASH type converter will be described in a later section of this chapter). Ideal non-leaky

integrators were assumed in all these works, in order to simplify the analysis, but, of course, any realistic implementation of the sigma delta modulator will have leaky integrators. Gray and Park [55] addressed this problem by attempting to apply piece-wise linear and piece-wise monotone transformations to the first order modulator with a leaky integrator and a d.c. input, to give a description of the quantiser output and error sequences.

In [56] an exact analysis of the output noise spectrum of a double-loop sigma delta modulator for d.c. inputs is achieved. The method used is that of ergodic theory, whereby the asymptotic autocorrelation of the quantisation error sequence is determined, and the noise spectrum calculated from the autocorrelation function. This method was extended to irrational sinusoidal inputs in [54]. Rangan and Leung achieved similar results, by a different method, in [57]. They used an open loop model for the sigma delta modulator and applied a Fourier series representation of the quantisation error function. These works showed that the output spectrum is composed of a number of discrete spectral lines, with the assumption that the input of the modulator is not over-loaded.

The stability of the sigma delta modulator has been addressed by a number of researchers. Hein and Zakhor have collaborated on a number of papers on the topic, in particular the work in [58] considers the double loop modulator. They examine the large-amplitude limit cycle behaviour of the modulator with a constant input, and apply their results to the design process. Wang applied a geometric method to the problem [59] to define a boundary for stable operation of a double loop modulator with a d.c. input, extending this to a generalised $n$th order device. Pinault and Lopestri [60] provided a stability theorem based on a class of input functions made up from summed sinusoids, using a discrete difference equation.

In recent years the presence and removal of tones in the output of the sigma delta modulator has been a topic for discussion. These tones are related to the limit cycle behaviour of the circuit. The problem was first addressed in [61], and the case of the first order modulator was completely described in [52]. For higher order modulators, the suggested solution is to move the integrator poles outside the unit circle [8, 9] to produce what has been labelled a chaotic configuration of the circuit. This is addressed further in the final section of this chapter.

It is hoped that this section has presented a brief taste of the range of approaches that have been applied to the analysis of sigma delta modulators, particularly from a non-linear standpoint, since their inception. The intention is to have shown that the modulator is a far more complex device than is immediately apparent, and that it has resisted attempts to fully analyse its behaviour with moving signals and for higher order modulators and alternative structures. Even the analyses of first and second order modulators tend to be somewhat esoteric and complex.

A good over-view of the work carried out on $\Sigma\Delta$M is contained in the introduction to [62]. The remainder of that book consists of an extensive collection of papers on the subject, more from

the point of view of designing sigma delta modulators than analysing their operation.

### 3.6 ALTERNATIVE STRUCTURES

Due to the lack of rigorous analysis of higher order sigma delta modulators, particularly in terms of the effects of the circuit coefficients on stability, a number of alternative structures have been proposed. The most common architecture is the MASH converter [63, 64], which consists of a series of first order modulators, each taking its input from the quantisation error of the previous stage. A three stage MASH converter is shown in Figure 3.10. Such devices have become the industry standard in audio applications such as compact disc technology. The acronym MASH appears to be a trademark of the Matsushita company, although I can find no reference to what it actually stands for.

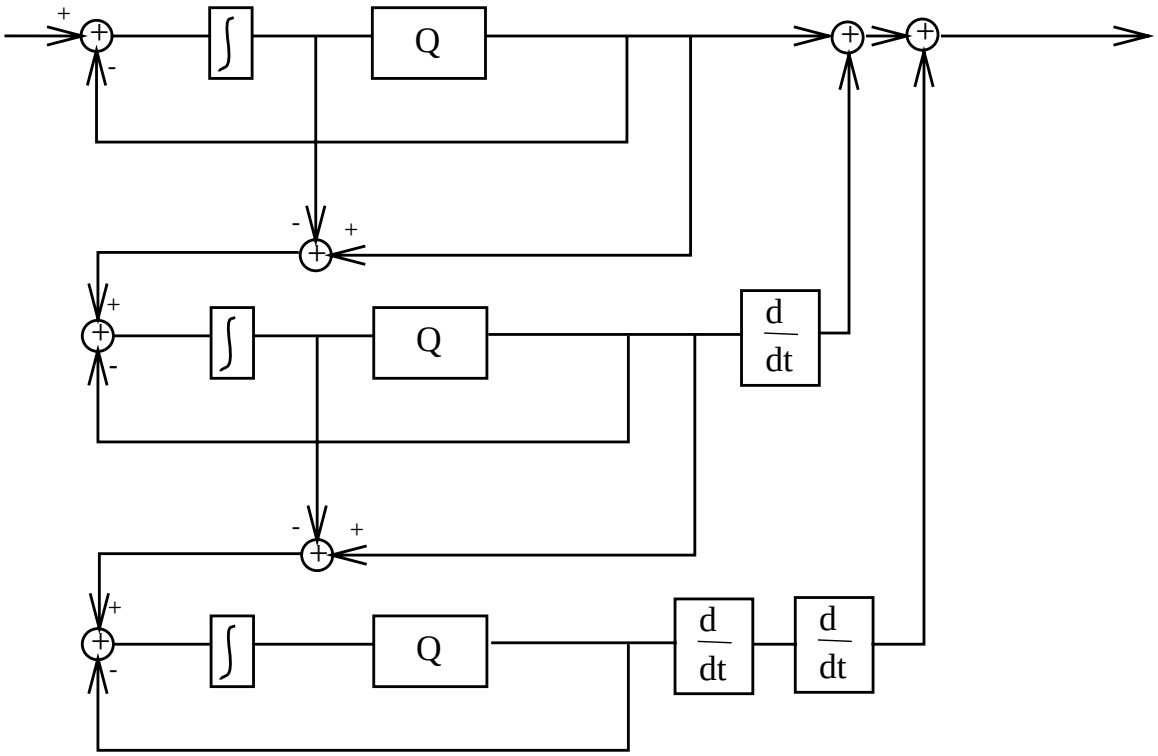


**Figure 3.10**: *A three stage MASH converter*

In general, other novel structures have been introduced to address a particular design problem or application. For example, the design in [65] consists of a two stage device, with each stage containing a second order modulator. The one-bit quantiser is sometimes replaced with a more complex n-bit device such as in [66], or Burr Brown's PCM1760P/U [67]. The outputs of the integrators in a higher order device have been combined according to a set of weights before being quantised (e.g. [68]), and combinations of feed-forward paths from the integrator outputs have also been implemented [69].

Although only a few examples are given here, it can be seen that a wide range of architectures

have been discussed or implemented. The approach in general, however, has been of a "suck it and see" nature, with simulations and experimental results being presented in lieu of rigorous analysis of the circuit, as evidence of the architecture's effectiveness against a specific set of criteria. We shall not discuss alternative architectures further, since this thesis is concerned with the conventional structure of sigma delta modulation.

## 3.7 SIGMA DELTA MODULATORS AND CHAOS

As has been demonstrated, the basic structure of a sigma delta modulator is a non-linearity (the one bit quantiser) within a feedback loop. This type of structure is a classic route to chaos, with many known chaotic systems (including the Henon map of the previous chapter) being describable in this way, i.e. a non-linearity which is folded back on itself by some means. Consequently we have the initial question of whether a sigma delta modulator may be capable of chaotic modes of operation.

Figure 3.11 shows a two-dimensional phase plot of the output from the integrator in a first order

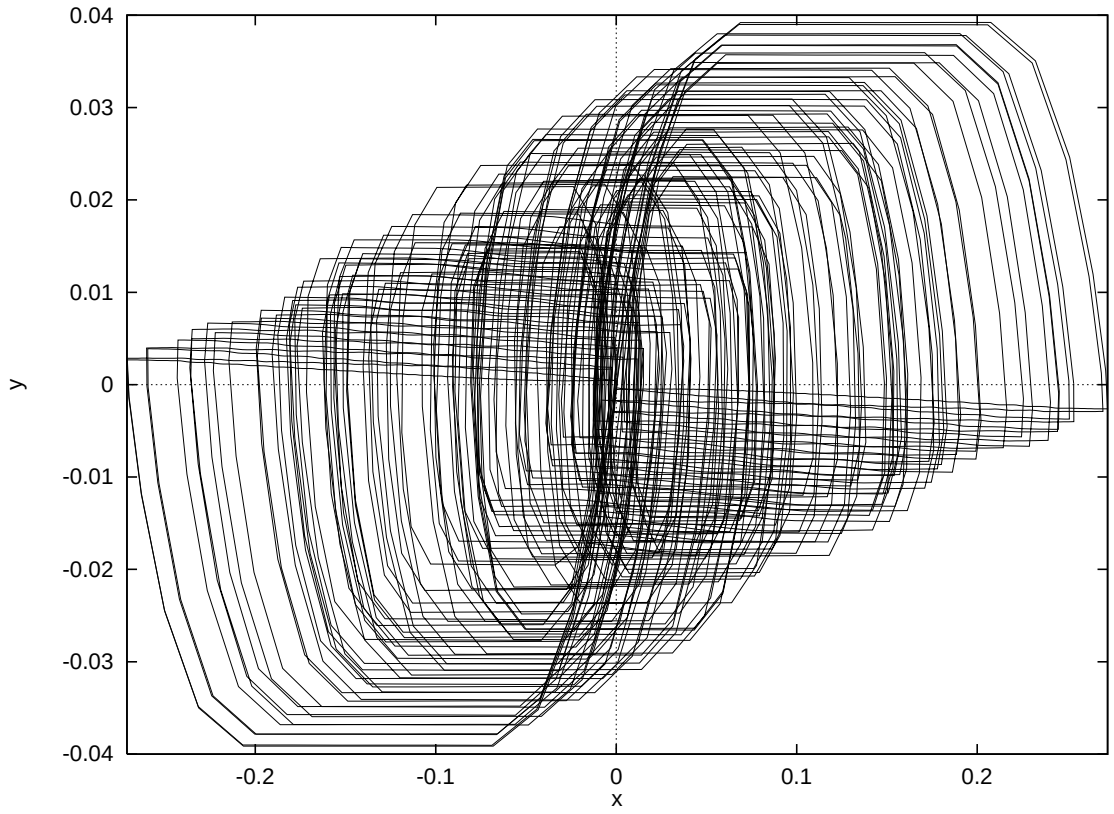


**Figure 3.11**: *Reconstructed attractor from the integrator output in a first order sigma delta modulator with a sinusoidal input*

sigma delta modulator with a sinusoidal input. The phase plot was constructed by the method of singular value decomposition reconstruction, as described in chapter 6. This method can change the shape of the resulting attractor, in comparison to that produced by a simple time delay embedding, but the dynamics of the attractor are not changed [37]. The figure clearly

shows that the signal at the output of the integrator has a complex attractor structure, which would support our worry that it may be chaotic.

Figure 3.12 shows a short section of this attractor, and it is apparent that the attractor consists of a basic shape which is repeated at different points in phase space as the attractor evolves. It would therefore seem that there are two sets of dynamics at work here: a small timescale dynamic producing this basic shape, and a larger timescale dynamic causing that shape to move around the phase space. An initial guess at explaining this would be to attribute the

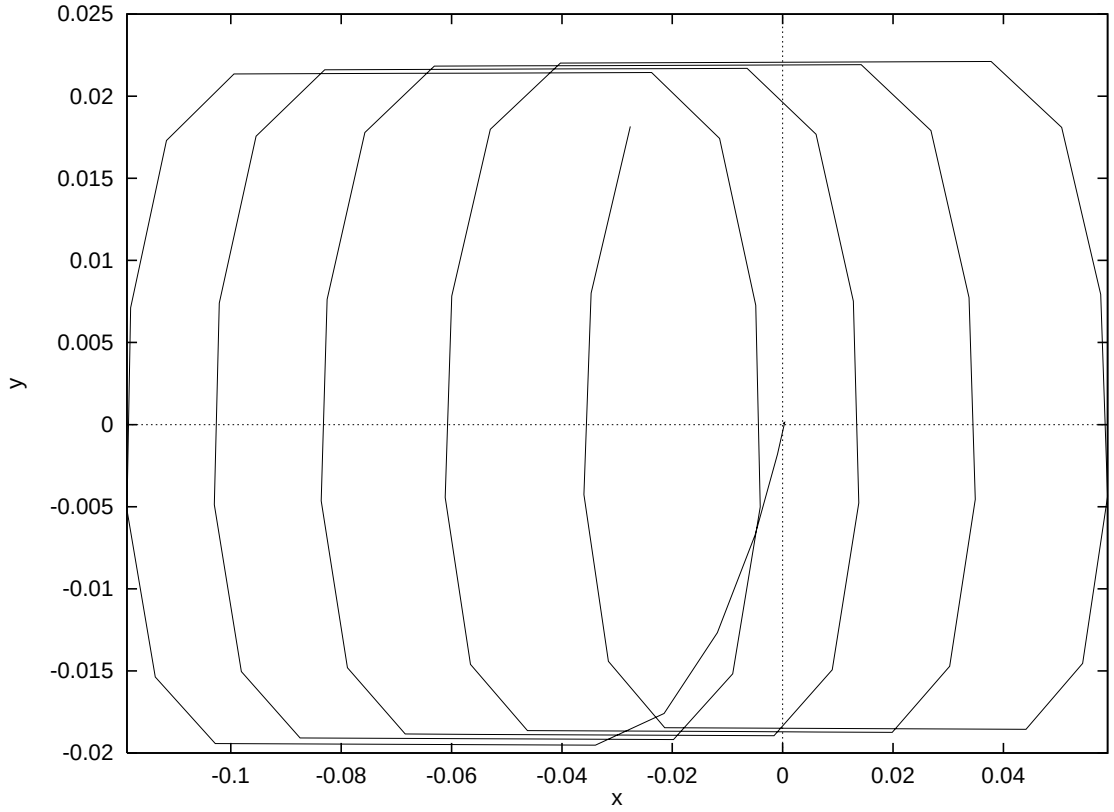


**Figure 3.12**: *Short section of reconstructed attractor from integrator output in first order modulator with sinusoidal input*

basic shape to the operation of the modulator, and the larger dynamic to the input signal.

In recent years, the problem of spurious tones in the output of a sigma delta modulator has been addressed by the suggestion of moving the poles of the circuit outside the unit circle [8,9]. This is achieved by causing the integrators to become locally unstable, by dint of their leakage coefficients. Such tone-suppressing architectures have been labelled chaotic. The reasoning behind such a label is that the integrator output consists of exponentially differing time series which are cut back and folded around by the quantiser and the feedback loop [8]. As pointed out in Chapter 2, rigorous definitions of chaos are hard to agree on, so we won't criticise this one too much, although it does seem that such a description could apply to the non-tone-suppressing architecture just as well. These structures are returned to in Chapter 7, when we consider their effect on chaotic signals, in terms of the measurable dynamics of the signal after modulation.

In this chapter we have introduced the concept of sigma delta modulation, and shown it to be a more complex process than is immediately apparent. We have described briefly some of the existing work on the structure, with particular reference to that part of the work immediately related to the problem of the $\Sigma\Delta$M of a chaotic signal. We have shown why chaotic modes of operation are likely to arise, and introduced some of the complexities involved in carrying out such an analysis. In the remaining chapters of this thesis, we will address these problems, discussing the dimension of the $\Sigma\Delta$M system, and the implications of considering the internal states of the circuit as opposed to the output after decimation.

# Chapter 4

# CONTINUOUS MODEL OF A SIGMA DELTA MODULATOR

## 4.1 INTRODUCTION

This chapter details a novel analysis of sigma delta modulation, based on devising an entirely continuous version of the circuit and constructing a system of ordinary differential equations to represent it. Some initial analysis, both numerical and algebraic, of these equations is presented to show that a reasonable model of $\Sigma\Delta$M is achieved. These equations are then used to comment on the effect of sigma delta modulation on the Lyapunov exponents of a signal. The equations are also used in the following chapter to develop a study of the stability and operation of $\Sigma\Delta$M.

As has been shown in chapter 3, work in the field to date has been confined almost exclusively to the analysis of sigma delta modulation in the discrete domain. However, since the initial motivation from the Defence Research Agency in Malvern was related to the sigma delta modulation of higher frequency signals such as radar, the devices used must have analogue integrators, rather than the digital ones often in use in other applications (for example, see [67]). Consequently our approach of considering a continuous model of the system is justified and, indeed, follows on from a similar approach adopted for a different, though related, problem by Badii and Politi [1]. Also the investigation was intended to centre around the Lyapunov exponents of the system in order to study the effects of long-term predictablilty. Although it may be possible to consider the Lyapunov exponents of a discrete model of the system in conjunction with, for example, the Henon map, such an investigation would have little meaning in the real world. A Henon map is essentially a set of completely discrete values, so over-sampling such a data set with a sigma delta modulator would have to involve either taking lots of samples at each value (i.e. modulating a series of d.c. inputs) or averaging a series of different values thus rendering them meaningless.

The particular approach adopted was to consider the effects of $\Sigma\Delta$M on an artificial chaotic time-series with known Lyapunov exponents generated from a set of differential equations such as Lorenz' equations [25] or Duffing's equations [70]. There are established methods [32, 42] for calculating the Lyapunov exponents of a system from its characteristic equations, as outlined in chapter 2, so if a set of differential equations can be constructed to represent $\Sigma\Delta$M then these need simply be combined with the equations generating the artificial time series to produce a

complete system. The Lyapunov exponents of this complete system should then be calculable for comparison to the exponents of the generating attractor before modulation.

## 4.2 CONTINUOUS MODEL

Before formulating a differential equation to represent sigma delta modulation, a continuous model of the analogue/digital hybrid circuit must be effected.

In order to construct a continuous model of a $\Sigma\Delta$M, the discrete elements of the circuit must each be addressed. The discrete elements in the sigma delta modulator in which we are interested are the one-bit quantiser and the digital to analogue converter (DAC) in the feedback path. In fact the DAC is not a problem, since the continuous equivalent of a Digital-to-Analogue converter would be an Analogue-to-Analogue converter, otherwise known as a piece of wire! There is however a delay introduced by the DAC in the conventional discrete case, which effects a comparison of the next period of analogue input to the previous digital output, and this will be addressed in our choice of a continuous representation of the one bit quantiser.

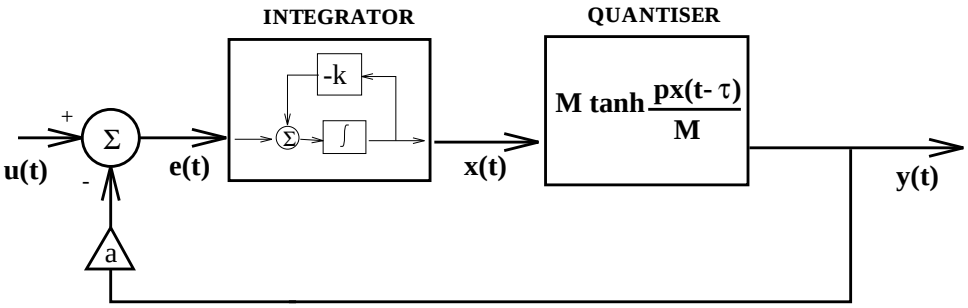


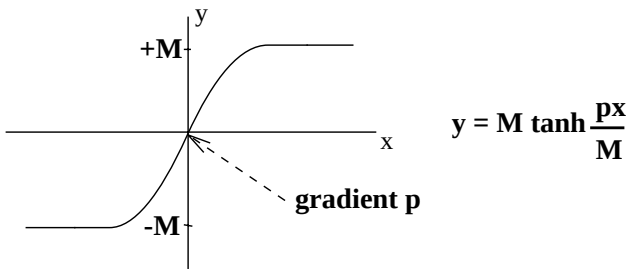


**Figure 4.1**: *First Order Continuous Sigma Delta Modulator*

The function which has been chosen to model the quantiser is a hyperbolic tangent function with a sufficiently steep gradient in the crossover region so that it tends toward the step function of the one bit quantiser. Figure 4.1 shows the resultant circuit for a first order $\Sigma\Delta$M with the quantiser represented by

$$M \tanh \frac{px(t-\tau)}{M} \tag{4.1}$$

where $M$ is the saturation level (i.e. 1 in this case), $p$ is the gradient of the tanh function as it passes through the origin ($\infty$ in an ideal quantiser) and $x(t-\tau)$ is the delayed input value. Note the inclusion of the delay at this point due to the absence of the DAC in the feedback path. Note also that this will result in the output of the continuous representation being delayed by $\tau$ seconds in comparison to the output of the conventional discrete circuit. As was noted in chapter 3, much analysis of $\Sigma\Delta$M has been in the discrete domain and often involves combining the delay of the DAC with the delay in the feedback path of a conventional discrete integrator to form a delay in the feed-forward path of the integrator [56,60,71]. A similar lag in the output of this model is thus experienced.

This continuous circuit is used to construct a series of ordinary differential equations which, if solvable, will make a full analysis of sigma delta modulation possible.

### 4.2.1 First order $\Sigma\Delta$M

In Figure 4.1 the integrator can be described by

$$e(t) = \frac{dx(t)}{dt} + kx(t). \tag{4.2}$$

A leaky integrator is used in the simulation, with $kx(t)$ representing a leakage current feeding back from the output to the input of the integrator. This is a necessity for the correct operation of an integrator circuit [72], and shall be commented upon in the stability study of the next chapter. Also note that this feedback is not the same as that on a digital integrator, which includes a feedback factor ideally equal to unity.

A quick comparison of the leakage factors in discrete and continuous integrators is worthwhile at this stage. Figure 4.2 shows a schematic of a discrete integrator and a continuous integrator.

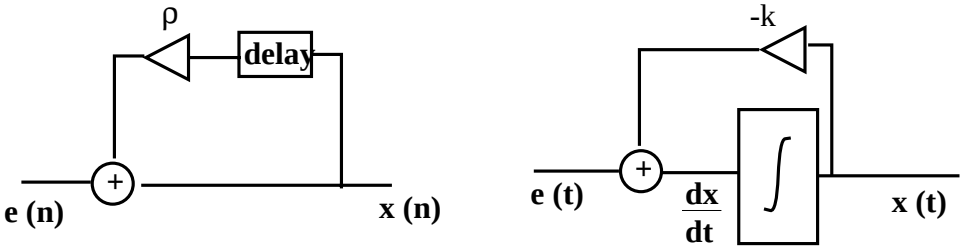


**Figure 4.2**: *Schematic of a discrete integrator and a continuous integrator*

In the discrete integrator

$$x(n) = e(n) + \rho x(n-1) \tag{4.3}$$

which can be rewritten, in differential form as

$$x(n) - x(n-1) = e(n) + [\rho - 1]x(n-1). \tag{4.4}$$

In the continuous integrator

$$\frac{dx(t)}{dt} = e(t) - kx(t). \tag{4.5}$$

It can be seen that these two equations are equivalent as the time step of the discrete circuit reduces. Hence

$$\rho - 1 \equiv -k. \tag{4.6}$$

When considering a leaky discrete integrator, the leakage factor $\rho$ is set to slightly less than unity, i.e. $\rho = 1 - \delta$; in the continuous case, the leakage factor $k$ is set to slightly more than zero, i.e. $k = 0 + \delta$. Substituting these values into 4.6 gives

$$1 - \delta - 1 \equiv -(0 + \delta) \tag{4.7}$$

and it can be seen that our representation of the leakage factor in the continuous case is in some way equivalent to that used in discrete analysis. However, taking a step back for a moment here, we have stated that equations 4.4 and 4.5 are equivalent in the limit of the time step of the discrete circuit approaching zero. Such a limit is not, in fact, practicable since the time step of the discrete circuit is equal to the input sampling rate. Consequently it would seem that, whereas the continuous representation has parallels with the discrete approach, it can not be viewed as being completely equivalent. This further supports our decision to consider the continuous form of sigma delta modulation (i.e. with analogue integrators) by means of a set of differential equations rather than by some discrete approximation.

Referring back to Figure 4.1: at the comparator

$$e(t) = u(t) - ay(t) \tag{4.8}$$

where

$$y(t) = M \tanh \frac{px(t-\tau)}{M} \tag{4.9}$$

is the output of the delayed hyperbolic tangent.

Note the inclusion of feedback factor $a$. The combination of feedback factor $a$ ($a_0$, $a_1$, etc. in higher order modulators) and leakage factor $k$ ($k_0$, $k_1$, etc. in higher order modulators) is often

termed the configuration of a sigma delta modulator. It is the combination of these coefficients which will form the basis of the stability study in the following chapter.

So equating 4.2 and 4.8

$$e(t) = u(t) - aM \tanh \frac{px(t-\tau)}{M} = \frac{dx(t)}{dt} + kx(t) \tag{4.10}$$

gives the first order sigma delta modulation differential equation

$$\frac{dx(t)}{dt} = u(t) - kx(t) - aM \tanh \frac{px(t-\tau)}{M} \tag{4.11}$$

### 4.2.2 Second order $\Sigma\Delta$M

Similarly equations can be formulated for higher order modulators. Consider the continuous model of a second order modulator shown in Figure 4.3.

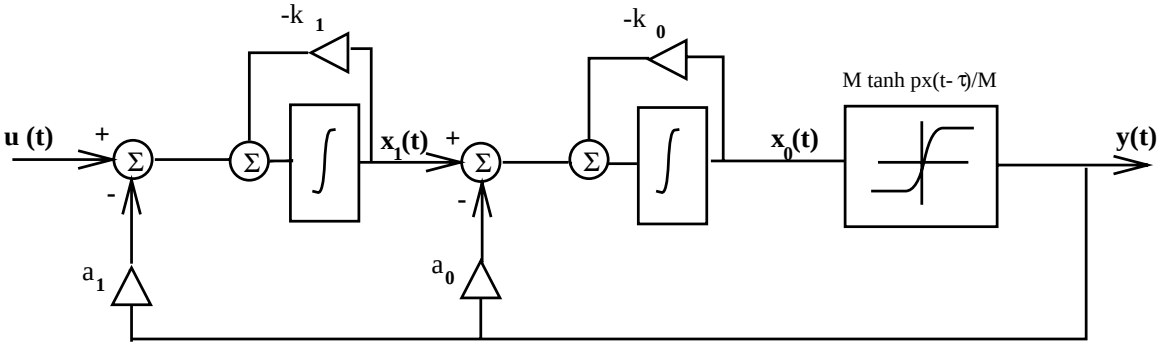


**Figure 4.3**: *First Order Continuous Sigma Delta Modulator*

An equivalent equation to 4.10 can be constructed for each of the integrators in the circuit, i.e. for the second integrator (the one next to the quantiser)

$$x_1(t) - a_0 M \tanh \frac{px_0(t-\tau)}{M} = \frac{dx_0(t)}{dt} + k_0 x_0(t) \tag{4.12}$$

and for the first integrator (the one by the comparator)

$$u(t) - a_1 M \tanh \frac{px_0(t-\tau)}{M} = \frac{dx_1(t)}{dt} + k_1 x_1(t) \tag{4.13}$$

leading to the differential equations defining second order sigma delta modulation

$$\frac{dx_0(t)}{dt} = x_1(t) - k_0 x_0(t) - a_0 M \tanh \frac{px_0(t-\tau)}{M} \tag{4.14}$$

$$\frac{dx_1(t)}{dt} = u(t) - k_1 x_1(t) - a_1 M \tanh \frac{px_0(t-\tau)}{M} \tag{4.15}$$

### 4.2.3 nth order ΣΔM

It is easy to see a recurring pattern here, and a generalised set of differential equations defining nth order sigma delta modulation can be constructed.

$$\frac{dx_0(t)}{dt} = x_1(t) - k_0 x_0(t) - a_0 M \tanh \frac{p x_0(t-\tau)}{M} \tag{4.16}$$

$$\vdots$$

$$\frac{dx_m(t)}{dt} = x_{m+1}(t) - k_m x_m(t) - a_m M \tanh \frac{p x_0(t-\tau)}{M} \tag{4.17}$$

$$\vdots$$

$$\frac{dx_n(t)}{dt} = u(t) - k_{n-1} x_{n-1}(t) - a_{n-1} M \tanh \frac{p x_0(t-\tau)}{M} \tag{4.18}$$

These equations have been constructed to solve for $x_m(t)$, the outputs of the integrators ($x_0(t)$ is also the input to the quantiser). They could have been constructed to solve for $y(t)$, the output of the quantiser and the modulator as a whole. The problem with this is that the time series would primarily be a huge list of $+1$s and $-1$s which would not allow for much insight into the interior workings of the sigma delta modulator under study and, indeed, the equation would almost definitely be intractable.

As mentioned, if these systems of differential equations are solvable then a complete analysis of ΣΔM becomes possible. However an analytic solution is far more complex than immediately apparent, and is discussed later in this and the following chapter. The equations are solvable numerically by using the Runge Kutta method for example, and this approach is first considered.

## 4.3 RUNGE KUTTA SOLUTION OF DIFFERENTIAL EQUATIONS REPRESENTING ΣΔM

The Runge Kutta (RK) method of numeric integration solves a set of differential equations one step at a time, feeding the results back into the equations to generate the next set of answers. This means that, for an initial set of conditions, the RK method can be used to produce a time series representing each of the components in the system of equations. The program used to solve these equations was a fourth order fixed time step RK process [73]. Fourth order in this context refers to the number of times the derivative is calculated at each step of the RK method – once at the start point, twice at trial mid-points, and once at a trial end point – in order to calculate the next iteration. Although an adaptive time step could give more accurate results, they would ultimately be on an irregular time scale which causes problems in analysis; consequently it was decided to stay with the fixed time step.

The waveforms acquired by the Runge Kutta method for a first order sigma delta modulator with a sinusoidal input are shown in Figure 4.4. Figure 4.4b shows the solution of the numerical integration of equation 4.11 (i.e. the output $x(t)$ of the integrator) with the input

$$u(t) = \sin \omega t \tag{4.19}$$

4.4a

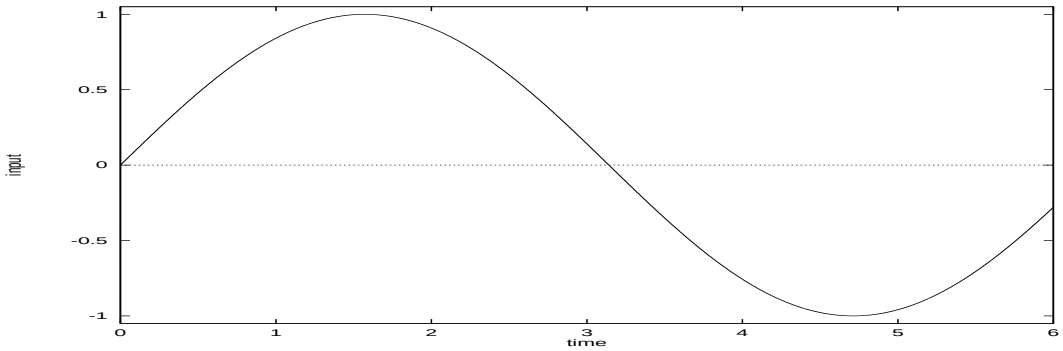


4.4b

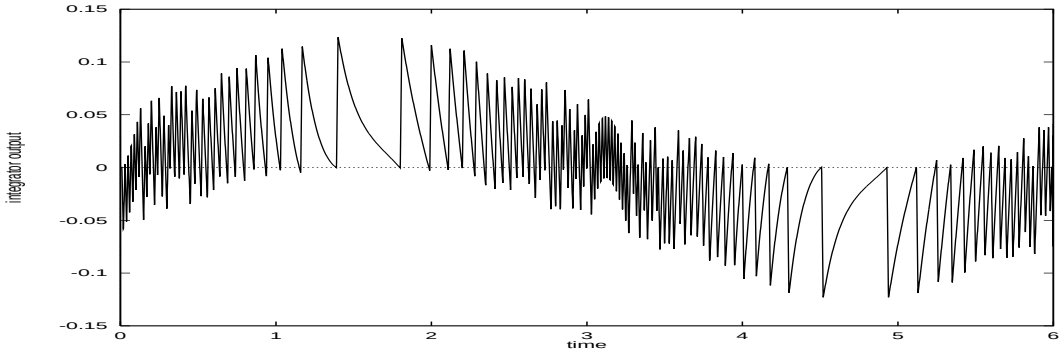


4.4c

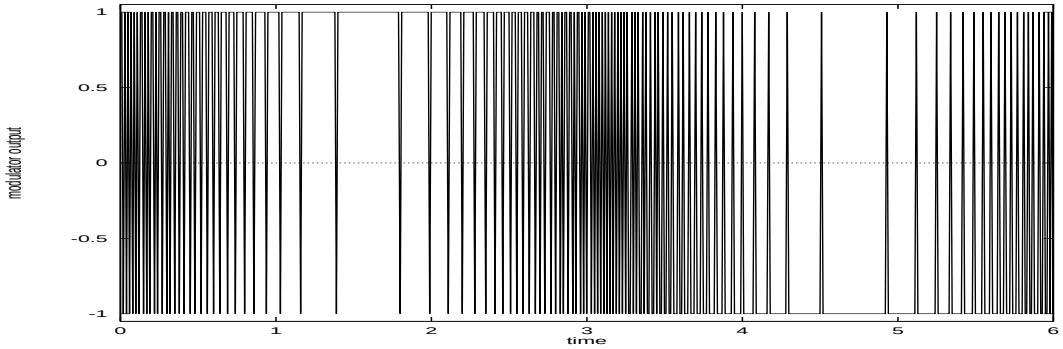


4.4d

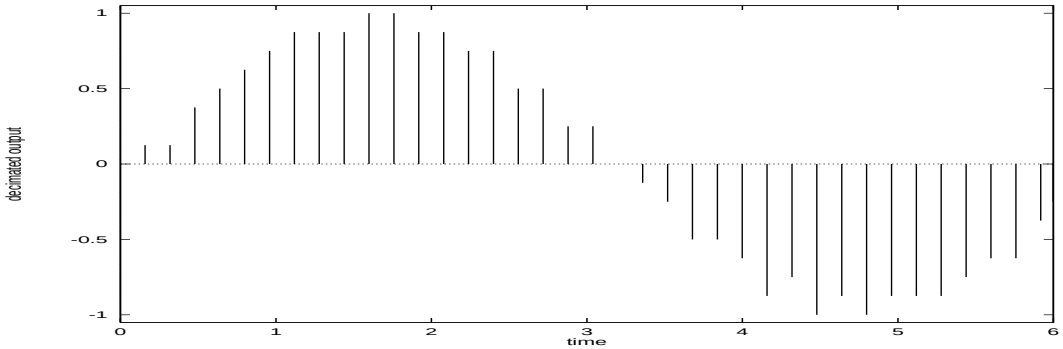


**Figure 4.4**: *Time series of a)* $u(t)$*, b)* $x(t)$*, c)* $y(t)$*, and d) decimated* $y(t)$ *for sinusoidal input to continuous first order sigma delta converter calculated by Runge Kutta method*

(shown in Figure 4.4a). Figure 4.4c shows the output of the quantiser, $y(t)$, calculated from

$$y(t) = M \tanh \frac{px(t-\tau)}{M} \tag{4.20}$$

where $p = 5000$ and $M = 1$, and Figure 4.4d shows this signal after decimation. The feedback coefficient $a$ was set to unity and the integrator leakage $k = 0.1$. If these plots are compared to those generated from the simulation of a conventional sigma delta modulator (Figure 3.5), it can be seen that they are very similar in structure. In particular the plot of the input to the quantiser, $x(t)$, exhibits the distinctive frequency change as the amplitude of the signal input changes – i.e. the frequency of the oscillation decreases as the input amplitude nears the quantiser (or hyperbolic tangent) limits, and increases as the input nears zero. The low-pass filtered output shows that the original signal can be retrieved in the same way as in the conventional device. These two factors imply that the differential equation modelling the continuous device is a sufficiently reasonable representation of first order sigma delta modulation to warrant further analysis. This claim will be corroborated later in this chapter and in the next.

Figure 4.5 shows the results for a second order sigma delta converter with a sinusoidal input. Again the outputs were calculated by using the fourth order Runge Kutta technique to numerically solve the differential equations 4.14 and 4.15 which have been constructed to represent the second order modulator.

From the results achieved with the Runge Kutta process presented here it would seem that the modulators can be represented as continuous systems and that a set of differential equations can be constructed to accurately represent them. Thus a basis for further analysis of $\Sigma\Delta$M has been achieved.

## 4.4 FIRST ORDER SIGMA DELTA MODULATOR WITH CONSTANT INPUT

This section is concerned with a detailed study of the differential equation (4.11) representing a first order sigma delta modulator with a constant input $\lambda$. This is first considered for a Runge Kutta numerical integration of the equation and the results compared with those achieved from a straight simulation of conventional sigma delta modulation. An analytical approach to solving the differential equation with a constant input is then presented and shown to predict the results achieved from the numerical methods.

### 4.4.1 Numerical Approach

Consider a sigma delta modulator with a constant input. It has been noted [58] that a constant input is a natural mode of operation to investigate in sigma delta converters due to the over-sampling nature of these devices, and indeed it makes the subsequent analysis simpler. We

4.5a

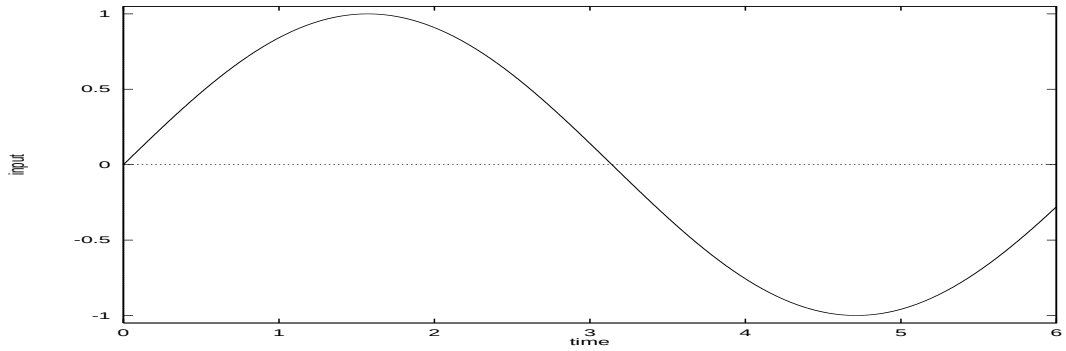


4.5b

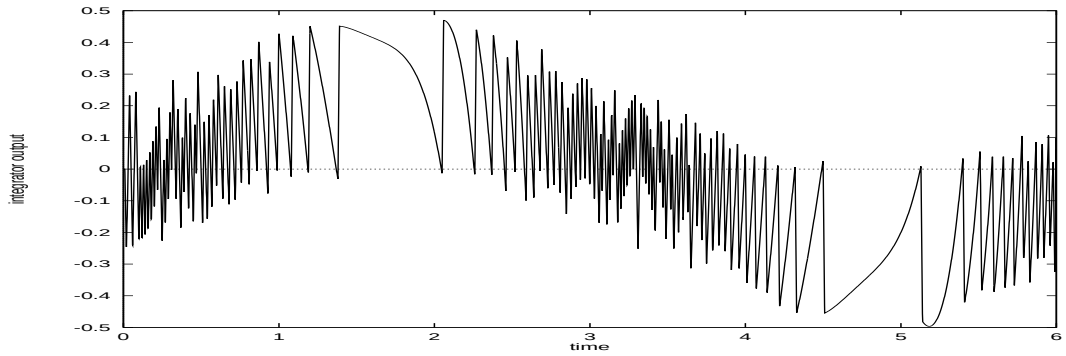


4.5c

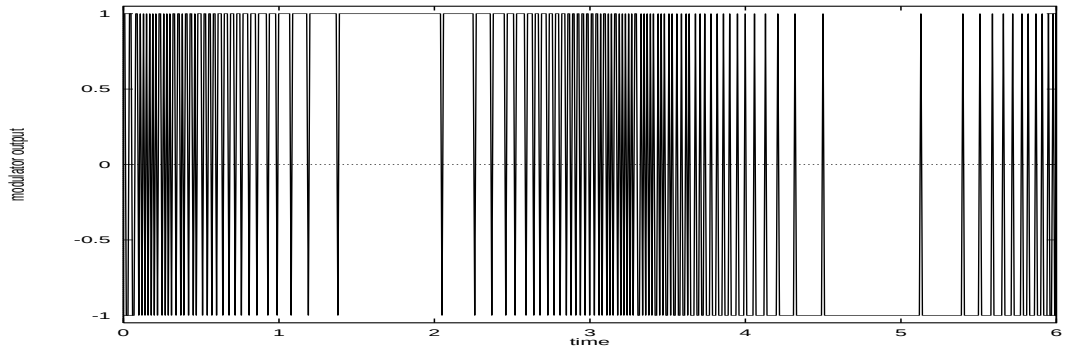


4.5d

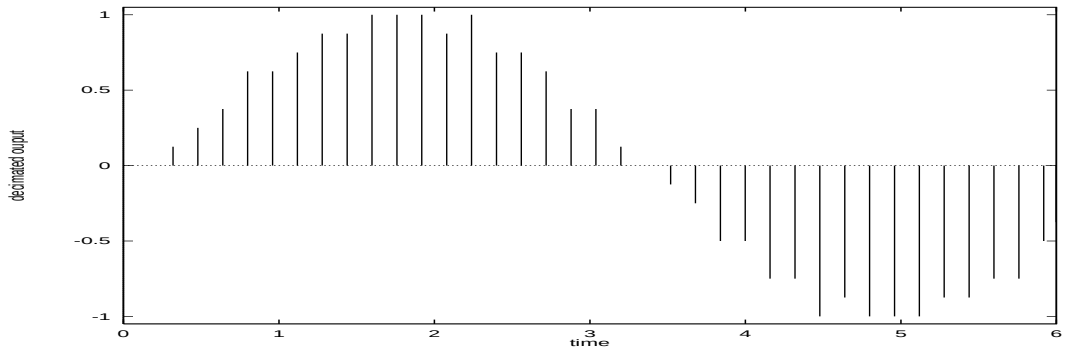


**Figure 4.5**: *Time series of a)* $u(t)$*, b)* $x(t)$*, c)* $y(t)$*, and d) decimated* $y(t)$ *for sinusoidal input to continuous second order sigma delta converter calculated by Runge Kutta method*

know that the output of the modulator, although a series of $+1$s and $-1$s, will average to the value of the input over a sufficiently long time period. For example, if the input is equal to $+0.5$, the output will be of the form $+1, +1, +1, -1$; which averages to $0.5$. This means that the input to the one-bit quantiser must be positive three times as often as it is negative. The initial question then is, does this happen for the Runge Kutta solution?

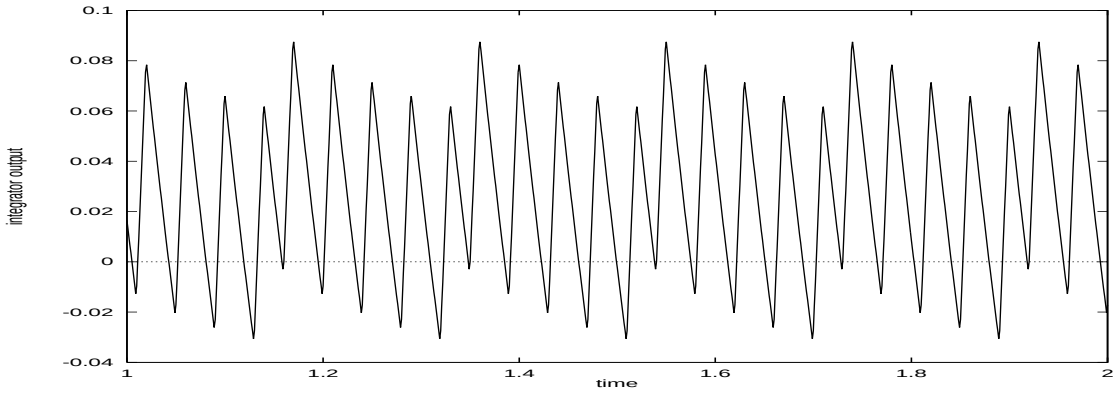


**Figure 4.6**: *Time series of* $x(t)$ *for constant input of* $0.5$ *to continuous first order sigma delta converter calculated by Runge Kutta method*

The plot in Figure 4.6 implies that this is the case, and an average of the quantised value of this waveform comes to $0.5$, although it should be noted that the small number of points plotted on each arm of the waveform causes the amplitude at each changeover to appear to vary depending on where the point happens to fall.

Also of concern is what happens if the input is over-driven with an input greater than one. In the straightforward simulation the output of the integrator becomes unstable, unless there is a feedback factor across the integrator (i.e. a leaky integrator). This isn't really surprising when you consider the circuit diagram (Figure 3.4) – for a positive input, the output will be $+1$ and the integrator will just keep integrating a d.c. value equal to the difference between the input and $+1$ (the output) – hence it will continually increase. Incorporating integrator leakage prevents this from happening, with the integrator output settling to a d.c. value.

This integrator feedback is equivalent to $kx(t)$ in the continuous equation and again the Runge Kutta solution matches the discrete simulation well. For an over-driven input (i.e. $u(t) > aM$ in Equation 4.11) with $k$ equal to zero, $x(t)$ is unstable, and with $k$ greater than zero, $x(t)$ tends toward a positive d.c. value, so the output after quantisation ($\tanh(px(t))$) stays at $+1$. Note that much work in the field would label both of these results (i.e. with and without integrator leakage) as instability; this will be greatly expanded upon in the following chapter. Again the Runge Kutta solution of the differential equation representing first order modulation gives the same results as the direct simulation.

### 4.4.2 Analytical Approach

There now follows some analysis of the equation for a first order modulator. Our approach is to first consider a general solution of the differential equation we have formulated to represent first order modulation, and then to consider the stability of the equation in a fixed point sense. The equation for a first order sigma delta modulator, incorporating feedback factor $a$ and integrator leakage $k$ is

$$\frac{dx}{dt} = \lambda - kx - aM \tanh \frac{px(t-\tau)}{M}. \tag{4.21}$$

We set the input $\lambda$ equal to a constant. Also assume that an ideal quantiser is used, so the hyperbolic tangent will only ever equal $\pm 1$. Both these steps simplify the analysis; the reasons for considering a constant input only at this stage have already been stated and the assumption of an ideal quantiser facilitates the general solution of the equation.

The equation now becomes

$$\frac{dx}{dt} = \lambda - kx \mp a. \tag{4.22}$$

This equation has the general solution

$$x = \frac{\lambda \mp a}{k} + \frac{A}{k} e^{-kt}. \tag{4.23}$$

where A is some constant. It can be seen that the analysis predicts an exponential waveform. The expression can be thought of in two parts; the first part $(\lambda \mp a)/k)$ is the value to which the exponential curve is heading, the second part $(A/k)e^{-kt}$ shows the rate at which the exponential is changing. The coefficient marked $\mp$ will change sign as the waveform crosses the zero axis, causing the direction of the exponential to change. This would seem to imply that the waveform will never leave the zero axis, since as soon as it crosses, its direction changes and it recrosses repeatedly. However remember that we have disregarded the delay in the hyperbolic tangent, which represents a very real delay in the circuit. This delay will cause the direction of the waveform to change a fixed time after it has crossed the zero axis. Hence the waveform of Figure 4.7 which shows the two exponential curves generated from the Runge Kutta solution of the equation for first order modulation.

Furthermore it is clear that for $\lambda > a$, the first part of the expression is always positive so switching of the circuit can not occur. This will be expanded upon greatly in the following chapter.

The period of this waveform may also be of interest. In particular, it is clear from the diagram of Figure 4.8 that the period is greater than twice the delay $\tau$. The delay $\tau$ defines the time

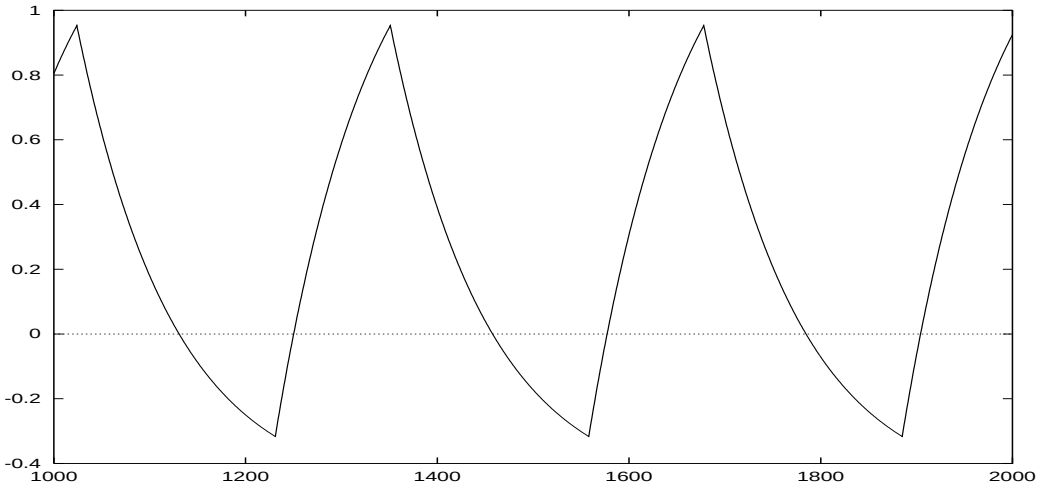


**Figure 4.7**: *Plot of* x(t)

after x(t) has crossed the zero axis, that the sign of the expression changes, and x(t) changes direction. Clearly there is some additional time in the period due to x(t) having first to reach the zero crossover point.

It will be noted at this point that we are assuming the waveform to be periodic. This is largely due to the obviously periodic nature of the empirical evidence, i.e. the numerical solution to the equation with a d.c. input appears to be periodic, and follows a repeated path in phase space. A full algebraic proof of periodicity is complicated due to the delayed nature of the equation and would involve a phase space reconstruction of the equation together with various dynamical considerations. A full proof that a generic version of our equation is indeed periodic (with the constant input) can be found in [74], whereby a global attractor of the equation is constructed and shown to be both continuous and periodic.

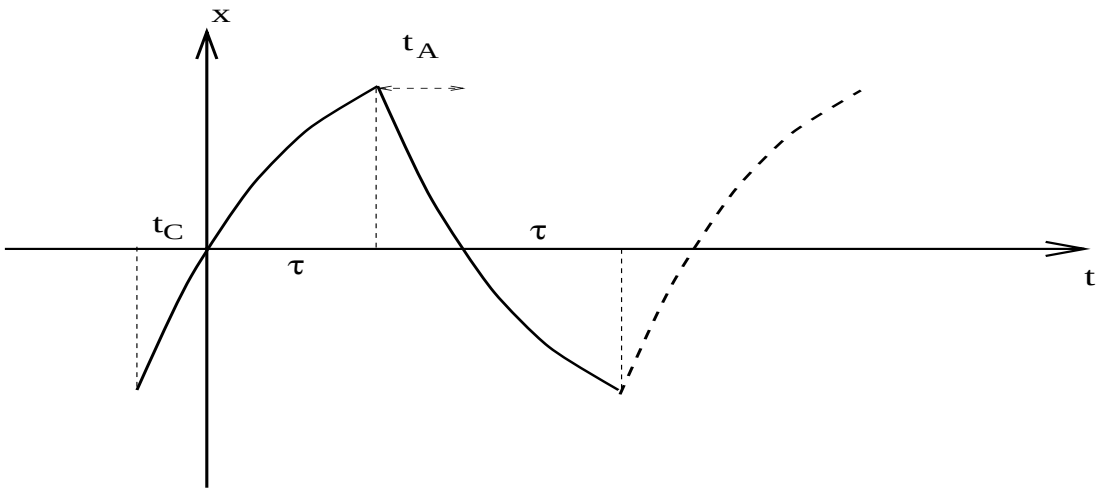


**Figure 4.8**: *Period of* x(t)

There now follows an analysis of the equation representing first order sigma delta modulation involving the construction of a limit cycle in phase space and the use of that limit cycle to

show that the output of the equation, after quantisation and decimation, tracks the input as would be expected in a sigma delta modulator. We begin by rewriting our equation with a set of unscaled parameters, marked with a prime($'$), and using an ideal quantisation function.

$$\frac{dx'}{dt'} = \lambda - kx' - a\mathrm{Sgn}[x'(t' - \tau')] \tag{4.24}$$

It is useful to rescale this equation in order to minimise the number of parameters, so we divide through by $a$ and write $x = \frac{k}{a}x'$

$$\frac{1}{k}\frac{dx}{dt'} = \frac{\lambda}{a} - x - \mathrm{Sgn}[x'(t' - \tau')] \tag{4.25}$$

Write

$$t = kt' \Rightarrow \frac{d}{dt} = \frac{1}{k}\frac{d}{dt'} \tag{4.26}$$

and think of $x$ as a function of $t$. That is,

$$x'(t') = \frac{a}{k}x(kt') \equiv \frac{a}{k}x(t) \tag{4.27}$$

In particular

$$\mathrm{Sgn}[x'(t' - \tau')] = \mathrm{Sgn}[\frac{a}{k}x(k(t' - \tau'))] = \mathrm{Sgn}[x(t - \tau)] \tag{4.28}$$

where $\tau = k\tau'$ and we use the fact that $\frac{a}{k} > 0$.

Introducing $\Lambda = \frac{\lambda}{a}$, we get the rescaled equation

$$\frac{dx}{dt} = \Lambda - x - \mathrm{Sgn}[x(t - \tau)] \tag{4.29}$$

This is equivalent to having two different differential equations

$$\frac{dx}{dt} = \Lambda - 1 - x \qquad x(t - \tau) > 0 \tag{4.30}$$

$$\frac{dx}{dt} = \Lambda + 1 - x \qquad x(t - \tau) < 0 \tag{4.31}$$

with the subtlety that we swap from one to the other when the delayed solution changes sign.

We can solve 4.30 and 4.31 to get two explicit flows:

$$\Phi_t^+ x = [\Lambda - 1] + (x - [\Lambda - 1])e^{-t} \tag{4.32}$$

$$\Phi_t^- x = [\Lambda + 1] + (x - [\Lambda + 1])e^{-t} \tag{4.33}$$

interpreting $\Phi_t^+$ as an operator which evolves $x$ under the influence of 4.30 for a time $t$; i.e. $\Phi_t^+ \equiv x(t)$. Similarly $\Phi_t^-$ is an operator which evolves $x$ under the influence of 4.31 for a time $t$.

Provided that we account for the times that we swap from $\Phi^+$ to $\Phi^-$ we now have an explicit solution.

In fact $\Phi^+$ (and similarly $\Phi^-$) is a one-parameter continuous group of diffeomorphisms of $\Re$. In particular, we have

$$\Phi_{t_1}^+ \Phi_{t_2}^+ = \Phi_{t_1+t_2}^+ \tag{4.34}$$

i.e. propagating for $t_2$ and then $t_1$ is the same as propagating for $t_1 + t_2$, and

$$\Phi_t^+ \Phi_{-t}^+ = \Phi_0^+ \tag{4.35}$$

so every map $\Phi_t^+$ has an inverse $\Phi_{-t}^+$ since $\Phi_0^+ \equiv$ identity, i.e. $\Phi_0^+ x = x$.

Proof:

$$\Phi_{t_1}^+ \Phi_{t_2}^+ x = \Phi_{t_1}^+ ([\Lambda - 1] + (x - [\Lambda - 1])e^{-t_2}) \tag{4.36}$$

$$= [\Lambda - 1] + (([\Lambda - 1] + (x - [\lambda - 1])e^{-t_2}) - [\Lambda - 1])e^{-t_1} \tag{4.37}$$

$$= [\Lambda - 1] + (x - [\Lambda - 1])e^{-(t_1+t_2)} \equiv \Phi_{t_1+t_2}^+ x \tag{4.38}$$

and, in particular

$$\Phi_t^+ \Phi_{-t}^+ x = [\Lambda - 1] + (x - [\Lambda - 1])e^{-(t-t)} = x \tag{4.39}$$

Clearly these properties hold for $\Phi_t^-$ also. We can prove the existence of a limit cycle solution of 4.29 using these simple properties of $\Phi_t^+$ and $\Phi_t^-$ together with the additional facts that:

$$\lim_{t\to\infty} \Phi_t^+ x = \Lambda - 1 < 0 \tag{4.40}$$

$$\lim_{t\to\infty} \Phi_t^- x = \Lambda + 1 > 0 \tag{4.41}$$

which mean that in the solution of 4.29 these limits can not be reached (because $x(t-\tau)$ will change sign first).

These are properties that hold for more general systems than 4.29, and we shall come back to this later.

Our proof of the existence of a limit cycle will work in a plane spanned by the variables $x(t)$ and $x(t-\tau)$ – i.e. a delay space with just two components. To avoid having to deal with some huge function space (where the solutions to 4.29 actually live) we shall choose special initial data.

We need to specify initial data on the interval $[-\tau, 0]$, i.e. our initial conditions for 4.29 will be a function on $[-\tau, 0]$ which we might write as $\{x(t) \mid t \in [-\tau, 0]\}$.

Our special initial functions can have one of two forms:

$$\{\Phi^+_{-\nu} x(0) \mid 0 \leq \nu \leq \tau \; ; \; x(0) > 0\} \tag{4.42}$$

$$\{\Phi^-_{-\nu} x(0) \mid 0 \leq \nu \leq \tau \; ; \; x(0) < 0\} \tag{4.43}$$

The easiest way to view this problem is with reference to Figure 4.9.

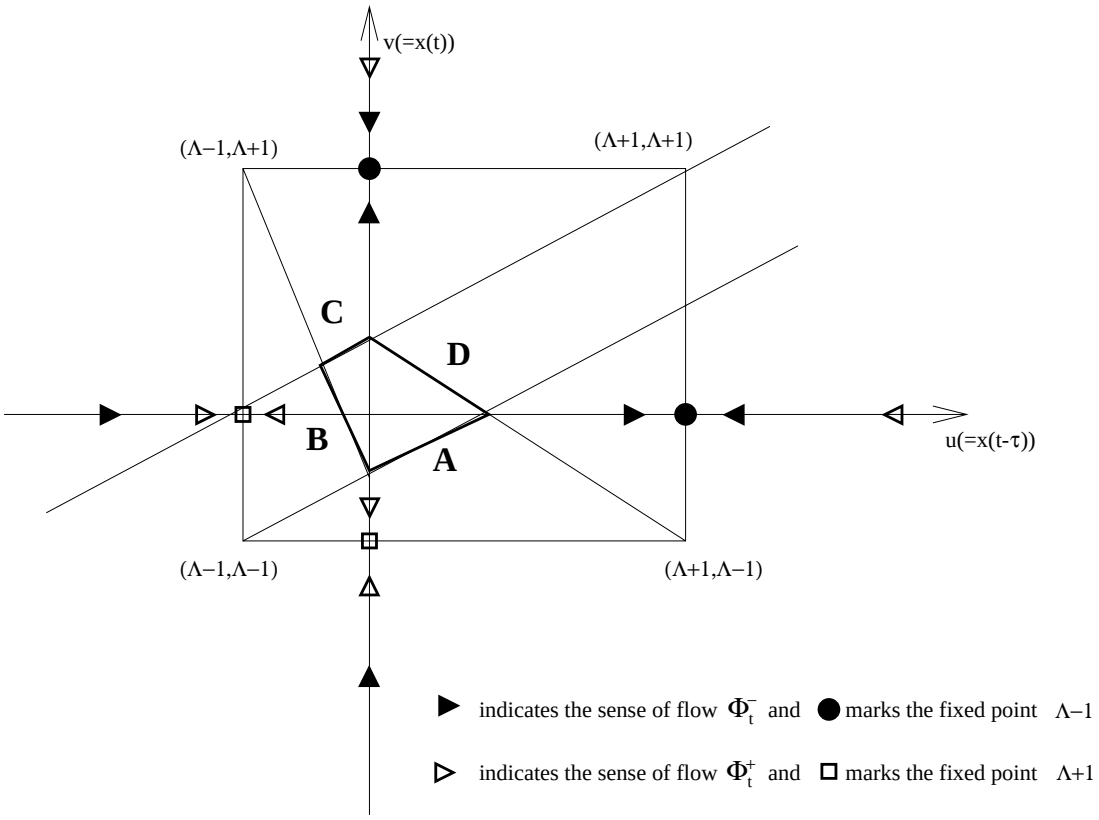


**Figure 4.9**: *Limit cycle of first order equation.*

Following simultaneously the behaviour of $x(t)$ and $x(t-\tau)$ gives us an evolving point in the plane. We shall call this point

$$\begin{pmatrix} u \\ v \end{pmatrix} \equiv \begin{pmatrix} x(t-\tau) \\ x(t) \end{pmatrix} \tag{4.44}$$

There are four solutions:

- A: $x(t)$ and $x(t-\tau)$ are both evolving under the action of $\Phi^+_t$.
- B: $x(t)$ evolves under $\Phi^-_t$ while $x(t-\tau)$ evolves under $\Phi^+_t$
- C: $x(t)$ and $x(t-\tau)$ are both evolving under the action of $\Phi^-_t$.

- D: $x(t)$ evolves under $\Phi_t^+$ while $x(t-\tau)$ evolves under $\Phi_t^-$

These are marked on the diagram as straight line segments. The fact that these are *straight* lines is a peculiarity of 4.29 as will now be shown. The existence of the limit cycles doesn't depend on this property, however.

We now consider the trajectories in the $(u,v)$ plane for each of the four regions. Starting with region A:

$$u(t) = \Phi^+_{t-\tau}x \qquad\qquad v(t) = \Phi^+_t x \tag{4.45}$$

for some initial $x$.

$$\Rightarrow\ u = \Phi^+_{-\tau}v \tag{4.46}$$

a time independent functional relationship between $u$ and $v$ which does not depend upon the initial condition of $x$.

Explicitly:

$$u = [\Lambda - 1] + (v - [\Lambda - 1])e^{\tau} \tag{4.47}$$

$$\Rightarrow\ v - [\Lambda - 1] = e^{-\tau}(u - [\Lambda - 1]) \tag{4.48}$$

i.e. a straight line through $([\Lambda - 1], [\Lambda - 1])$ with positive gradient $e^{-\tau}$.

Similarly we have for region C:

$$u(t) = \Phi^-_{t-\tau}x \qquad\qquad v(t) = \Phi^-_t x \tag{4.49}$$

for some initial $x$.

$$\Rightarrow\ u = \Phi^-_{-\tau}v \tag{4.50}$$

and the same remarks apply as for A.

$$\Rightarrow\ v - [\Lambda + 1] = e^{-\tau}(u - [\Lambda + 1]) \tag{4.51}$$

i.e. a straight line, parallel to the one for A, but passing through $([\Lambda + 1], [\Lambda + 1])$. Note the initial data lies on either of these two lines with $v(0) > 0$, $v(0) < 0$ respectively. To find the line segments B and D we need to impose an extra condition because these regions correspond

to $x(t)$ and $x(t-\tau)$ evolving under different flows and we have freedom to specify when the changeover took place. To obtain our limit cycle we would like line B to intersect line A on the line $u = 0$ (the $v$-axis) because $u = 0 \Leftrightarrow x(t-\tau) = 0$ is the point at which the flow for $x(t)$ swaps from $\Phi^+$ to $\Phi^-$. The argument for D and C is completely analogous.

From equation 4.48 the A line hits the $v$-axis at

$$v = [\Lambda - 1](1 - e^{-\tau}) \tag{4.52}$$

In region B, doing things explicitly:

$$u(t) = \Phi^+_{t-\tau} x \qquad\qquad v(t) = \Phi^-_t x \tag{4.53}$$

$$u = [\Lambda - 1] + (x - [\Lambda - 1])e^{-(t-\tau)} \tag{4.54}$$

$$v = [\Lambda + 1] + (x - [\Lambda + 1])e^{-t} \tag{4.55}$$

$$\Rightarrow \ (v - [\Lambda + 1]) = \left(\frac{x - [\Lambda + 1]}{x - [\Lambda - 1]}\right) e^{-\tau}(u - [\Lambda - 1]) \tag{4.56}$$

This is a line of slope $m = \left(\frac{x - [\Lambda + 1]}{x - [\Lambda - 1]}\right) e^{-\tau}$ which passes through the point $([\Lambda - 1], [\Lambda + 1])$. We are free to choose $x$, and hence $m$ (since the mapping $\frac{x - [\Lambda + 1]}{x - [\Lambda - 1]} \to m$ is one to one and hence invertible for all $(x, m)$ where $x$ is finite and $m \neq 1$), so we choose $m$ such that the line passes through $(0, [\Lambda - 1](1 - e^{-\tau}))$ also. That is, choose $m$ such that

$$m = \frac{[\Lambda - 1](1 - e^{-\tau}) - [\Lambda + 1]}{0 - [\Lambda - 1]} \tag{4.57}$$

$$\Rightarrow \ m = \frac{\Lambda + 1}{\Lambda - 1} - (1 - e^{-\tau}) \tag{4.58}$$

So, in region B the path is a straight line:

$$v - [\Lambda + 1] = \left(\frac{\Lambda + 1}{\Lambda - 1} - (1 - e^{-\tau})\right)(u - [\Lambda - 1]) \tag{4.59}$$

In region D things work out to be pretty much the same:

$$u(t) = \Phi^-_{t-\tau} x \qquad\qquad v(t) = \Phi^+_t x \tag{4.60}$$

$$u = [\Lambda + 1] + (x - [\Lambda + 1])e^{-(t-\tau)} \tag{4.61}$$

$$v = [\Lambda - 1] + (x - [\Lambda - 1])e^{-t} \tag{4.62}$$

and we need the line to go through $(0, [\Lambda + 1](1 - e^{-\tau}))$. So the result follows from 4.59 by exchanging $[\Lambda + 1]$ and $[\Lambda - 1]$:

$$v - [\Lambda - 1] = \left(\frac{\Lambda - 1}{\Lambda + 1} - (1 - e^{-\tau})\right)(u - [\Lambda + 1]) \tag{4.63}$$

This is a straight line passing through $(\Lambda+1, \Lambda-1)$ and $(0, [\Lambda+1](1-e^{-\tau}))$; it is not parallel to line B.

Since line B must intersect line C, and D must intersect A, and, by construction, A and B intersect as do C and D, we have found the closed cycle shown in the figure.

We can follow this through without making use of the explicit formulae. We again divide the dynamics into four regions according to the definitions already given.

- A: Assume at $t = 0$ we begin at a point $x_0$ (to be determined) which will be the point of crossover from region D to region A. Assume that we spend $t_A$ in region A, so

$$0 \le t \le t_A \qquad \begin{pmatrix} u \\ v \end{pmatrix} = \begin{pmatrix} \Phi^+_{t-\tau} x_0 \\ \Phi^+_t x_0 \end{pmatrix} \tag{4.64}$$

  $t_A$ is the time at which $u$ goes through zero, so

$$\begin{pmatrix} u(t_A) \\ v(t_A) \end{pmatrix} = \begin{pmatrix} \Phi^+_{t_\Lambda - \tau} x_0 \\ \Phi^+_{t_\Lambda} x_0 \end{pmatrix} = \begin{pmatrix} 0 \\ \Phi^+_{t_\Lambda} x_0 \end{pmatrix} \tag{4.65}$$

  but

$$\Phi^+_{t_\Lambda - \tau} x_0 = 0 \;\Rightarrow\; \Phi^+_{t_\Lambda} x_0 = \Phi^+_\tau 0 \tag{4.66}$$

  so

$$\begin{pmatrix} u(t_A) \\ v(t_A) \end{pmatrix} = \begin{pmatrix} 0 \\ \Phi^+_\tau 0 \end{pmatrix} \tag{4.67}$$

- B: If $x(t-\tau)$ changes sign at $t = t_A$, there will be a delay of $\tau$ before the evolution of $x(t-\tau)$ also is according to $\Phi^-_t$. For this interval the flow is in region B.

$$t_A \le t \le t_A + \tau \qquad \begin{pmatrix} u \\ v \end{pmatrix} = \begin{pmatrix} \Phi^+_{t-t_\Lambda} 0 \\ \Phi^-_{t-t_\Lambda} \Phi^+_\tau 0 \end{pmatrix} \tag{4.68}$$

  and

$$\begin{pmatrix} u(t_A+\tau) \\ v(t_A+\tau) \end{pmatrix} = \begin{pmatrix} \Phi^+_\tau 0 \\ \Phi^-_\tau \Phi^+_\tau 0 \end{pmatrix} \tag{4.69}$$

  is the end point.

- C: Now both components evolve under $\Phi^-_t$

$$t_A + \tau \le t \le t_C + t_A + \tau \qquad \begin{pmatrix} u \\ v \end{pmatrix} = \begin{pmatrix} \Phi^-_{t-t_\Lambda-\tau} \Phi^+_\tau 0 \\ \Phi^-_{t-t_\Lambda-\tau} \Phi^-_\tau \Phi^+_\tau 0 \end{pmatrix} \tag{4.70}$$

$$\Rightarrow \qquad \begin{pmatrix} u \\ v \end{pmatrix} = \begin{pmatrix} \Phi^-_{t-t_\Lambda-\tau} \Phi^+_\tau 0 \\ \Phi^-_{t-t_\Lambda} \Phi^+_\tau 0 \end{pmatrix} \tag{4.71}$$

The time $t_C$ is defined to be the time at which $u$ changes sign:

$$\Phi^-_{t_C+t_A+\tau-t_A-\tau}\Phi^+_\tau 0 = 0 \tag{4.72}$$

$$\Rightarrow\ \Phi^-_{t_C}\Phi^+_\tau 0 = 0 \tag{4.73}$$

So the end point of C is

$$\begin{pmatrix} u(t_C+t_A+\tau) \\ v(t_C+t_A+\tau) \end{pmatrix} = \begin{pmatrix} 0 \\ \Phi^-_{t_C+t_A+\tau-t_A}\Phi^+_\tau 0 \end{pmatrix} \tag{4.74}$$

$$= \begin{pmatrix} 0 \\ \Phi^-_{t_C+\tau}\Phi^+_\tau 0 \end{pmatrix} \tag{4.75}$$

but the condition given in 4.73 means that

$$\Phi^-_{t_C+\tau}\Phi^+_\tau 0 = \Phi^-_\tau 0 \tag{4.76}$$

so

$$\begin{pmatrix} u(t_C+t_A+\tau) \\ v(t_C+t_A+\tau) \end{pmatrix} = \begin{pmatrix} 0 \\ \Phi^-_\tau 0 \end{pmatrix} \tag{4.77}$$

as should be expected since $v$ is $\tau$ ahead of $u$ and we are in the region where everything propogates under $\Phi^-_t$.

- D: As before in region B there is a delay between $x(t-\tau)$ changing sign and $x(t-\tau)$ actually being determined by the new flow ($\Phi^+_t$ in this case). So

$$t_C+t_A+\tau \le t \le t_C+t_A+2\tau \qquad \begin{pmatrix} u \\ v \end{pmatrix} = \begin{pmatrix} \Phi^-_{t-(t_C+t_A+\tau)}0 \\ \Phi^+_{t-(t_C+t_A+\tau)}\Phi^-_\tau 0 \end{pmatrix} \tag{4.78}$$

so

$$\begin{pmatrix} u(t_C+t_A+2\tau) \\ v(t_C+t_A+2\tau) \end{pmatrix} = \begin{pmatrix} \Phi^-_\tau 0 \\ \Phi^+_\tau\Phi^-_\tau 0 \end{pmatrix} \tag{4.79}$$

Now we must ask the question, can we find $x_0$ such that $\begin{pmatrix} u(0) \\ v(0) \end{pmatrix} = \begin{pmatrix} u(t_C+t_A+2\tau) \\ v(t_C+t_A+2\tau) \end{pmatrix}$ ?

The condition is:

$$\begin{pmatrix} \Phi^+_{-\tau}x_0 \\ x_0 \end{pmatrix} = \begin{pmatrix} \Phi^-_\tau 0 \\ \Phi^+_\tau\Phi^-_\tau 0 \end{pmatrix} \tag{4.80}$$

Clearly these two conditions are actually the same, so we need $x_0$ such that

$$x_0 = \Phi^+_\tau\Phi^-_\tau 0 \tag{4.81}$$

We have conditions 4.66 and 4.73 which define $t_A$ and $t_C$:

From 4.66

$$\Phi^+_{t_A} x_0 = \Phi^+_\tau 0 \tag{4.82}$$

$$\Phi^+_{t_A+\tau}\Phi^-_\tau 0 = \Phi^+_\tau 0 \tag{4.83}$$

$$\Phi^+_{t_A}\Phi^-_\tau 0 = 0 \tag{4.84}$$

and from 4.73

$$\Phi^-_{t_C}\Phi^+_\tau 0 = 0 \tag{4.85}$$

We can find $t_A$ and $t_C$ using the explicit form of the flows $\Phi^+_t$ and $\Phi^-_t$:

$$\Phi^+_{t_A}([\Lambda+1](1-e^{-\tau})) = 0 \tag{4.86}$$

$$[\Lambda-1] + ([\Lambda+1](1-e^{-\tau}) - [\Lambda-1])e^{-t_A} = 0 \tag{4.87}$$

$$e^{-t_A} = \frac{-[\Lambda-1]}{[\Lambda+1](1-e^{-\tau}) - [\Lambda-1]} \tag{4.88}$$

$$t_A = \log\left(1 - \frac{\Lambda+1}{\Lambda-1}(1-e^{-\tau})\right) \tag{4.89}$$

And

$$\Phi^-_{t_C}([\Lambda-1](1-e^{-\tau})) = 0 \tag{4.90}$$

$$[\Lambda+1] + ([\Lambda-1](1-e^{-\tau}) - [\Lambda+1])e^{-t_C} = 0 \tag{4.91}$$

$$e^{-t_C} = \frac{-[\Lambda+1]}{[\Lambda-1](1-e^{-\tau}) - [\Lambda+1]} \tag{4.92}$$

$$t_C = \log\left(1 - \frac{\Lambda-1}{\Lambda+1}(1-e^{-\tau})\right) \tag{4.93}$$

From Figure 4.8, the approximate output of the averaging filter (i.e. after quantisation and decimation) is given by

$$\frac{t_A + \tau - (t_C + \tau)}{t_A + t_C + 2\tau} \tag{4.94}$$

substituting for the values of $t_A$ and $t_C$ calculated above gives

$$\text{out} \approx \frac{\log\left(\frac{1+\Gamma(1-e^{-\tau})}{1+\Gamma^{-1}(1-e^{-\tau})}\right)}{2\tau + \log((1+\Gamma(1-e^{-\tau}))(1+\Gamma^{-1}(1-e^{-\tau})))} \tag{4.95}$$

where $\Gamma = \frac{1+\Lambda}{1-\Lambda}$.

Figure 4.10 shows the output as a function of $\Lambda$, the scaled d.c. input, for a number of values of $\tau$. Clearly, as $\tau \to 0$ the function is nearly linear with unity slope. For larger $\tau$ there is still

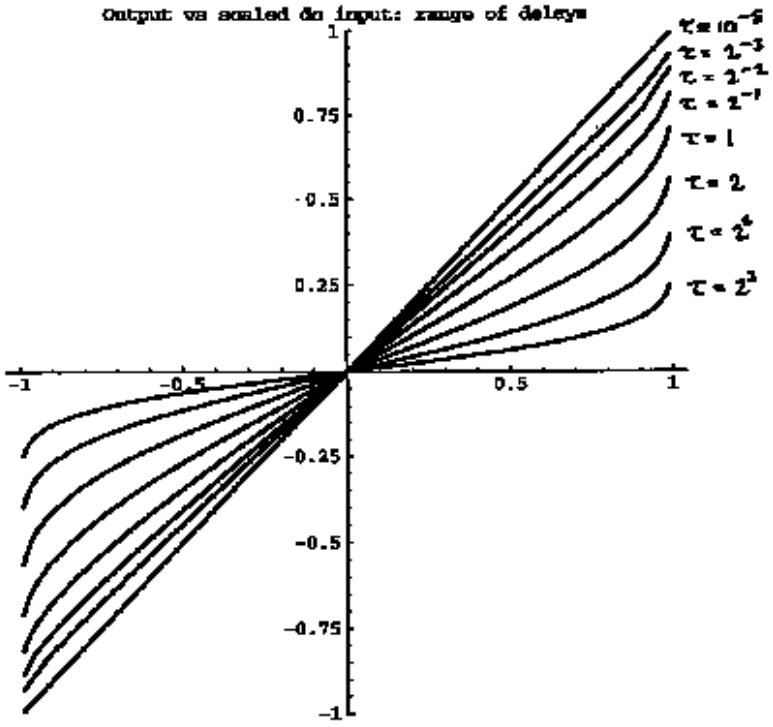


**Figure 4.10**: *Output vs scaled d.c. input.*

a largish linear region, but the gain is less than unity.

We can investigate these two limits. First, as $\tau \to \infty$

$$\lim_{\tau\to\infty} 1 + \Gamma(1 - e^{-\tau}) = 1 + \Gamma = \frac{2}{1-\Lambda} \tag{4.96}$$

$$\lim_{\tau\to\infty} 1 + \Gamma^{-1}(1 - e^{-\tau}) = 1 + \Gamma^{-1} = \frac{2}{1+\Lambda} \tag{4.97}$$

So, as $\tau \to \infty$

$$\text{out} \to \frac{\log\left(\frac{1-\Lambda}{1+\Lambda}\right)}{2\tau + \log\left(\frac{4}{1-\Lambda^2}\right)} \tag{4.98}$$

So, if $\Lambda \neq \pm 1$

$$\text{out} \to \frac{1}{2\tau}\log\left(\frac{1-\Lambda}{1+\Lambda}\right) \to 0 \tag{4.99}$$

If we allow $|\Lambda| \to 1$ first

$$\text{out} \to \frac{\log[1-\Lambda] - \log[1+\Lambda]}{\log[1-\Lambda] + \log[1+\Lambda]} \to \text{Sgn}\Lambda \tag{4.100}$$

So, as $\tau \to \infty$ the output becomes rather singular, tending to zero everywhere except $\Lambda = \pm 1$.

In the limit $\tau \to 0$ on the other hand,

$$\lim_{\tau \to 0} 1 + \Gamma(1 - e^{-\tau}) = 1 + \Gamma\tau + 0(\tau^2) \tag{4.101}$$

$$\lim_{\tau \to 0} 1 + \Gamma^{-1}(1 - e^{-\tau}) = 1 + \Gamma^{-1}\tau + 0(\tau^2) \tag{4.102}$$

So

$$\frac{1 + \Gamma(1 - e^{-\tau})}{1 + \Gamma^{-1}(1 - e^{-\tau})} \to (1 + \Gamma\tau)(1 - \Gamma^{-1}\tau) + 0(\tau^2) \tag{4.103}$$

assuming that $\Gamma^{-1}\tau \approx \tau$, so $\Lambda$ isn't too close to $\pm 1$.

$$\to 1 + (\Gamma - \Gamma^{-1})\tau + 0(\tau^2) \tag{4.104}$$

$$\log\left(\frac{1 + \Gamma(1 - e^{-\tau})}{1 + \Gamma^{-1}(1 - e^{-\tau})}\right) \to (\Gamma - \Gamma^{-1}\tau + 0(\tau^2) \tag{4.105}$$

and

$$\log((1 + \Gamma(1 - e^{-\tau}))(1 + \Gamma^{-1}(1 - e^{-\tau}))) \to \log((1 + \Gamma\tau)(1 + \Gamma^{-1}\tau)) \tag{4.106}$$

$$\to \log(1 + (\Gamma + \Gamma^{-1})\tau + \ldots) \tag{4.107}$$

$$\to (\Gamma + \Gamma^{-1})\tau \tag{4.108}$$

So

$$\text{out} \to \frac{(\Gamma - \Gamma^{-1})\tau}{2\tau + (\Gamma + \Gamma^{-1})\tau} = \frac{\Gamma - \Gamma^{-1}}{2 + \Gamma + \Gamma^{-1}} \tag{4.109}$$

$$= \frac{\frac{1+\Lambda}{1-\Lambda} - \frac{1-\Lambda}{1+\Lambda}}{2 + \frac{1+\Lambda}{1-\Lambda} + \frac{1-\Lambda}{1+\Lambda}} \tag{4.110}$$

$$\frac{\frac{(1+\Lambda)^2 - (1-\Lambda)^2}{1-\Lambda^2}}{\frac{2(1-\Lambda^2) + (1+\Lambda)^2 + (1-\Lambda)^2}{1-\Lambda^2}} \tag{4.111}$$

$$= \frac{4\Lambda}{2 - 2\Lambda^2 + 2 + 2\Lambda^2} \tag{4.112}$$

So

$$\lim_{\tau \to 0} \text{out} = \Lambda \tag{4.113}$$

i.e. a linear, unit slope (except perhaps under $\Lambda = \pm 1$)l.

This subsection has shown that the differential equation representing first order sigma delta modulation takes a periodic form with a d.c. input, and has shown that the output of that equation, after quantisation and decimation, tracks the input as would be expected for an accurate model of $\Sigma\Delta$M.

### 4.4.3 Fixed Point Analysis

This section details a fixed point analysis study of the differential equation (4.11) that has been constructed to represent first order ΣΔM with a constant input.

It is worth noting that we only search for fixed points in this analysis. This is because the equation under study is a first order differential equation, so limit cycles will not be present and searching for fixed points will be sufficient [75,76]. Further to this, the plots of $x(t)$ (e.g. Figure 4.7) and the general solution of the generating equation given in equation 4.23 suggest that the time series under consideration consists of two separate exponential curves, switching over as the output of the quantiser changes. Each of these curves is, in the absence of a switchover at least, asymptotic to a d.c. value, or a fixed point, by its very nature. Consequently we are justified in only considering a fixed point analysis as an indication of the viability of our equation representing sigma delta modulation.

For a fixed point solution, $x(t)$ is constant – i.e. $x(t) = x(t-\tau)$ and $\frac{dx}{dt} = 0$. Also take $a = M = 1$ for simplicity.

$$0 = \lambda - kx - \tanh px \tag{4.114}$$

$$\lambda - kx = \tanh px \tag{4.115}$$

This equation will always have a solution for a particular set of $\lambda$, $k$ and $p$. That solution can be found graphically – see Figure 4.11, which assumes $\lambda > 1$, $k > 0$. (We will consider $\lambda < -1$ and $-1 < \lambda < 1$ presently).

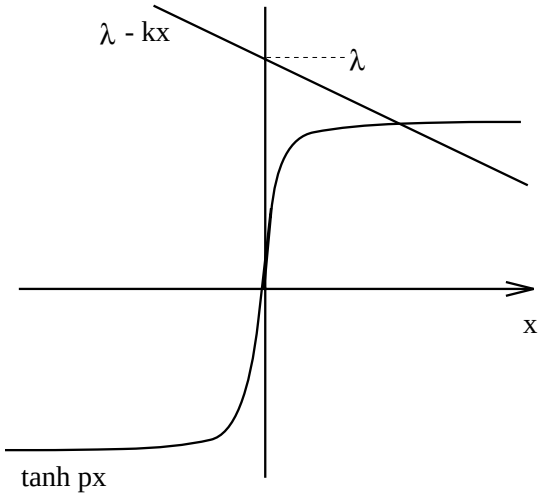


**Figure 4.11**: *Graphical solution for* $\lambda > 1$

In Figure 4.11 $\tanh px \simeq 1$ at the point where the lines intersect, so the solution becomes

$$X = \frac{\lambda - 1}{k}. \tag{4.116}$$

It is reasonable to extend this to all $\lambda > 1$, if $p >> 0$, which is the case since $\tanh px$ must realistically model a quantiser ($p$ is the gradient of the $\tanh$ function at the origin). Equation 4.116 shows a fixed point for the system and the local stability of that fixed point must now be considered.

Consider $\nu$, a small change in $x$.

$$x(t) = X + \nu(t) \tag{4.117}$$

Equation 4.11 becomes

$$\frac{d\nu}{dt} = \lambda - kX - k\nu - \tanh(p\nu(t-\tau) + pX) \tag{4.118}$$

since $X$ is a constant. As $\nu$ is very small in comparison with $X$, we can write

$$\tanh(p\nu(t-\tau) + pX) \simeq p\nu(t-\tau)\,\mathrm{sech}^2\,pX + \tanh pX \tag{4.119}$$

from a Taylor expansion

$$f(a+h) \simeq f(a) + hf'(a) \tag{4.120}$$

so

$$\frac{d\nu}{dt} = \lambda - kX - \tanh pX - k\nu - \nu(t-\tau)p\,\mathrm{sech}^2\,pX \tag{4.121}$$

Substitute for 4.115

$$\frac{d\nu}{dt} = -k\nu - \nu(t-\tau)p\,\mathrm{sech}^2\,pX \tag{4.122}$$

Since we have said that $\tanh pX = 1$, it is also the case that $\mathrm{sech}^2\,pX = 0$. So equation 4.122 becomes

$$\frac{d\nu}{dt} = -k\nu \tag{4.123}$$

i.e. the fixed point is locally stable and the rate of convergence to the fixed point is determined by k. For a rigorous analysis it should be shown that the fixed point is globally stable; however, this is mathematically complex and beyond the scope of this thesis. A paper by Walther [74] considers a generalised version of the delay equation we have constructed to represent first order sigma delta modulation and shows that such analysis does indeed require much time

and mathematical insight. It is hoped that, for the purposes of this thesis, the evidence that the fixed point is locally stable is sufficient to imbue the reader with some confidence in the remainder of the results and analysis presented on this topic.

The above analysis implies that for $\lambda > 1$, $p >> 0$, $x(t)$ has a stable fixed point at $(\lambda - 1)/k)$. In other words, when the input is overdriven ($\lambda > 1$), so long as the slope of the hyperbolic tangent is sufficiently steep ($p >> 0$), the output of the integrator will be a positive d.c. value and so the output of the modulator will be a steady $+1$.

The case for $\lambda < -1$ can be treated similarly to give much the same result – i.e. a negative d.c. output from the integrator for $k > 0$, resulting in a steady quantiser output of $-1$, so we'll move straight on to the case for $-1 < \lambda < 1$.

Again the solution can be written as equation 4.115:

$$\lambda - kx = \tanh px \tag{4.124}$$

Figure 4.12 shows the graphical solution to Equation 4.124 for $-1 < \lambda < 1$.

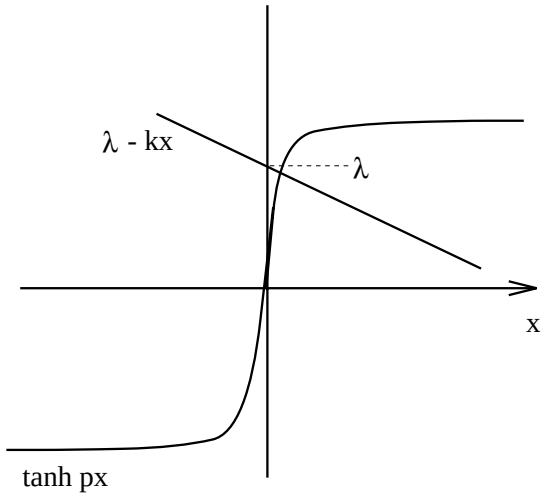


**Figure 4.12**: *Graphical solution for* $-1 < \lambda < 1$

However $\tanh px$ can not be assumed to be equal to $\pm 1$. Again a solution (i.e. a fixed point) will always exist for any given set of $\lambda$, $k$ and $p$ so we'll just consider the stability of such a solution. Equation 4.122 still holds

$$\frac{dv}{dt} = -kv - v(t - \tau)p\,\mathrm{sech}^2\,pX \tag{4.125}$$

However $X$ may now be sufficiently small that even for large $p$, $\mathrm{sech}^2\,pX$ can not be assumed to be zero. A more complete analysis is now undertaken, in which no assumption about the input to the modulator being sufficiently higher than the input to the quantiser is made.

Making the substitution

$$\alpha = p\,\mathrm{sech}^2\, pX \tag{4.126}$$

and assuming $v(t) = 0$ for $t < 0$, we now consider the Laplace transform of equation 4.125 in order to consider the stability of the fixed points.

$$sv(s) - v(0) = -kv(s) - \alpha e^{-\tau s} v(s) \tag{4.127}$$

$$v(s) = \frac{v(0)}{s + k + \alpha e^{-\tau s}} \tag{4.128}$$

We are interested in the poles of this expression, i.e. solutions to

$$s + k + \alpha e^{-\tau s} = 0 \tag{4.129}$$

$s$ may be complex, so substitute $s = \sigma + j\omega$

$$\sigma + j\omega + k + \alpha e^{-(\sigma + j\omega)\tau} = 0 \tag{4.130}$$

Splitting this expression into real and imaginary parts:

$$\sigma + k + \alpha e^{-\sigma\tau} \cos \omega\tau = 0 \tag{4.131}$$

$$\omega - \alpha e^{-\sigma\tau} \sin \omega\tau = 0 \tag{4.132}$$

For stability, the poles must be in the left half of the Argand diagram, i.e. the real part must be negative. Consequently we now adopt a bifurcation theory approach and consider what happens at the boundary between stability and instability, i.e. we solve the equations for the boundary condition of $\sigma = 0$.

$$k + \alpha \cos \omega\tau = 0 \tag{4.133}$$

$$\omega - \alpha \sin \omega\tau = 0 \tag{4.134}$$

Squaring these equations gives

$$k^2 = \alpha^2 \cos^2 \omega\tau \tag{4.135}$$

$$\omega^2 = \alpha^2 \sin^2 \omega\tau \tag{4.136}$$

Adding together gives an expression for $\omega$

$$\omega^2 = \alpha^2 - k^2 \tag{4.137}$$

From the definition of $\omega$, it must be real, therefore

$$\alpha^2 > k^2 \tag{4.138}$$

and $\alpha$ and $k$ are both positive, so

$$\alpha > k \tag{4.139}$$

Thus we have the condition that $\alpha > k$ for a pole to be on the imaginary axis, and the fixed point to be unstable. In general $\alpha = p\,\mathrm{sech}^2 pX$ is less than $k$ (in the ideal case it is zero) and so the fixed point is almost always stable. Note also that this finding fits the special case of $\lambda > 1$ as described in equation 4.123.

As an aside, it is worth noting that equations 4.133 and 4.134 have another solution whereby $\omega = 0$. This would mean that $\alpha = -k$ however, and, since both $\alpha$ and $k$ must be positive, this solution can be discarded. We now consider what other conditions must hold at this boundary point.

Substituting 4.137 into 4.133

$$k + \alpha\cos(\alpha^2 - k^2)^{\frac{1}{2}}\tau = 0 \tag{4.140}$$

$$\cos(\alpha^2 - k^2)^{\frac{1}{2}}\tau = \frac{-k}{\alpha} \tag{4.141}$$

Consequently the solution occurs where a cosine wave passes through a particular value, which will happen twice on each cycle of the wave ($\alpha > k$ so the value is always less than 1). This solution represents a pair of poles on the imaginary axis (i.e. a complex conjugate pair) since any solution for $\omega$ must also be true for $-\omega$ due to the symmetrical nature of the cosine function.

We now have this bifurcation occurring between stability and instability, and we need to consider the sign of the rate of change of the real part of the pole $\sigma$ with respect to the delay $\tau$. Consider equations 4.131 and 4.132. $k$ and $\alpha$ are fixed, subject to $\alpha > k$, we now regard $\sigma(t)$ and $\omega(t)$ as solutions to these equations, specifically we want to find $\frac{d\sigma}{d\tau}$ at $\sigma = 0$.

$$\frac{d\sigma}{d\tau} + \alpha(-(\sigma + \frac{d\sigma}{d\tau}\tau)e^{-\sigma\tau}\cos\omega\tau - e^{-\sigma\tau}\sin\omega\tau(\frac{d\omega}{d\tau}\tau + \omega)) = 0 \tag{4.142}$$

$$\frac{d\omega}{d\tau} - \alpha(-(\sigma + \frac{d\sigma}{d\tau}\tau)e^{-\sigma\tau}\sin\omega\tau + e^{-\sigma\tau}\cos\omega\tau(\frac{d\omega}{d\tau}\tau + \omega)) = 0 \tag{4.143}$$

Substitute for $\sigma = 0$

$$\frac{d\sigma}{d\tau} + \alpha(-\frac{d\sigma}{d\tau}\tau\cos\omega\tau - (\frac{d\omega}{d\tau}\tau + \omega)\sin\omega\tau) = 0 \tag{4.144}$$

$$\frac{d\omega}{d\tau} - \alpha(-\frac{d\sigma}{d\tau}\tau\sin\omega\tau + (\frac{d\omega}{d\tau}\tau + \omega)\cos\omega\tau) = 0 \tag{4.145}$$

Substitute $w = (\alpha^2 - k^2)^{\frac{1}{2}}$ and values of $\cos\omega\tau$ and $\sin\omega\tau$ from equations 4.135 and 4.136

$$\frac{d\sigma}{d\tau} + k\tau\frac{d\sigma}{d\tau} - (1 - \frac{k^2}{\alpha^2})^{\frac{1}{2}}(\omega + \tau\frac{d\omega}{d\tau}) = 0 \tag{4.146}$$

$$(1 + k\tau)\frac{d\sigma}{d\tau} - \alpha(\alpha^2 - k^2) - \alpha\tau(\alpha^2 - k^2)^{\frac{1}{2}}\frac{d\omega}{d\tau} = 0 \tag{4.147}$$

Making the same substitutions in equation 4.145:

$$\frac{d\omega}{d\tau} + \alpha\tau(1 - \frac{k^2}{\alpha^2})^{\frac{1}{2}}\frac{d\sigma}{d\tau} + k((\alpha^2 - k^2)^{\frac{1}{2}} + \tau\frac{d\omega}{d\tau}) = 0 \tag{4.148}$$

$$(1 + k\tau)\frac{d\omega}{d\tau} + \tau(\alpha^2 - k^2)^{\frac{1}{2}}\frac{d\sigma}{d\tau} + k(\alpha^2 + k^2)^{\frac{1}{2}} = 0 \tag{4.149}$$

Now express equations 4.147 and 4.149 in matrix format

$$\begin{pmatrix} 1 + k\tau & -\alpha\tau(\alpha^2 - k^2)^{\frac{1}{2}} \\ \tau(\alpha^2 - k^2)^{\frac{1}{2}} & 1 + k\tau \end{pmatrix} \begin{pmatrix} \frac{d\sigma}{d\tau} \\ \frac{d\omega}{d\tau} \end{pmatrix} = \begin{pmatrix} \alpha(\alpha^2 - k^2) \\ -k(\alpha^2 - k^2)^{\frac{1}{2}} \end{pmatrix} \tag{4.150}$$

The determinant of the first matrix is:

$$\det = (1 + k\tau)^2 + \alpha\tau^2(\alpha^2 - k^2) \tag{4.151}$$

which is positive. The inverse of that matrix is:

$$\text{inv} = \frac{1}{\det}\begin{pmatrix} 1 + k\tau & \alpha\tau(\alpha^2 - k^2)^{\frac{1}{2}} \\ -\tau(\alpha^2 - k^2)^{\frac{1}{2}} & 1 + k\tau \end{pmatrix} \tag{4.152}$$

So

$$\begin{pmatrix} \frac{d\sigma}{d\tau} \\ \frac{d\omega}{d\tau} \end{pmatrix} = \frac{1}{\det}\begin{pmatrix} 1 + k\tau & \alpha\tau(\alpha^2 - k^2)^{\frac{1}{2}} \\ -\tau(\alpha^2 - k^2)^{\frac{1}{2}} & 1 + k\tau \end{pmatrix} \begin{pmatrix} \alpha(\alpha^2 - k^2) \\ -k(\alpha^2 - k^2)^{\frac{1}{2}} \end{pmatrix} \tag{4.153}$$

Thus the expression for $\frac{d\sigma}{d\tau}$ is

$$\frac{d\sigma}{d\tau} = \frac{1}{\det}((1 + k\tau)\alpha(\alpha^2 - k^2) - \alpha k\tau(\alpha^2 - k^2)) \tag{4.154}$$

$$= \frac{1}{\det}\alpha(\alpha^2 - k^2) \tag{4.155}$$

Since the determinant is positive and $\alpha > k$, the derivative of $\sigma$ must be positive at $\sigma = 0$.

This shows that the poles of the solution have a positive rate of change at the imaginary axis, which means that for values of the delay slightly less than the bifurcation value, the fixed point is stable, and for values slightly more the fixed point is unstable. Consequently even given the condition for instability $\alpha > k$, the fixed point is stable for small values of $\tau$ and, as $\tau$ increases, the poles are pushed over the imaginary axis and the fixed point becomes unstable. This is probably sufficient evidence that a Hopf bifurcation is taking place.

This section has shown that the fixed points of the system are stable for all $\alpha < k$, which is usually the case for a realistic implementation since $\alpha$ is a $\text{sech}^2$ term which is ideally equal to zero, and that they can go unstable when that condition is not met and the delay time is sufficiently high.

Consequently, for positive $k$ and an approaching ideal tanh function the equation representing

sigma delta modulation behaves in the manner intended, i.e. as an accurate representation of a sigma delta modulator.

These analytic results can be extended to higher order sigma delta modulators, since equation 4.115 will always take the form

$$0 = \lambda - Ax - B\tanh px \tag{4.156}$$

when looking for a fixed point, where $A$ and $B$ are some combination of the integrator leakage ($k_0$, $k_1$, etc.) and feedback ($a_0$, $a_1$, etc.) coefficients. For example, the equation for second order modulation becomes

$$0 = \lambda - k_0 k_1 x - (k_1 a_0 + a_1)\tanh px \tag{4.157}$$

This is further investigated in the subsequent chapter on the stability of sigma delta modulation.

The results of this section suggest that the differential equation formulated does behave similarly to a sigma delta modulator. The numerical solutions show comparable behaviour to that of a conventional simulation of $\Sigma\Delta$M. The fixed point study shows that the equation reacts to an over-driven input in the same way that a sigma delta modulator does. The generalised solution shows that this constantly changing output follows two distinct exponential curves, switching between them as the delayed output changes sign; this behaviour is also observable in a conventional $\Sigma\Delta$M simulation, and is returned to in greater detail in the following chapter.

These three factors are sufficient for us to consider the equation as a viable model of sigma delta modulation. The following section attempts to utilise this equation to calculate the Lyapunov exponents of the system.

## 4.5 PRELIMINARY ANALYSIS OF THE LYAPUNOV EXPONENTS OF A SIGMA DELTA MODULATED SIGNAL

The initial motivation for developing a set of differential equations to represent sigma delta modulation was to calculate the Lyapunov exponents introduced to a signal by such modulation, using for example the method of Wolf *et al* [32]. This section sets out the method utilised and the results achieved; the reasons for not continuing with this line of research are also addressed. As described in chapter 2, Wolf *et al*'s method involves constructing a linearised set of equations representing the system, each equation leading to the calculation of a single Lyapunov exponent.

The problem which first presents itself in the process of obtaining the Lyapunov exponents of the differential equation representing first order sigma delta modulation is a result of the delayed nature of this equation. A delay in a continuous system is in fact infinite dimensional. Consider the initial conditions of such a system; in order to fully define them, the delay $x(t-\tau)$ must

be fully defined. In a continuous system this would require either an infinite number of initial conditions or a well-defined function. Such a function is not available in this instance, which leaves us with the infinite initial conditions solution. An infinite number of initial conditions, however, leads to an infinite number of dimensions and hence an infinite number of Lyapunov exponents and our problem is apparent.

Fortunately, Farmer [27] proposes an approach for getting around this problem in a numerical manner. The delay interval $[t-\tau, t]$ is sampled to give $j$ variables for a $j$-dimensional discrete mapping of the delay. These variables are iterated by using a Runge Kutta numerical integration scheme on the linearised set of $j$ equations

$$\frac{d\delta x_j}{dt} = -k\delta x_j - p\,\mathrm{sech}^2(px)\delta x(t-\tau)_j \tag{4.158}$$

where the $j$ small separations $\delta x_j$ between two infinite-dimensional vectors are known as separation functions. Note that this is a linearised form of the equation for first order sigma delta modulation, as was derived in Equation 4.122.

According to the method of Farmer, it is now possible to calculate the Lyapunov exponents by observing how much these separation functions grow in a timestep $\tau$.

Figure 4.13 shows the results achieved from applying this method to the equation representing first order sigma delta modulation with a constant input (equation 4.21). The first 25 Lyapunov exponents have been plotted for $\tau = 0.006$, $p = 120.0$, $k = 0.1$ and $\lambda = 0.5$. As can be seen the first exponent is zero, indicating that we are studying a flow; the rest of the exponents are negative which implies that the system is stable as has been shown in the analysis of previous sections. Similar results were found when a sinusoidal input was used.

It should be pointed out that these results were only achieved with very careful selection of the parameter values $\tau$ and $p$, so that the switchover period, when the hyperbolic tangent has an effect, is both sufficiently long and sufficiently frequent for its effect to be calculable in the estimation of the Lyapunov exponents. Hence, we have used an artificially low value of both $p$ and $\tau$ in this calculation. In general, the fact that the switching occurs over such a short period of time in comparison to the time between switchings (i.e. the portion of time when the hyperbolic tangent comes into play, or the hyperbolic secant in the linearised equations) means that the various exponents decay away to virtually nothing before the next switching takes place, leading to numerical instability of the process.

This is apparent from consideration of the plot of the output of the integrator $x(t)$ shown in Figure 4.6, where the switch-over is sufficiently fast to result in a discontinuity between the two exponential curves. This effectively leads to two separate sets of dynamics at work, on completely different time scales. At the lowest level are the dynamics of the switch-over itself; at a higher level are the dynamics of the exponentials. This situation is further complicated

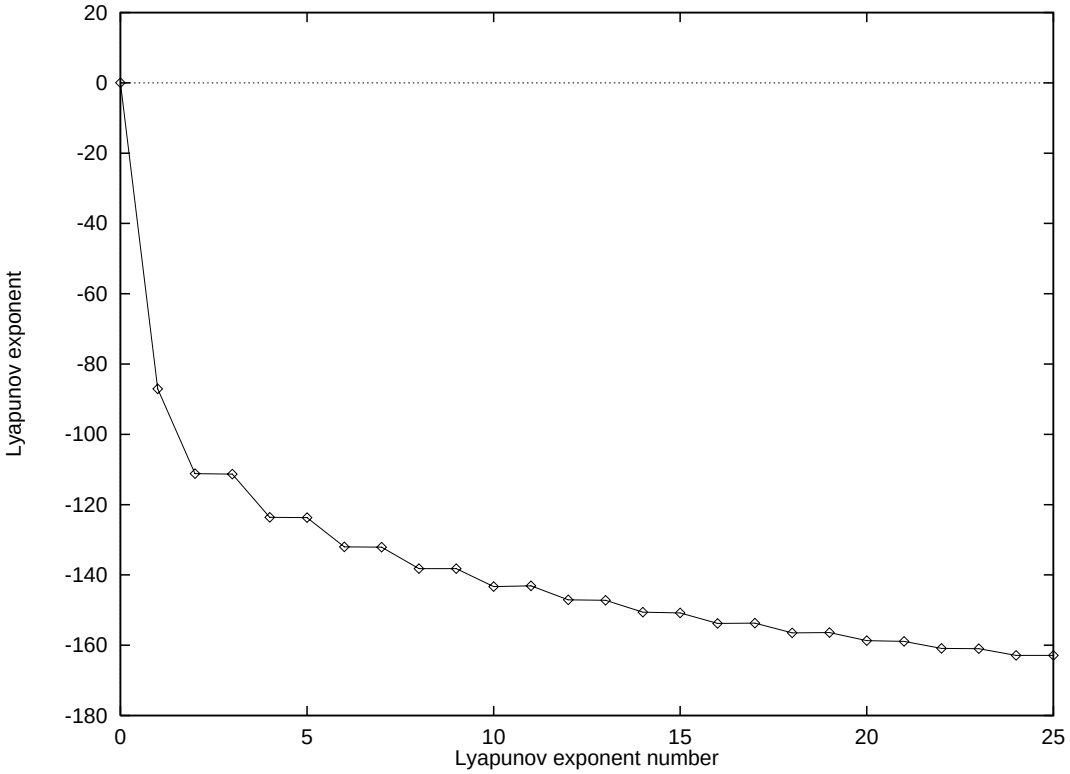


**Figure 4.13**: *Lyapunov exponents calculated from the differential equation representing first order sigma delta modulation with a constant input.*

when considering the ΣΔM of a moving signal, since, at an even higher level, there are the dynamics of that signal. The over-sampling nature of ΣΔM must result in the dynamics of the modulator being on a significantly smaller time scale than the dynamics of the input. An examination of the phase plots in Figures 3.11 and 3.12 showing the integrator output x(t) reveal these phenomena: the phase plot shows a basic repetitive structure, which moves around the phase space over time and as the input to the modulator changes; also the sharp corners of the plot show the discontinuities of the switch-over points.

Perhaps ironically, if we could apply Wolf *et al*'s method directly to the differential equation under study, these problems would not arise in that they would be accounted for within the Jacobian of the system automatically. However, the approach of Farmer necessitated by the delay is a numerical one, which means that the the differing time scales of the dynamics take their effect.

Consequently, although some results could be achieved with very careful (and intrinsically artificial) choice of the parameter values, the process was found to be unusable in any general case.

The results which were achieved are of some interest however. In particular they tend to imply that the first order sigma delta modulator is not inherently a chaotic device as has been speculated, since no positive Lyapunov exponents is apparent in the calculated spectrum.

Indeed, the fact that the small-scale dynamics of the modulator are dying out before their full effect can be brought to bear on the calculation implies that the system is not chaotic. In a chaotic system, as we have seen, a change in a system value, however small, will have a far-reaching effect on the overall state of the system. This does not appear to be the case here, so our sigma delta modulator with a constant input seems to be non-chaotic.

## 4.6 CONCLUSIONS

In this chapter a possible basis for the analytical study of sigma delta modulators and their effects on and interactions with chaotic signals has been described, and a set of reasons have been given for not taking this particular approach to the problem.

A set of differential equations have been constructed to represent a sigma delta modulator and it has been shown that a successful model is achieved providing certain assumptions hold. The slope of the hyperbolic tangent, $p$, must be high; this is a reasonable assumption since the tangent is modelling a one bit quantiser in which the slope is ideally infinite. The delay $\tau$ is intended to tie the continuous system to the discrete one by modelling the sampling rate of the modulator, it also incorporates any delay introduced by the quantiser and other circuit elements.

The equation for a first order modulator has been considered for calculation of Lyapunov exponents. Although some results were forthcoming, the necessity of a low value of the slope $p$ (in conflict with the assumptions necessary to the formulation of the equation in the first place), and the wide range of time scales on which the system's dynamics take place, has led us to discard this method as a tool for further study.

The results achieved do suggest that the sigma delta modulator is not capable of chaotic modes of operation with a non-chaotic input.

It has been implied that the continuous model of the sigma delta modulator may be used to investigate the stability behaviour of such devices. The next chapter will deal with this aspect of the work.

# Chapter 5

# STABILITY AND CONFIGURATION OF SIGMA DELTA MODULATORS

## 5.1 INTRODUCTION

A method for the stability analysis of sigma delta modulators is presented in this chapter. The model also defines a set of constraints on the configuration of sigma delta modulation for avoiding a mode of operation which we have chosen to call asymptotic operation. It will be shown that, although this mode of operation is equally as undesirable as unstable operation, it is a stable mode. It is apparent that some researchers may have mistakenly labelled this asymptotic mode as instability and grouped it with genuinely unstable behaviour (e.g. [58]). Perhaps it is somewhat pedantic to point this out, since the asymptotic behaviour is certainly something to be avoided, however it is not, rigourously speaking, an unstable mode in the sense of being unbounded, and should not be described as such. A set of differential equations representing a continuous sigma delta modulator was constructed in the previous chapter. These equations are now used to study the stability of continuous sigma delta modulation and the results obtained are compared to the operation of a conventional sigma delta converter.

In the analysis of these equations, particular reference is made to values representing the gains of the feedback loop and the integrator leakage. The results are presented in the form of plots showing regions of asymptotic and correct operation of the modulator. Conditions for the stability and correct operation of the equations representing $\Sigma\Delta$M are derived. The results from this process are used on a conventional simulation of $\Sigma\Delta$M and shown to give the results predicted.

A recurrent problem in the design of sigma delta modulators is predicting the stability of higher order modulators. Alternative circuit architectures are often used in lieu of a high order sigma delta modulator due to this difficulty. In this chapter criteria for the stability and desirable operation of a $n^{th}$ order modulator are derived from the continuous differential equations.

## 5.2 SIGMA DELTA MODULATION AS DIFFERENTIAL EQUATIONS

A set of ordinary differential equations has been derived to represent a continuous model of sigma delta modulation. The equations for second order modulation are

$$\frac{dx_0(t)}{dt} = x_1(t) - k_0 x_0(t) - a_0 M \tanh\frac{p x_0(t-\tau)}{M} \tag{5.1}$$

$$\frac{dx_1(t)}{dt} = \lambda - k_1 x_1(t) - a_1 M \tanh\frac{p x_0(t-\tau)}{M}. \tag{5.2}$$

It has been shown in the previous chapter that these equations, when solved numerically by the Runge Kutta method for example, are an accurate model of sigma delta modulation providing certain assumptions hold. The coefficients $k_0, k_1, a_0, a_1$ represent the integrator leakages and the feedback constants respectively in an attempt to correctly model the circuit characteristics of a sigma delta modulator. These are the coefficients which define the configuration of the circuit. Note that the input $\lambda$ will be taken to be constant for the analysis of this chapter. As mentioned in the previous chapter a constant input is a natural mode of operation to investigate in these over-sampling devices and, of course, it simplifies the analysis. The meanings of the various symbols are best made clear with reference to Figure 5.1.

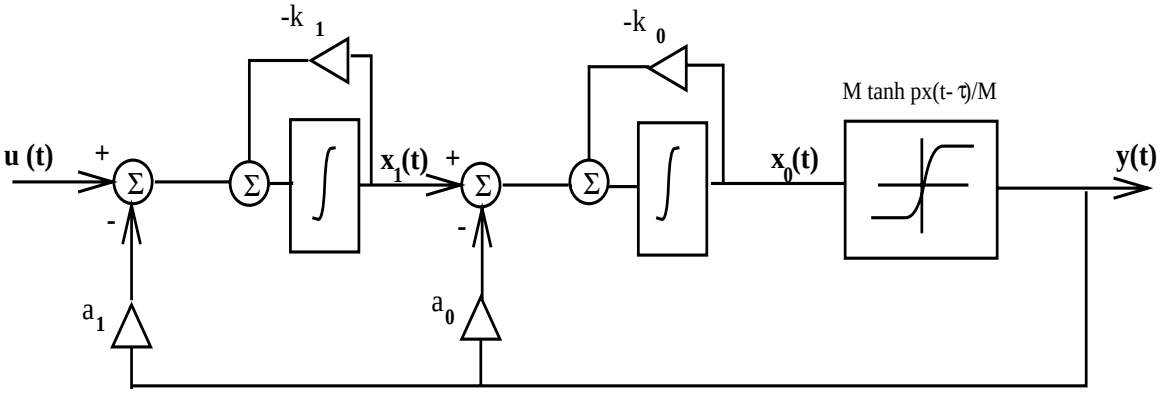


**Figure 5.1**: *Second Order Continuous Sigma Delta Modulator*

It seems reasonable to suppose that if these equations representing the continuous sigma delta modulator give an accurate model of conventional sigma delta modulation, then a stability analysis of those equations could lead to a full understanding of the stability of $\Sigma\Delta$M. This analysis concentrates on the equations representing second order modulation (5.1 and 5.2), before it is applied to third order, first order and a general $n^{th}$ order modulator.

## 5.3 OPERATIONAL BOUNDARIES FROM SIMULATION

The algebraic analysis of equations 5.1 and 5.2 is more complicated than is perhaps apparent. Indeed a full integration of these equations would seem to be beyond the capabilities of any texts or computer packages consulted. However, as was demonstrated in the previous chapter, it is possible to solve these equations numerically using an iterative method such as the Runge Kutta method. The results achieved in this manner lead to a simplified analysis of the equations, since

they imply the nature of the solutions being searched for, as shall be shown.

Again a fourth order fixed time step Runge Kutta iterative process was used to numerically solve the system of differential equations representing second order $\Sigma\Delta$M. It was found that three distinct modes of operation occurred. Of these, only one mode was genuinely unstable, and this mode only occurred under very specific circumstances. The only configurations of the equations which led to instability were those with zero integrator leakage (i.e. zero values of $k_0$ or $k_1$) and some other criterion which will be discussed in full presently. That these configurations should be unstable is unsurprising, since it is a well-known fact that zero integrator leakage can lead to an unstable integrator [72]. Indeed, had this result not been observed then the whole analysis would be of little worth. However, the fact that these are the only genuinely unstable configurations of the equations, and hence the circuit that they represent, is surprising. The reasons for this behaviour will be explained in the analysis of the following section.

Examples of the two stable modes of operation are shown in Figure 5.2.

5.2a

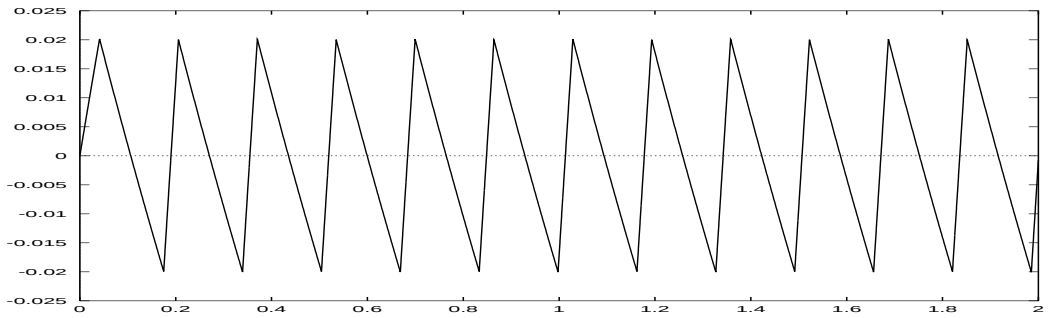


5.2b

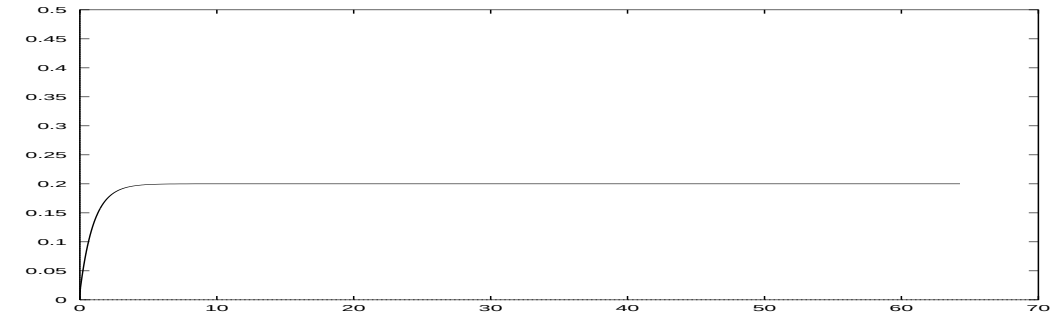


**Figure 5.2**: *Plot of input to quantiser, $x_0(t)$, during a)correct operation and b)asymptotic operation*

As can be seen, both of these modes of operation are stable, however only the time series for $x_0(t)$ in Figure 5.2a is of a form which can result in correct modulation of the input. The oscillatory nature of this plot is the sort of waveform expected if the circuit is configured in a desirable mode. The time series for $x_0(t)$ shown in Figure 5.2b is clearly an undesirable one since, if quantised, it will result in a steady stream of +1s in the output of the modulator. We have chosen to label this mode of operation *asymptotic operation*, as the waveform of $x_0(t)$

tends toward a d.c. value and stays there.

It is perhaps worth noting at this point that, whereas this asymptotic operation is not unstable, it would seem that a number of researchers have mistaken it for instability. Often when searching for instability the output of the quantiser is considered; of course the quantiser output will never become genuinely unstable as it can never have any value other than $+1$ or $-1$, depending on the sign of its input. Consequently some researchers have looked for limit-cycles in the output as a clue to instability at the quantiser input. If the input to the quantiser is moving toward positive infinity then the output of the quantiser will remain at $+1$. However, if the input to the quantiser is a d.c. level, as in the case of this asymptotic operation, the situation could easily be mistaken for instability, when only the output of the quantiser is considered. It is also possible that if the asymptotic level toward which $x_0(t)$ is tending is higher than the power rails of the integrator then the integrator will saturate before that level is reached and again the modulator will appear to be unstable. This is an important part of this chapter and will be considered at some length in a later section.

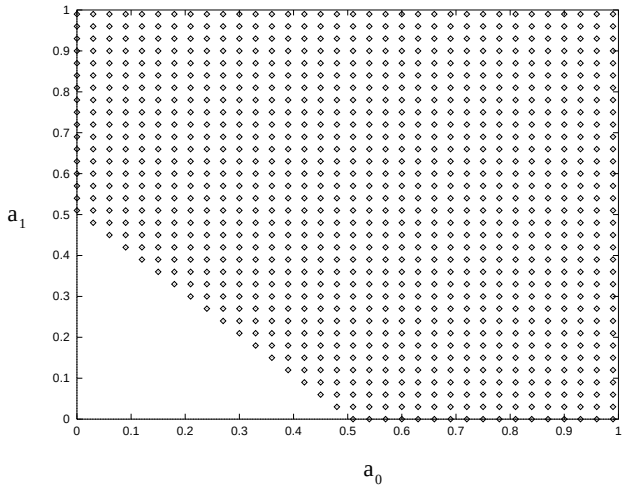


**Figure 5.3**: *Operational plot of Runge Kutta solution to differential equations representing second order* $C\Sigma\Delta M$ *with varying* $a_0$ *(abscissa) and* $a_1$ *(ordinate).*

It was discovered that the configurations leading to the two different types of operation (i.e. asymptotic and oscillatory) were divided by a well-defined boundary. Consider Figure 5.3 which shows the occurrence of the two types of operation for $\lambda = 0.5$ and $k_0 = k_1 = 1$ as $a_0$ and $a_1$ are varied. The dark area represents the configurations leading to an oscillatory response, the light area shows the configurations giving an asymptotic response. The values of the integrator leakages were set to an unrealistically high value (i.e. unity) in order to move the boundary to a position on the graph where it is more visible for a wide range of feedback coefficients. If more realistic values are used (e.g. $k_0 = k_1 = 0.01$) then the following analysis and results still hold true. If the integrator leakage is zero then this same line shows the boundary between unstable behaviour and a triangular wave.

As can be seen a straight line divides the two areas. From replotting this boundary for a range

of values of the coefficients it was found that the equation of this line is

$$\lambda = a_1 + a_0 k_1. \tag{5.3}$$

A time domain model of each circuit element was constructed to form a direct simulation of a second order sigma delta modulator. Note that this is a simulation of a conventional $\Sigma\Delta$M with discrete elements as well as continuous elements; a computer simulation can never be truly continuous, but the iteration frequency was sufficiently high to appear continuous in relation to the sampling period of the discrete elements. This simulation was used to investigate the effects of the values of the feedback constants $a_0$ and $a_1$ and the integrator leakages $k_0$ and $k_1$ on the operation of the modulator.

It was found that certain configurations (i.e. certain combinations of values of these coefficients) caused the modulator to operate incorrectly, in that the output remained at $+1$ at all times. On further investigation it was apparent that this was due to the input to the quantiser being asymptotic to a d.c. level. This is exactly the behaviour observed in the numerical solutions of the differential equations as outlined above. Again the only true instability arose when either of the integrator leakages was set to zero.

With this in mind consider the plot in Figure 5.4, which shows the results for a simulated second order sigma delta modulator with an input $\lambda = 0.5$, and $k_0 = k_1 = 1$, whilst $a_0$ and $a_1$ are varied (i.e. the same configuration as for the results from the Runge Kutta method).

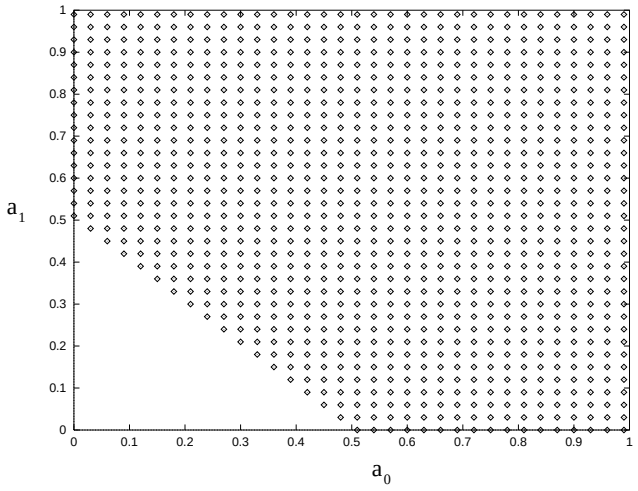


**Figure 5.4**: *Operational plot of second order $\Sigma\Delta M$ with varying $a_0$ (abscissa) and $a_1$ (ordinate).*

The dark area is where correct operation occurs, the light area where asymptotic operation is observed. It can be seen that a straight line divides the two areas. By taking a number of further plots with a range of values of $\lambda$, $k_0$ and $k_1$ it was found that the equation of this

straight line boundary is again

$$\lambda = a_1 + a_0 k_1. \tag{5.4}$$

Consequently it can be seen that the same results have been observed in both a direct simulation of a second order sigma delta converter, and the iterative solution of the differential equations representing such a device. This provides further evidence that the differential equations in question are an accurate model of $\Sigma\Delta$M and it implies that an algebraic analysis of those equations should give a full description of the stability and asymptotic behaviour of these circuits.

## 5.4 STABILITY ANALYSIS OF DIFFERENTIAL EQUATIONS

Two methods have been utilised to investigate the stability of the ordinary differential equations representing a second order sigma delta modulator. The two techniques provide equivalent results. Only the fixed point method will be used in subsequent sections of this chapter, as it gives a more intuitive understanding of the processes involved in this particular system. In this first instance however, the Laplace transform method is also presented as this is a form which is more often used in the study of the stability of circuits. In both methods a constant input $\lambda$ has been utilised. It has been noted already that the constant input is a natural object to investigate in the analysis of sigma delta modulation. This is largely due to the oversampling nature of this type of converter which means that any input will at most be changing slowly in comparison with the sampling rate.

### 5.4.1 General Dynamics

Strictly speaking, for a rigorous analysis, a full dynamical study of the equations should first be carried out, however, as we have seen in the previous chapter, these equations do not yield up meaningful results easily and such an investigation would involve extensive work with no guarantee of meaningful results, and be of little interest in the context of the thesis as a whole. In the previous chapter, before considering the behaviour of the equation representing first order sigma delta modulation in detail, the general dynamics were described in terms of a general solution to the equation of the form

$$x = A + Be^{-kt}. \tag{5.5}$$

For the second order system, however, such a general solution has not been forthcoming. The general solution to the equation involving the input $\lambda$ can be shown to take this form, but the other equation must involve a second exponential term in some manner, which seems to preclude such an equation from being written. This is not surprising, as most nonlinear second order systems do not have general solutions [75, 76]. However, as is common in the analysis of

nonlinear differential equations, we can fall back on numerical approaches. Specifically we can see from the Runge Kutta solutions that the waveforms take the form once more of two rising or falling lines, switching between the two as the quantiser switches state. Whether these lines are formed by a single exponential variable, or the sum of two such variables, does not stop us from considering them as lines heading toward some fixed point. The asymptotic mode of operation identified in the Runge Kutta solutions further leads us toward considering a fixed point approach.

Since the form of the equations is the same as that of the first order system and, perhaps more importantly, since their behaviour when numerically solved is similar (i.e. two switched curves or an asymptotic line) we shall jump straight to the search for fixed points.

### 5.4.2 Fixed Point Method

The numerical analysis of the previous section implies that a search for the causes of asymptotic operation should be instigated. Since in this mode the value of $x_0(t)$ heads to a d.c. value and stays there, we can think of this as a fixed point. Consequently the fixed points of the equations representing second order $\Sigma\Delta$M (5.1 and 5.2) are considered. At a fixed point the derivatives of $x_0$ and of $x_1$ are zero. Although the quantiser was replaced with a hyperbolic tangent in the construction of the differential equations and in the numerical solution of those equations, we shall revert to an ideal delayed quantiser in this analysis. This is simply a measure to aid clarity and reduce the complexity of the analysis. Assuming the hyperbolic tangent can only output $\pm 1$ (i.e. we set $M = 1$), equation 5.1 can be solved for the fixed point $\hat{x}_1$.

$$\hat{x}_1 = \frac{\lambda \mp a_1}{k_1} \tag{5.6}$$

Substituting this into 5.2 gives an expression for fixed point $\hat{x}_0$.

$$\hat{x}_0 = \frac{\lambda \mp (a_1 + a_0 k_1)}{k_0 k_1} \tag{5.7}$$

### 5.4.3 Laplace Transform Method

Alternatively, the stability can be analysed via Laplace transform, again the tanh function is set to $\pm 1$ for simplicity. The ODEs then become

$$sX_0(s) - x_0(0) = X_1(s) - k_0 X_0(s) \pm \frac{a_0}{s} \tag{5.8}$$

$$sX_1(s) - x_1(0) = \frac{\lambda}{s} - k_1 X_1(s) \pm \frac{a_1}{s}. \tag{5.9}$$

Setting initial conditions $(x_0(0), x_1(0))$ to zero, gives

$$X_0(s) = -\frac{a_0 s + a_1 + a_0 k_1 \mp \lambda}{s(s + k_0)(s + k_1)}. \tag{5.10}$$

It can be seen that a similar expression has occurred in the numerator. This expression in the numerator of the expression from both the fixed point analysis and the Laplace transform analysis will be of importance in the following section.

## 5.5 DISCUSSION OF RESULTS FOR SECOND ORDER MODULATION

We have seen that a definite boundary exists between oscillatory and asymptotic operating modes, or, in the case of zero integrator leakage, between an oscillatory mode and instability. In order to understand why this boundary arises, we turn to Figure 5.5.

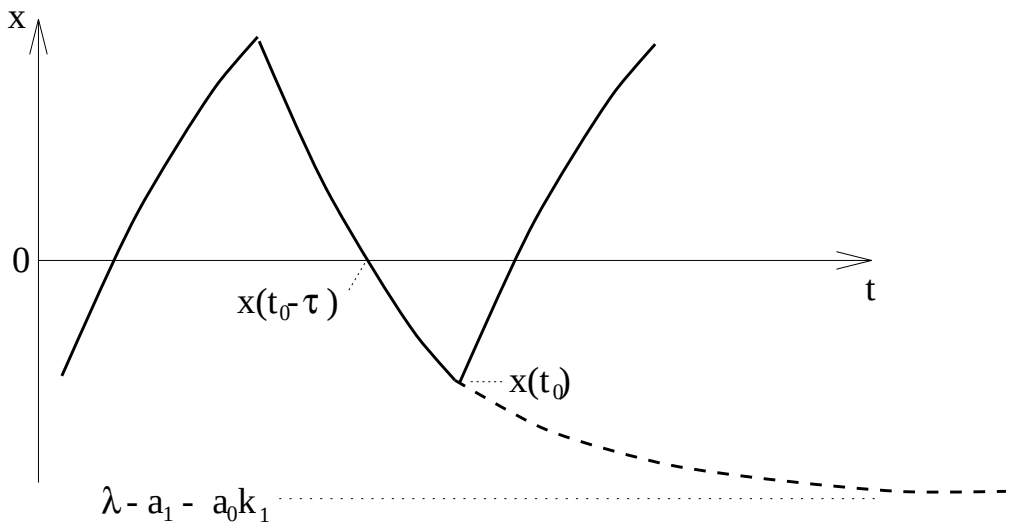


**Figure 5.5**: *Schematic showing evolution of* $x(t)$ *with reference to fixed points*

If we consider a point in time at which the output of the quantiser is $+1$ then this gives a fixed point at $\hat{x}_0 = \lambda - a_1 - a_0 k_1$ and the waveform of $x_0(t)$ is on the downward slope as shown in Figure 5.5. When the delayed value of $x_0$, i.e. $x_0(t-\tau)$, becomes negative the output of the quantiser switches to $-1$ and the fixed point is now at $\hat{x}_0 = \lambda + a_1 + a_0 k_1$. Consequently the direction of $x_0(t)$ reverses and it evolves along the upward slope. It can be seen that this leads to the desirable oscillatory mode of operation which will result in a reliable modulation of the input signal.

However, consider the case when

$$\lambda > a_1 + a_0 k_1. \tag{5.11}$$

In this case the value of $\hat{x}_0$ remains positive whatever the output of the quantiser for positive $k_0$ and $k_1$ (If $k_0 k_1$ gives a negative value, $\hat{x}$ will remain negative – the point being that the sign of the fixed point expression of equation 5.7 never changes). Consequently $x_0(t)$ reaches the fixed point value and stays there, since it never crosses the zero line as it approaches that fixed point and so the output of the quantiser never switches over and a new fixed point is not generated. This is the asymptotic mode of operation observed in both the numerical solution

of the equations and the direct simulation of the circuit. A similar argument can be made for the modulator getting into an asymptotic mode with negative $x_0(t)$.

It is worth considering the case of zero integrator leakage at this point. Since no leakage factor is involved, the waveform is no longer exponential, but a straight line (i.e. $k$ has been set to zero in equation 4.22, giving a straight line as the solution), so, if the parameters are such as to preclude a changeover of the quantiser, this line will simply continue to rise toward infinity. If a changeover can occur then a triangular wave will result as the time series switches between the two straight line solutions.

Hence a general rule can be written for the correct operation of second order sigma delta modulators

$$|\lambda| < a_1 + a_0 k_1 \tag{5.12}$$

with the additional factor that the second order modulator is stable (in the sense that its states are bounded) for non-zero values of the integrator leakages

$$|k_0|, |k_1| > 0. \tag{5.13}$$

## 5.6 ASYMPTOTIC BEHAVIOUR OR INSTABILITY?

In the past, the asymptotic behaviour described in this chapter appears to have been considered as a form of unstable behaviour, and has been grouped together with other unstable modes of operation of the sigma delta converter. As has been shown, the asymptotic mode of operation is not, strictly speaking, an unstable one and it is therefore possible that incorrectly labelling it as such could lead to some confusion or misunderstanding in the study of the phenomenon.

To the author's knowledge, the nearest anyone has come to making this distinction is in [58], in which the stability of the sigma delta modulator is considered to be a matter of degrees (i.e. some configurations are said to be more stable than others). This work acknowledges that instability, in terms of an unbounded output, will not be observed in a sigma delta modulator since the output is consistently bounded by the one bit quantiser, and hence it considers the interior signal levels. It goes on to describe a configuration as *very unstable* if the signal levels seen in a simulation without boundaries such as clipping implemented are vastly larger than those seen in a full simulation with all clipping present. However, the concept of asymptotic modes of operation does not appear to be discussed, and no case is made for this particular response to an input (again it would seem that this undesirable mode of operation is lumped in with other modes, some of which lead to genuine unbounded instability– with the caveat that clipping boundaries are removed). As with our own study, the work is based upon DC signal inputs to the modulator for ease of analysis.

In general, however, the study of the stability of sigma delta modulators has concentrated on the search for limit cycles at the output of the quantiser (e.g. [77]) whereby there is no way of telling whether such a limit cycle is caused by an internal signal reaching an asymptotic level, or whether it is genuinely unbounded. Whether or not such mis-labelling has lead to problems or obstacles in the field is debatable, since both modes of operation are equally undesirable and result in similar outputs to the modulator anyway, so perhaps only a pedant would make the distinction, but the findings of this work indicate that such a distinction exists.

## 5.7 THIRD ORDER MODULATION

It has been shown that a form of analysis exists which describes both the stability constraints and the constraints for non-asymptotic operation of a second order sigma delta modulator. This section uses that analysis to predict the constraints on third order modulation. A set of results will then be derived both from numerically solving the differential equations and from a direct simulation of third order modulation and shown to match the results predicted from the analysis.

The ordinary differential equations representing third order continuous sigma delta modulation are:

$$\frac{dx_0(t)}{dt} = x_1(t) - k_0 x_0(t) - a_0 M \tanh\frac{p x_0(t-\tau)}{M} \tag{5.14}$$

$$\frac{dx_1(t)}{dt} = x_2(t) - k_1 x_1(t) - a_1 M \tanh\frac{p x_0(t-\tau)}{M} \tag{5.15}$$

$$\frac{dx_2(t)}{dt} = \lambda - k_2 x_2(t) - a_2 M \tanh\frac{p x_0(t-\tau)}{M}. \tag{5.16}$$

The coefficients represent the circuit elements as shown in Figure 5.6.

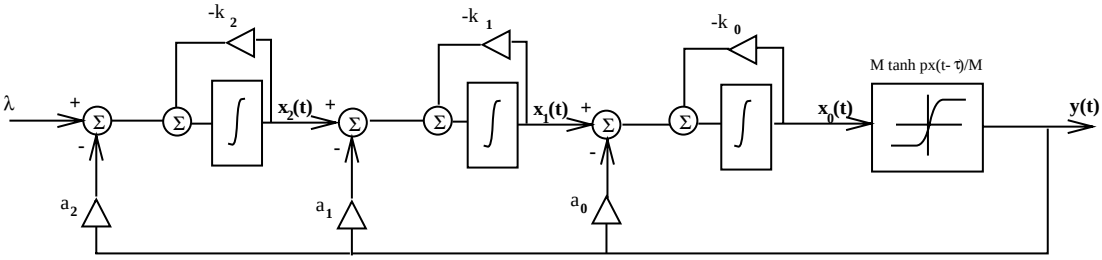


**Figure 5.6**: *Continuous circuit representation of third order sigma delta modulator.*

Solving for the fixed point $\hat{x}_0$, gives :

$$\hat{x}_0 = \frac{\lambda \mp (a_2 + a_1 k_2 + a_0 k_2 k_1)}{k_2 k_1 k_0}. \tag{5.17}$$

Note that the hyperbolic tangent has again been replaced with an ideal quantiser for simplicity of analysis.

The expression for $\hat{x}_0$ remains positive, independent of the quantiser output (for positive $k_0$, $k_1$, $k_2$), when

$$\lambda > a_2 + a_1 k_2 + a_0 k_2 k_1 \tag{5.18}$$

and hence it is expected that such configurations of the third order modulator will give rise to the asymptotic behaviour described in the second order analysis.

A number of plots have been made for a range of modulator configurations, using both the direct simulation of a third order modulator and the Runge Kutta iterative process on the third order equations, and the results are presented in Figures 5.7 and 5.8 respectively. Each plot shows the boundary between correct operation and asymptotic operation predicted by the above expression and the boundary observed from running the simulations. In each case the results are plotted for three different third order modulator configurations. In fact, the results match the theory very well and the two lines of each plot coincide to such an extent that it is impossible to see that two lines are actually plotted on each graph.

The theory fits the experimental results, so a general rule for non-asymptotic operation of third order sigma delta modulators can be written as

$$|\lambda| < a_2 + a_1 k_2 + a_0 k_2 k_1 \tag{5.19}$$

and the system is always stable (i.e. bounded states) for

$$|k_2|, |k_1|, |k_0| > 0. \tag{5.20}$$

## 5.8 FIRST ORDER MODULATION: A REPRISE

The question now arises as to whether this type of analysis can be applied to the first order sigma delta modulator. In fact this has already been considered in the previous chapter, but couched in somewhat different terms. The differential equation representing first order modulation is

$$\frac{dx(t)}{dt} = \lambda - k_0 x(t) - a_0 M \tanh \frac{p x(t-\tau)}{M} \tag{5.21}$$

and a fixed point occurs at

$$\hat{x} = \frac{\lambda - a_0}{k_0} \tag{5.22}$$

when the same assumptions are made as in the formulation of 5.7. Consequently the modulator is expected to be non-asymptotic for

5.7a : $\lambda = 0.5$, $a_0 = 1.0$, $a_1 = 1.0$, $a_2 = 0.1$ and $k_0 = 0.5$. the abscissa shows $k_1$, and the ordinate $k_2$. Theory predicts line at $k_2 = \frac{0.4}{k_1+1}$.

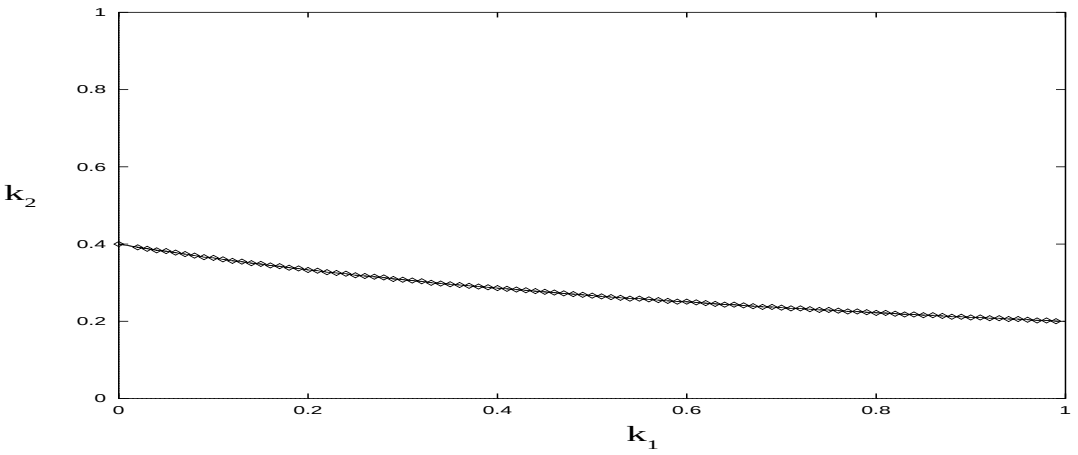


5.7b : $\lambda = 0.5$, $a_1 = 1.0$, $a_2 = 0.1$, $k_0 = 0.5$ and $k_1 = 1.0$. the abscissa shows $k_2$, and the ordinate $a_0$. Theory predicts line at $a_0 = \frac{0.4-k_2}{k_2}$.

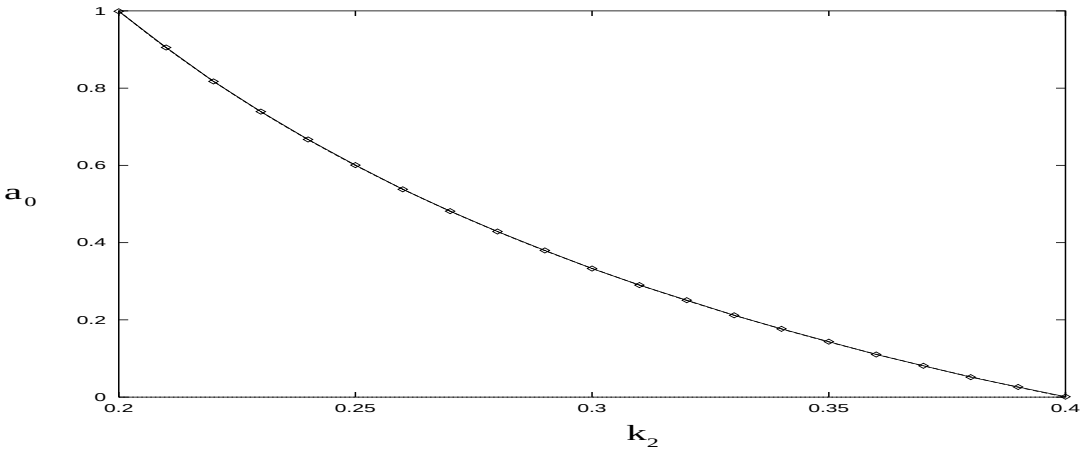


5.7c : $\lambda = 0.5$, $a_2 = 0.1$, $k_0 = 0.5$, $k_1 = 1.0$ and $k_2 = 1.0$. the abscissa shows $a_1$, and the ordinate $a_0$. Theory predicts line at $a_0 = 0.4 - a_1$.

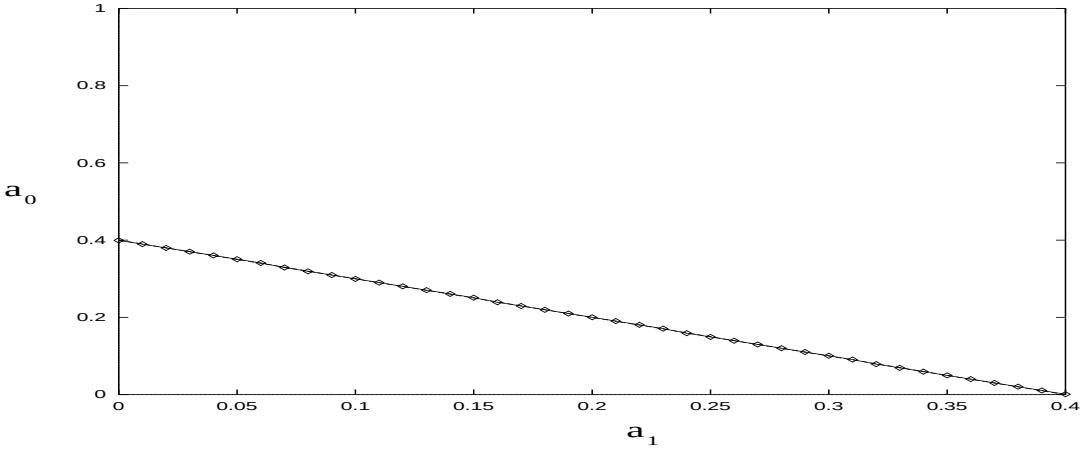


**Figure 5.7**: *Plots of results showing boundary between asymptotic and oscillatory behaviour of direct simulation of third order modulator*

5.8a : $\lambda = 0.5$, $a_0 = 1.0$, $a_1 = 1.0$, $a_2 = 0.1$ and $k_0 = 0.5$. the abscissa shows $k_1$, and the ordinate $k_2$. Theory predicts line at $k_2 = \frac{0.4}{k_1+1}$.

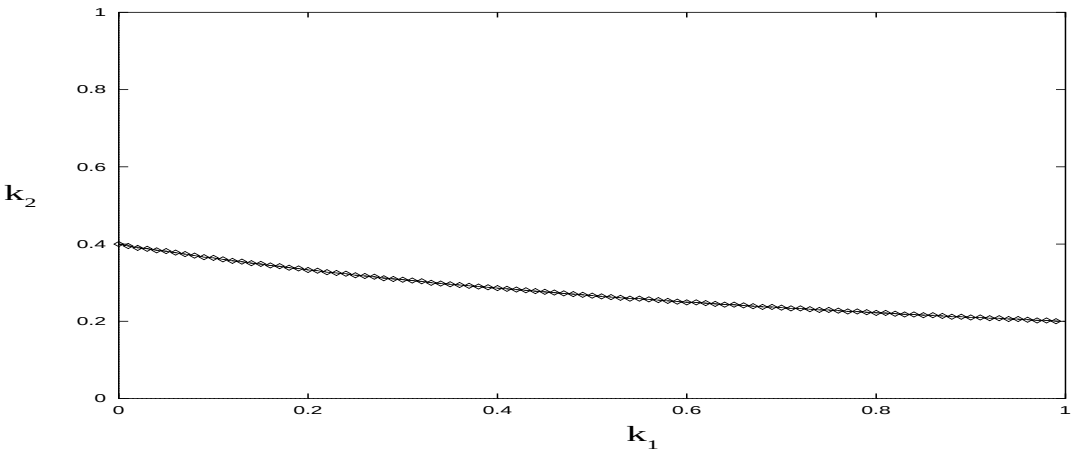


5.8b : $\lambda = 0.5$, $a_1 = 1.0$, $a_2 = 0.1$, $k_0 = 0.5$ and $k_1 = 1.0$. the abscissa shows $k_2$, and the ordinate $a_0$. Theory predicts line at $a_0 = \frac{0.4-k_2}{k_2}$.

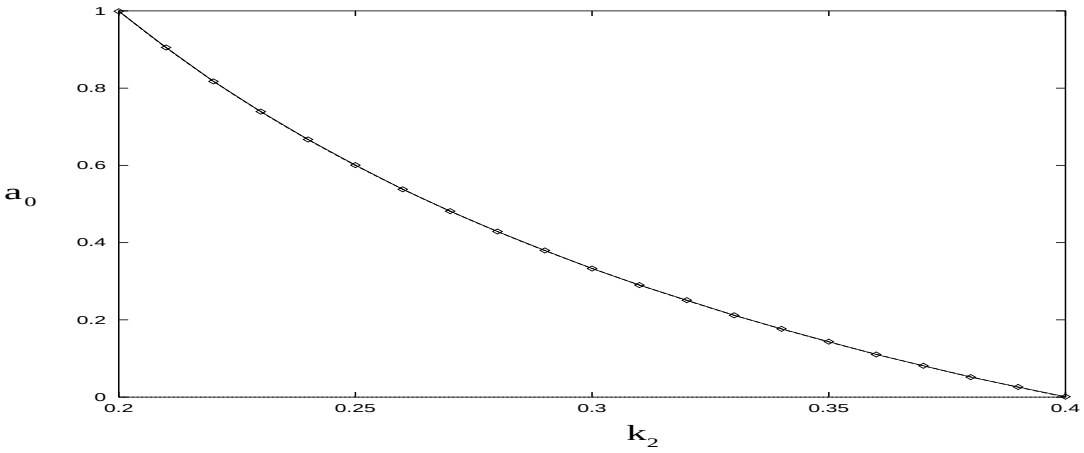


5.8c : $\lambda = 0.5$, $a_2 = 0.1$, $k_0 = 0.5$, $k_1 = 1.0$ and $k_2 = 1.0$. the abscissa shows $a_1$, and the ordinate $a_0$. Theory predicts line at $a_0 = 0.4 - a_1$.

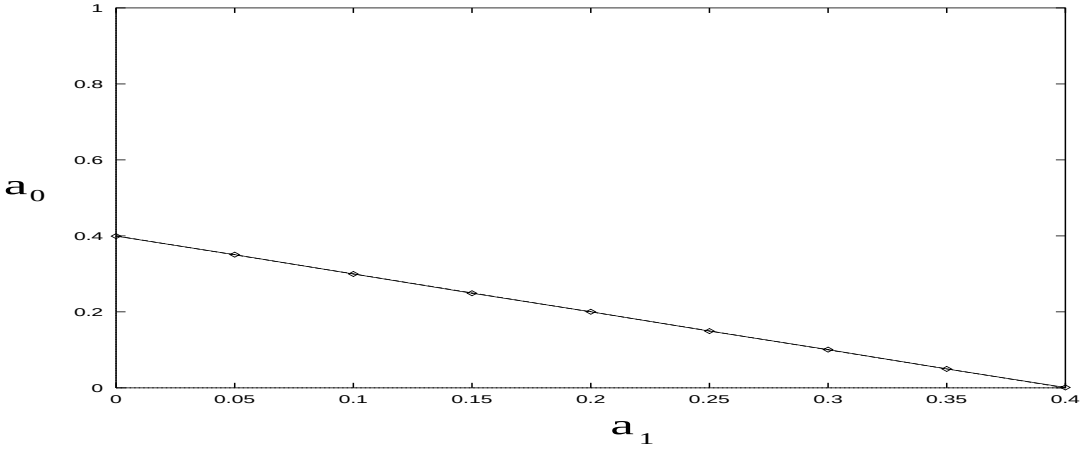


**Figure 5.8**: *Plots of results showing boundary between asymptotic and oscillatory behaviour of Runge Kutta solutions to equations representing third order modulator*

$$|\lambda| < a_0. \tag{5.23}$$

This proves to be the case for both the Runge Kutta solution to the equation and for the direct simulation of the circuit. Typically there is unity feedback in a first order modulator, i.e. $a_0 = 1$, so this implies that for an input greater than $+1$ or less than $-1$ (i.e. the limits of the quantiser) the modulator operates in an asymptotic mode. For inputs between the limits of the quantiser the modulator operates normally. It is a well established rule that the input to a first order sigma delta modulator should not exceed the limits of the quantiser for a successful analogue to digital conversion to take place [58]. This was demonstrated in the previous chapter. Again there is agreement between the fixed point analysis and the results from simulation.

## 5.9 HIGHER ORDER MODULATORS

It would seem that this analysis can be extended to higher order sigma delta modulators. Consider the criteria for non-asymptotic operation of first, second and third order sigma delta modulation:

First order 5.23

$$|\lambda| < a_0$$

Second order 5.12

$$|\lambda| < a_1 + a_0 k_1$$

Third order 5.19

$$|\lambda| < a_2 + a_1 k_2 + a_0 k_2 k_1.$$

It can be shown that for non-asymptotic behaviour of an $n^{th}$ order modulator

$$|\lambda| < I_n \tag{5.24}$$

where

$$I_n = a_{n-1} + k_{n-1} I_{n-1} \tag{5.25}$$

and

$$I_1 = a_0. \tag{5.26}$$

Alternatively this criterion can be written as

$$|\lambda| < \sum_{p=0}^{n-1} a_p \frac{1}{k_p} \prod_{m=p}^{n-1} k_m. \tag{5.27}$$

For stability of an $n^{th}$ order modulator

$$|k_0|, |k_1|, |k_2| ... |k_{n-1}| > 0. \tag{5.28}$$

An inductive proof of this reasoning is now presented. The differential equations representing a $n^{th}$ order sigma delta modulator are

$$\frac{dx_0(t)}{dt} = x_1 - k_0 x_0 - a_0 M \tanh \frac{p x_0(t-\tau)}{M} \tag{5.29}$$

$$\frac{dx_1(t)}{dt} = x_2 - k_1 x_1 - a_1 M \tanh \frac{p x_0(t-\tau)}{M} \tag{5.30}$$

$$\frac{dx_2(t)}{dt} = x_3 - k_2 x_2 - a_2 M \tanh \frac{p x_0(t-\tau)}{M} \tag{5.31}$$

$$\frac{dx_{n-1}(t)}{dt} = \lambda_n - k_{n-1} x_{n-1} - a_{n-1} M \tanh \frac{p x_0(t-\tau)}{M}. \tag{5.32}$$

Assume that the boundary between normal and asymptotic operation of the $n^{th}$ order modulator is

$$\lambda_n = I_n = a_{n-1} + k_{n-1} I_{n-1}. \tag{5.33}$$

Now consider the differential equations representing a $(n+1)^{th}$ order modulator

$$\frac{dx_0(t)}{dt} = x_1 - k_0 x_0 - a_0 M \tanh \frac{p x_0(t-\tau)}{M} \tag{5.34}$$

$$\frac{dx_1(t)}{dt} = x_2 - k_1 x_1 - a_1 M \tanh \frac{p x_0(t-\tau)}{M} \tag{5.35}$$

$$\frac{dx_2(t)}{dt} = x_3 - k_2 x_2 - a_2 M \tanh \frac{p x_0(t-\tau)}{M} \tag{5.36}$$

$$\frac{dx_{n-1}(t)}{dt} = x_n - k_{n-1} x_{n-1} - a_{n-1} M \tanh \frac{p x_0(t-\tau)}{M} \tag{5.37}$$

$$\frac{dx_n(t)}{dt} = \lambda_{n+1} - k_n x_n - a_n M \tanh \frac{p x_0(t-\tau)}{M}. \tag{5.38}$$

It can be seen that an extra equation 5.38 has been added and $\lambda_n$ in equation 5.32 has been replaced by $x_n$ in equation 5.37. $x_n$ in the $(n+1)^{th}$ modulator can be thought of as the input to a $n^{th}$ order modulator. Equating $\lambda_n$ to $x_n$, 5.33 can be rewritten

$$x_n = \lambda_n = I_n \tag{5.39}$$

and substituting this into 5.38 gives

$$\frac{dx_n(t)}{dt} = \lambda_{n+1} - k_n I_n - a_n M \tanh \frac{p x_0(t-\tau)}{M}. \tag{5.40}$$

For stability, search for a fixed point (i.e. set derivatives to zero), and set tanh function to $+1$ as in the analysis of the second order system.

$$0 = \lambda_{n+1} - k_n I_n - a_n \tag{5.41}$$

$$\lambda_{n+1} = k_n I_n + a_n \tag{5.42}$$

This is the same expression as in 5.33. Hence if 5.33 is true for a $n^{th}$ order modulator then it is true for a $n+1^{th}$ order modulator. This chapter has shown that the expression is true for first, second and third order modulators, so it can be stated by induction that it is true for $n^{th}$ order modulators.

## 5.10 GENERALISED SIGMA DELTA MODULATOR

Some configurations of sigma delta modulators involve coefficients in the feedforward path rather than the feedback path [51]. Figure 5.9 shows a generalised second order sigma delta architecture incorporating these variations.

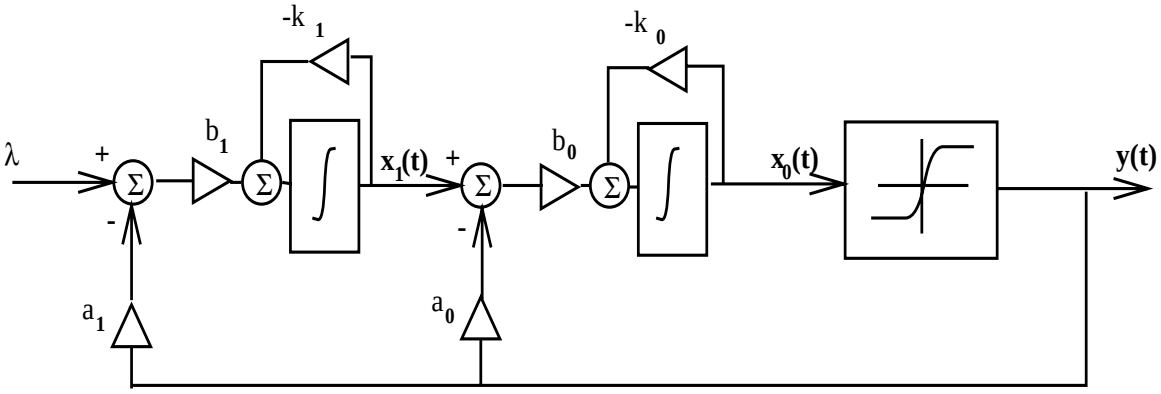


**Figure 5.9**: *Generalised second order sigma delta modulator*

The criterion for non-asymptotic operation of a $n^{th}$ order generalised sigma delta modulator can be written as

$$|\lambda| < \sum_{p=0}^{n-1} a_p \frac{b_p}{k_p} \prod_{m=p}^{n-1} \frac{k_m}{b_m}. \tag{5.43}$$

This expression is formulated in the same manner as Equation 5.27, with the extra feed-forward factors $b_n$ being taken into account. For example, the differential equations describing the generalised second order modulator shown in Figure 5.9 are

$$\frac{dx_0(t)}{dt} = b_0 x_1 - k_0 x_0 - b_0 a_0 M \tanh \frac{p x_0(t-\tau)}{M} \tag{5.44}$$

$$\frac{dx_1(t)}{dt} = b_1 \lambda - k_1 x_1 - b_1 a_1 M \tanh \frac{p x_0(t-\tau)}{M} \tag{5.45}$$

which have a fixed point at

$$\hat{x}_0 = \frac{b_0(b_1\lambda \pm (b_1 a_1 + a_0 k_1))}{k_1 k_0} \tag{5.46}$$

leading to a criterion for non-asymptotic operation of

$$|\lambda| < a_1 + \frac{a_0 k_1}{b_1}. \tag{5.47}$$

Note that $b_0$ does not figure in the expression for non-asymptotic operation. This is because this coefficient acts as a scaling factor on the final state variable – i.e. the input to the quantiser. The output of the quantiser depends only on the sign of the input, not its size, so a scaling factor has no effect on the overall circuit operation. A similar, though more complicated, argument can be made for the absence of the final integrator leakage coefficient $k_0$ from the expression.

## 5.11 DISCUSSION

Investigation of the stability of sigma delta analogue to digital converters has recently centred around the search for limit cycles in the output of the modulator. A $\Sigma\Delta$M is considered stable if limit cycles cannot occur [77] – with the proviso that two types of limit cycle, whilst undesirable, do not necessarily imply instability: when the absence of both noise and an input signal produces a one-zero pattern at half the sampling frequency, and when some offset in the modulator or a d.c. input gives rise to a nearly stable pattern at the modulator output. However there are modes of operation other than instability which can result in limit cycles at the output of the quantiser. In particular we would argue that the asymptotic behaviour described in this chapter has been mistaken for instability in the past. True instability is better defined as when the integrator outputs become unbounded.

It has also been noted [58] that the poles of the transfer function $H(z)$ affect the stability of a sigma delta modulator – this is not usually the case as we generally look to the zeroes of $(1 + H(z))$ for stability criteria. It is likely that what is being labelled as instability due to the limit cycles observed at the output is actually the asymptotic behaviour described in this chapter. It should be remembered that this behaviour was defined by the numerator of the fixed point expression (5.7) rather than the denominator which would generally give the stability condition.

Hein and Zakhor [58] show that the first order modulator is inherently stable for inputs less than the feedback factor (labelled $a_0$ in this work). This result is in agreement with our findings, although we would argue that inputs outside this range cause asymptotic behaviour at the integrator output rather than true instability. They also concur on the effect, or rather lack of effect, of the final feedforward coefficient (which we have labelled $b_0$) on the stability criteria for second order and higher modulators.

This chapter has set out a method of considering the stability and desirable operation of $\Sigma\Delta$M which does not rely on the limitations imposed by the limit cycle approach. It has also gone

some way toward explaining results produced by that approach.

## 5.12 CONCLUSIONS

This chapter has used the differential equations representing $\Sigma\Delta$M to suggest that a stability constraint on a sigma delta modulator is the requirement for non-zero leakage in the integrators. It has been pointed out that this ensures the stability of each integrator and is therefore a result to be expected (it must once more be underlined that in this analysis we are considering analogue integrators rather than discrete ones). However, much work has shown that unstable behaviour can result from other circuit factors, in particular the feedback coefficients. We would argue that at least some cases of what is being labelled unstable behaviour is actually asymptotic behaviour. For true instability a state variable (in this case, the output of an integrator) must become unbounded. In the case of the sigma delta modulator we have shown that this does not happen (except for certain cases with zero integrator leakages as noted). What has been observed is the saturation of a state variable – this is caused either by the variable reaching the asymptotic level defined in this chapter, or reaching the saturation point of the device on its way to the asymptotic level. Of course, whilst this asymptotic behaviour is not true instability, it is still a mode of operation to be avoided in the design and use of sigma delta modulators. This chapter has presented a full description of how and when this behaviour occurs. It should however be noted that there are many circuit imperfections and design criteria missing from our model, and we have only addressed one aspect of the operation of a sigma delta converter.

A stability criterion has been laid down for second order sigma delta modulators. Also a criterion for avoiding asymptotic operation has been derived theoretically and shown to occur via simulation. The results from the direct simulation of a second order sigma delta modulator, the Runge Kutta numerical solution to the differential equations representing second order $\Sigma\Delta$M and the algebraic analysis of these equations were in agreement. This analysis has also been shown to hold true for first and third order modulator structures and has been extended to $n^{th}$ order modulators.

# Chapter 6

# LYAPUNOV EXPONENTS

## 6.1 INTRODUCTION

It was indicated in chapter 4 that, although the sigma delta modulator is a non-linear device, it is not capable of chaotic modes of operation with a constant input, for normal configurations of the circuit. However, what has not yet been addressed is the effect of sigma delta modulation on signals of more practical interest. Of particular concern is how sigma delta modulation may affect a chaotic signal. In this chapter and the next, this issue is investigated, firstly by considering the modulation of a simple non-chaotic input, a sine wave, and then moving on to the more complex situation of a chaotic input. It should be pointed out that a full mathematical description of sigma delta modulation of a moving input has not been achieved in the field [54, 57], and that the work presented in this part of the thesis is primarily based upon experimental results from numerical simulation.

In order to ascribe specific attributes to the sigma delta modulation of a chaotic signal, some measure of chaos is needed. The measure considered in this thesis is the Lyapunov spectrum. This chapter describes a methodology for extraction of Lyapunov exponents from a time series, while the following chapter applies that method to the sigma delta modulated data.

The definition and meaning of an attractor's Lyapunov spectrum has already been discussed in chapter 2, but it is worth repeating the salient points here, before moving on to a description of the algorithm developed at Edinburgh University for determining all the Lyapunov exponents of an attractor from a single time series obtained from that attractor's generating system.

The algorithm is described in sufficient detail to enable the interested reader to implement a version of it without reference elsewhere. A discussion of the factors to be borne in mind when applying the algorithm to a particular time series is included, as are some guidelines on the interpretation of the results produced by it.

The Lyapunov spectra of the attractors were chosen as the tools of analysis as they provide an intuitive feel for the dynamics of the system, and describe the predictability of the data. Other predictability measures exist and were initially considered for utilisation alongside the Lyapunov exponents. However, it became apparent that these measures did not provide any more information about a system's predictability than was already available from the Lyapunov

exponents calculated. Also, the methodology of these measures could lead to ambiguous results in the particular application, i.e. to a chaotic system. The majority of the measures [78,79] are based on an attempt to fit a linear predictive model to an attractor, gradually increasing the extent of that model from a local neighbourhood up to the global phase space. Clearly, this approach quickly becomes meaningless for a chaotic attractor. Alternative approaches have been suggested involving fitting a non-linear predictive model [80], which would initially appear to be an improvement; however, it became apparent that the choice of which particular non-linear model to utilise could severely affect the results. The implication was that a great deal of time would be required to construct such an algorithm, and a great deal of care required to implement it, possibly to no additional benefit. Consequently, it was decided not to continue with the development of these tools, and to rely on the results provided by the Lyapunov exponent extraction algorithm detailed herein, which, in itself, is not the straightforward task it may first appear to be.

## 6.2 LYAPUNOV SPECTRA

The Lyapunov exponents of an attractor are a set of invariant geometric measures which describe, in an intuitive way, the dynamical content of the attractor. In particular, they serve as a measure of how easy it is to perform prediction on the system.

Lyapunov exponents quantify the average rate of convergence or divergence of nearby trajectories, in a global sense. A positive exponent implies divergence, a negative one convergence, and a zero exponent indicates the temporally continuous nature of a flow. Consequently an attractor with positive exponents has positive entropy, in that trajectories that are initially close together move apart over time. The more positive the exponent, the faster they move apart. Similarly, for negative exponents, the trajectories move together. An attractor with both a positive and negative Lyapunov exponents is said to be chaotic.

Mathematically, the Lyapunov spectrum ($\lambda_{i=1..k}$) can be defined by:

$$\lambda_i = \lim_{n\to\infty} \left(\frac{1}{n} \ln(\mathrm{eig}(\prod_{q=0}^{n} T(q))\right) \tag{6.1}$$

where $T$ is the local tangent map as $q$ moves around the attractor [40,41]. As such, it can be seen that the Lyapunov exponents give an average rate of exponential change in the distance between trajectories, in each of a set of orthonormal directions in the embedding space.

If the differential equations defining the system are known, then there are established techniques [32,41] for applying this formula, and the entire Lyapunov spectrum can be calculated. However, as discussed in chapter 4, the sigma delta modulator presents us with a number of problems here.

It was decided to consider the output of the modulator, after decimation, and to calculate the

Lyapunov exponents from there. Unfortunately, the formulation of a set of differential equations describing this process proved unwieldy, and a method for extracting Lyapunov exponents directly from a time series was decided upon.

A number of researchers have recently published algorithms on this subject [32, 33, 44, 45, 81], but on investigation of these algorithms it was found that they either relied upon more *a priori* knowledge of the generating attractor than was necessarily available, or they included so many variable "twiddle factors", that they were essentially unreliable. It became clear that the best course of action was to formulate our own algorithm, based largely on the work of Broomhead and King [44]. What follows is a description of the algorithm developed by Mike Banbrook and myself, for the extraction of the entire Lyapunov spectrum of an attractor from a single time series generated from that attractor. Since carrying out this work, a virtually identical algorithm has been brought to our attention by Darbyshire and Broomhead [40], who offered us much-appreciated advice and discussion during the development of the algorithm.

## 6.3 LYAPUNOV EXPONENTS FROM TIME SERIES

The algorithm for extracting exponents from a time series is complex and requires care in its application and the interpretation of its results. This section describes the algorithm itself and is broken down into a series of subsections, each dealing with a separate process making up the extraction algorithm.

### 6.3.1 Overview

Before describing each step of the algorithm in detail, it is worth discussing the over-all philosophy of the algorithm, so as to more fully appreciate the purpose of each process involved. In order to calculate the Lyapunov exponents of an attractor, we consider the evolution of a sphere of points on the trajectory of that attractor as they move around the phase space. By averaging the rate of convergence or diversion of these points, as the sphere performs an orbit of the attractor, we can arrive at estimates of the attractor's Lyapunov spectrum. Consequently, the first step is to construct a $\mathbf{d}$-dimensional phase space trajectory of the attractor from the one-dimensional time series. The points within the sphere to be considered, or the *neighbourhood*, must then be chosen. This neighbourhood is then evolved, simply by observation of the time series data, and a transformation calculated which, when applied to the initial neighbourhood, produces the evolved neighbourhood. The eigenvalues of this transformation give the expansion or contraction occurring during that evolve step (i.e. the local Lyapunov exponents). Averaging those values across a sufficient expanse of the attractor then results in the global Lyapunov spectrum.

### 6.3.2 Time Series Embedding

A time series measurement from a system is, loosely speaking, a measurement of only one particular dimension of that system. The initial problem, therefore, is to reconstruct the full dynamics of the system from that one dimension. The most common way of doing this is to use Takens' method of delays [35].

Simply stated, this involves moving a window of length $w$ through the data, and taking each snap-shot seen in the window as a row of a $w$-column matrix. That is, for a time series

$$x(t) = (x_0, x_1, x_2, x_3, \ldots x_i, \ldots) \tag{6.2}$$

the reconstructed trajectory matrix takes the form

$$\mathbf{X} = \begin{pmatrix} x_0 & x_1 & x_2 & \ldots & x_{w-1} \\ x_1 & x_2 & x_3 & \ldots & x_w \\ x_2 & x_3 & x_4 & \ldots & x_{w+1} \\ \vdots & & & & \end{pmatrix}. \tag{6.3}$$

Takens showed that such a matrix exhibits the general dynamics of the original $d$-dimensional system if $w \geq 2d + 1$. Careful choice of the delay time, i.e. the sampling period between successive values of $x_i$, improves the results by, in effect, opening up the attractor.

For clean data, this method is often sufficient, however its performance in conjunction with the algorithms for extracting Lyapunov spectra is severely curtailed by the presence of noise on the signal. The method of singular value decomposition (*svd*) reduction described by Broomhead and King [37] addresses this problem, as well as providing information about the number of linear independent dimensions of the attractor under construction.

The *svd* reduction method involves an analysis of the number of degrees of freedom in the data, which is equivalent to the dimension of the phase space containing the dynamical information. The data are projected onto a phase space defined by the singular vectors of the data, which can then be partitioned into a signal subspace and a noise subspace.

A time delay embedding is first carried out, producing a $N \times w$ trajectory matrix $\mathbf{X}$, where the window length $w$ (i.e. the number of columns in $\mathbf{X}$) is chosen to be much greater than the expected dimension of the attractor. This matrix is then factorised into its singular values

$$\mathbf{X} = \mathbf{S}\mathbf{\Sigma}\mathbf{C}^T \tag{6.4}$$

where $\mathbf{\Sigma}$ is a diagonal matrix containing the singular values of $\mathbf{X}$ with the ordering $|\sigma_1| \geq |\sigma_2| \geq |\sigma_3| \geq \ldots \geq |\sigma_n| \geq 0$, and $\mathbf{S}$ and $\mathbf{C}$ are matrices of the singular vectors associated with $\mathbf{\Sigma}$.

The singular vectors $\underline{s}_i$ comprising $\mathbf{S}$ are the eigenvectors of the *structure matrix*, $\mathbf{\Theta} = \mathbf{X}\mathbf{X}^T$. The singular vectors $\underline{c}_i$ comprising $\mathbf{C}$ are the eigenvectors of the *covariance matrix*, $\mathbf{\Xi} = \mathbf{X}^T\mathbf{X}$. The singular values in $\mathbf{\Sigma}$ are the square roots of the eigenvalues of either $\mathbf{\Xi}$ or $\mathbf{\Theta}$ (the structure matrix and the covariance matrix have the same eigenvalues). Rewriting Equation 6.4,

$$\mathbf{\Sigma} = \mathbf{S}^T\mathbf{X}\mathbf{C} \tag{6.5}$$

facilitates the calculation of these singular values.

Since the singular values contained in $\mathbf{\Sigma}$ are the root mean square projections onto the basis vectors, the number of non-zero values in $\mathbf{\Sigma}$ should give the number of degrees of freedom in $\mathbf{X}$. Noise on the data, however, will generate spurious degrees of freedom, evident as extra non-zero values in $\mathbf{\Sigma}$. It is theoretically possible to identify these extra values from a plot of the singular values of $\mathbf{X}$, since they will be of the same order of magnitude, and of less magnitude than the singular values pertaining to the signal. A plot of the form shown in Figure 6.1 is produced, and the noise floor is apparent. Hence a measure of the dimension of the signal is achieved and labelled $\mathrm{d}$.

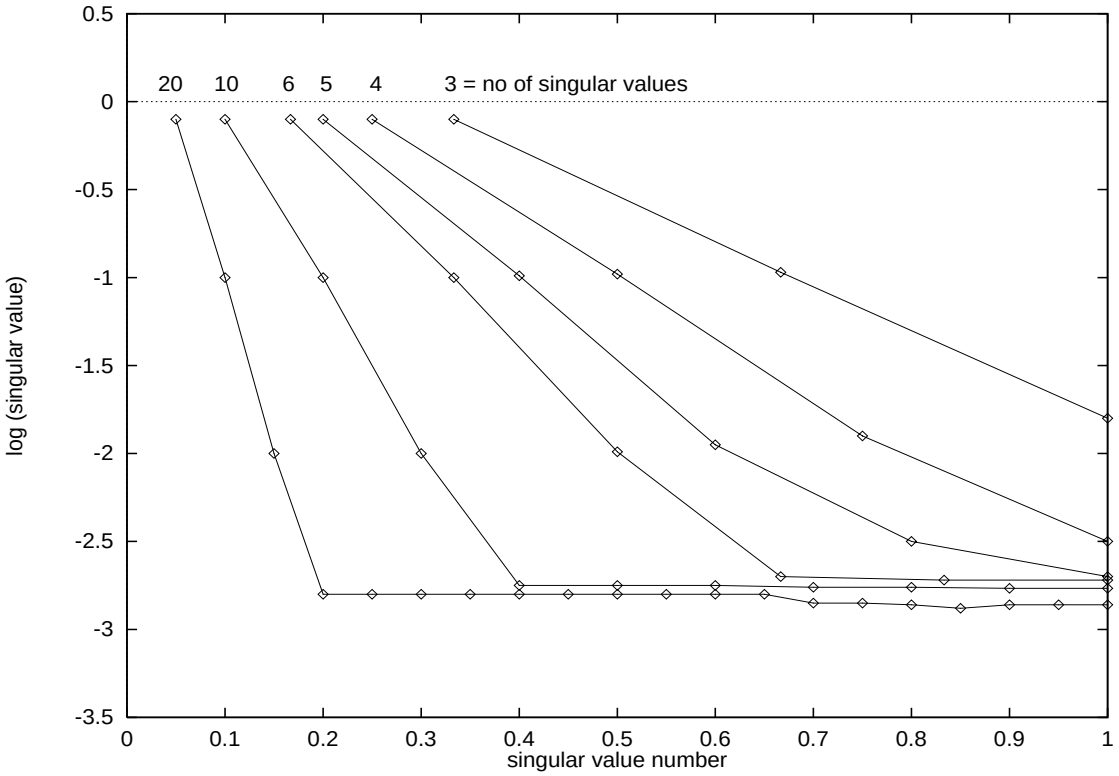


**Figure 6.1**: *Example of results from singular value reduction of data. The three degrees of freedom in time series data generated from the Lorenz system can clearly be seen above the noise floor for a range of embedding dimensions. The data was generated at floating point precision, and analysed at double floating point precision.*

It should be noted that this process is reliant on choosing an appropriate sampling rate for the data (generally taken as the Nyquist frequency). Also, for data generated artificially, from a

set of differential equations for example, no noise floor will be apparent since the precision of the data in the time series will be equal to the precision of the calculation.

The embedding space has now been partitioned into a $\mathsf{d}$-dimensional signal subspace and its orthogonal complement, the $(w - \mathsf{d})$-dimensional noise subspace. The dynamical information of interest is contained within the signal subspace, so it is now desirable to reduce the $w$-dimensional trajectory matrix $\mathbf{X}$ to a $\mathsf{d}$-dimensional reduced trajectory matrix $\hat{\mathbf{X}}$. In effect, what this achieves is a separation of the signal from out of band noise. Any dynamical information due to the signal that is contained within the noise subspace is inextractable due to the noise dominance. As with any technique in this field, if the noise floor is higher than amplitude variations due to the system dynamics in one time step, then this dynamical information will be thrown out with the noise. This places obvious requirements on both the sampling time and, for measured real-world signals, the accuracy of the measurement. This latter point is at the very heart of this thesis and will be returned to at length.

The reduced trajectory matrix $\hat{\mathbf{X}}$ is calculated from

$$\hat{\mathbf{X}} = \mathbf{X}\mathbf{C}_{(\mathsf{d})} \tag{6.6}$$

where $\mathbf{C}_{(\mathsf{d})}$ consists of the first $\mathsf{d}$ columns of $\mathbf{C}$. Remember that $\mathbf{C}$ contains the ordered eigenvectors of the covariance matrix $\Xi$. $\hat{\mathbf{X}}$ is thus a $\mathsf{N} \times \mathsf{d}$ matrix, containing a reduced trajectory representing the noise-reduced dynamics of the system under study, where $\mathsf{N}$ is the number of points on the trajectory, and $\mathsf{d}$ is the perceived dimension of the attractor.

### 6.3.3 Choosing The Neighbourhood

In order to calculate the Lyapunov exponents of the attractor, an average of the local Lyapunov exponents is taken for a number of revolutions of the attractor. To achieve this, we consider the evolution of a $\mathsf{d}$-dimensional hyper-sphere as it traverses the trajectory. First, we must define how the points within that $\mathsf{d}$-dimensional hyper-sphere are chosen.

If the time step to be considered is sufficiently small, then we can consider the evolution of our sphere to be a linear process over that time step. However, for this to be the case, the radius of the sphere itself must be small so that it does not contain points outside the local linear space. This radius, $\epsilon$, is one of the 'twiddle factors' of the algorithm, which will be discussed later in this chapter, but for now consider $\epsilon$ to be of the order of 3% of the attractor's largest radius [44].

It is a simple matter to construct a *neighbourhood matrix* $\mathbf{B}$, containing all the points within the $\epsilon$-radius hypersphere. First, consider a *neighbourhood set* $\mathbf{\Gamma}_0$

$$\mathbf{\Gamma}_0(\underline{x}_0, \epsilon) = (k \in J : \epsilon > |\ \underline{x}_k - \underline{x}_0\ |) \tag{6.7}$$

where $\underline{x}_n$ represents the $n$th row of matrix $\hat{\mathbf{X}}$ and $J \subseteq [1, N - a]$ such that all points will be further away from the end of the time series than the number of evolutions $a$ to be carried out. $\mathbf{\Gamma}_0$ thus contains a list of the row numbers of $\hat{\mathbf{X}}$ corresponding to points within a $\epsilon$-radius hypersphere centred on $\underline{x}_0$.

The neighbourhood matrix $\mathbf{B}_0$ can now be constructed as a series of rows defined from

$$(\underline{x}_k - \underline{x}_0 : k \in \mathbf{\Gamma}_0(\underline{x}_0, \epsilon)) \tag{6.8}$$

again $\underline{x}_n$ represents the $n$th row of matrix $\hat{\mathbf{X}}$. $\mathbf{B}_0$ contains the vector distance to each point within the $\epsilon$-radius hypersphere from the centre.

However, in practice, it is possible to achieve better results from considering a $d$-dimensional hyper-annulus, rather than a hyper-sphere. This is due to the difficulty in measuring the contraction between two points which start very close together, particularly in the presence of noise; if a minimum radius $\epsilon_m$ is also set, then any point will begin the evolution period at least $\epsilon_m$ away from the centre and the measurement of its movement toward the centre is more apparent. Consequently, if the neighbourhood matrix is chosen to represent a hyper-annulus, rather than a sphere, increased accuracy in the calculation of the negative Lyapunov exponents results.

Equation 6.7 now becomes

$$\mathbf{\Gamma}_0(\underline{x}_0, \epsilon, \epsilon_m) = (k \in J : \epsilon > |\ \underline{x}_k - \underline{x}_0\ | > \epsilon_m) \tag{6.9}$$

with the rows of $\mathbf{B}_0$ being chosen from this new neighbourhood set as before ($\underline{x}_n$ represents the $n$th row of matrix $\hat{\mathbf{X}}$). It is generally sufficient to choose $\epsilon_m$ to be higher than the level of noise on the signal, as measured by the $(d + 1)$th singular value, calculated during the *svd* reduction.

As the neighbourhood moves around a chaotic attractor, the points within the hyper-annulus eventually become separated, as the non-linear aspect of long term evolution takes effect (or, to put it differently, there goes the neighbourhood!). Consequently it is necessary to reconstruct a new neighbourhood after a number of evolve steps. As with the radius, the number of evolve steps carried out between reinitialisations of the neighbourhood is a coefficient that can be varied in order to achieve some confidence in the results. This is discussed in a later section.

### 6.3.4 Calculating The Tangent Maps

The next stage is to estimate the *tangent map* $\mathbf{T}_i$ which operates on the neighbourhood matrix $\mathbf{B}_i$ to produce the evolved neighbourhood matrix $\mathbf{B}_{i+a}$. The eigenvalues of this tangent map give the local Lyapunov exponents at that point in phase space, in that $\mathbf{T}_i$ defines the linear transformation from $\mathbf{B}_i$ to $\mathbf{B}_{i+a}$.

The tangent map $\mathbf{T}_0$ for the first $a$ evolve steps from the initial neighbourhood $\mathbf{B}_0$ is estimated from a series of matrix operations $\tau_k$ on each point in the neighbourhood. So

$$\underline{b}_{a_k} = \tau_k \underline{b}_{0_k} \tag{6.10}$$

where $\underline{b}_{0_k}$ is the kth row of $\mathbf{B}_0$. Combining each of these $\tau_k$ gives an expression for the transformation of the whole neighbourhood

$$\mathbf{B}_a^T = \mathbf{T}_0 \mathbf{B}_0^T \tag{6.11}$$

which can be rewritten as

$$\mathbf{B}_a = \mathbf{B}_0 \mathbf{T}_0^T. \tag{6.12}$$

Note that, in solving this equation, $\mathbf{T}_0$ is an approximation to the transformation of any particular point in the neighbourhood, based upon an assumption of a linear transformation throughout the neighbourhood. Figure 6.2 shows this graphically.

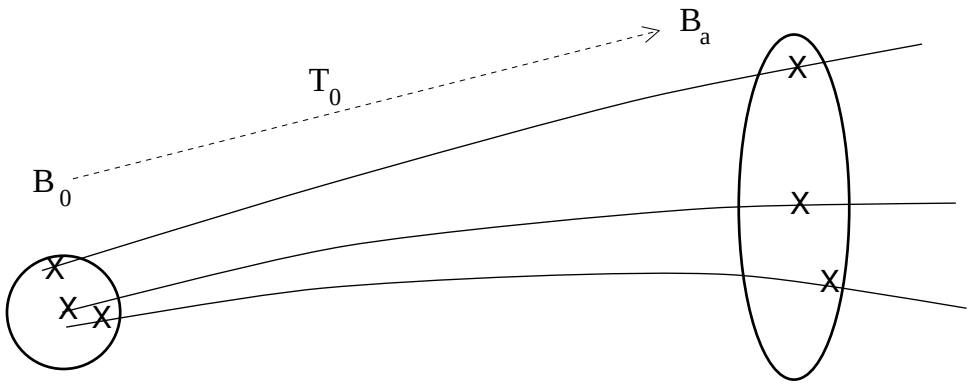


**Figure 6.2**: *Evolution of hypersphere for $a$ time steps around attractor.*

The evolved neighbourhood matrix $\mathbf{B}_a$ is constructed by taking the values of $\underline{x}(t)$ $a$ steps further on from those points contained within $\mathbf{B}_0$. This is achieved by adding $a$ to each of the row numbers contained in $\mathbf{\Gamma}_0$, to produce $\mathbf{\Gamma}_a$, and then constructing the evolved neighbourhood matrix $\mathbf{B}_a$ from this evolved neighbourhood set in the same manner as shown in 6.8.

In order to calculate $\mathbf{T}_0$ from 6.12, the inverse of $\mathbf{B}_0$ is needed, i.e.

$$\mathbf{B}_0^{-1}\mathbf{B}_a = \mathbf{T}_0^{\top} \tag{6.13}$$

but, in general, the inverse of $\mathbf{B}_0$ does not exist. Moore and Penrose [82] have described the *pseudo-inverse* of a matrix, however, and this is the method adopted here. The left pseudo-inverse of $\mathbf{B}$, represented as $\mathbf{B}^+$, has the following properties

$$\mathbf{B}^+\mathbf{B} = \mathbf{I} \qquad\qquad \mathbf{B}\mathbf{B}^+ \neq \mathbf{I}. \tag{6.14}$$

It should be noted that for a successful construction of the pseudo-inverse $\mathbf{B}$ must be full rank, which is always the case in our problem as each line of $\mathbf{B}$ contains a phase space vector.

Thus 6.12 can be written as

$$\mathbf{B}_0^+\mathbf{B}_a = \mathbf{T}_0^{\top} \tag{6.15}$$

and the desired tangent map $\mathbf{T}_0$ can be estimated.

The left pseudo-inverse of $\mathbf{B}_0$ is constructed from its singular value decomposition

$$\mathbf{B}_0 = \mathbf{S}_0\mathbf{\Sigma}_0\mathbf{C}_0^{\top} \tag{6.16}$$

where $\mathbf{S}_0$,$\mathbf{\Sigma}_0$ and $\mathbf{C}_0$ are calculated as described in the subsection on time series embedding. Specifically, the columns of $\mathbf{S}_0$ contain the eigenvectors of the structure matrix $\mathbf{\Theta}_0 = \mathbf{B}_0\mathbf{B}_0^{\top}$, and the columns of $\mathbf{C}_0$ contain the eigenvectors of the covariance matrix $\mathbf{\Xi}_0 = \mathbf{B}_0^{\top}\mathbf{B}_0$. $\mathbf{\Sigma}_0$ is a diagonal matrix containing the square roots of the eigenvalues of $\mathbf{\Theta}_0$ or $\mathbf{\Xi}_0$, either giving the same values. However, when used in conjunction with some techniques for calculating eigenvectors and eigenvalues, it is not clear which root to take of each eigenvalue, so in practice, $\mathbf{\Sigma}_0$ is calculated from

$$\mathbf{\Sigma}_0 = \mathbf{S}_0^{\top}\mathbf{B}_0\mathbf{C}_0 \tag{6.17}$$

bearing in mind that, since $\mathbf{S}_0$ and $\mathbf{C}_0$ are matrices of normalised eigenvectors calculated from originally symmetric matrices, they are orthogonal, so multiplication by their transpose results in the unit matrix. The left pseudo-inverse of $\mathbf{B}_0$ is defined by

$$\mathbf{B}_0^+ = \mathbf{C}_0\mathbf{\Sigma}_0^+\mathbf{S}_0^{\top} \tag{6.18}$$

where $\mathbf{\Sigma}_0^+$ is the pseudo-inverse of $\mathbf{\Sigma}_0$, calculated simply by replacing each non-zero element of the diagonal matrix $\mathbf{\Sigma}_0$ with its reciprocal. Note that the pseudo-inverse of such a diagonal matrix is also its actual inverse, if it has no zero elements in the diagonal.

From 6.13, the tangent map $\mathbf{T}_0$ can now be calculated, giving the local linear dynamics at that point in the attractor. In order to assess the global dynamics, this process must be repeated across a sufficient expanse of the attractor and the local exponents averaged to give the global exponents. Before considering the technique that achieves this, however, an improvement to our tangent map calculation is described.

### 6.3.5 Applying Local Noise Reduction To Tangent Mapping

It has been noted [40, 83] that the straightforward method of constructing the tangent maps outlined in the previous subsection is not very robust to noise. Indeed, adding as little as 1% noise to the signal causes problems in estimating these tangent maps. This may be due to the fact that the method involves an estimate of the local tangent map based on an assumption of a locally linear model, but the *svd* reduction process is an attempt to account for noise on a global level, rather than a local one. Consequently, a local noise reduction routine may show an improvement.

The method suggested by Darbyshire and Broomhead [40] is to utilise a local *svd* reduction at each point of the evolution. This is, in fact, a natural extension of the pseudo-inverse method in that we now consider the tangent spaces mapped onto a set of local bases, which have already been calculated for the construction of the pseudo-inverse. When the trajectory matrix is initially constructed, the time series is embedded in a dimension $\mathfrak{d}$, that is higher than the dimension of the attractor under consideration, $\mathfrak{m}$. The neighbourhood is calculated, as before, in $\mathfrak{d}$ dimensions and is then reduced to the desired $\mathfrak{m}$ dimensions, by means of multiplying it by the first $\mathfrak{m}$ columns of $\mathbf{C}_0$, i.e.

$$\hat{\mathbf{B}}_0 = \mathbf{B}_0 \hat{\mathbf{C}}_0 \tag{6.19}$$

where the hat indicates a reduced matrix. $\mathbf{C}_0$ is the matrix made up of the eigenvectors of the covariance matrix $\mathbf{\Xi} = \mathbf{B}_0^+ \mathbf{B}_0$, and $\hat{\mathbf{C}}_0$ contains the first $\mathfrak{m}$ columns of this matrix. It can be seen that this achieves a local mapping onto the singular vectors, in the same way as the global reduction was achieved in subsection 6.3.2.

Similarly, the evolved matrix $\mathbf{B}_a$ is reduced to $\mathfrak{m}$ dimensions by multiplying it with the first $\mathfrak{m}$ columns of the $\mathbf{C}$ matrix at the evolved point, i.e.

$$\hat{\mathbf{B}}_a = \mathbf{B}_a \hat{\mathbf{C}}_a. \tag{6.20}$$

The tangent mapping $\hat{\mathbf{T}}_0$ is constructed in the same way as before, so

$$\hat{\mathbf{B}}_a = \hat{\mathbf{B}}_0 \hat{\mathbf{T}}_0^{\mathrm{T}} \tag{6.21}$$

although in this case, since the neighbourhood matrix ought to be full rank, a true inverse should exist. In practice, where a true inverse exists, the pseudo-inverse algorithm finds it anyway. It is therefore safer to continue to use the pseudo-inverse routine, in case the dimension of the reduced neighbourhoods has been over-estimated and the matrices are not actually full rank.

### 6.3.6 Averaging The Exponents

We have now achieved an algorithm for calculating a string of tangent maps for a point evolving around an attractor. The final hurdle is to formulate an expression for averaging the contraction and expansion of the phase space represented therein. Note that in the section on applying local noise reduction, the tangent maps were labelled with a hat; this was for consistency within that section and the continued use of the hat (representing the locally reduced phase space) is no longer of importance. Consequently, we revert to labelling the string of tangent maps as $\mathbf{T}_0, \mathbf{T}_1, \mathbf{T}_2 \ldots \mathbf{T}_k \ldots$ hereafter.

The method for formulating the global Lyapunov exponents from the local mappings is taken from the work of Eckman and Ruelle [84], which in turn is based upon the QR-factorisation technique used by Johnson, Palmer and Sell (later described in [85]) in proving the multiplicative ergodic theorem.

First, we need to consider what a QR-factorisation is and how it is achieved. In general, any matrix $\mathbf{A}$ can be written

$$\mathbf{A} = \mathbf{QR} \tag{6.22}$$

where $\mathbf{Q}$ has orthogonal columns and $\mathbf{R}$ is a square upper-right triangular matrix with positive values on the diagonal. The method for constructing these matrices is best described in a series of steps [86]:

i) Write $\mathbf{A}$ as a series of columns $\mathbf{A} = [\underline{a}_1, \underline{a}_2, \ldots, \underline{a}_m]$.

ii) If $\underline{a}_1 = 0$, set $\underline{q}_1 = 0$; otherwise set

$$\underline{q}_1 = \frac{\underline{a}_1}{\sqrt{(\underline{a}_1^* \underline{a}_1)}}.$$

iii) For each $k = 2, 3, \ldots, m$

$$\underline{y}_k = \underline{a}_k - \sum_{i=1}^{k-1} (\underline{q}_i^* \underline{a}_k) \underline{q}_i.$$

iv) If $\underline{y}_k = 0$, set $\underline{q}_k = 0$; otherwise set

$$\underline{q}_k = \frac{\underline{y}_k}{\sqrt{(\underline{y}_k^* \underline{y}_k)}}.$$

v) Build up $\mathbf{Q}$ from the columns $\mathbf{Q} = [\underline{q}_1, \underline{q}_2, \ldots, \underline{q}_m]$.

vi) $\mathbf{R}$ is calculated as $\mathbf{R} = \mathbf{Q}^T \mathbf{A}$, since $\mathbf{Q}$ is an orthogonal matrix.

This method is, in effect, the result of applying a Gram Schmidt process to each of the columns of $\mathbf{A}$.

Now this QR-factorisation is applied to the problem at hand. We start with a purely arbitrary orthogonal matrix, which we label $\mathbf{Q}_0$ for reasons which will become apparent; the columns of this matrix we take as the basis for the initial tangent space. For simplicity's sake, we take this arbitrary matrix to be the identity matrix.

$$\mathbf{Q}_0 = \mathbf{I}_m \tag{6.23}$$

By applying our first tangent map $\mathbf{T}_1$ to this basis set we construct the set of tangent vectors at the next evolved point on the trajectory, $\mathbf{T}_1 \mathbf{Q}_0$. Carrying out a QR-factorisation on this matrix, produces an orthogonal set of basis vectors for the evolved tangent space, i.e.

$$\mathbf{T}_1 \mathbf{Q}_0 = \mathbf{Q}_1 \mathbf{R}_1 \tag{6.24}$$

where $\mathbf{Q}_1$ is the new set of basis vectors. This process is repeated through the string of tangent maps, giving a string of orthogonalised basis vectors as the attractor evolves. So, in general

$$\mathbf{T}_k \mathbf{Q}_{k-1} = \mathbf{Q}_k \mathbf{R}_k. \tag{6.25}$$

Now, in order to trace the evolution of the attractor, the tangent maps $\mathbf{T}_1$, $\mathbf{T}_2 \ldots$ need to be multiplied together, i.e.

$$\mathbf{T}_{1 \to n} = \mathbf{T}_n \mathbf{T}_{n-1} \ldots \mathbf{T}_2 \mathbf{T}_1 \tag{6.26}$$

but by rewriting equation 6.25 as

$$\mathbf{T}_k = \mathbf{Q}_k \mathbf{R}_k \mathbf{Q}_{k-1}^T \tag{6.27}$$

and substituting this into equation 6.26

$$\mathbf{T}_{1\to n} = \mathbf{Q}_n\mathbf{R}_n\mathbf{Q}_{n-1}^{\mathsf{T}}\mathbf{Q}_{n-1}\mathbf{R}_{n-1}\mathbf{Q}_{n-2}^{\mathsf{T}}\ldots\mathbf{Q}_2\mathbf{R}_2\mathbf{Q}_1^{\mathsf{T}}\mathbf{Q}_1\mathbf{R}_1\mathbf{Q}_0^{\mathsf{T}} \tag{6.28}$$

the expression can be written

$$\mathbf{T}_{1\to n} = \mathbf{Q}_n\mathbf{R}_n\mathbf{R}_{n-1}\ldots\mathbf{R}_2\mathbf{R}_1 \tag{6.29}$$

since the $\mathbf{Q}$ matrices are orthogonal and $\mathbf{Q}_0$ has been chosen to be the identity matrix. It is evident that the necessary information can be taken directly from the $\mathbf{R}$ matrices as they are calculated. In fact the diagonal entries of the $\mathbf{R}$ matrices contain the relationship between these bases and the evolution of the $\mathbf{Q}$ matrices due to the tangent maps. This means that these diagonal values effectively contain the local Lyapunov exponents, so the global exponents $\lambda_i$ can be calculated from

$$\lambda_i = \lim_{n\to\infty}\frac{1}{n}\sum_{j=1}^{n}\log(\mathbf{R}_j)_{ii} \tag{6.30}$$

where $n$ is the number of evolve steps carried out.

## 6.4 USING THE ALGORITHM

The previous section described in detail our algorithm for computing the Lyapunov exponents of an attractor from a single time series, however, due to the complexity of the algorithm, this is not the whole story. Care must be taken both in the choice of parameters used when applying the algorithm to a particular time series, and in the interpretation of the results derived from it. In this section an artificially generated Lorenz time series is used to explore the application of the algorithm, and to demonstrate the process of gathering information about a time series under study.

The Lorenz system [25] was chosen because it is easy to generate, and its dynamics are well-known, including the values of its Lyapunov exponents. The differential equations are

$$\dot{X} = \sigma(Y - X) \qquad \dot{Y} = rX - Y - XZ \qquad \dot{Z} = -bZ + XY \tag{6.31}$$

with the parameters $\sigma = 16.0$, $r = 40.0$ and $b = 4.0$. Figure 6.3 shows the attractor under consideration. It is generally accepted that this attractor has a correlation dimension of 2.06, and three Lyapunov exponents of size $+1.37$, $0$ and $-22.37$ [32].

The results from the *svd* reduction of the Lorenz time series were shown previously in Figure 6.1 and imply that we need to search for three Lyapunov exponents. This is in agreement with the value of the correlation dimension, since it is necessary to round up this figure to the next integer to give the number of dimensions to be considered (i.e. correlation dimension of 2.06 implies three exponents). Note however that, for a measured time series, this figure is not

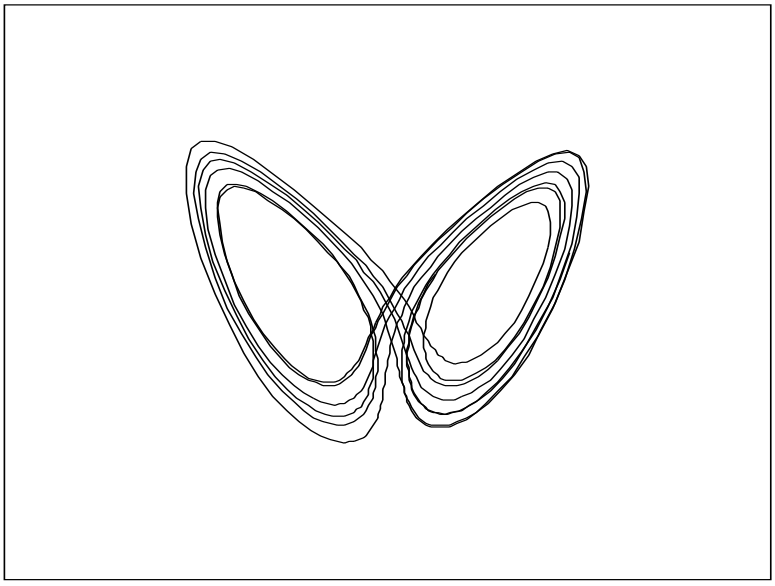

**Figure 6.3**: *The Lorenz attractor*

initially known; also the method of determining the dimension from the *svd* reduction does not always give clear results. In practice, a range of methods for determining the dimension of the signal should be utilised, including, but not necessarily limited to, measuring the correlation dimension [30] and considering the *svd* reduction.

It has been intimated that there are a number of parameters to be chosen when applying the Lyapunov exponent algorithm to a time series. In fact, the best approach is to vary each of these parameters across a suitable range of values and then to assimilate the results in some way. The main parameters of interest, or, if you prefer, 'twiddle factors', are:

- outer radius of hyper-annulus. It has been recommended [45] that this should be set to around 3% of the overall radius of the attractor. This is a good value to start at, but it is well worth trying a range of radii around this value, since not all attractors will yield optimum results at this radius. Too small a radius will make it difficult to measure contraction of the phase space and will affect the negative exponents. Too large a radius will cause the local neighbourhood to cover a volume which can not be approximated by the linear model; it may also include points from nearby arms of the attractor moving in a completely different direction.

- number of neighbours. In essence, this parameter is similar to the size of radius, in that the more neighbours searched for, the greater the radius necessary to find them. However, including more points within the same linear space can lead to a better approximation of the local tangent maps since a better average can be achieved.

- size of *svd* window. In the presence of noise, a larger window is recommended, as it reduces the noise content of the embedded attractor. Indeed, since the *svd* is used for a global embedding, it is advisable to use a window length approximately equal to a single

revolution of the attractor. However, it should be noted that a longer window appears to curtail the calculation of the negative exponent [40].

- dimension. In practice, it is worth analysing the data for a range of dimensions higher than the actual (or estimated) dimension of the attractor. This results in more accurate values for the 'true' exponents, but introduces an extra spurious exponent for each additional dimension. Identifying which exponents are true, and which are spurious, is an ongoing problem however, to which no method known to the author offers an unambiguous solution.

- the number of steps between reinitialisations of the neighbourhood. A reinitialisation must occur before the neighbourhood becomes unwieldy in size, but it is often worth postponing this as long as possible in order to see a greater expansion or contraction. As a rule of thumb, implementing a check that, at the end of the set of evolve steps between re-initialisations, the points in the neighbourhood are no more than twice as far from the centre as the original neighbourhood radius has proved effective.

There are further parameters which can and will affect the results: the total number of points on the attractor as a whole (clearly increasing this number increases our knowledge of the attractor but also increases computing time); the number of evolve steps to take, i.e the total number of tangent maps produced (again, the higher the better, but the longer it takes); the size of the inner radius of the hyper-annulus containing the neighbourhood (needs to be higher than the noise level).

It can be seen that applying the Lyapunov exponent algorithm to a time series is not an exercise to be taken lightly. There is really no substitute for becoming intimately familiar with the attractor in question and gaining a good knowledge of how the algorithm behaves under a large range of parameters on the particular time series under study.

### 6.4.1 The Lorenz time series: an example of applying the algorithm

We now devote some time to considering the application of our algorithm for extracting Lyapunov spectra to a time series with known Lyapunov exponents. The time series to be analysed is derived from the Lorenz system.

Consider Figure 6.4 which shows the Lyapunov exponents calculated for the Lorenz time series over a range of values of the *svd* window. The other parameters were set at: number of neighbours = 15; outer radius < 1.0; globally embedded in 7 dimensions and reduced to 3 dimensions by the local *svd* method; 49000 points on attractor at sample time of 0.01; 1000 evolve steps with a reinitialisation after every 8 steps.

The figure reveals that, whereas the program calculates the positive and the zero exponent to

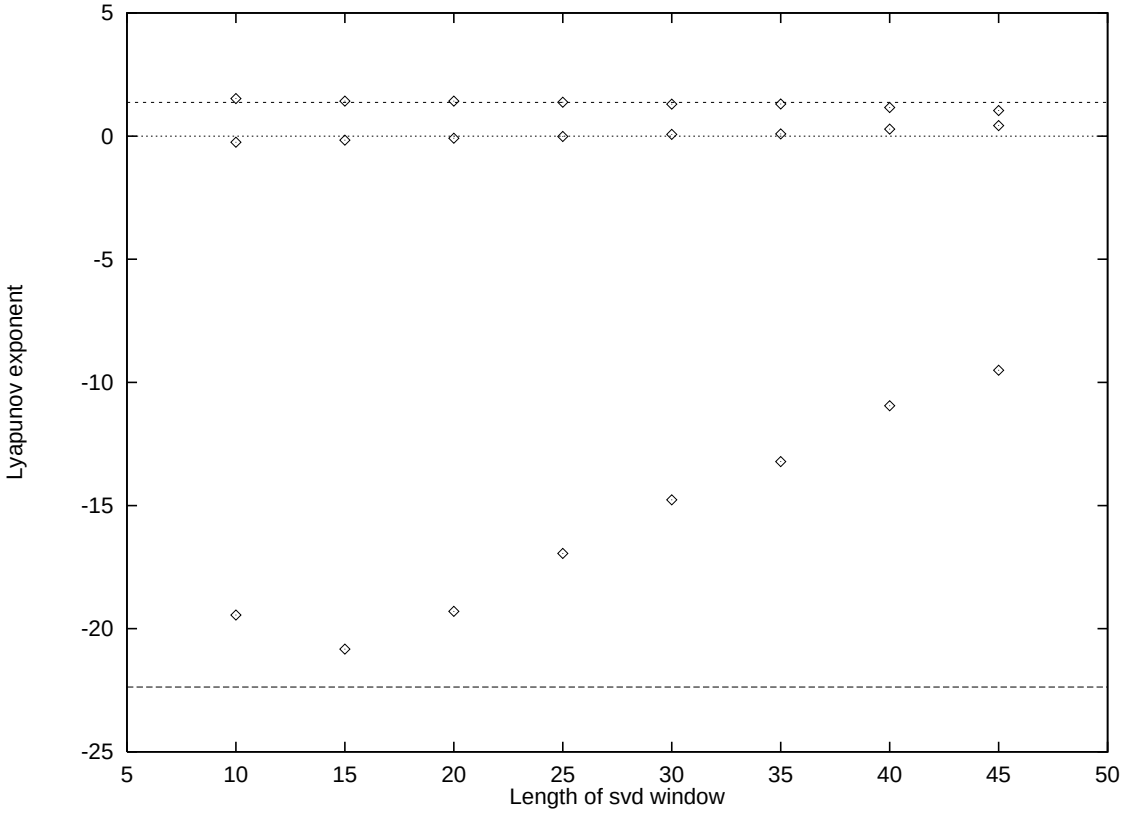


**Figure 6.4**: *Lyapunov exponents of Lorenz time series over a varying window length, with accepted values of* $+1.37$, $0$ *and* $-22.37$ *indicated.*

be reasonably close to the accepted values, the negative exponent is seriously under-estimated. In fact, this is a problem with all algorithms for extracting Lyapunov exponents from a time series that are known to the author (e.g. [40, 87]). The accepted values generally come from a solution of the differential equations that make up the Lorenz system, rather than from analysis of time series. With *a priori* knowledge, it is easy to say that the best results are achieved with a *svd* window size of 15, though, of course, in the case of a measured real-world signal this advance information on the size of the exponents is not available (indeed, if it were, there'd be no point in trying to calculate them). However, the *svd* window size of 15 produces the lowest value of the negative exponent on the plot, and this is our pointer toward further investigation.

Figure 6.5 shows the Lyapunov exponents calculated for this same time series, with the *svd* window fixed at 15, over a range of number of neighbours. All other parameters are as before. The positive and zero exponents are each still calculated with acceptable precision, and the consistency of the negative exponent has improved greatly. In fact, the results are sufficiently consistent that, in the absence of any *a priori* knowledge about the size of the exponents, a value of around $-21.0$ could be attributed to the negative exponent with some confidence. Of course, further tweaking of the parameters could probably result in an even more accurate value here, but, as has been noted, this is only really possible when the correct value is already known.

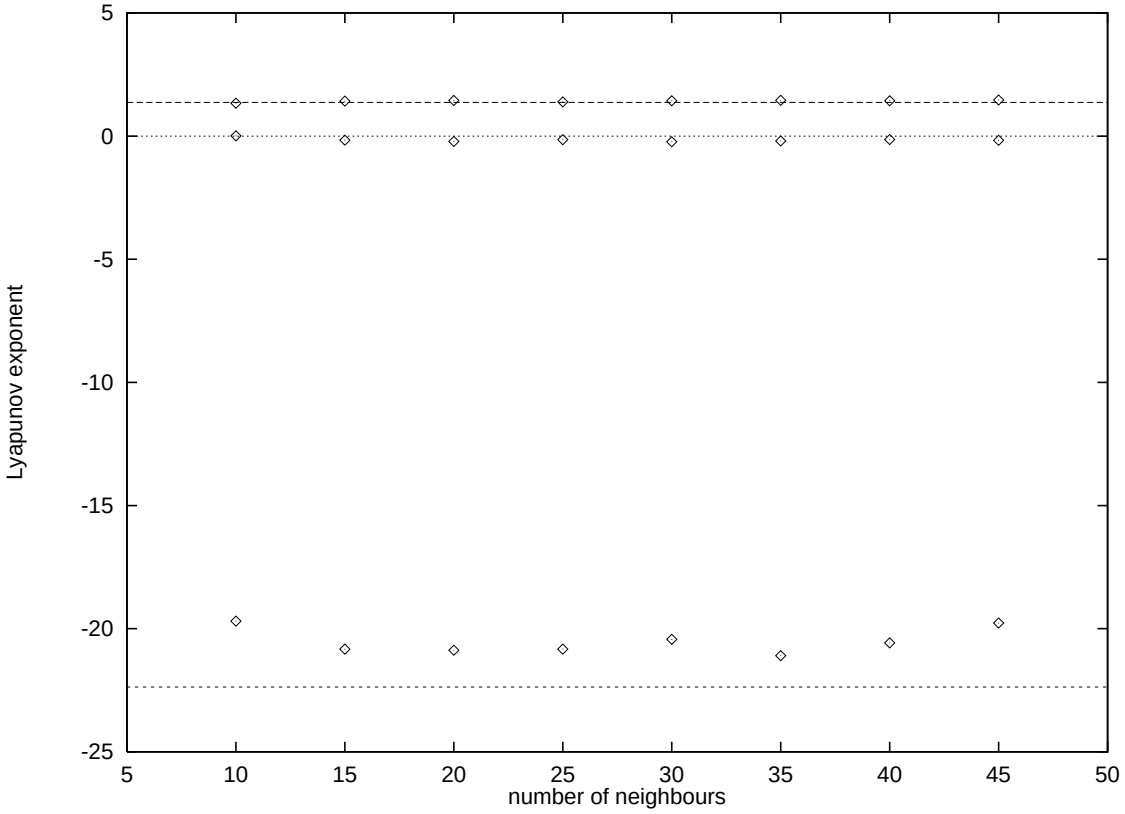


**Figure 6.5**: *Lyapunov exponents of Lorenz time series for a varying size of neighbourhood set, with accepted values of* $+1.37$, $0$ *and* $-22.37$ *indicated.*

The fact that this tweaking of the parameters can affect the results to such an extent, implies that they can be manipulated so that pretty much any result you want can be calculated. To call this a problem would be an understatement, and, in general, the literature on the subject has only considered time series such as Lorenz, where the desired results are already known. This effect becomes far more apparent when analysing a time series with noise on it, which, of course, will be true of any measured time series.

Consider the results given over a range of *svd* window sizes, with all parameters set as in Figure 6.4, for a Lorenz time series with added Gaussian noise of power $0.05$, which is only around $0.35\%$ of the signal.

Figure 6.6 shows that the noise has affected the results considerably, to such an extent that it's not worth marking the negative value of $-22.37$ on the same plot. In the previous case, we took the lowest point on the negative plot and considered a varying size of neighbourhood set for that *svd* window; in this case, however, we take the trough at the *svd* window size of $40$. We won't claim that this decision has not been influenced by the knowledge of the values of exponents sought after, however the fact that the time series under consideration is a flow leads us to search for a zero exponent, and the best zero occurs at a window size of around $40$. In general, it should be known whether or not a measured time series represents a flow, i.e. a continuous system. Also a higher *svd* window size is desirable in the presence of noise, and so

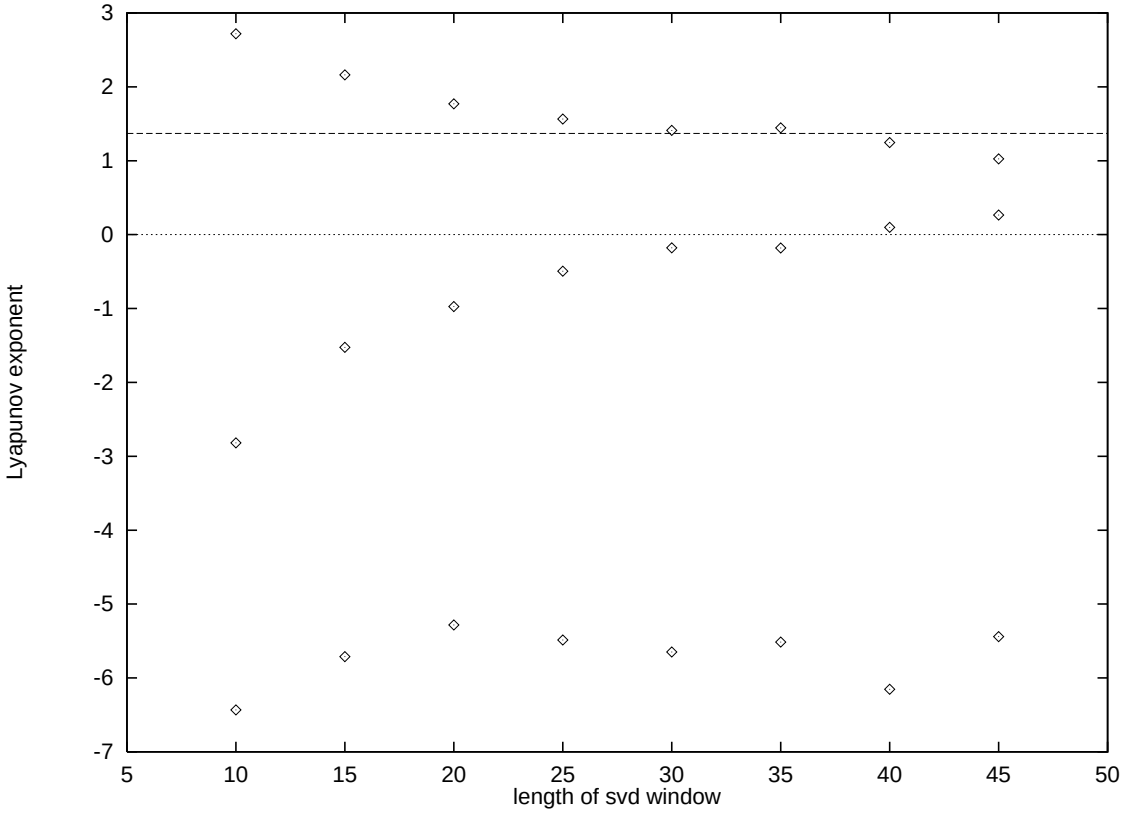


**Figure 6.6**: *Lyapunov exponents of Lorenz time series with added noise for a varying size of svd window, with accepted values of* $+1.37$ *and* $0$ *indicated.*

the lower values can be discarded. The general shape of the plot, along with our knowledge of the exponent values, supports this line of argument.

Figure 6.7 shows the plot for a range of number of neighbours, with a *svd* window size of 40, and all other parameters set as before. Again, it is not at all clear what values to choose as the definitive exponents, and the negative one in particular has been grossly underestimated. It is, however, noticeable that the point on the plot which gives the best zero exponent (a value we expect to see) coincides with the best estimate of the positive exponent. We could continue to try to home in on the accepted values, but, in practice, we'd just end up going around in circles without ever really improving on the plots presented, and certainly without applying much in the way of un-biased logic in achieving such results. It should be noted that all published work on extracting Lyapunov exponents from noisy time series known to the author seem to have met with this same problem, though generally this is not admitted in so many words, with the values being arrived at through tweaking of parameters to bring them closer to the figures that are already known from analysing clean data. What can be said with some confidence is that the presence of noise on the signal has seriously affected the accuracy with which the Lyapunov exponents can be calculated. This is easily apparent when comparing the plots for the clean data (Figures 6.4 and 6.5) with those for the noisy data (Figures 6.6 and 6.7).

That is, in fact, the key to how the Lyapunov exponent algorithm must be used within this

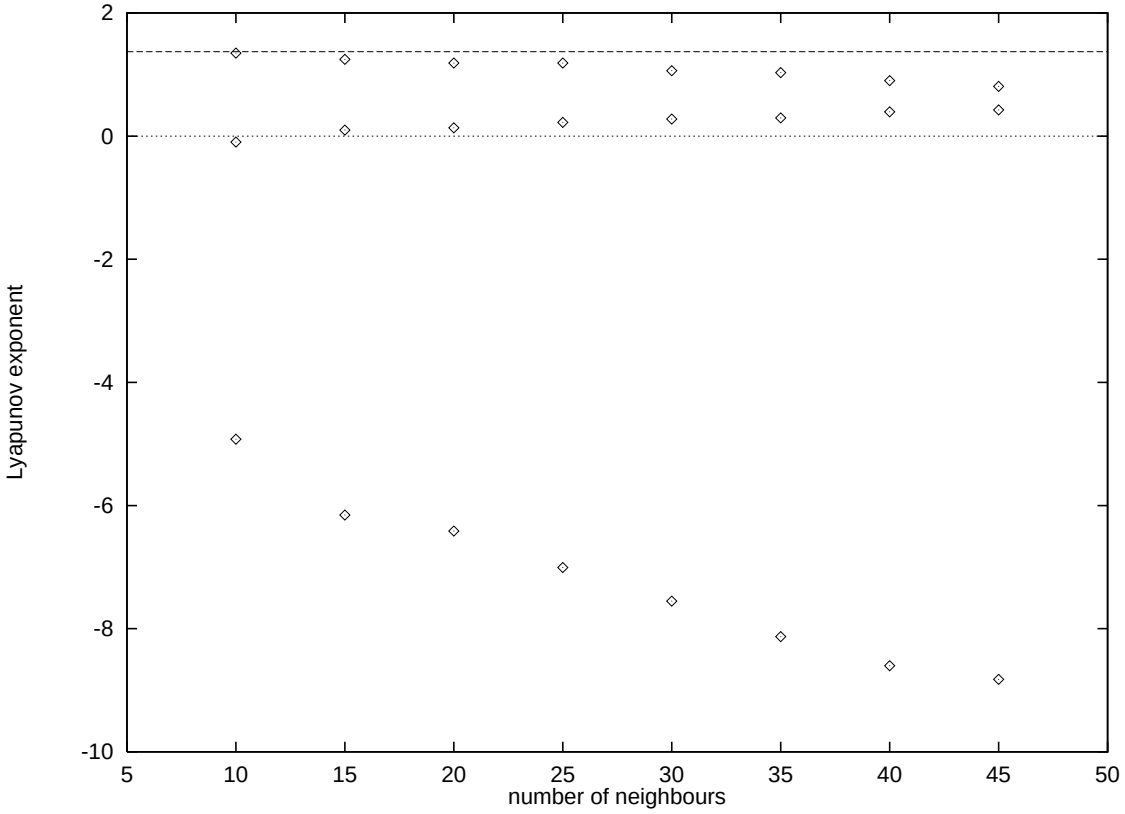


**Figure 6.7**: *Lyapunov exponents of Lorenz time series with added noise for varying number of neighbours, with accepted values of* $+1.37$ *and* $0$ *indicated.*

thesis: as a tool for *comparison*.

## 6.5 DISCUSSION

It is worthwhile at this point taking a step back and considering the aims of this thesis as a whole in relation to what has become apparent about the application of a Lyapunov exponent extraction algorithm to time series. Our ultimate goal is to provide a basis for commenting on the effect sigma delta modulation has on the predictability of a time series, specifically a chaotic time series. Lyapunov exponents ought to be a useful tool in achieving this. We have concluded in chapter 4 that our approach must be to measure Lyapunov exponents directly from the time series. However, we have shown that the presence of noise on the signal under consideration severely curtails the ease with which such exponents may be calculated, in particular the negative exponent can be lost altogether. Bear in mind here, that, in contemplating the effect of sigma delta modulation on a time series, we are, by definition, considering a time series with added noise.

All is not lost, though, since it is possible to treat these results in a qualitative sense, rather than a rigourously quantitative one. By starting with a single time series (e.g. Lorenz) and then adding Gaussian noise, direct quantisation noise, and noise from a sigma delta modulator respectively, it is possible to make comparisons and draw conclusions on the effects these various

types of noise have on the calculation of Lyapunov exponents. The use of a common underlying signal gives us a basis for comparison on a qualitative level.

It is also likely that any prediction carried out on such a signal will be based upon the same or similar principles to our Lyapunov exponent extraction algorithm (i.e. a locally linear model mapping to a global average), and difficulties in calculating the Lyapunov exponents will directly translate to difficulties in predicting the time series.

In this chapter we have described an algorithm for extracting Lyapunov exponents from time series. We have demonstrated that this algorithm performs well when the time series is noise-free. We have also shown that, for a time series that is known to be a flow, a positive exponent can be accurately estimated in the presence of noise, while the negative exponents estimated from noisy time series should only be used for comparative purposes.

# Chapter 7

# EFFECT OF ΣΔM ON LYAPUNOV EXPONENTS

## 7.1 INTRODUCTION

In this chapter, the algorithm for the extraction of Lyapunov exponents outlined in the previous chapter is applied to a range of time series after sigma delta modulation. Although the emphasis of this chapter is on chaotic signals, a simple sinusoidal time series is initially considered.

However, a comparison of the sigma delta modulated time series to data derived directly from the chaotic system under consideration would not be very informative, since any ADC process is bound to affect a signal's dynamics due to quantisation noise. To address this, the results are compared to those achieved for time series generated by a direct quantisation method; by *direct quantisation*, a simple software implementation of choosing the nearest quantisation level to the input at each sampling instant is referred to.

Time series derived from the Lorenz, Duffing and Rossler systems are considered; these are all artificially generated systems but, since the differential equations generating them are known, the expected values of the Lyapunov exponents have been calculated, and can be considered in the subsequent analysis. Results are also presented for a second order modulator and a tone-suppressing modulator. Gaussian noise of an equal variance to the quantisation noise is added to the time series and the results compared to those from ΣΔM. The question of the dimension of the system, after ΣΔM, is also addressed.

## 7.2 A SINE WAVE

A sine wave has a simple periodic structure and, as such, an analysis of its Lyapunov spectrum should reveal only zero and negative exponents. Figure 7.1 shows the exponents calculated for clean sine wave data over a range of numbers of neighbours. The other parameters used are: globally embedded in 5 dimensions, reduced to 3; outer radius at 3% of overall attractor size; evolved over 1000 periods, taking 8 steps between reinitialisations; data set of 15000 points sampled at a period of 0.06; *svd* window size of 15; the inner radius is set to zero, since the data are noise-free and periodic (i.e. all data points lie exactly on the attractor so looking for points further afield will prove useless).

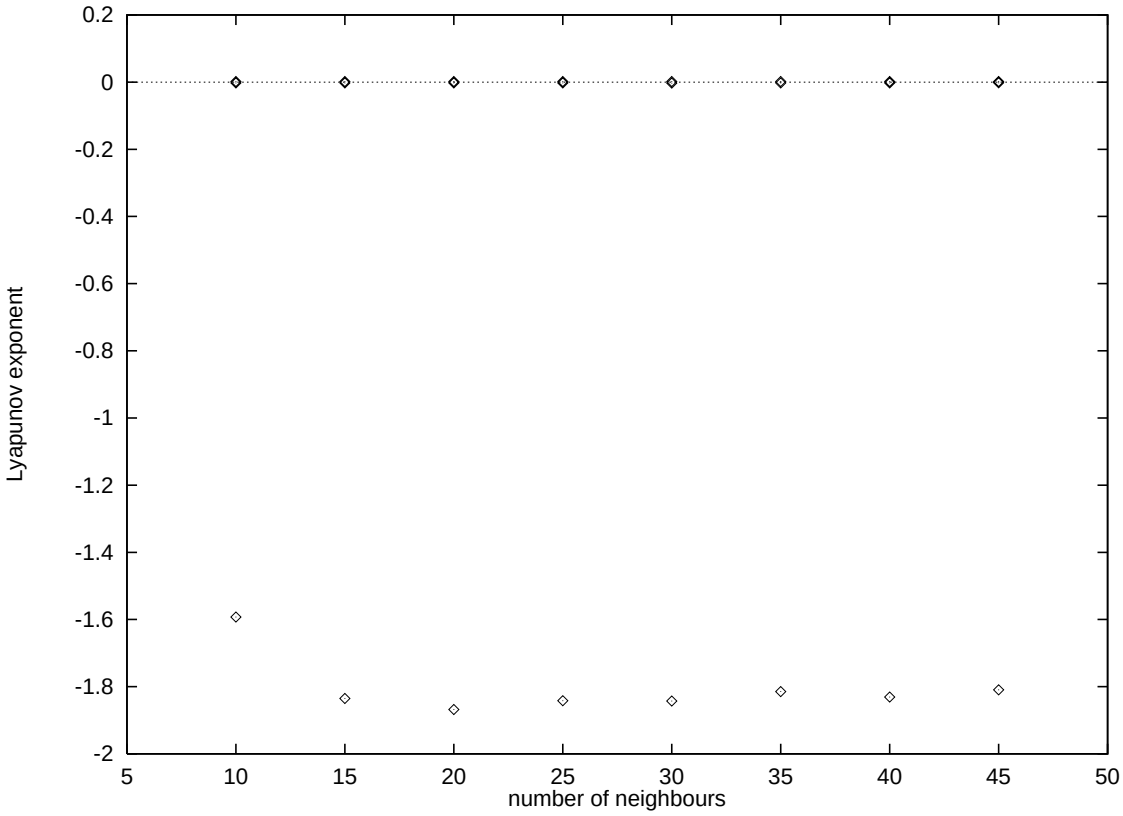


**Figure 7.1**: *Lyapunov exponents of noiseless sine wave time series for varying number of neighbours.*

Inspection of the data reveals that there are two zero exponents and a negative one which is reasonably stable at around $-1.85$. These results are sensible for the system under consideration, i.e. a periodic flow; the zero exponents imply that it is indeed a flow that is under consideration, the negative one shows that any points straying from the attractor are pulled back onto it. It should be noted that a sine wave, being a one-dimensional system, only has one Lyapunov exponent, a zero. However, since we are considering empirical data, we have calculated three exponents so that comparison to the sigma delta modulated data can reveal any extra exponents introduced.

If the results of applying the Lyapunov exponent extraction routine to a quantised version of this time series, and to one after sigma delta modulation, are added to this plot, Figure 7.2 is produced. In both cases 4096 quantisation levels (i.e. 12 bit quantisation) were used; the sigma delta modulator was first order.

It can be seen from the graph that quantisation of the data has affected the measured Lyapunov exponents considerably, although there is no discernible difference in the effect of sigma delta modulation compared to direct quantisation. A single zero exponent is still apparent, but the other has been pushed into the negative; the existing negative one has also been pushed further negative. In practice, these changes are not as drastic as they at first may appear: it is still possible to conclude from the plots that the system under consideration is a periodic flow since

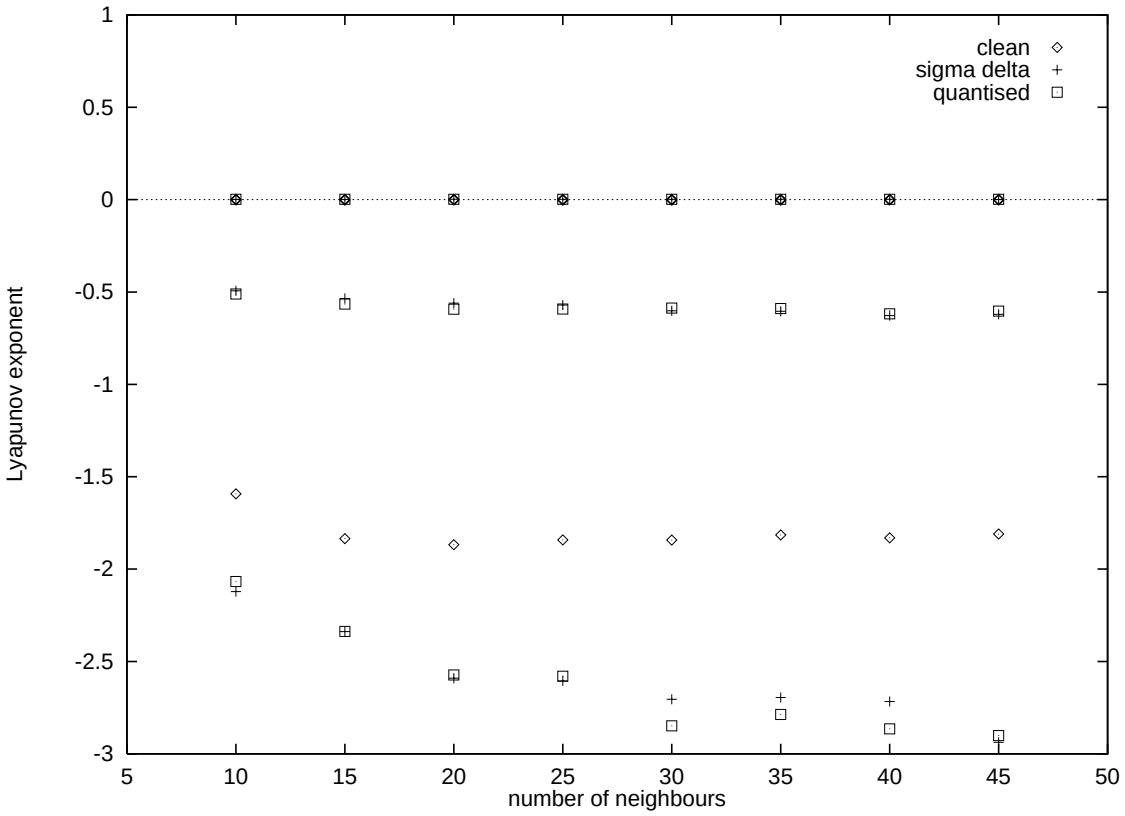


**Figure 7.2**: *Lyapunov exponents of sine wave time series for varying number of neighbours, for clean data, sigma delta modulated and direct quantised.*

zero and negative exponents are present and there is no positive exponent.

The increase in the amplitude of the negative exponents can be explained by the presence of the quantisation noise, in that particular points can now occur at a distance from the attractor. Their trajectory is pulled back toward the attractor within a sample or two, so that larger contractions on to the attractor are present than with the clean data. It should be noted that this effect is not seen in the subsequent analyses of chaotic time series after quantisation. This is probably due to the fact that the sine wave is a periodic signal so, in the case of no noise, points always lie on the same strand of the attractor; indeed the attractor only has one strand. Consequently a noisy point will always be attracted back on to this single strand as the attractor evolves, resulting in a more negative Lyapunov exponent. In a chaotic attractor, however, a noisy point will have a number of possible strands to which it should belong, and to which it can be attracted, which is obviously going to degrade predictability, and the increased negativity of the exponents is no longer apparent. It should be borne in mind here that these negatives are not "real": they are spurious results from analysing the signal in too many dimensions. Their value is essentially a factor of the accuracy of the time series measurement, so the greater inaccuracy of the quantised data leads to more negative spurious exponents.

These results echo those achieved by the analysis of the differential equations in chapter 4, establishing that sigma delta modulation of a non-linear function does not result in the onset

of chaos. We now move on to considering the sigma delta modulation of a chaotic signal.

### 7.3 TIME SERIES GENERATED FROM LORENZ SYSTEM

The first chaotic signal to be considered is a time series generated from the X component of Lorenz' equations:

$$\dot{X} = \sigma(Y - X) \qquad \dot{Y} = rX - Y - XZ \qquad \dot{Z} = -bZ + XY \tag{7.1}$$

with the parameters $\sigma = 16.0$, $r = 40.0$ and $b = 4.0$. Figure 7.3 shows a section of the time series, and the corresponding trajectory of the attractor.

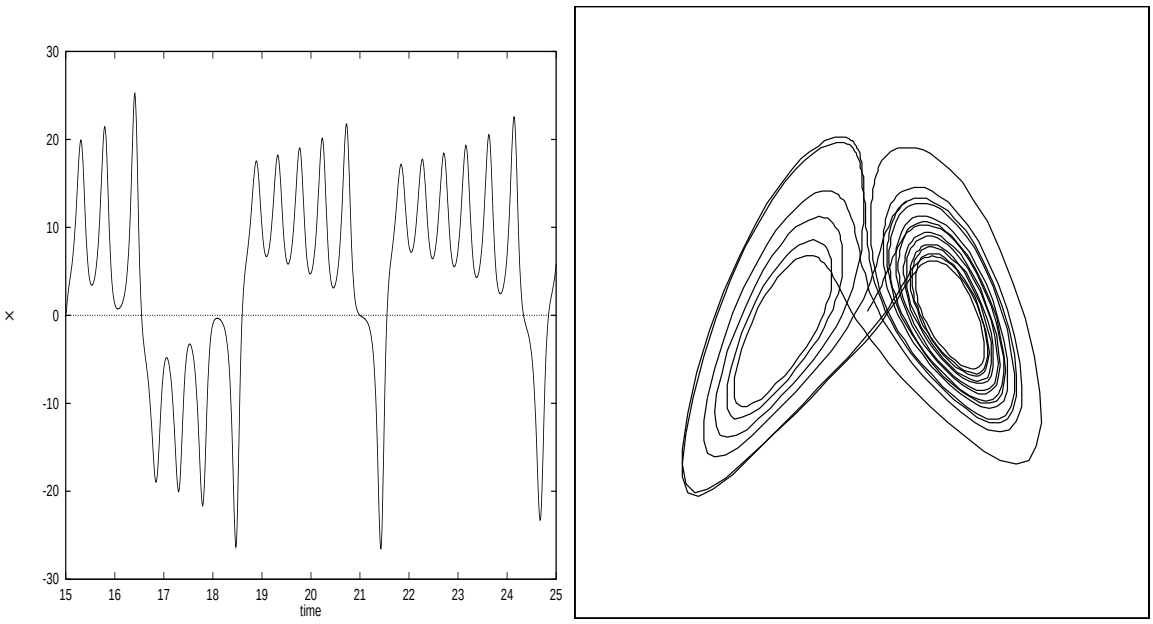


**Figure 7.3**: *A short section of the Lorenz time series, and the corresponding trajectory of the attractor*

The data used in this section have a sample time of 0.01s over 500s, giving a data set of 50000 points. It was generated using a fourth order Runge Kutta process to iteratively solve the differential equations of 7.1. The Lyapunov spectrum of this time series has already been calculated and presented in the section on using the exponent extraction algorithm, see Figures 6.4 and 6.5.

Figure 7.4 shows the Lyapunov exponents calculated by the extraction algorithm for time series of Lorenz data after first order sigma delta modulation, and direct quantisation respectively. Again 4096 quantisation levels have been implemented in each case, which is equivalent to 12 bit quantisation. The accepted Lyapunov exponents of $+1.37$, 0 and $-21.37$ for this Lorenz data are marked with dotted lines, and the number of neighbours in the neighbourhood set was

varied from ten to forty-five. All other parameters are the same as in the calculation of the exponents of the noiseless data, as depicted in figure 6.5.

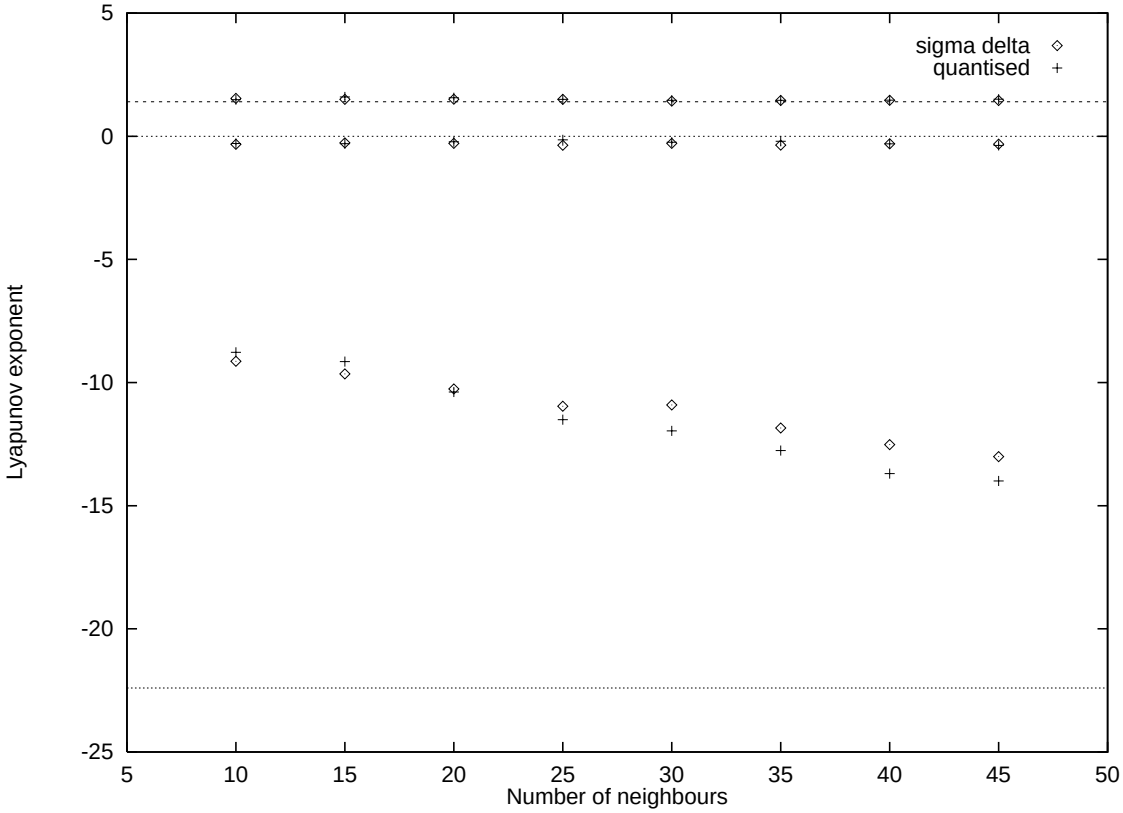


**Figure 7.4**: *Lyapunov exponents of Lorenz time series for varying number of neighbours, sigma delta modulated and direct quantised data.*

It can be seen that the positive exponent has not been affected, with the algorithm successfully calculating a reasonable approximation to +1.37. The zero exponent has been moved slightly negative, and this may be due to noisy points being pulled back toward the attractor, as conjectured in the previous section on the sine wave. It could even be argued that this shows that we are no longer strictly considering a flow, since it has been quantised to a number of discrete levels.

The negative exponent is of more interest, however, since it has been affected quite drastically, being considerably less negative than before quantisation. Once more, there is little to distinguish the exponents calculated for the sigma delta modulated time series from those calculated from the directly quantised data.

Before continuing with a discussion of these results, it is worth considering that a longer *svd* window size tends to improve the robustness of the algorithm to noise on the signal. Figure 7.5 shows the results over a range of window sizes and it can be seen that results closer to those achieved from noiseless data are evident at higher *svd* window sizes, particularly in the case of the positive and zero exponents. In order to investigate this further, Figure 7.6 shows the Lyapunov exponents calculated from these time series for a *svd* window size of 30 over a range of

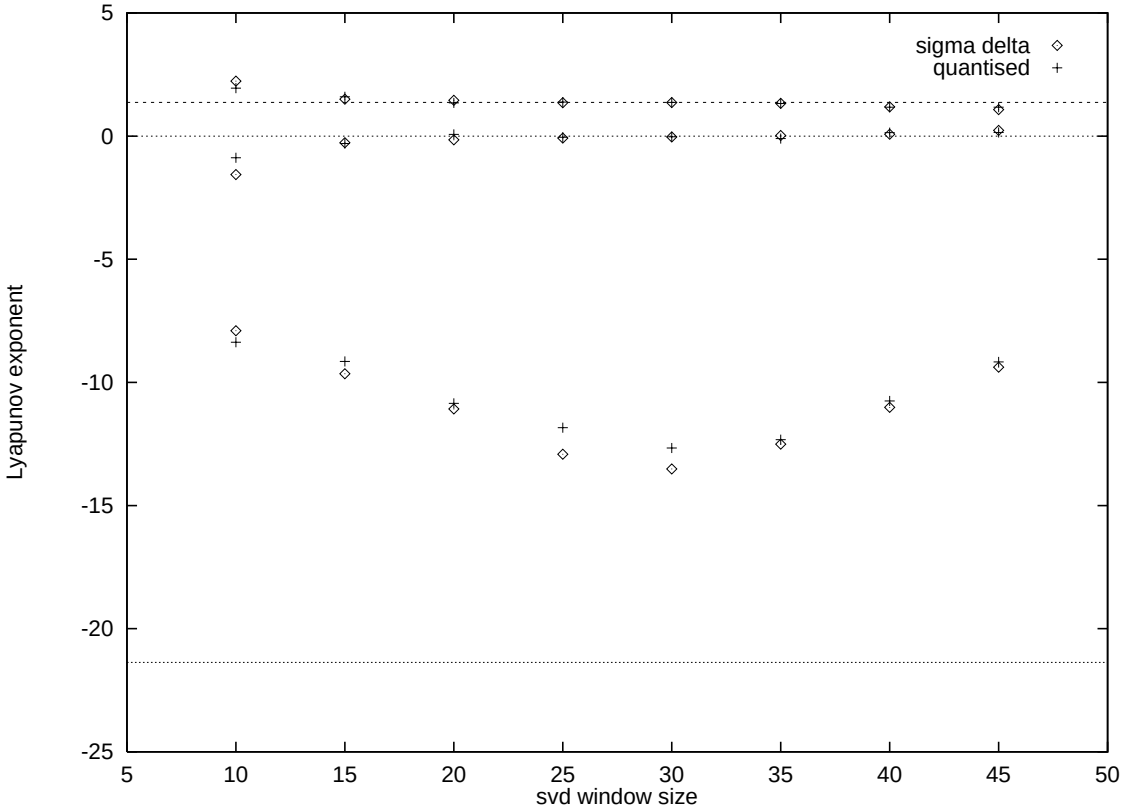


**Figure 7.5**: *Lyapunov exponents of Lorenz time series for varying svd window size showing sigma delta modulated and direct quantised data.*

neighbourhood set sizes (the *svd* window size of 30 gives the most negative value for the negative exponent on the plot, and also the best zero). All other parameters remain unchanged. It is important to note that these results are now for a different set of parameters (i.e. a different *svd* window size) to those presented for the un-quantised data. It is assumed that this difference does not hamper comparison of the results, since it is intended only to increase the algorithm's robustness to noise.

This could be a dangerous assumption to make, since it is based upon the idea that the modulated (i.e. noisy) data actually have the same Lyapunov exponents as the un-modulated (i.e. clean) data, and the extra noise only serves to hamper the algorithm's ability to calculate those exponents. Making such an assumption rather negates the whole point of this chapter, which is to establish whether or not sigma delta modulation of a time series affects the Lyapunov exponents of that time series. In fact, we would have arrived at the same results by only considering the accuracy of the zero exponent; a valid assumption as long as we can continue to regard the time series as a flow.

Consideration of the results, however, shows that even in the case of the higher *svd* window size, the negative exponent is considerably less negative for the modulated and quantised time series than for the original data. Indeed, we have shown that even by tweaking the parameters toward the results calculated from the un-quantised data, the exponent remains less negative.

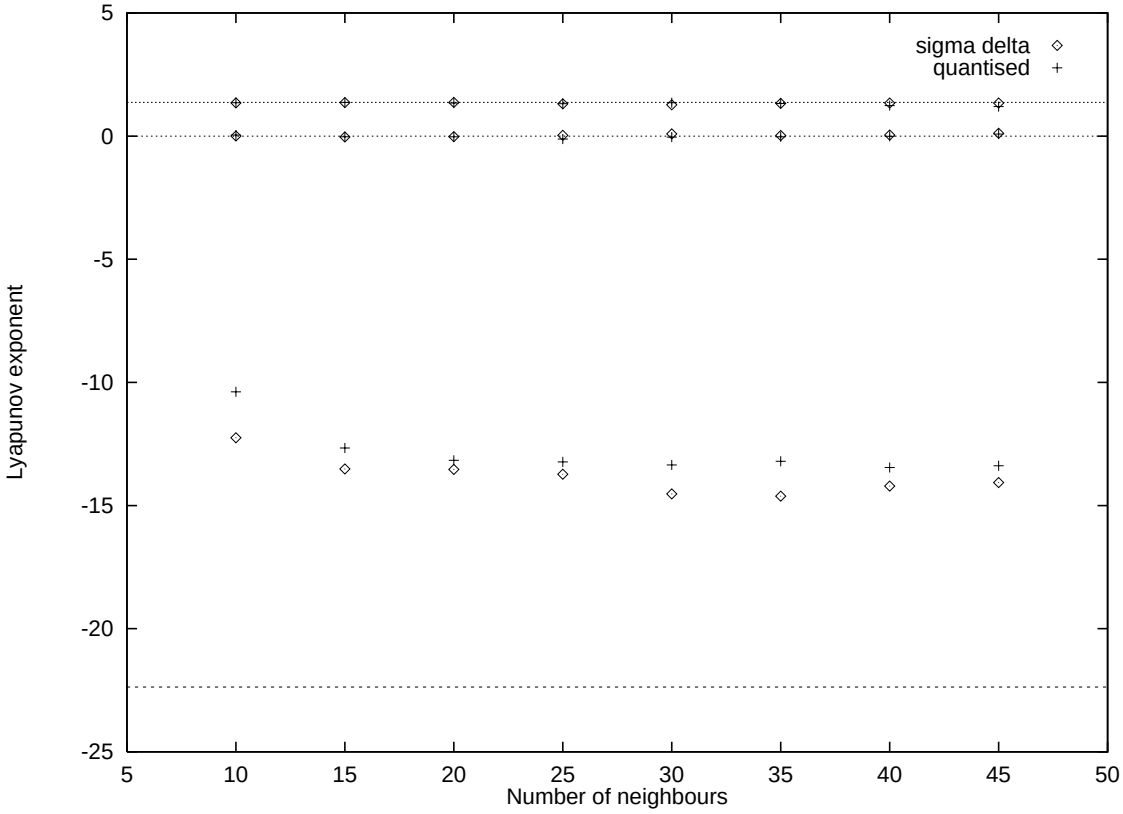


**Figure 7.6**: *Lyapunov exponents of Lorenz time series for varying numbers of neighbours with svd window size of* 30 *showing sigma delta modulated and direct quantised data.*

This implies, qualitatively at least, that quantisation, whether achieved directly or by $\Sigma\Delta$M, of the chaotic signal under study either decreases the accuracy with which the lowest Lyapunov exponent can be calculated, or actually decreases the value of that exponent, while not affecting the zero or positive exponents.

In fact, these two possibilities are indistinguishable at this stage, since either one will result in a decreased ability to predict the signal. A less negative Lyapunov exponent implies this directly, whereas the factors affecting our ability to correctly calculate the negative Lyapunov exponent will also affect our ability to perform prediction on the signal.

There is, however, a further point to discuss in relation to this negative exponent. Although we have seen that, in order to achieve a good zero exponent, a high value of *svd* window is necessary, such a high value tends to decrease the amplitude of the calculated negative exponents. This point is returned to in the discussion of the next set of results.

So far, we have only considered 12-bit quantisation (i.e. 4096 quantisation levels). Figure 7.7 shows the Lyapunov spectra calculated at a range of quantisation levels from 5-bit (32 levels) to 16-bit (65536 levels) for both first order sigma delta modulated and directly quantised data. The parameters for the algorithm were: *svd* window of 30; 40 neighbours; 1000 evolution periods of 8 steps apiece.

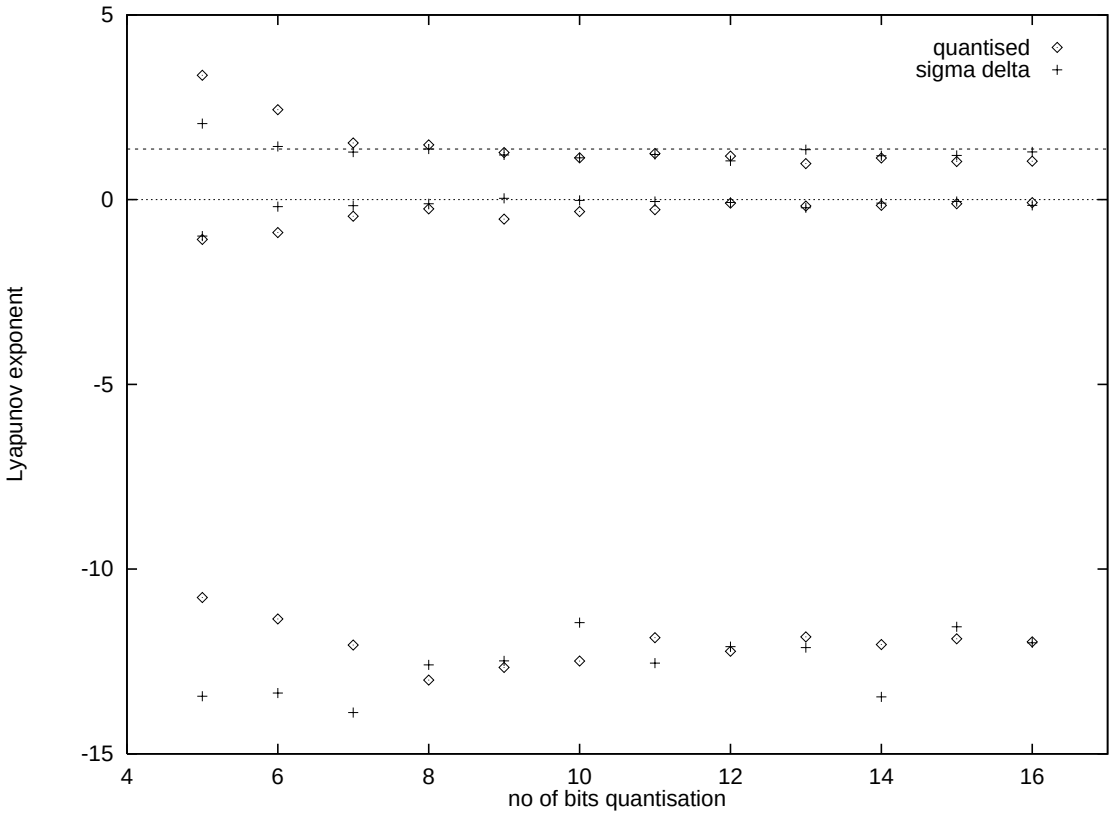


**Figure 7.7**: *Lyapunov exponents of Lorenz time series for varying quantisation levels showing both sigma delta modulated and directly quantised results.*

Again there is little to choose between the performance of the sigma delta modulated data and the directly quantised signal; particularly at quantisation levels greater than around 8-bits. The improved nature of the results can be seen as the number of quantisation levels increases, particularly with respect to the positive and zero exponents.

It is apparent that there is little change in the calculated Lyapunov exponents for quantisation levels above 8 bits or so, with the positive and zero exponents in particular levelling out above this value. This is actually a manifestation of the noise reduction techniques of the extraction algorithm, which appears to be capable of ignoring all the noise on the signal at quantisation levels above 8 bits. As the number of quantisation levels is reduced to below 8 bits, so the noise on the signal increases beyond the algorithm's noise reduction capabilities, and the algorithm loses its ability to completely deal with the noise.

However, in order to facilitate the algorithm's robustness to noise, as evidenced by the appearance of the zero exponent in the results, a long *svd* window must be implemented. This long *svd* window tends to decrease the amplitude of any negative exponents calculated, a problem encountered by other researchers [40,87], and leads to the levelling off of the negative exponent at a higher level than the results for the clean data.

Consequently, it would seem that neither sigma delta modulation or direct quantisation affect the Lorenz time series' Lyapunov exponents, although they do affect our ability to calculate them. If we were seeing a change in the actual Lyapunov exponents of the attractor, then we would expect to observe a gradual improvement in the results as the number of quantisation levels is increased, rather than the tendency toward a particular value that has been shown.

This highlights a problem with measuring chaos in the real world, generally. Any measured time series will be quantised for storage and analysis on a digital medium which, of course, introduces quantisation noise. As the tools available for analysis of such signals stand, this quantisation noise severely hampers our ability to rigourously assign quantitative results to the data. We have shown that it is possible to achieve good approximations of the positive and zero exponents, but our calculation of the negative exponent is severely curtailed by the method in which the algorithm cancels out noise on the signal.

## 7.4 FOUR DIMENSIONAL ANALYSIS

So far in this investigation, we have assumed that the three dimensional Lorenz system remains three dimensional after sigma delta modulation. However, it is possible that the act of $\Sigma\Delta$M introduces one or more additional exponents to the attractor's Lyapunov spectrum. As has been pointed out in Chapter 2, the methods known to the author of calculating an attractor's dimension from a time series derived from that attractor are both ambiguous and unreliable. Rather than attempting to interpret the results from applying such algorithms to the sigma delta modulated Lorenz data, we elected to simply calculate the Lyapunov spectrum of this data after embedding them in four dimensions.

If an extra dimension (and hence an extra Lyapunov exponent) is introduced by $\Sigma\Delta$M, then such analysis should reveal it when compared to a similar calculation made from the un-modulated data. The clean data are known to be three dimensional, and, as such, the spectrum calculated in four dimensions must contain one spurious exponent along with poor approximations of the three actual exponents. If the modulated time series is four dimensional, then it ought to be possible to calculate good approximations of the three Lorenz exponents, plus an extra stable exponent.

Figure 7.8 shows plots of the Lyapunov exponents of clean Lorenz data and Lorenz data after 12 bit $\Sigma\Delta$M embedded in four dimensions, for a range of values of the evolve period between re-initialisations, the number of vectors in the neighbourhood, and the size of the *svd* window.

It is clear from these plots that the two sets of data are behaving in the same manner when analysed in four dimensions. Since we know that the artificially generated clean data set is three dimensional, this implies that the sigma delta modulated data set is also three dimensional, so $\Sigma\Delta$M does not add an extra Lyapunov exponent, or dimension, to the signal being modulated.

In fact, if the sigma delta modulated data were of a higher dimension than three, this would

7.8a

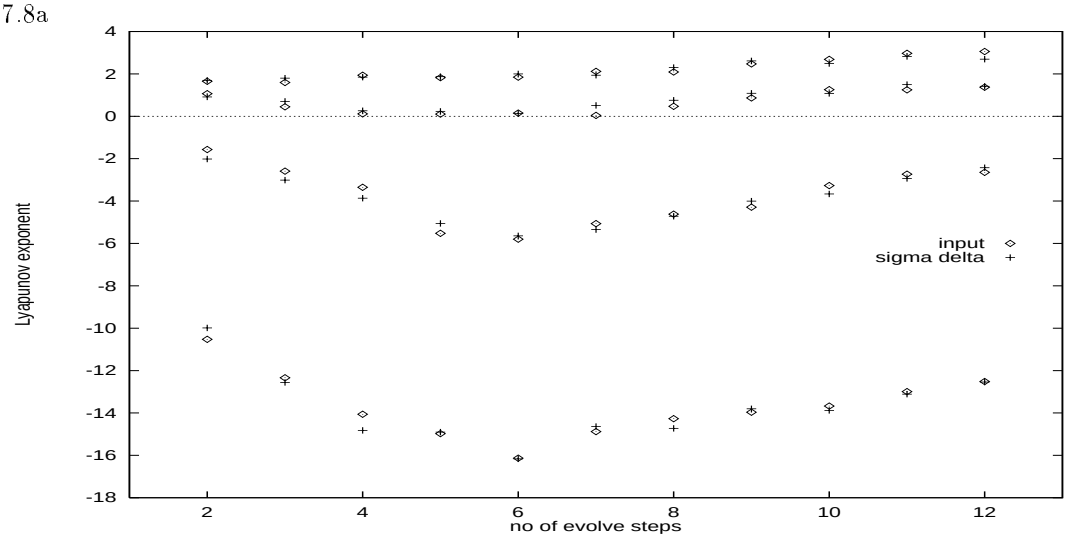


7.8b

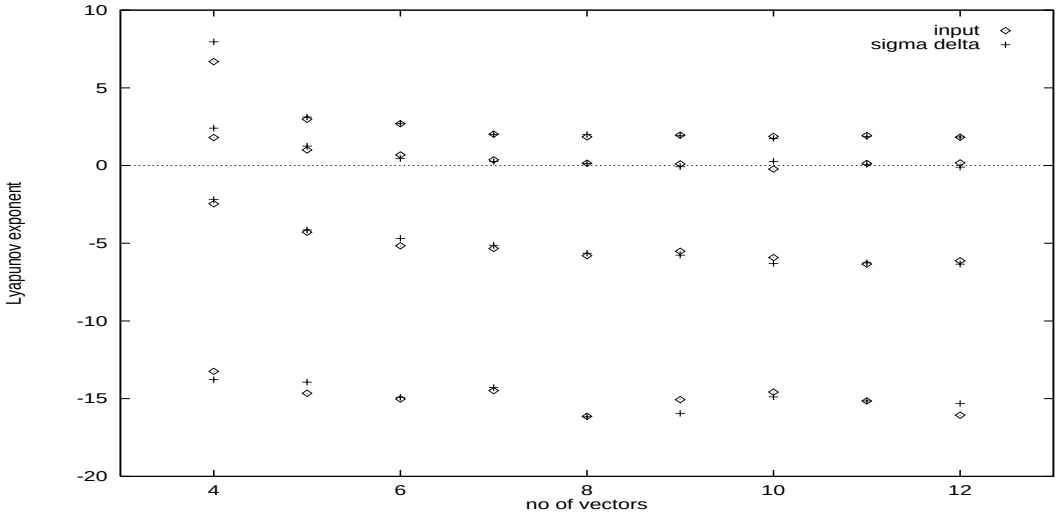


7.8c

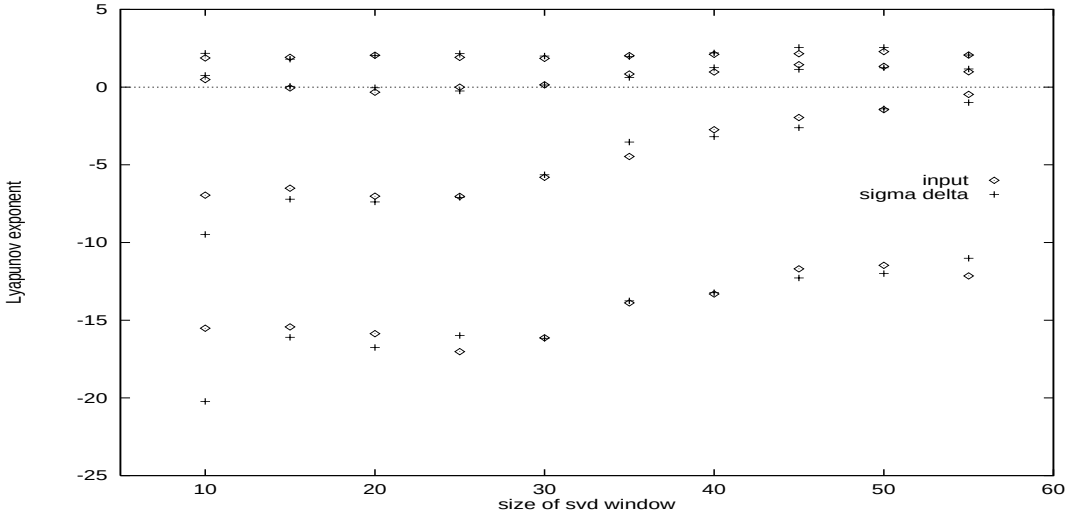


**Figure 7.8**: *Lyapunov exponents of Lorenz time series analysed in four dimensions for a) varying evolve period, b) number of vectors in neighbourhood matrix, and c) size of svd window. Results presented for both sigma delta modulated data and clean data.*

be clear from the three dimensional results, in that a higher dimensional attractor could not be adequately embedded in three dimensions, which would lead to vastly inaccurate estimates of the three exponents calculated. The results already presented show that this is not the case, with the known values of the Lorenz attractor's Lyapunov exponents being easily apparent.

The results from the four dimensional analysis further assure us that we are treating the data in the correct number of dimensions, and that $\Sigma\Delta$M does not introduce an extra Lyapunov exponent, and therefore dimension, into the attractor under study. This was also the case when considering the sigma delta modulation of a sine wave earlier in this chapter. However it is worth bearing in mind that the sigma delta modulation of a d.c. input results in a periodic output before decimation which may well still have some periodic content after passing through the decimation filter. This appears to be indicative that sigma delta modulation can increase the dimension of a modulated signal, although whether or not such an increase is measurable or cab have a measurable effect on the dynamics of the signal is debatable. We won't present results for a d.c. input, since, for comparison, the Lyapunov exponents of that input would need to be measured, and it's somewhat tricky to do so for a zero dimensional system since, of course, it does not have any Lyapunov exponents. Equally analysing the d.c. input after modulation would be a non-starter since it would consist of a d.c. signal with a very small amount of noise, of whatever form, on it, and the algorithm would not be able to produce meaningful or trustworthy results due to the extremely compact nature of such an attractor.

However, a sigma delta modulator must have some dimension which, it seems reasonable to claim, is equal to the number of integrators or order of the modulator [8]. This being the case it is also reasonable to assume that a modulated signal should have increased in dimensionality by a number equal to the order of the modulator. Work by Badii and Politi [1], and Broomhead *et al* [5] has shown that a signal after filtering has an increased dimension due to the filtering process. In the case of our sigma delta modulator this increased dimension has not been observed for any of the range of signals considered: how can this be?

In order to understand this, we need to consider how the two parts of sigma delta modulation are likely to affect a signal's dimension. As described in the previous paragraph, the act of sigma delta modulation itself ought to increase a signal's dimension, which is plainly seen when a d.c. input gives a periodic output from the quantiser. However, the the decimation filter can be viewed as attempting to remove this extra dimensionality, by averaging over some period of the output (e.g. the periodic output from the d.c. input is averaged to an approximation of the d.c. input with some periodic noise on it). Whilst this is an heuristic argument, it seems to fit the observed measurements, and it is further supported by considering the Lyapunov dimension of the output.

As was described in chapter 2, the Lyapunov dimension is calculated by keeping a running total of the Lyapunov exponents of an attractor up until that running total goes negative. That is, if the $n$th Lyapunov exponent is sufficiently negative to pull the running total of the exponents

below zero, then that is the last Lyapunov exponent of consequence. Referring back to Figure 4.13 produced during the preliminary consideration of the Lyapunov exponents introduced by a sigma delta modulator, we can see that the Lyapunov exponents measured (discounting the initial zero which results from the signal under consideration being a flow) are very negative (the most positive being in the region of $-90$). Indeed, these results were only attained by using somewhat unrealistic values of the system parameters in order to pull the Lyapunov exponents sufficiently positive to be measurable. Consequently that work implies that the Lyapunov exponents introduced by sigma delta modulation (in that case on to a d.c. input) are negative to the point of being unmeasurable within the time-scales of the signal being modulated.

These findings appear to support our results here whereby, whatever Lyapunov exponents that are being introduced by the extra dimensionality of the sigma delta modulator are so negative as to have no measurable effect on our calculation, or on the dynamics of the modulated signal in general. Consideration of the effect of such highly negative exponents on the value of the Lyapunov dimension (i.e. there would be no effect) suggests why no observable change in the attractor's dimension is found.

Consequently, whereas the first order sigma delta modulator is a one dimensional system, it does not add a measurable extra dimension to either of the two signals considered so far. We will assume that this continues to be the case for the remaining chaotic time series considered, since the results presented for those signals are sufficiently similar to suggest that no extra dimension is measurable (bearing in mind that a four dimensional attractor considered in three dimensions should give wildly wrong values for the three Lyapunov exponents calculated).

## 7.5 TIME SERIES GENERATED FROM DUFFING SYSTEM

We now turn our attention to another known chaotic time series: that generated from Duffing's equation [70, 88]. Duffing's equation is

$$\frac{d^2x}{dt^2} = x - x^3 - \delta\frac{dx}{dt} - \gamma\cos\omega t \tag{7.2}$$

which is rewritten as two first order differential equations, for numerical solution by the Runge Kutta method, as follows:

$$\left.\begin{aligned} \frac{dy}{dt} &= x - x^3 - \delta y - \gamma\cos\omega t \\ \frac{dx}{dt} &= y \end{aligned}\right\} \tag{7.3}$$

in order to generate the time series data. The values of the coefficients used are $\delta = 0.1$, $\gamma = 10.0$ and $\omega = 1.0$. A section of the data is shown in Figure 7.9, both as a time series, and as a three-dimensional embedded phase plot.

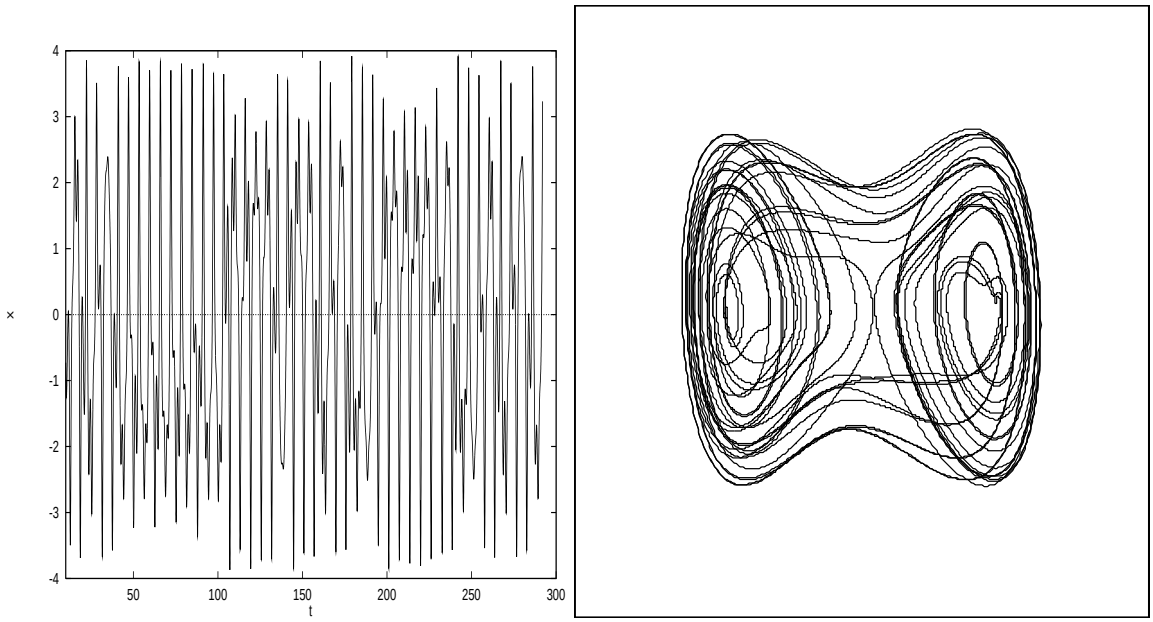


**Figure 7.9**: *A short section of the Duffing time series, and the corresponding trajectory of the attractor*

By applying the algorithm of Wolf *et al* [32] to these equations, the Lyapunov spectrum is calculated as $\lambda_1 = 0.75, \lambda_2 = 0.0, \lambda_3 = -1.38$. Note that a third exponent has been calculated, by making the substitution $z = \omega t$ and creating a third differential equation. This is due to advance knowledge that the Duffing system is three dimensional.

The trace of the Jacobian can be utilised to check the veracity of these figures, in that this trace should be equal to the sum of the Lyapunov exponents. This arises from the general rule that the trace of a matrix (i.e. the sum of the diagonal elements) is equal to the sum of the eigenvalues. In the case of the Jacobian, the eigenvalues are the Lyapunov exponents. Substituting the values of the coefficients into the three differential equations defining the Duffing system gives

$$\left.\begin{aligned} \dot{x} &= y \\ \dot{y} &= x - x^3 - 0.1y - 10\cos z \\ \dot{z} &= 1 \end{aligned}\right\} \tag{7.4}$$

which gives a trace of

$$\frac{\partial \dot{x}}{\partial x} + \frac{\partial \dot{y}}{\partial y} + \frac{\partial \dot{z}}{\partial z} = 0 - 0.1 + 0 = -0.1. \tag{7.5}$$

The sum of the calculated Lyapunov exponents, however, is $0.75 + 0 - 1.38 = -0.63$. This apparent discrepancy is explained by the presence of a time term in the equations, which requires the introduction of a factor of $2\pi$ (i.e. the base period of the function) into the process. The results are thus sufficiently close to give us confidence in our calculated values of the Lyapunov exponents.

Figure 7.10 shows the Lyapunov exponents calculated by the extraction algorithm for a Duffing time series after both sigma delta modulation and direct quantisation. The results are presented for a range of number of bits precision in the analogue to digital process. The parameters used in the calculation were: 35000 points sampled at 0.12s; *svd* window size of 30; 1000 iterations of 6 evolve steps each; 120 neighbours in a radius of less than 0.075.

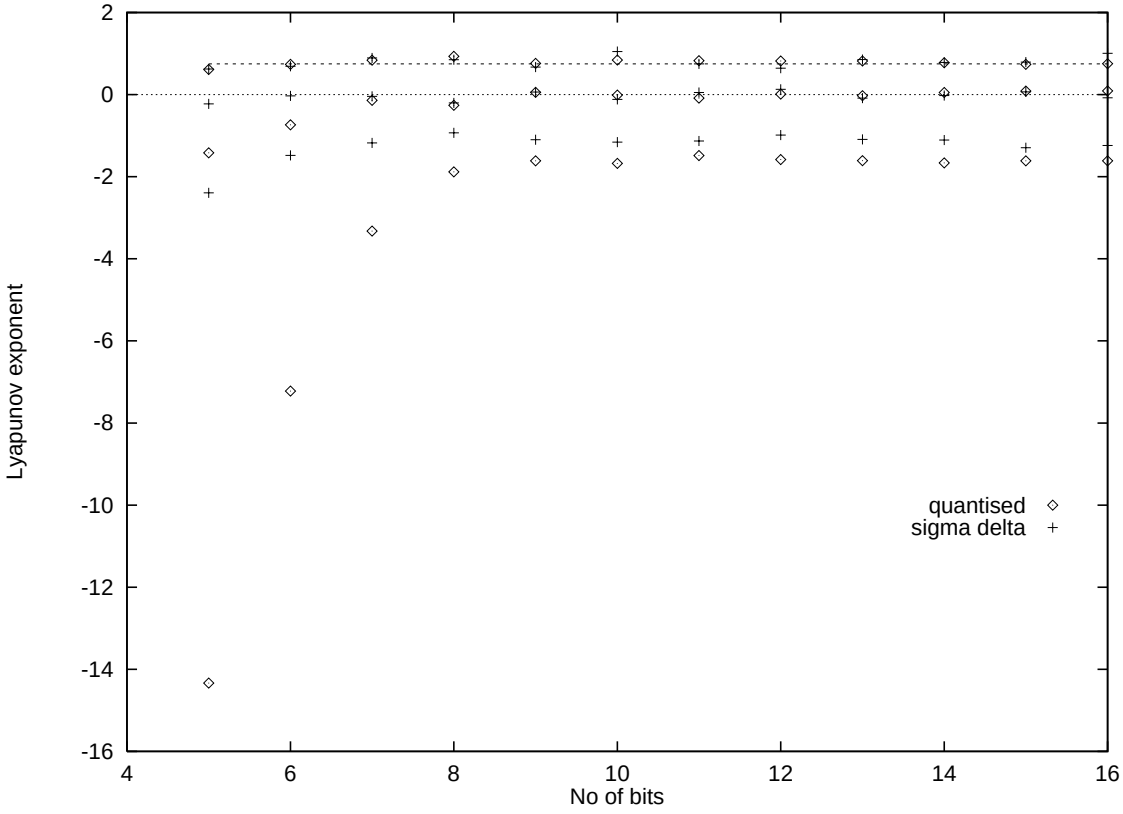


**Figure 7.10**: *Lyapunov exponents of Duffing time series for varying number of quantisation levels, sigma delta modulated and direct quantised data.*

The positive exponent calculated by the Wolf method (0.75) is marked by the dotted line, and it can be seen that this exponent is unaffected by either ΣΔM or direct quantisation. The zero exponent is also successfully extracted, except for very low precisions of the direct quantisation. The negative exponent, however, is of more interest. The sigma delta modulated data consistently produce a less negative exponent than the directly quantised data, an effect which is especially pronounced at lower sampling rates.

This phenomenon appears to be due to the fact that the Duffing time series under analysis is somewhat over-sampled, producing a sampled value, by whatever means, at a sample time of 0.012s. Figure 7.11 shows sections of this time series after 5-bit ΣΔM and 5-bit direct quantisation.

It is clear that the sigma delta modulated time series has far noisier transitions from one quantisation level to the next, in comparison to the clean transitions of the directly quantised

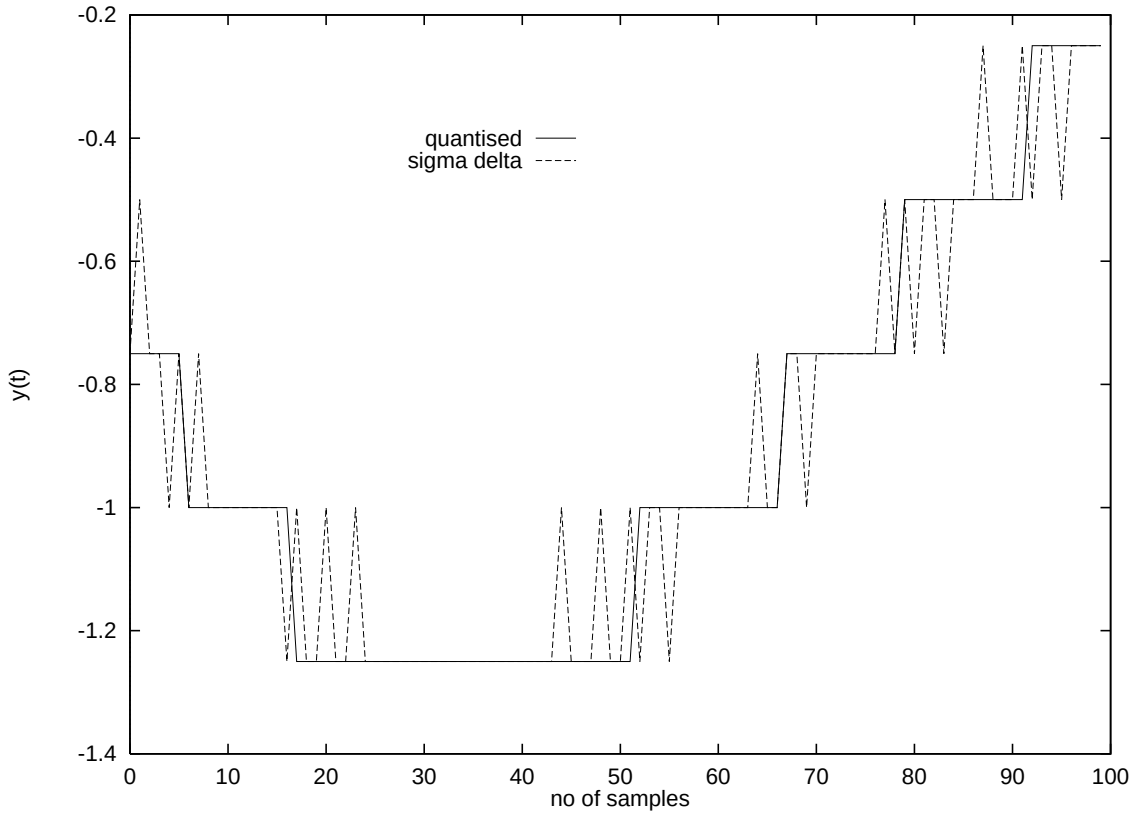


**Figure 7.11**: *Time series plots of sigma delta modulated and quantised Duffing data.*

data. Perhaps paradoxically, this extra noise on the transition can actually create a *less noisy* attractor due to the *svd* process that is utilised by the Lyapunov exponent extraction algorithm. That is to say that, due to the averaging nature of this *svd* process in embedding the time series as an attractor, the transitions become much smoother in the sigma delta modulated case than in the directly quantised case. Consequently the sigma delta modulated data, after *svd* reconstruction, are closer to the 'smooth' dynamics of the clean Duffing attractor than the directly quantised data are. Since the *svd* reduction process is analogous to a low pass filter, it is not surprising that this effect is observed as we are, effectively, carrying out a partial demodulation on the signal.

This does appear to be an artefact of the data being somewhat over-sampled, so the obvious next step is to reduce the sampling rate in order to decrease the vacillations between quantisation levels at each transition point.

Figure 7.12 shows the results produced from investigating this line of reasoning. The Lyapunov exponents calculated from both sigma delta modulated and directly quantised Duffing time series are presented for a range of sampling periods. The parameters of the algorithm were as before, except that the number of points on the attractor was reduced in proportion to the increased sample period, in order to consider a comparable temporal section of the attractor.

Once more a large discrepancy in the calculated exponents is evident for the sample period

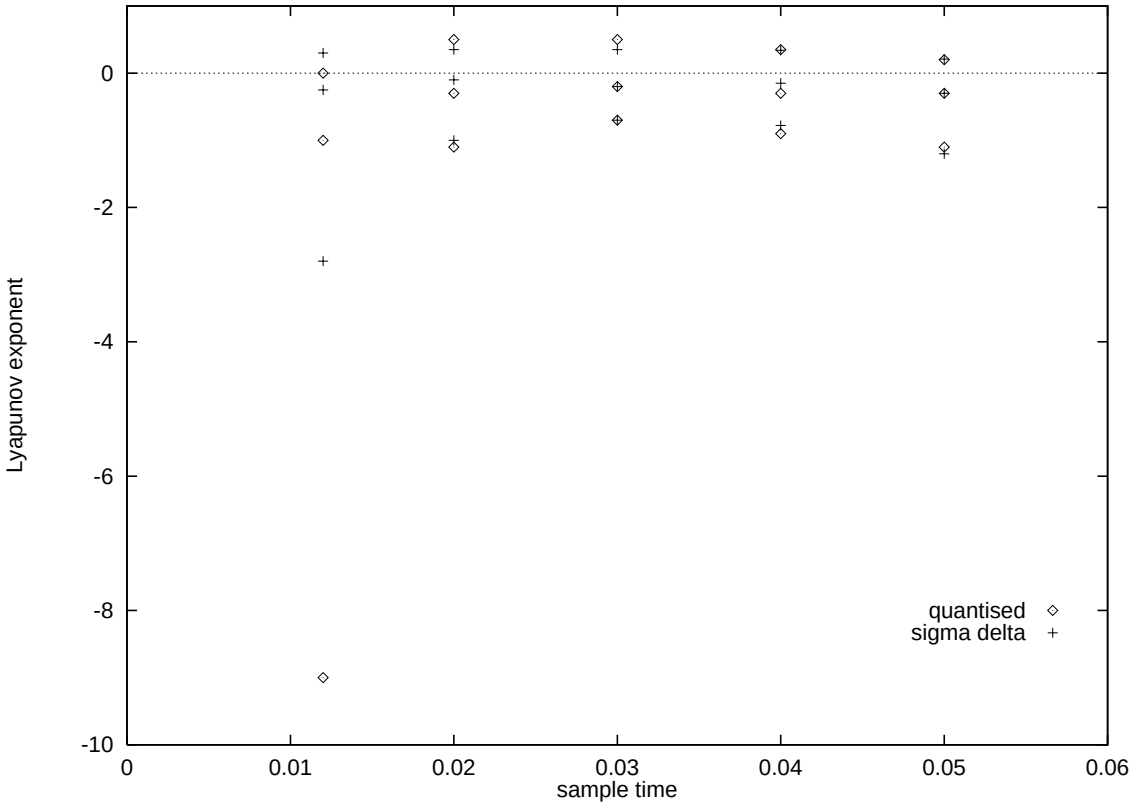


**Figure 7.12**: *Calculated Lyapunov exponents of Duffing time series after sigma delta modulation and direct quantisation for a range of sample times.*

of 0.012s. As the sample period is increased, and thus the sample rate reduced, the two sets of Lyapunov exponents quickly come into alignment, with the best agreement occurring at a sample period of around 0.03s. This is likely to be due to the time series no longer being over-sampled, so the vacillations of the sigma delta modulator are not having an increased smoothing effect during the embedding process. Equally the clean steps of the directly quantised data are now part of a temporally longer *svd* window so they are averaged out more.

It will have been noted that the zero exponent has been lost in these calculations. With careful choice of the algorithm's parameters for each sample period, the zeroes could be re-established, but it was decided to present the results using the same parameters as have been used previously. Since the plot is serving as a comparison between the results calculated from the sigma delta modulated data, to those calculated from the directly quantised data, this does not affect its meaningfulness.

It would seem from this section that the measured dynamics of a low precision quantisation of a non-linear signal can be improved by over-sampling with a sigma delta modulator, as opposed to a direct quantisation at the same sample rate. These effects were not observable at higher precisions, however, since the noise introduced was within the boundaries of the algorithm's suppression capabilities.

## 7.6 TIME SERIES GENERATED FROM ROSSLER SYSTEM

The final chaotic time series we shall consider is that generated by the Rossler system [89]. Rossler's system is defined by the equations

$$\dot{x} = -(y + z) \qquad \dot{y} = x + \alpha z \qquad \dot{z} = \mu + z(x - \gamma) \tag{7.6}$$

and has accepted Lyapunov exponent values of $\lambda_1 = 0.13$, $\lambda_2 = 0$ and $\lambda_3 = -14.1$ with the coefficients $\alpha = 0.15$, $\mu = 0.2$ and $\gamma = 10$ [32]. A portion of the time series, and of the attractor in a three-dimensional embedding is shown in Figure 7.13.

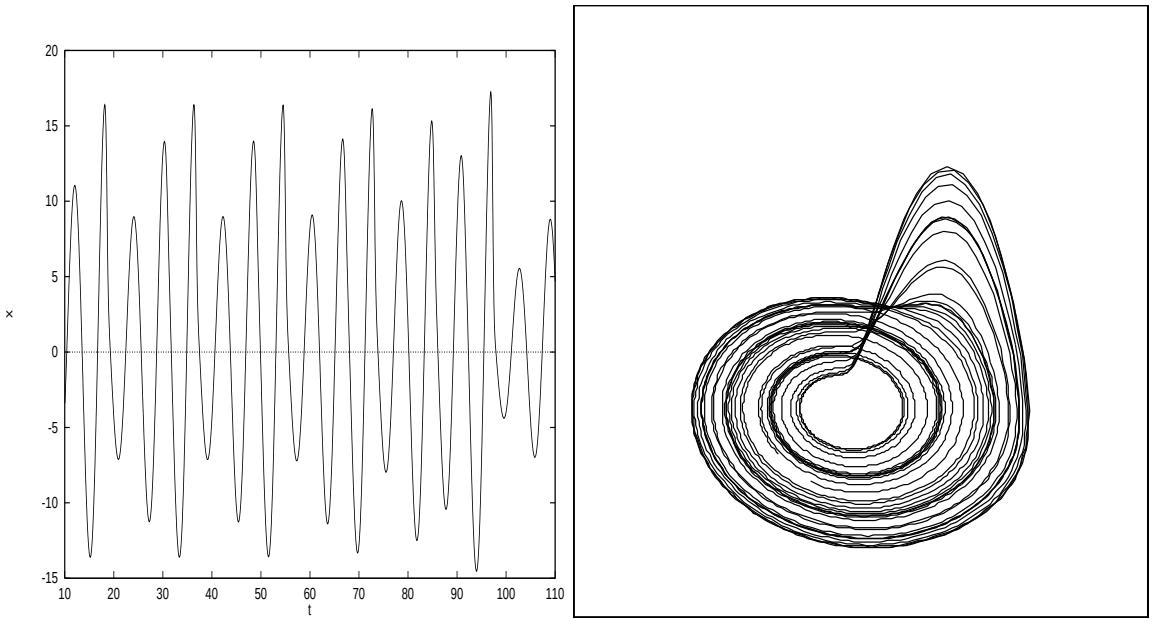


**Figure 7.13**: *A short section of the Rossler time series, and a longer trajectory of the attractor*

It should be noted that, in the case of the Rossler attractor, the positive exponent is very close to zero which precludes accurate estimation of it. Figure 7.14 shows the estimated Lyapunov exponents for both a sigma delta modulated and a directly quantised Rossler time series for a range of quantisation precisions. The accepted positive value of 0.15 is marked by the horizontal line. The parameters used in the application of the algorithm were: 49000 points sampled at 0.04s; 180 neighbours within a radius of 0.75; 4000 iterations of 6 evolve points each; *svd* window size of 30. The long evolve period was used in an attempt to more accurately measure the positive exponent, by allowing the algorithm time to successfully distinguish it from the zero exponent.

The plot reveals that, once more, there is little to consistently distinguish the two sets of data when examining the positive and zero exponents. However, as with the Duffing data, the negative exponents reveal slightly less negative values for the sigma delta modulated data, compared to the directly quantised data.

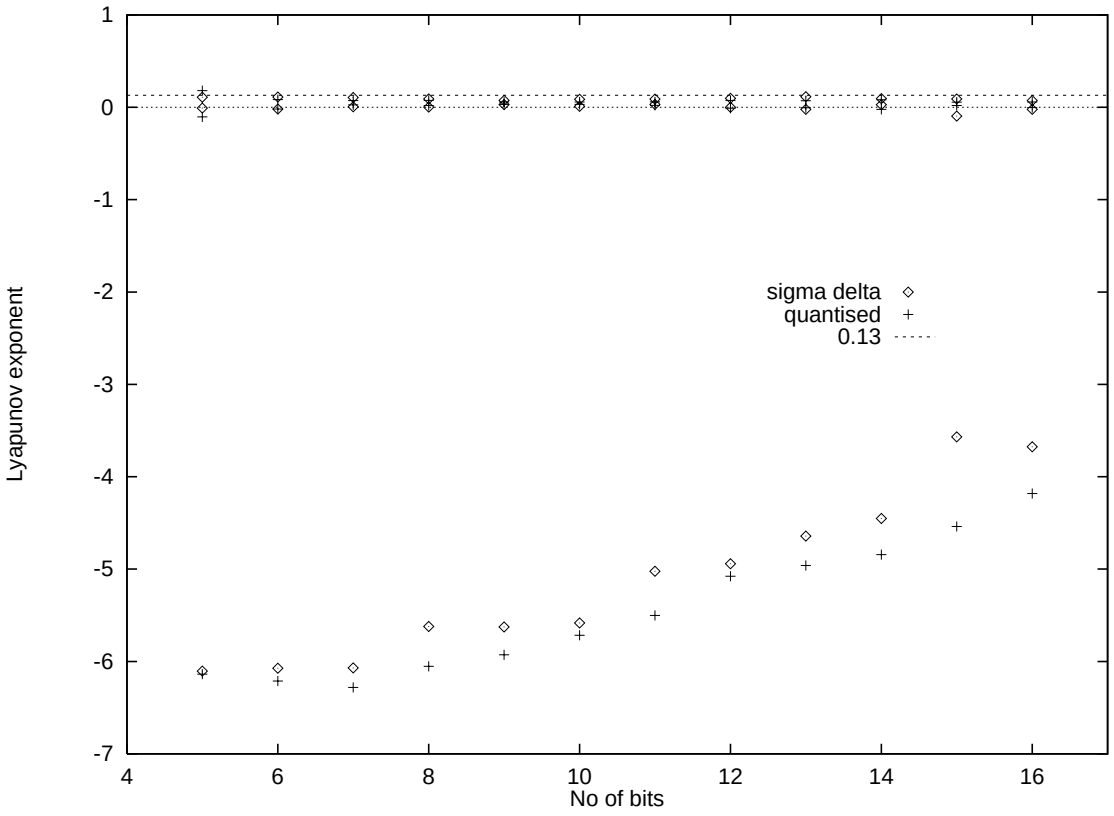


**Figure 7.14**: *Calculated Lyapunov exponents for Rossler time series after sigma delta modulation and direct quantisation over a range of oversampling rates.*

## 7.7 LOCAL SINGULAR VALUE DECOMPOSITION

The results presented for both the Duffing and the Rossler time series would suggest that the act of sigma delta modulating those signals has had an adverse effect on the negative Lyapunov exponents of the measured attractors. However, this phenomenon was not observed when considering the data generated by the Lorenz system. This would appear to be a contradiction in the results presented in this chapter.

In order to explain this, it should be recalled that the Lorenz system is an unusual one, dynamically speaking, in that it can successfully be analysed using an embedding dimension equal to the order of the system. In general, this is not the case, so by analysing both the Rossler and the Duffing data in a three dimensional phase space, we may have inadvertently introduced problems into the calculation. Indeed, if the data have not been embedded in a sufficient number of dimensions, then the extra errors caused by the "wrong" quantisations of the sigma delta modulator may have increased the number of false nearest neighbours introduced into each neighbourhood during the calculation. This would, in turn, reduce the amplitude of the negative Lyapunov exponents estimated.

To investigate this further, we utilise the local *svd* technique described in section 6.3.5. In each case, the data are globally embedded in 6 dimensions and the neighbourhoods constructed

and evolved as before. Prior to calculating the tangent maps, however, each neighbourhood is reduced to three dimensions, i.e. a three column matrix, by means of a singular value decomposition.

The results achieved by applying this process to the Duffing time series data are shown in Figure 7.15. Clearly, the analysis of the data in 6 dimensions has brought the two sets of Lyapunov

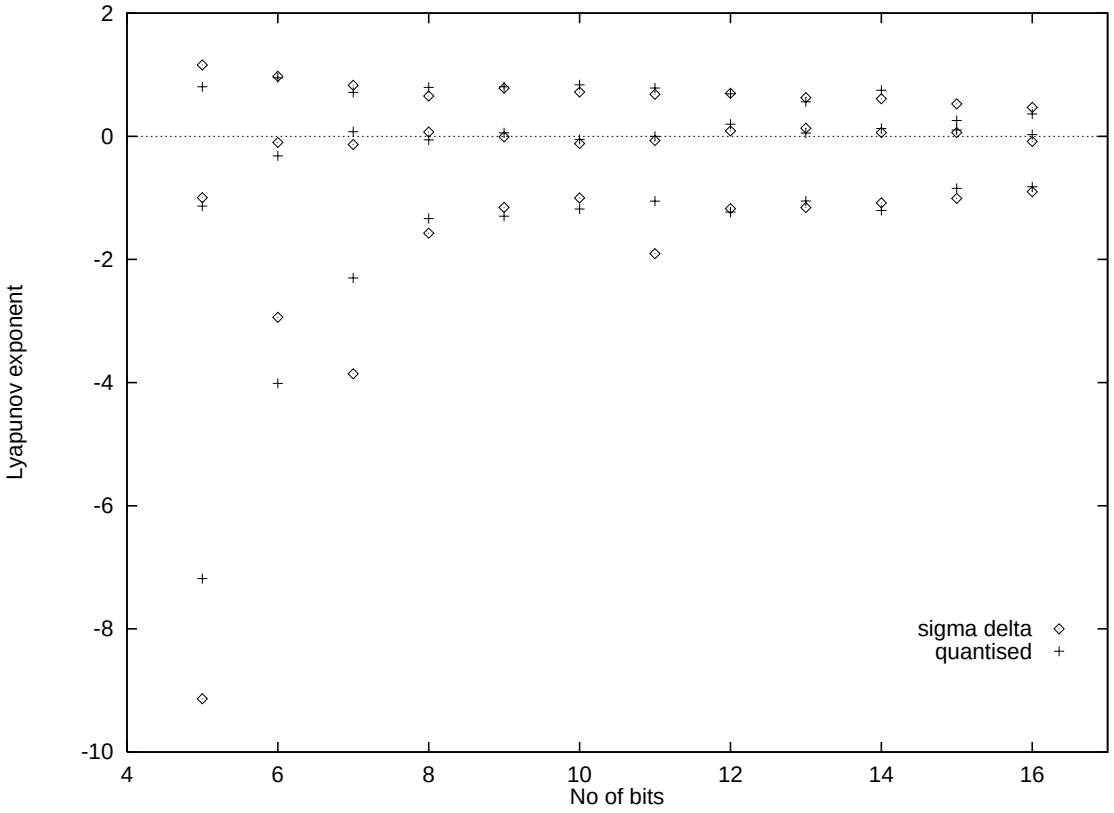


**Figure 7.15**: *Calculated Lyapunov exponents for Duffing time series after sigma delta modulation and direct quantisation over a range of oversampling rates, with local svd reduction.*

exponents into much closer agreement. Indeed, once more, there is no consistently identifiable difference between the Lyapunov spectrum of the sigma delta modulated data and that of the directly quantised data, across a range of quantisation precisions.

## 7.8 GAUSSIAN NOISE

This section compares the results attained so far to the Lyapunov exponents estimated from Lorenz time series with equivalent amounts of Gaussian noise added. The noise was calculated to have the same average absolute value as the quantisation noise at each precision level.

The results are shown in Figure 7.16, and were produced using the same algorithm coefficients as previously used for the Lorenz time series. Unfortunately, the results are less than conclusive since the algorithm lost the zero exponent for the data with added Gaussian noise. This implies that the dynamics of the noise being added by the sigma delta modulator (and indeed the

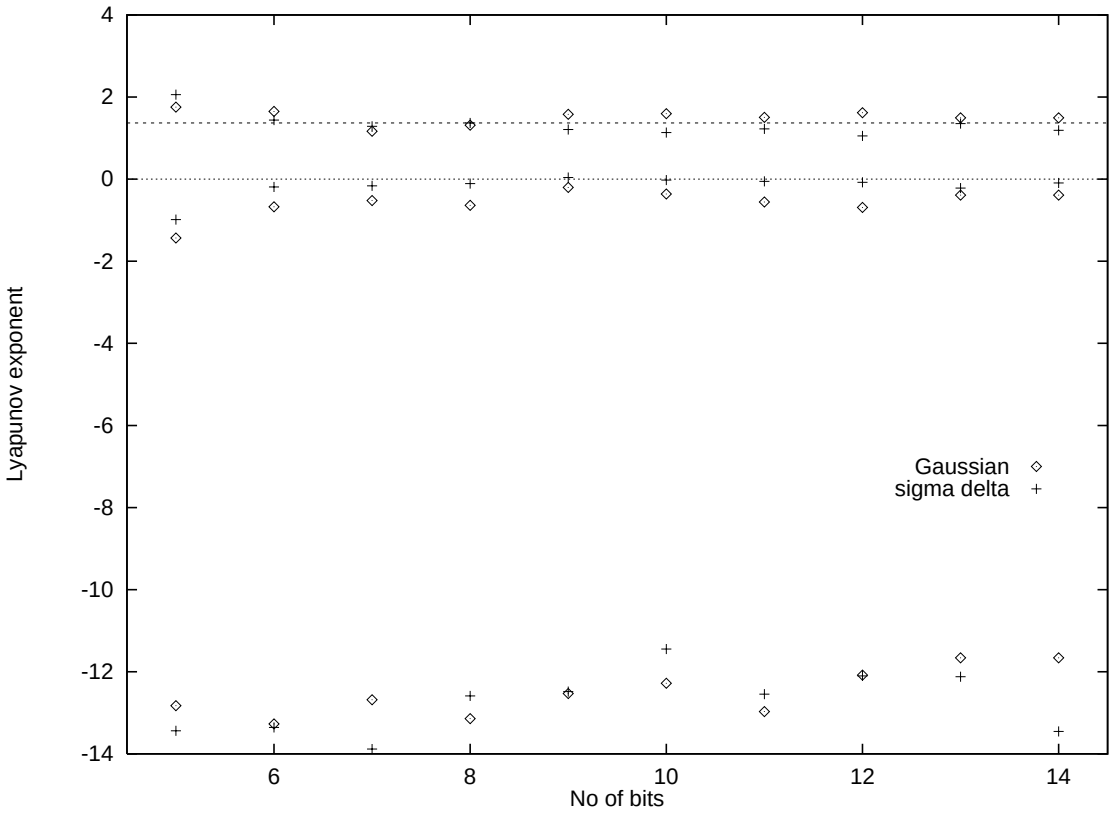


**Figure 7.16**: *Calculated Lyapunov exponents for Lorenz time series after sigma delta modulation and equivalent additive Gaussian noise over a range of oversampling rates.*

direct quantisation) are markedly different to those of Gaussian noise. This is, of course, to be expected.

## 7.9 SECOND ORDER MODULATION

So far only the first order sigma delta modulator has been considered. In this section we briefly discuss the case of the second order device. Modulators of higher orders are not considered, since establishing reliable and stable circuit configurations is not a straightforward process and, as we shall see in this section, may not add anything to our knowledge of the situation.

Figure 7.17 shows the Lyapunov exponents calculated for a Lorenz time series after first and second order sigma delta modulation. The number of bits precision in the quantisation process was varied from five to sixteen. The parameters used by the algorithm were: *svd* window of 30; 40 neighbours; 1000 evolution periods of 8 steps apiece; 49000 points sampled at 0.01s.

Figure 7.17 indicates that the dynamics of the data which have been modulated by the second order system have not been further affected, in comparison to the results from the first order system. Indeed, if there is a consistent difference between the two sets of results, it is that the data that has been modulated by the second order device have a negative exponent of slightly greater magnitude. This implies a slight improvement in the data, which is, of course, the

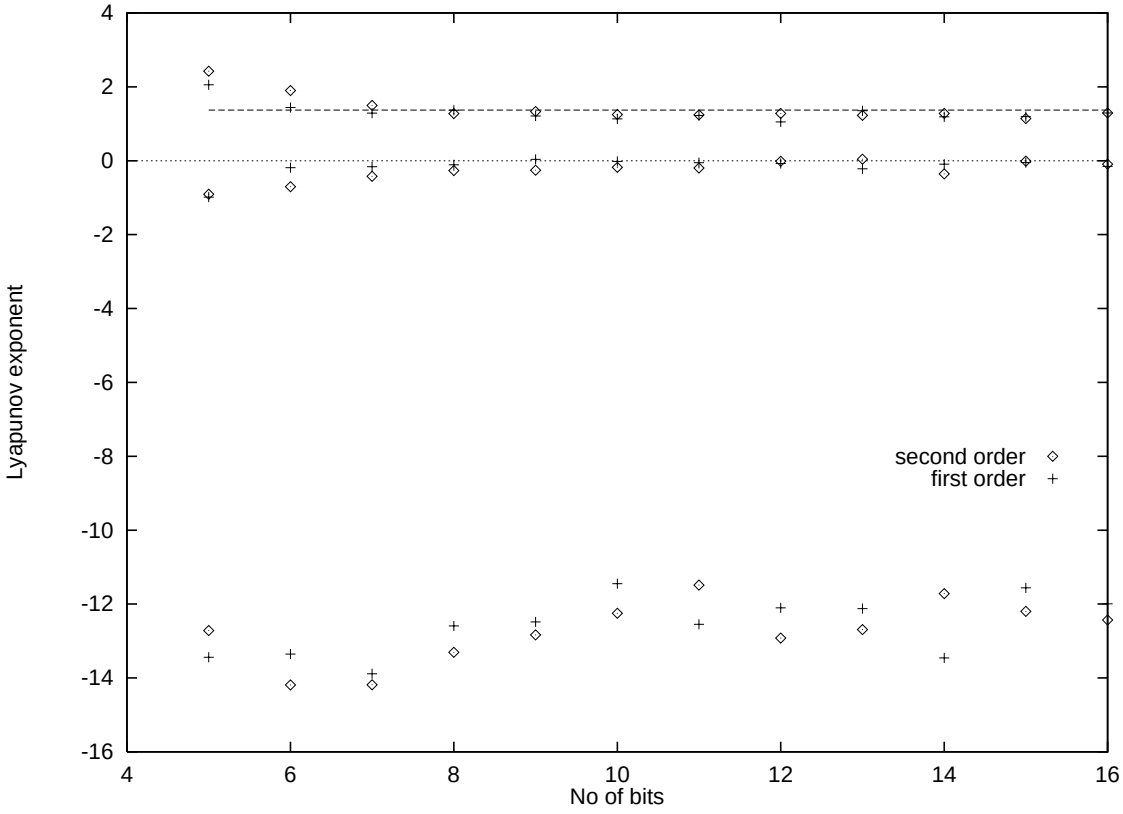


**Figure 7.17**: *Calculated Lyapunov exponents for Lorenz time series after first order and second order sigma delta modulation over a range of oversampling rates.*

desired effect of using a higher order modulator.

This section suggests that it is valid to concentrate on the first order modulator, and that there is little point in considering higher order structures for the purposes of this thesis, since no further effect on the measurable Lyapunov exponents is introduced.

## 7.10 SIGMA DELTA MODULATION WITH TONE SUPPRESSION

So far, in this chapter, we have established that sigma delta modulation of a chaotic signal does not affect the Lyapunov exponents of that signal, or therefore its predictability, in comparison to a direct quantisation of the signal to the same precision. However, we have only considered a conventional implementation of sigma delta modulation in this analysis.

We now turn to the tone suppression architecture discussed in chapter 3, which has been described as a chaotic configuration of $\Sigma\Delta$M [8,9]. In general, these tone suppression configurations are represented in the discrete domain, as containing integrators with a feedback factor slightly higher than unity, as opposed to slightly less than unity as is conventional. As was shown in equations 4.3 to 4.7 this is equivalent to changing the sign of the integrator feedback coefficient in the continuous representation of the circuit.

Figure 7.18 shows the results of applying the Lyapunov exponent extraction algorithm to Lorenz

7.18a

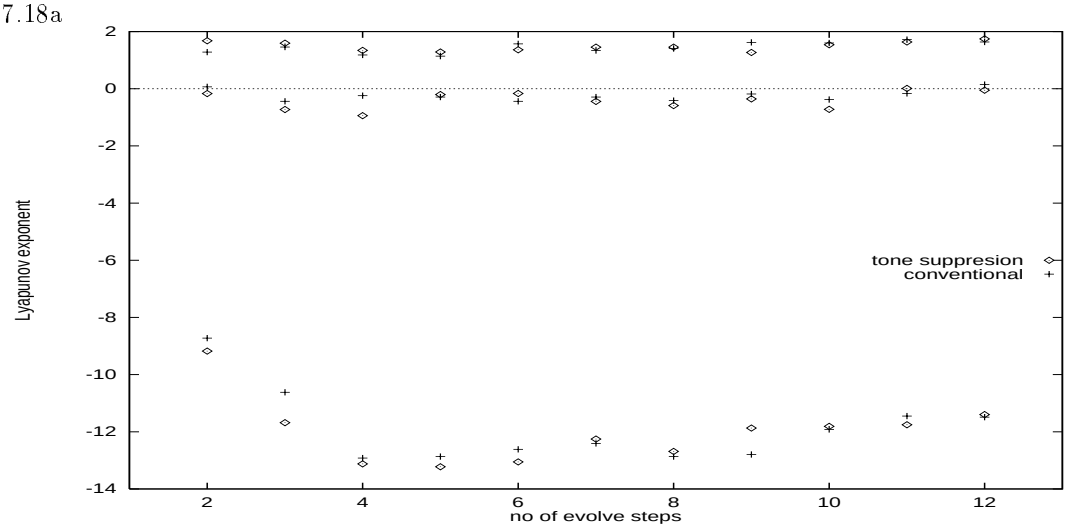


7.18b

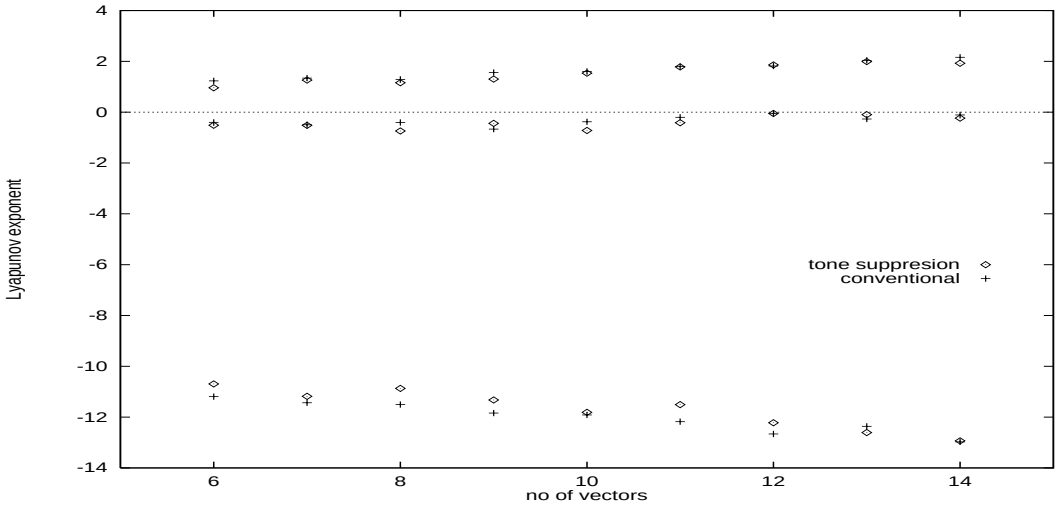


7.18c

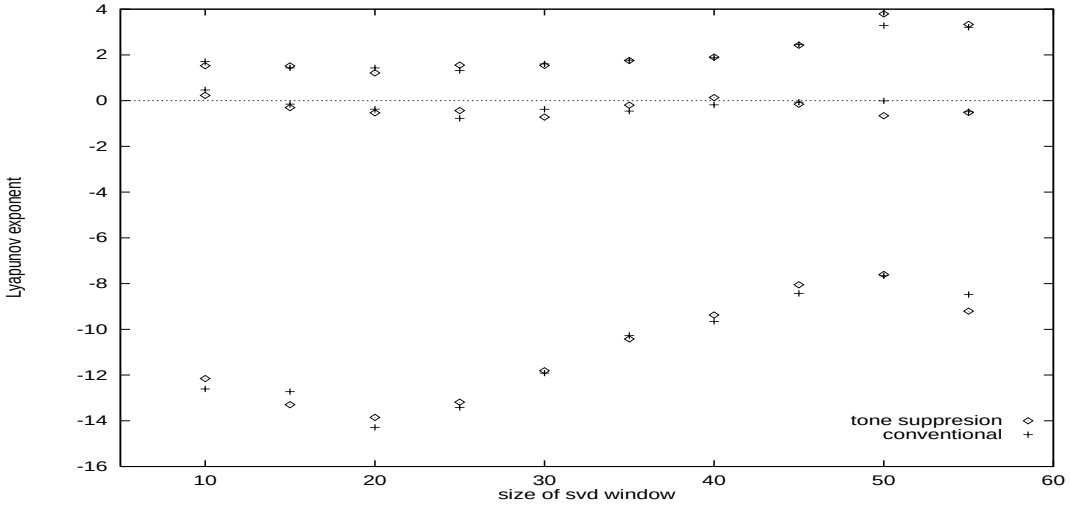


**Figure 7.18**: *Lyapunov exponents of Lorenz time series for a) varying evolve period, b) number of vectors in neighbourhood matrix, and c) size of svd window. Results presented for both conventionally sigma delta modulated data and tone suppressed sigma delta modulated data.*

data which have been conventionally sigma delta modulated, and tone suppression sigma delta modulated respectively. In each case, the modulator is a first order 12-bit device.

Examination of these results shows little distinction between the two sets of Lyapunov spectra, with no consistent difference apparent. Exponents are present at values of around +1.37 and 0, as before, with the calculation of the negative exponent equally curtailed by the long *svd* window in both cases.

This shows that the tone suppression architecture of sigma delta modulation does not adversely affect the chaotic signal under consideration, despite claims that such a configuration is itself chaotic [8]. Such claims appear to be based on the idea that the integrator with a pole outside the unit circle is unstable, causing trajectories in phase space to diverge exponentially, but these trajectories are folded back in on themselves by the one-bit quantiser. In fact, this is not a very rigorous way of labelling a system chaotic, but, as was discussed in chapter 2, such a rigorous definition is a matter of some controversy and this definition is as good as any. The important point is that the tone suppression architecture, whether it is genuinely chaotic or not, does not affect the Lyapunov exponents of the modulated signal any more than conventional ΣΔM does.

## 7.11 DISCUSSION

In this chapter, it has been shown that ΣΔM of a chaotic signal does not adversely affect the measurable Lyapunov spectrum of the attractor, in comparison to a direct quantisation of the same data. It was also shown that, for quantisation precisions greater than around 8 bits, the positive and zero exponents can be calculated with some reliability. The measurable negative exponents of the original attractor are compromised, however, due to the *svd* reduction of the data. This is a common problem throughout the field, but it has been shown that the effects are not worsened by the use of ΣΔM.

The possibility that ΣΔM may introduce an extra dimension, and therefore an extra Lyapunov exponent, into the system was also considered. The results show that this does not, in fact, occur for the three chaotic signals considered, nor for the sine wave. It would not seem unreasonable to make a more general statement based on this evidence that sigma delta modulation does not affect the dimension of a modulated input, with the possible exception of a d.c. input. It was further indicated that higher order modulators do not have any further degrading effect on the measurable dynamics of a signal under study.

It was made clear that the number of dimensions in which a signal is embedded for analysis can affect the results. The majority of signals must be embedded in a greater dimension than the dynamical dimension of the system initially implies.

The tone-suppressing architecture suggested for ΣΔM was finally considered. This architecture has been labelled chaotic in the past, though we show that its effects on the measurable dynamics of a modulated Lorenz signal are negligible in comparison to the effects of conventional ΣΔM

or direct quantisation.

Consequently, the results of this chapter imply that the sigma delta modulator is a "safe" way of measuring a chaotic signal, taking into account such caveats already mentioned whereby care must be taken over the sampling rate and the embedding dimension.

# Chapter 8

# CONCLUSIONS AND DISCUSSION

## 8.1 PRELIMINARY DISCUSSION

This thesis set out to investigate the effect the sigma delta modulator, a form of analogue to digital converter, has on a chaotic signal. The fact that the sigma delta modulator consists of a non-linear element, a one bit quantiser, within a feedback loop, a classic route to chaos in itself, implied that using such a device to measure a chaotic signal may adversely affect the measurable dynamics of that signal. This basic structure, a non-linearity which is somehow folded back on itself, is a well-documented cause of chaotic dynamics, with many known chaotic systems being describable in this generalised manner.

The question was of particular concern due to both the increasing popularity and availability of sigma delta modulators across an increasingly broad spectrum of applications, and the continually burgeoning amount of research being carried out on sampled chaotic systems. It was further motivated by a body of evidence indicating that a variety of signals frequently undergoing sigma delta modulation, such as speech and medical signals, may be chaotic in nature, as well as research implying that circuit structures similar to that of the sigma delta modulator were capable of chaotic modes of operation with a non-chaotic input. The sigma delta modulators considered involved analogue integrators rather than the more commonly used discrete variety.

Clearly, if the method of measuring a chaotic signal has an adverse effect on the measurable dynamics of that signal, then action must be taken to either include this effect in the subsequent analysis, or to nullify its consequences.

To date, a full description of the sigma delta modulator with a moving input signal has not been achieved. The analyses which have been published are mathematically complex and highly involved, even for a d.c. or single sinusoid input to the modulator, and, as such, would be extremely unwieldy to apply under the added complexities involved in considering a chaotic signal input. Consequently, the bulk of the work and results contained in this thesis has been experimental in nature, based on observations derived from simulations of $\Sigma\Delta$M. However, this approach introduced further problems, since, to date, the vast majority, and certainly the

most successful, of published work on analysing chaotic systems has been based on considering systems with a known algebraic description. In considering a measured time series, generated by a system for which a full dynamical description does not exist, the current knowledge of chaos science is stretched to its limits.

This chapter details the progress made in researching this topic, the conclusions drawn from the results, and suggestions for further work in the area.

## 8.2 ACHIEVEMENTS

The initial approach was to formulate a set of differential equations representing $\Sigma\Delta$M. Necessarily, this involved a continuous approximation of the circuit, which is partly analogue, partly digital, and a hyperbolic tangent function was chosen to model the one bit quantiser. Using this differential equation, it was hoped to consider the equation as a system in itself and thus to investigate the possibility of chaotic modes of operation of the sigma delta modulator. It would then be informative to introduce the equation into a set of $n$ equations representing a $n$-dimensional system to produce a $n+1$-dimensional system. The analysis of this system ought to be equivalent to considering the action of a sigma delta modulator with an input taken from the $n$-dimensional system.

However, in order to fully represent the structure of the sigma delta modulator, a delay differential equation had to be formulated, which led to problems in applying the Lyapunov exponent calculation procedure. These problems were addressed using Farmer's approach of splitting the delay period into a series of discrete steps. Unfortunately, this still did not suffice to allow a satisfactory calculation of the Lyapunov exponents of the attractor as a whole. Although it was indicated that, on its own, the equation representing $\Sigma\Delta$M was not chaotic, producing only zero and negative Lyapunov exponents, the choice of parameters required to provide this result proved incompatible with allowing the input to the modulator to be driven by a chaotic system. Essentially, what was happening was that the dynamics of the modulator were on a vastly different time-scale to the dynamics of the input signal, and thus analysing their interaction was not possible by this method, since the changes wrought by the modulator were dying away too quickly to affect the long term calculation. It could be argued that this implies that the modulator is non-chaotic, since what is essentially happening is that a small change in the dynamics is not resulting in a great change over time; i.e. the system does not exhibit sensitive dependence on initial conditions. This chapter of the work did imply that the first order sigma delta modulator is not capable of chaotic modes of operation with a non-chaotic input. It also indicated that further work on the effects of $\Sigma\Delta$M on a chaotic signal would have to be based on analysis of the time series produced after $\Sigma\Delta$M, rather than the interior states of the circuit during modulation.

Before moving on to this topic, the differential equations constructed to represent $\Sigma\Delta$M were utilised in a stability study of the circuit. Since the equations appear to give an accurate

representation of the modulator, information about the modulator's stability behaviour may be gleaned from the application of a stability analysis to the equations. It was discovered empirically that the equations were only genuinely unstable under certain conditions with zero integrator leakages; for other values of the circuit coefficients, the equations behaved in either oscillatory or asymptotic modes. Since the oscillatory mode would lead to correct operation of the modulator, and the asymptotic mode would not, the factors leading to the occurrence of these two modes of behaviour were investigated. In the asymptotic mode, the output of the equations tends toward a d.c. value and stays there, i.e. a fixed point is attained. Consequently a fixed point analysis was applied to the differential equations, and it was found that the results from this analysis matched exactly the boundaries between the asymptotic and oscillatory modes of operation observed in the numerical solution of the differential equations, and also in a software simulation of the sigma delta modulator itself. These results were presented for first, second and third order modulators, and the analysis was shown to be applicable to a generalised $n$th order sigma delta modulator.

The thesis then moved on to the central problem of the effect of $\Sigma\Delta$M on a chaotic signal. To investigate this, the Lyapunov exponents of an attractor were considered before and after $\Sigma\Delta$M, and compared to a direct quantisation of the data. In order to achieve this, an algorithm had to be implemented for the extraction of Lyapunov spectra from the time series data. It became clear from the literature that a robust and unambiguous method of achieving this, particularly in the presence of noise inevitably introduced into the time series to be considered by the two methods of quantisation under investigation, was not in existence. Consequently, an algorithm was developed to extract Lyapunov exponents from a single time series. The efficacy of this algorithm was demonstrated, and the limitations of its applications were discussed, before invoking it in conjunction with the sigma delta modulated data.

The final part of the thesis dealt with results achieved by applying this algorithm to a range of time series after both $\Sigma\Delta$M and direct quantisation. It was shown that, over a range of sampling precisions, the positive and zero exponents of a number of chaotic attractors were not affected, to within the calculation limits of the algorithm, by either $\Sigma\Delta$M or direct quantisation. The negative exponents, however, were more difficult to estimate due to the noise reduction techniques inherent in the algorithm. However, it was clear that no consistent difference occurred between the negative exponents estimated from the sigma delta modulated data and those from the directly quantised data.

These results imply that the sigma delta modulator does not, as feared, adversely affect the measurable dynamical properties of the system being converted. Indeed, the results would suggest that $\Sigma\Delta$M is as valid a method of measuring a chaotic signal as any other.

However, it was implied in the section on the Duffing attractor, that the choice of sample period is of some importance. The vacillations introduced by errors in the sigma delta modulator's attempts to quantise an input signal around half-way between two quantisation levels actually

appeared to improve the calculation of the negative exponent at higher sample rates. This is probably due to these oscillations improving the averaging nature of the noise reduction processes employed by the Lyapunov exponent extraction algorithm, and, indeed, mirroring the demodulation process to return to a better approximation of the original signal. It was also made clear that the choice of embedding dimension is important in the analysis of these chaotic systems. At too low an embedding dimension, the extra errors introduced by the sigma delta modulator occasionally being one quantisation level out in its estimate appeared to be sufficient to introduce extra false nearest neighbours into the calculation and thus reduce the amplitude of the negative exponent. By embedding in a higher dimension and then performing a local reduction at each step of the calculation, these effects were nullified and the results shown to match those from the directly quantised data.

Although the majority of the work considered only a first order sigma delta modulator, it was briefly shown that a second order modulator does not exacerbate the situation. This is to be expected since the purpose of employing a higher order modulator is to reduce the frequency of wrong quantisations. The recently developed tone-suppressing architecture for $\Sigma\Delta$M was also considered. Although this type of converter has been labelled as chaotic in the literature, due to the behaviour of its internal states, it was shown that it does not affect the Lyapunov exponents of a time series generated from Lorenz' equations.

The fact that no consistent deterioration in the measured Lyapunov exponents is observable for the sigma delta modulated data, in comparison to the directly quantised data, implies that the predictability of a time series is not compromised by the choice of a sigma delta modulator to measure it.

## 8.3 LIMITATIONS

The limitations of this work can be grouped into two areas: those caused by the lack of a complete analysis or information on sigma delta modulators, and those caused by the fact that the study of chaos theory, particularly "real-world" chaos, is very much a science in its infancy.

Although the majority of the work presented in this thesis, especially the study of the effects of $\Sigma\Delta$M on the Lyapunov exponents of a signal, has been confined to considering a first order modulator, it would perhaps have been informative to consider some higher order or more complex architectures that are actually in use in commercially available packages. Unfortunately, the manufacturers of these devices are somewhat leery of describing their product in the kind of detail required for this type of investigation. This is understandable given that there are no rigorous analyses, or design guidelines, for higher order sigma delta modulators. Consequently the design of a commercially viable circuit is a complex process, and companies are unlikely to give away such designs for free. However, as was discussed during the thesis, higher order modulators do not introduce extra non-linearities into the circuit, and the implication of the research presented here is that the study of the first order modulator is sufficient. This does

not apply to the increasingly popular MASH converter, however, which does contain extra non-linearities in the form of additional one-bit quantisers.

The first two chapters of research are based on a continuous model of a sigma delta modulator. Again, due to the lack of rigorous descriptions of $\Sigma\Delta$M, the evidence that this model is an accurate representation of a sigma delta modulator is largely empirical, although it is hoped that the subsequent algebraic and stability analyses support this view.

Indeed, it is this empirical nature of the work that is, perhaps, its biggest limitation. This is especially true of the study of the effects of $\Sigma\Delta$M on the dynamics of a chaotic signal, as indicated by the change in the Lyapunov spectrum of that signal. Work on analysing the dynamics of measured chaotic time series is often unwieldy and ambiguous. We hope that the results presented in this thesis are sufficiently rigorous and consistent to support the theories put forward. However, it ought to be pointed out that a certain amount of interpretation was inevitably brought to bear on the results, particularly in the claims that there is no discernible difference between the exponents calculated from modulated data to those calculated from directly quantised data.

Although we discuss the signal's predictability in terms of its Lyapunov spectrum, it may have been of further interest to consider some other predictability measure, such as that described in [78]. However, since the indications were that no reduction in predictability was occurring, this was considered superfluous to the work. It is also worth noting that any such predictability measure will suffer from the same drawbacks of interpretation and application that are inherent in a Lyapunov exponent extraction algorithm.

## 8.4 FURTHER WORK

An amount of further work has been suggested in the preceding discussion of the limitations of the work. In particular, it would be desirable to carry out the Lyapunov exponent analysis on commercially available sigma delta modulator architectures, as well as on the MASH type converter.

There are a multitude of opportunities for further research into the area of analysing the dynamical properties of a chaotic system using a time series derived from that system. The question of estimating the dimension of an attractor has not been adequately addressed, and is an on-going topic of discussion. We would certainly not claim that our method of extracting Lyapunov exponents from a time series is the be-all and end-all on the subject. The results from our algorithm still require some interpretation and a great deal of care is required in applying the algorithm. Further noise-cancellation techniques have been suggested and work is continuing at Edinburgh University to improve on the algorithm described in this thesis.

Taking a broader view of the aims of this thesis, although it was shown that this specific example of a sigma delta modulator does not appear to adversely affect the measurable dynamics of a

chaotic signal, there are many more non-linear filters of which this may not be true. The initial problem of what happens when a non-linear signal is processed by a non-linear filter still exists.

# References


[1] R.Badii and A.Politi. *Dimensions and entropies in chaotic systems*, chapter On the fractal dimension of filtered chaotic signals, pages 67–73. Berlin: Springer, 1986.

[2] R.Badii, G.Broggi, B.Derighetti, M.Ravani, S.Ciliberto, A.Politi, and M.A.Rubio, "Dimension increase in filtered chaotic signals", *Physical Review Letters*, vol. 60, no. 11, pp. 979–82, Mar 1988.

[3] F.Mitschke, "Acausal filters for chaotic signals", *Physical Review A*, vol. 41, no. 2, pp. 1169–71, Jan 1990.

[4] F.Mitschke, M.Moller, and W.Lange, "Measuring filtered chaotic signals", *Physical Review A*, vol. 37, no. 11, pp. 4518–21, Jun 1988.

[5] D.S.Broomhead, J.P.Huke, and M.R.Muldoon, "Linear filters and non-linear systems", *J.R. Statist Soc. B*, no. 2, 1992.

[6] M.Jaidane-Saidane and O.Macchi, "Quasi-periodic self-stabilisation of adaptive ARMA predictors", *Int Jnl Adaptive Control and Signal Processing*, vol. 2, pp. 1–31, 1988.

[7] O.Macchi and C.Uhl, "Stability of the DPCM transmission system", *IEEE Trans Circuits and Systems II*, vol. 39, no. 10, pp. 705–22, Oct 1992.

[8] S.Hein, "Exploiting chaos to suppress spurious tones in general double-loop sigma delta converters", *IEEE Trans Circuits and Systems II*, vol. 40, no. 10, pp. 651–659, Oct 1993.

[9] O.Feely, "Nonlinear dynamics of chaotic double-loop sigma-delta modulation", in Proceedings *IEEE Proc ISCAS*, vol. 6, pages 101–106, 1994.

[10] M.Banbrook and S.McLaughlin, "Speech characterisation by nonlinear methods", in Proceedings *IEEE Workshop Nonlinear Signal and Image Processing*, pages 396–9, Jun 1995.

[11] S.S.Narayanann and A.A.Alwan, "A nonlinear dynamical systems analysis of fricative consonants", *Jnl of Acoustical Society of America*, vol. 97, no. 4, pp. 2511–24, Apr 1995.

[12] H.Leung and S.Haykin, "Is there a radar clutter attractor?", *Applied Physics Letters*, vol. 36, no. 6, June 1990.

[13] M.G.Signorini, S.Cerutti, A.Filannimo, and S.Guzzetti, "Nonlinear dynamics in heart-rate variability signal through deterministic chaotic approach", in Proceedings *IEEE Workshop Nonlinear Signal and Image Processing*, pages 499–503, Jun 1995.

[14] K.Vibe and J-M.Vesin, "Chaos detection methods with application to heart rate variability", in Proceedings *IEEE Workshop Nonlinear Signal and Image Processing*, pages 125–9, Jun 1995.

[15] E.Lorenz, *The essence of chaos*. UCL Press, 1993.

[16] M.Feigenbaum, "Qualitative universality for a class of nonlinear transformations", *Jnl of Statistical Physics*, vol. 19, pp. 25–52, 1978.

[17] M.Feigenbaum, "The universal metric properties of nonlinear transformations", *Jnl of Statistical Physics*, vol. 21, pp. 669–706, 1979.

[18] T.Y.Li and J.Yorke, "Period three implies chaos", *American nMathematical Monthly*, vol. 82, pp. 985–92, 1975.

[19] R.May, "Simple mathematical dynamics with very complicated dynamics", *Nature*, vol. 261, pp. 459–67, 1976.

[20] B.Mandelbrot, *The fractal geometry of nature*. Freeman, New York, 1977.

[21] D.Ruelle and F.Takens, "On the nature of turbulence", *Communications in Mathematical Physics*, vol. 20, pp. 167–92, 1971.

[22] D.Ruelle, "Strange attractors", *Mathematical Intelligencer*, vol. 2, pp. 126–37, 1980.

[23] J.Gleick, *Chaos: making a new science*. Cardinal, London, 1987.

[24] M.Henon, "A two-dimensional mapping with strange attractor", *Communications in Mathematical Physics*, vol. 50, pp. 69–77, 1976.

[25] E.N.Lorenz, "Deterministic non-periodic flow", *J. Atmos. Sci*, vol. 20, pp. 130–141, 1963.

[26] M.C.Mackey and L.Glass, "Oscillation and chaos in physiological control systems", *Science*, vol. 197, pp. 287, 1977.

[27] J.D.Farmer, "Chaotic attractors of an infinite dimensional dynamical system.", *Physica D*, pp. 366–393, 1982.

[28] G.L.Baker and J.P.Gollub, *Chaotic dynamics: an introduction*. Cambridge University Press, 1990.

[29] T.S.Parker and L.O.Chua, "Chaos: a tutorial for engineers", *Proc IEEE*, vol. 75, no. 8, pp. 982–1007, Aug 1987.

[30] P. Grassberger and I. Procaccia, "Characterization of strange attractors", *Physical Review Letters*, vol. 50, no. 5, pp. 346–349, January 1983.

[31] P.Frederickson, J.L.Kaplan, E.D.Yorke, and J.A.Yorke, "The Liapunov dimension of strange attractors", *Jnl of Differential Equations*, vol. 49, pp. 185–207, 1983.

[32] A. Wolf, J.B. Swift, H.L. Swinney, and J.A. Vastano, "Determining Lyapunov exponents from a time series", *Physica D*, vol. 16, pp. 285–317, 1965.

[33] J.P. Eckmann and D. Ruelle, "Fundamental limitations for estimating dimensions and Lyapunov exponents in dynamical systems", *Physica D*, vol. 56, pp. 185–187, 1992.

[34] R.L.Smith, "Estimating dimension in noisy chaotic time series", *Jnl R Statist Soc B*, vol. 54, no. 2, 1992.

[35] F.Takens. *Dynamical Systems and Turbulence*, vol. 898 of *Lecture Notes in Mathematics*, pages 366–381. Berlin: Springer, 1981.

[36] A.M. Fraser and H.L. Swinney, "Independent coordinates for strange attractors from mutual information", *Physical Review A*, vol. 33, no. 2, pp. 1134–1140, February 1986.

[37] D.S. Broomhead and G.P. King, "Extracting qualitative dynamics from experimental data", *Physica D*, vol. 20, pp. 217–236, 1986.

[38] D.S.Broomhead, "Private communication".

[39] O.E.Rossler, "An equation for hyper-chaos", *Physics Letters*, vol. 71A, pp. 155, 1979.

[40] A.G.Darbyshire and D.S.Broomhead, "The calculation of Liapunov exponents from time series data", *Submitted to Physica D*, 1995.

[41] D.Kugiumtzis, B.Lillekjendlie, and N.Christophersen, "Chaotic time series. part 1: estimation of invariant properties in state space", *Modeling, identification and control*, vol. 15, no. 4, 1994.

[42] G.Benettin, L.Galgani, A.Giorgilli, and J.M.Strelcyn, "Lyapunov characteristic exponents for smooth dynamical systems and for Hamiltonian systems: a method for computing all of them.", *Mechanica 15*, vol. 9, 1980.

[43] J. Holzfuss and W. Lauterborn, "Liapunov exponents from a time series of acoustic chaos", *Physical Review A*, vol. 39, no. 4, pp. 2146–2152, February 1989.

[44] D.S. Broomhead and G.P. King. *Nonlinear phenonema and chaos*, chapter On the qualitative analysis of experimental dynamical systems, pages 113–144. Malvern science series. Adam Hilger, Bristol, 1986.

[45] M.Sano and Y.Sawada, "Measurement of the Lyapunov spectrum from a chaotic time series", *Physical review letters*, vol. 55, no. 10, pp. 1082–1085, September 1985.

[46] H.D.I.Abarbanel, R.Brown, and M.B.Kennel, "Local Lyapunov exponents computed from observed data", *Journal of Nonlinear Science*, vol. 1, pp. 175–199, 1991.

[47] R.Steele, *Delta modulation systems*. Pentech Press, London, England, 1975.

[48] H.Inose, Y.Yasuda, and J.Marakami, "A telemetering system by code modulation, delta-sigma modulation", *IRE Trans Space, Electronics and Telemetry*, pp. 204–209, Sept 1962.

[49] J.C.Candy and O.J.Benjamin, "The structure of quantisation noise from sigma-delta modulation", *IEEE Trans Communications*, vol. 29, pp. 1316–29, Sep 1981.

[50] J.E.Iwersen, "Calculated quantising noise of single-integration delta modulation coders", *Bell Syst Tech Jnl*, vol. 48, pp. 2359–89, Sep 1969.

[51] S.H.Ardalan and J.J.Paulos, "An analysis of nonlinear behaviour in delta sigma modulators", *IEEE Trans Circuits and Systems*, vol. 36, no. 6, Jun 1987.

[52] R.M.Gray, "Oversampled sigma-delta modulation", *IEEE Trans Communications*, vol. COM35, no. 5, pp. 481–9, May 1987.

[53] R.M.Gray, W.Chou, and P.W.Wong, "Quantization noise in single-loop sigma-delta modulation with sinusoidal inputs", *IEEE Trans Communications*, vol. 37, no. 9, pp. 956–67, Sep 1989.

[54] P.W.Wong and R.M.Gray, "Two-stage sigma delta modulation", *IEEE Trans Acoustics Speech and Signal Processing*, vol. 38, no. 11, pp. 1937–51, Nov 1990.

[55] P.W.Wong and R.M.Gray, "Two-stage sigma delta modulation", *IEEE Trans Acoustics, Speech and Signal Processing*, vol. 38, no. 11, pp. 1937–51, Nov 1992.

[56] N.He, F.Kulhmann, and A.Buzo, "Double loop sigma delta modulation with dc input", *IEEE Trans Communications*, vol. 38, pp. 487–95, Apr 1990.

[57] S.Rangan and B.Leung, "Quantisation noise spectrum of double-loop sigma-delta converter with sinusoidal input.", *IEEE Trans Circuits and Systems*, vol. 41, no. 2, pp. 168–173, Feb 1994.

[58] S.Hein and A.Zakhor, "On the stability of sigma delta modulators", *IEEE Trans Signal Processing*, vol. 41, no. 7, Jul 1993.

[59] H.Wang, "A geometric view of sigma delta modulation", *Iee Trans Circuits and Systems*, vol. 39, no. 6, pp. 402–5, Jun 1992.

[60] May R, "On the behaviour of the double-loop sigma delta modulator", *IEEE Trans Circuits and Systems*, vol. 40, no. 8, pp. 467–79, Aug 1993.

[61] B.E.Boser and B.A.Wooley, "Quantisation error spectrum of sigma delta modulators", *IEEE Proc ISCAS*, 1988.

[62] J.C.Candy and G.C.Temes, editors, *Oversampling delta-sigma converters – theory, design and simulation.* IEEE Press, 92.

[63] Y.Matsuya, K.Uchimara, A.Iwata, T.Kobayashi, M.Ishikawa, and T.Yoshitome, "A 16-bit oversampling A-to-D conversion technology using triple-integration noise-shaping", *IEEE Jnl solid state circuits*, vol. SC-22, no. 6, pp. 921–9, Dec 1987.

[64] K.Uchimura, T.Hayashi, T.Kimura, and A.Iwata, "Oversampling A-to-D and D-to-A converters with multisatge noise shaping modulators", *IEEE Trans Acoustics, Speech and Signal Processing*, vol. 36, no. 12, pp. 1899–1905, Dec 1988.

[65] T.Karema, T.Ritoniemi, and H.Tenhunen, "An over-sampled sigma delta A/D converter circuit using two stage fourth order modulator", *IEEE Proc ISCAS*, pp. 3279–82, May 1990.

[66] L.R.Carley, "A noise-shaping coder topology for 15+ bit converters", *IEEE Jnl Solid-state circuits*, vol. SC24, pp. 267–73, Apr 1989.

[67] PCM1760P/U. Multi-bit enhanced noise shaping 20 bit analog to digital conversion system. Technical Report PDS 1174a, Burr Brown, Sep 1993.

[68] D.R.Welland, B.P.D.Signore, E.J.Swanson, T.Tanaka, K.Hamashita, S.Hara, and K.Takasuka, "A stereo 16-bit sigma delta converter for digital audio", *Jnl of the Audio Engineering Society*, vol. 37, pp. 476–86, Jun 1989.

[69] C.Dunn and M.Sandler, "Use of clipping in sigma-delta modulators", in Proceedings *IEE Coll Oversampling Techniques and Sigma-Delta Modulation*, pages 8/1–9, Mar 1994.

[70] G.Duffing, "Erzwungene schwingungen bei veranderlicher eigenfrequenz vieweg", *Braunschweig*, 1918.

[71] R.M.Gray, "Quantisation noise spectra", *IEEE Trans Information Theory*, vol. 36, no. 6, pp. 1220–1244, Nov 1990.

[72] J.Millman and C.C.Halkias, *Integrated Electronics.* McGraw Hill, 1971.

[73] W.H.Press, B.P.Fleming, S.A.Teukolsky, and W.T.Vetterling, editors, *Numerical recipes in C: the art of scientific computing.* Cambridge University Press, 92.

[74] H.O.Walther, "The 2-dimensional attractor of $x'(t) = -\mu x(t) + f(x(t-1))$", *Memoirs of the American Mathematical Society*, vol. 113, no. 544, pp. 1–76, Jan 1995.

[75] P.Glendinning, *Stability, instability and chaos: an introduction to the theory of nonlinear differential equations.* Cambridge University Press, 1994.

[76] N.V.Tu Pierre, *Dynamical systems: an introduction with applications in economics and biology.* Springer-Verlang, 1992.

[77] E.F.Stikvoort, "Some remarks on the stability of the noise shaper or sigma delta modulator", *IEEE Trans Communications*, vol. 36, no. 10, Oct 1988.

[78] M.Casdagli, "Nonlinear prediction of chaotic time series", *Physica D*, vol. 35, pp. 335–356, 1989.

[79] M.Casdagli, "Chaos and deterministic versus stochastic non-linear modelling", *Journal of the Royal Statistical Society B*, vol. 54, no. 2, pp. 303–328, 1991.

[80] G.Sugihara, "Non-linear forecasting for the classification of natural time series", *Phil. Trans. Royal Society of London Series A (Physical Sciences and Engineering)*, vol. 348, no. 1688, pp. 477–95, Sep 1994.

[81] W.E. Weisel, "Continuous time algorithm for Lyapunov exponents. I and II", *Physical Review E*, vol. 47, no. 5, pp. 3686–3697, May 1993.

[82] R.Penrose, "A generalised inverse for matrices", *Proc Camb Phil Soc*, vol. 51, pp. 406–13, 1955.

[83] J. Theiler, "Spurious dimension from correlation algorithms applied to limited time-series data", *Physical Review A*, vol. 34, no. 3, pp. 2427–2432, September 1986.

[84] J.P.Eckmann and D.Ruelle, "Ergodic theory of chaos and strange attractors", *Rev. Mod. Phys.*, vol. 57, pp. 617–56, 1985.

[85] R.A.Johnson, K.J.Palmer, and G.R.Sell, "Ergodic properties of linear dynamical systems", *SIAM J. Math. Anal.*, vol. 18, pp. 1–33, 1987.

[86] R.A.Horn and C.R.Johnson, *Matrix analysis*. Cambridge University Press, 1985.

[87] J.P. Eckmann, S.O.Kamphorst, D. Ruelle, and S. Ciliberto, "Liapunov exponents from time series", *Physical Review A*, vol. 34, no. 6, pp. 4971–4979, December 1986.

[88] J.T.Thompson and H.B.Stewart, *Nonlinear dynamics and chaos*. J.Wiley, 1986.

[89] O.E.Rossler, "An equation for continuous chaos", *Physics Letters*, vol. 57A, pp. 397, 1976.

# Appendix A
# Original publications

The work described in this thesis has been reported in the following publications:

- † M.Banbrook, G.Ushaw and S.McLaughlin, "Lyapunov exponents from short and noisy time series", in Chaos, Solitons and Fractals, vol7, no 7, pages 973-976.
- † G.Ushaw and S.McLaughlin, "To sigma delta modulate or not to sigma delta modulate: the chaos question", in Proceedings 3rd International Workshop on Nonlinear Dynamics of Electronic Systems, UCD, Dublin, pages 29-32, July, 1995.
- G.Ushaw and S.McLaughlin, "Sigma delta modulation of a chaotic time series: a nonlinear signal in a nonlinear system", in Proceedings 6th IEEE DSP Workshop, Yosemite, California, pages 63-66, October, 1994.
- † G.Ushaw and S.McLaughlin, "On the stabilty and configuration of sigma delta modulators", Proceedings IEEE ISCAS, London, UK, vol 5 pages 349-52, May, 1994.
- G.Ushaw and S.McLaughlin, "On the configuration of second order sigma delta modulator", in Proceedings IEE Colloquium "Over-sampling techniques and sigma delta modulation", London, UK, Digest no 1994/083, pages 2/1-4, March, 1994.
- G.Ushaw, S.McLaughlin, D.T.Hughes and B.Mulgrew, "A representation of sigma delta modulators as continuous systems for analysis of their effect on chaotic signals", in Proceedings SPIE Chaos in Communications, San Diego, California, Volume 2038, pages 103-14, July, 1993.
- D.T.Hughes, G.Ushaw, S.McLaughlin, B.Mulgrew and D.S.Broomhead, "The search for chaotic output from the sigma delta modulator: an archetypal retarded nonlinear system", in Proceedings SPIE Chaos in Communications, San Diego, California, Volume 2038, pages 194-204, July, 1993.
- G.Ushaw, S.McLaughlin and B.Mulgrew, "An analysis of sigma delta modulators as continuous systems", in Proceedings IEE Colloquium "Advanced A-D and D-A conversion techniques and applications", London, UK,, Digest no 1993/128, pages 3/1-5, May, 1993.

† Reprinted in this appendix.

Paper submitted:

- M.Banbrook, G.Ushaw and S.McLaughlin, "How to extract Lyapunov exponents from short and noisy time series", *IEEE Trans. Signal Processing*, submitted July 1995.

# On the stability and configuration of sigma delta modulators

G. Ushaw
Department of Electrical Engineering,
The University of Edinburgh,
Scotland. EH9 3JL
gu@ee.ed.ac.uk (+44) 31 650 5660

S. McLaughlin
Department of Electrical Engineering,
The University of Edinburgh,
Scotland. EH9 3JL
sml@ee.ed.ac.uk (+44) 31 650 5578

## ABSTRACT

A set of ordinary differential equations (ODEs) has been constructed to represent a continuous sigma delta modulator ($C\Sigma\Delta M$) [1] – i.e. a continuous equivalent of a conventional sigma delta modulator ($\Sigma\Delta M$). This paper is concerned with a stability analysis of these equations with particular reference being made to values representing the gains of the feedback loop and the integrator leakage in the circuit. Conditions for the stability of the equations representing second and third order modulation are derived. The results from this process are used on a conventional simulation of sigma-delta modulation, and the applicability of this method is discussed. The criteria for stable operation are extended to $n^{th}$ order sigma delta modulation and to a generalised architecture for sigma delta modulation. The results are compared to the conditions for stability derived from the work of various authors.

## SIGMA DELTA MODULATION AS ODES

A set of differential equations has been derived to represent a continuous model of sigma delta modulation. The equations for second order modulation are:

$$\frac{dx(t)}{dt} = w(t) - k_0 x(t) - a_0 M \tanh \frac{px(t-\tau)}{M} \quad (1)$$

$$\frac{dw(t)}{dt} = \lambda - k_1 w(t) - a_1 M \tanh \frac{px(t-\tau)}{M} \quad (2)$$

It has been shown in a previous paper [1] that these equations, when solved numerically by the Runge Kutta method for example, are an accurate model of sigma delta modulation providing certain assumptions hold. The slope of the hyperbolic tangent must be steep (i.e. $p$ high) – this is reasonable since the purpose of the tanh function is to model a one-bit quantiser. The delay $\tau$ is intended to tie the continuous system to the discrete circuit by modelling the sampling rate of the modulator, although it also incorporates any delay introduced by the switching time of the quantiser and other circuit elements. The coefficients $k_0, k_1, a_0, a_1$ represent integrator leakages and the feedback constants respectively, in an attempt to correctly model the circuit characteristics of a $\Sigma\Delta M$. The meanings of the various symbols are best made clear with reference to figure 1.

GU thanks SERC and DRA for their support in this work, SML similarly thanks the Royal Society.

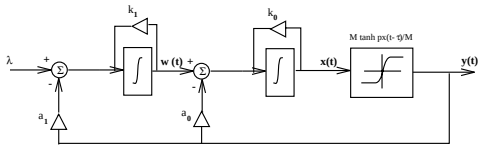


Figure 1: *Second Order Continuous Sigma Delta Modulator*

## STABILITY ANALYSIS OF ODES

Two methods have been utilised to investigate the stability of the ordinary differential equations representing second order $C\Sigma\Delta M$. The fact that both techniques provide similar results suggests that they are mathematically equivalent. Consequently only the fixed point method will be used in subsequent sections of the paper. In this first instance however, the Laplace transform method is also presented as this is a form with which the signal processing community is more familiar. In both methods a constant input $\lambda$ has been assumed; this is a reasonable mode to investigate due to the oversampling nature of the device. First, the fixed point method.

At a fixed point the derivatives of $x$ and of $w$ are zero. To aid clarity, assume that the tanh function can only equal $\pm 1$ – in the case when it is $+1$, (2) can be solved for $\hat{w}$:

$$\hat{w} = \frac{\lambda - a_1}{k_1} \quad (3)$$

Substituting this into (1) gives an expression for $\hat{x}$:

$$\hat{x} = \frac{\lambda - a_1 - a_0 k_1}{k_0 k_1} \quad (4)$$

This fixed point $\hat{x}$ will be finite, and hence the system will be stable, for all non-zero values of the integrator leakages $k_0$

and $k_1$. The numerator of this expression is of interest also and shall be discussed later in this paper.

Alternatively, the stability can be analysed via Laplace Transform, again the tanh function is set to $+1$ for simplicity. The ODEs become

$$sx(s) - x_0 = w(s) - k_0 x(s) - a_0 \quad (5)$$

$$sw(s) - w_0 = \lambda - k_1 w(s) - a_1 \quad (6)$$

Setting initial conditions ($x_0, w_0$) to zero, gives

$$x(s) = -\frac{s + \frac{a_1 + a_0 k_1 - \lambda}{a_0}}{(s + k_0)(s + k_1)} \quad (7)$$

The implications for stability are the same as for the fixed point method and it can be seen that the same expression has occurred in the numerator.

## OPERATIONAL BOUNDARIES FROM SIMULATION

A simulation of a second order sigma delta modulator was used to investigate the effects of the values of the feedback constants $a_0$ and $a_1$ and the integrator leakages $k_0$ and $k_1$ on the operation of the modulator. It was found that certain configurations (i.e. certain combinations of values of these coefficients) caused the modulator to operate incorrectly, in that the output remained at $+1$ at all times. It is tempting to call this condition instability; the output of the modulator is bounded by the one-bit quantiser so a $\Sigma\Delta M$ is labelled unstable when the input to the quantiser becomes unbounded resulting in long periods of time when the output is at the same value (i.e $\pm 1$). However, this type of output will also be observed when the input to the quantiser simply remains positive as was found to be the case here, indeed the input to the quantiser was seen to be asymptotic to a dc level. Hence the term instability is inappropriate in this situation. We have chosen to label the condition arising from such configurations as asymptotic operation of the modulator. Figure 2 shows the two different types of time series seen at $x(t)$.

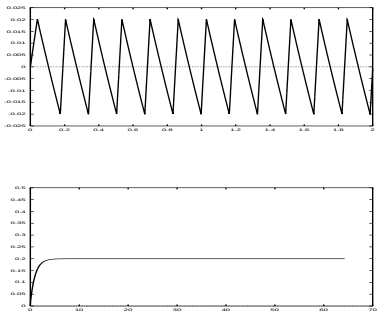

Figure 2: *Plot of input to quantiser, $x(t)$, during a)correct operation and b)asymptotic operation*

With this in mind consider the plot in figure 3, which shows the results for a second order sigma delta modulator with an input $\lambda = 0.5$, and $k_0 = k_1 = 1$. The dark area is where correct operation occurs, the light area where asymptotic operation is observed.

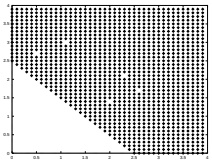

Figure 3: *Operational plot of second order $\Sigma\Delta M$ with varying $a_0$ (abscissa) and $a_1$ (ordinate)*

It can be seen that a straight line divides the two areas. By taking a number of further plots with a range of values of $\lambda$, $k_0$ and $k_1$ it was found that the equation of this straight line boundary is

$$\lambda = a_1 + a_0 k_1 \quad (8)$$

A Runge Kutta iterative process was used to solve the ordinary differential equations representing the second order $C\Sigma\Delta M$ and a number of similar plots were taken. Again a straight line boundary was seen and its equation proved to be the same as in (8).

## DISCUSSION OF RESULTS FOR SECOND ORDER MODULATION

Consider the numerators of (4) and (7). In each case, for the numerator to be positive

$$\lambda > a_1 + a_0 k_1 \quad (9)$$

Now, if this were the case then the value of $x$ would remain positive at all times for positive $k_0$ and $k_1$. Remember that $x(t)$ represents the signal at the input to the quantiser. Consequently when (9) is true the output of the modulator is a constant $+1$ and the modulator is in an asymptotic operation configuration. If $\hat{x}(t)$ can go negative, i.e. if (9) is untrue, then the output of the quantiser can switch to $-1$, changing the sign of $a_0$ and $a_1$ in (4). At first sight this seems to imply that the output will flip back and forth at an infinite rate, but bear in mind that (4) gives an expression for the fixed point of the system, that is the value to which $x(t)$ tends, also (4) was derived from an approximation of the differential equations representing $C\Sigma\Delta M$ – in particular note that the delay $\tau$ will cause this switching to occur over some time period.

Hence a more general rule can be written for the correct operation of second order sigma delta modulators

$$|\lambda| < a_1 + a_0 k_1 \quad (10)$$

and the second order modulator is stable for all non-zero values of the integrator leakages

$$|k_0|, |k_1| > 0 \tag{11}$$

## THIRD ORDER MODULATION

The ordinary differential equations representing third order continuous sigma delta modulation are:

$$\frac{dx(t)}{dt} = w(t) - k_0 x(t) - a_0 M tanh \frac{px(t-\tau)}{M} \tag{12}$$

$$\frac{dw(t)}{dt} = u(t) - k_1 w(t) - a_1 M tanh \frac{px(t-\tau)}{M} \tag{13}$$

$$\frac{du(t)}{dt} = \lambda - k_2 u(t) - a_2 M tanh \frac{px(t-\tau)}{M} \tag{14}$$

Solving for the fixed point $\hat{x}$, gives :

$$\hat{x} = \frac{\lambda - a_2 - a_1 k_2 - a_0 k_2 k_1}{k_2 k_1 k_0} \tag{15}$$

Note that the hyperbolic tangent has again been set to $+1$. The fixed point is finite, and hence the third order modulator is stable, for non-zero values of the integrator leakages $k_0, k_1, k_2$ as was the case with the second order modulator.

The expression for $\hat{x}$ is positive when

$$\lambda > a_2 + a_1 k_2 + a_0 k_2 k_1 \tag{16}$$

and hence it is expected that such configurations of the third order modulator will give rise to the asymptotic behaviour described in the second order analysis.

A : $\lambda = 0.5$, $a_1 = 1.0$, $a_2 = 0.1$, $k_0 = 0.5$ and $k_1 = 1.0$. Theory predicts line at $a_0 = \frac{0.4 - k_2}{k_2}$.

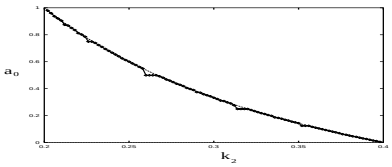


B : $\lambda = 0.5$, $a_2 = 0.1$, $k_0 = 0.5$, $k_1 = 1.0$ and $k_2 = 1.0$. Theory predicts line at $a_0 = 0.4 - a_1$.

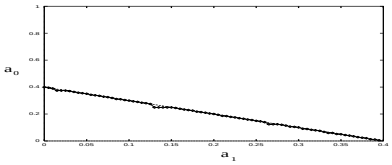


Figure 4: *Plots of results from direct simulation of third order modulator*

A number of plots have been made, using both the direct simulation of a third order modulator and the Runge Kutta iterative process on the third order equations, and some results for the direct simulation are presented in figure 4. Each plot shows the boundary between correct operation and asymptotic operation predicted by the above expression and the boundary observed from running the simulations for a particular set of configurations of third order modulator.

The theory fits the experimental results well, so a general rule for non-asymptotic operation of third order sigma delta modulators can be written as

$$|\lambda| < a_2 + a_1 k_2 + a_0 k_2 k_1 \tag{17}$$

and for stability

$$|k_2|, |k_1|, |k_0| > 0 \tag{18}$$

## FIRST ORDER SIGMA MODULATION

The question now arises as to whether this type of analysis can be applied to the first order sigma delta modulator. The differential equation representing first order modulation is

$$\frac{dx(t)}{dt} = \lambda - k_0 x(t) - a_0 M tanh \frac{px(t-\tau)}{M} \tag{19}$$

and a fixed point occurs at

$$\hat{x} = \frac{\lambda - a_0}{k_0} \tag{20}$$

when the same assumptions are made as in the formulation of (4). Consequently the modulator is stable for all non-zero values of the integrator leakage $k_0$ and is expected to be non-asymptotic for

$$|\lambda| < a_0 \tag{21}$$

This proves to be the case for both the Runge Kutta solution to the equation and for the direct simulation of the circuit. Typically there is unity feedback in a first order modulator, i.e. $a_0 = 1$, so what this implies, and what is seen to occur, is that for an input greater than $+1$ or less than $-1$ (i.e. the limits of the quantiser) the modulator operates in an asymptotic mode. For inputs between the limits of the quantiser the modulator operates normally. It is a well established rule that the input to a first order sigma delta modulator should not exceed the limits of the quantiser for a successful analogue to digital conversion to take place [5].

## HIGHER ORDER MODULATORS

It would seem that this analysis can be extended to higher order sigma delta modulators. Consider the criteria for non-asymptotic operation of first, second and third order sigma delta modulation:

First order

$$|\lambda| < a_0 \tag{22}$$

Second order

$$|\lambda| < a_1 + a_0 k_1 \tag{23}$$

Third order

$$|\lambda| < a_2 + a_1 k_2 + a_0 k_2 k_1 \tag{24}$$

It can be shown [6] that for non-asymptotic behaviour of an $n^{th}$ order modulator

$$|\lambda| < I_n \tag{25}$$

where

$$I_n = a_{n-1} + k_{n-1} I_{n-1} \tag{26}$$

and

$$I_1 = a_0 \tag{27}$$

Alternatively this criterion can be written as

$$|\lambda| < \sum_{p=0}^{n-1} a_p \frac{1}{k_p} \prod_{m=p}^{n-1} k_m \tag{28}$$

For stability of an $n^{th}$ order modulator

$$|k_0|, |k_1|, |k_2| ... |k_{n-1}| > 0 \tag{29}$$

## GENERALISED SIGMA DELTA ARCHITECTURE

Some configurations of sigma delta modulators involve coefficients in the feedforward path rather than the feedback path [2]. Figure 5 shows a generalised second order sigma delta architecture incorporating these variations. The criterion for

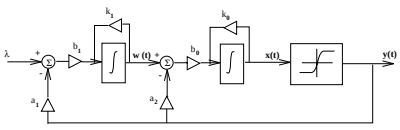


Figure 5: *Generalised second order sigma delta modulator*

non-asymptotic operation of a $n^{th}$ order generalised sigma delta modulator can be written as

$$|\lambda| < \sum_{p=0}^{n-1} a_p \frac{b_p}{k_p} \prod_{m=p}^{n-1} \frac{k_m}{b_m} \tag{30}$$

## DISCUSSION

Investigation of the stability of sigma delta analogue to digital converters has recently centred around the search for limit cycles in the output of the modulator. A $\Sigma\Delta M$ is considered stable if limit cycles cannot occur [4] – with the proviso that two types of limit cycle, whilst undesirable, do not neccessarily imply instability: when the absence of both noise and an input signal produces a one-zero pattern at half the sampling frequency, and when some offset in the modulator or a dc input gives rise to a nearly stable pattern at the modulator output.

It has also been noted [3] that the poles of the transfer function $H(z)$ affect the stability of a $\Sigma\Delta M$ – this is not usually the case as we generally look to the zeroes of $(1 + H(z))$ for stability criteria. It is likely that what is being labelled as instability due to the limit cycles observed at the output is actually the asymptotic behaviour described in this report. Remember that this behaviour was defined by the numerator of the fixed point expression (4) rather than the denominator which would generally give the stability condition.

This paper sets out a method of considering the stability and desirable operation of $\Sigma\Delta M$ which does not rely on the limitations imposed by the limit cycle approach, it has also gone some way toward explaining results produced by that approach.

## CONCLUSIONS

A stability criterion has been laid down for second order sigma delta modulators. Also a criterion for avoiding asymptotic operation has been derived theoretically and shown to occur via simulation. A good match of results occurred between the direct simulation of a second order $\Sigma\Delta M$, the Runge Kutta numerical solution to the differential equations representing second order $C\Sigma\Delta M$ and the algebraic analysis of these equations.

This analysis has also been shown to hold true for first and third order modulator structures and has been extended to $n^{th}$ order modulators and to a generalised configuration for $\Sigma\Delta M$.

## REFERENCES


[1] Ushaw G. McLaughlin S. Hughes D.T.& Mulgrew B. Representation of sigma delta modulators as continuous systems for analysis of their effect on chaotic signals. *SPIE Proc Chaos in Communications*, 2038, July 93.

[2] Ardalan S.H. Paulos J.J. An analysis of nonlinear behaviour in delta sigma modulators. *IEEE Trans Circuits and Systems*, 36(6), June 87.

[3] Hein S. & Zakhor A. On the stability of sigma delta modulators. *IEEE Trans Signal Processing*, 41(7), Jul 93.

[4] Stikvoort E.F. Some remarks on the stability of the noise shaper or sigma delta modulator. *IEEE Trans Comms*, 36(10), Oct 88.

[5] Hughes D.T. Ushaw G. McLaughlin S. Mulgrew B. & Broomhead D.S. The search for chaotic output from a sigma delta modulator: an archetypal retarded nonlinear system. *SPIE Proc Chaos in Communications*, 2038, July 93.

[6] Hughes D.T. private communication.

# TO SIGMA DELTA MODULATE OR NOT TO SIGMA DELTA MODULATE: THE CHAOS QUESTION

Gary Ushaw Steve McLaughlin

Department of Electrical Engineering
University of Edinburgh
The Kings Buildings
Mayfield Road
Edinburgh
EH9 2JL
SCOTLAND
gu@ee.ed.ac.uk (+44) 31 650 5660

**Abstract**

The effects of sigma delta modulation, a form of analogue to digital conversion, on a chaotic signal are discussed. A sigma delta modulator is a non-linear device that has not been fully described analytically. In this paper we pose the question of whether such a device is capable of chaotic modes of operation with a linear input, and whether it can adversely affect the predictability of a chaotic signal by causing it to become more chaotic. We utilise a simulation of such a modulator to show, in an experimental sense, that neither of these effects occur. In particular, we measure the Lyapunov spectra of a number of signals before and after modulation, to show that the process does not affect the predictability of the signal any more than direct quantisation does. We also address the tone-suppression architecture of sigma delta modulation which has recently been labelled as chaotic. We conclude that sigma delta modulation provides a reliable tool for analogue to digital conversion of a chaotic signal.

## 1 Introduction

Sigma delta modulation ($\Sigma\Delta$M) has become a widespread method of analogue to digital conversion, however its operation has not been completely defined. The majority of the analysis carried out on the circuit has been from a linear standpoint, with non-linear analysis hinting at hidden complexities in the modulator's operation [1] [2]. The sigma delta modulator itself is a non-linear system consisting, as it does, of a number of integrators and a one bit quantiser in a feedback loop. This configuration can be generalised as a non-linearity within a feedback path, which is a classic route to chaos.

This initially raises the prospect that a sigma delta modulator may be capable of chaotic modes of operation with a linear input. In fact, the problem does not arise and we briefly show why not. Of more interest, and more uncertainty, is the effect sigma delta modulation may have on a chaotic signal. If $\Sigma\Delta$M makes a chaotic signal more chaotic then this will have serious repercussions on the predictability of that signal. In the past, analysis of the circuit has tended to be based around a steady state input or a slowly moving linear input such as a low frequency sine wave [3] [4]. This has greatly eased the complexity of such analyses, but it does not address the problem at hand.

In this paper we present the results of comparing the sigma delta modulation of a chaotic signal to a direct quantisation of the same signal. The tool we use to investigate this is the Lyapunov spectrum of the time series, measured using an algorithm developed at Edinburgh University [5] which follows on from the work in [6]. The Lyapunov exponents of a chaotic signal are presented before and after both $\Sigma\Delta$M and direct quantisation, and it is shown that $\Sigma\Delta$M does not increase the chaotic content of the signal.

The problem is summarised in Figure 1, which shows a first order sigma delta modulator. The non-linear nature of the circuit is apparent from the presence of the one bit quantiser in the feedback loop. The chaotic signal to be considered is derived from the Lorenz system, the attractor of which is shown in the figure.

The Lyapunov spectrum of a system provides information about the dynamics of that system in an intuitive way. They describe the expansion and contraction of a system's phase space in a global sense.

[0]GU thanks EPSRC and DRA for their support in this work, SML similarly thanks the Royal Society.

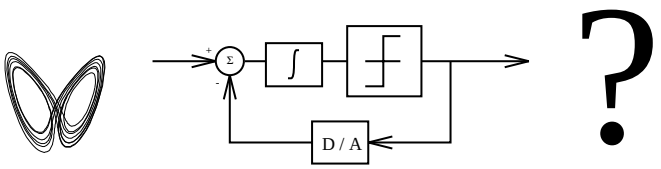


Figure 1: *What effect does sigma delta modulation have on a chaotic signal?*

A system with both positive and negative exponents is said to be chaotic. The effect that sigma delta modulation and direct quantisation have on these values will provide us with information about how the measured dynamics of the original chaotic system are affected by the particular method of measuring it.

It should be pointed out that, due to the incompleteness of rigorous analysis of ΣΔM and the complex processes involved in applying such analysis to a chaotic signal, the results of this paper are based upon experimentation and observation from a simulation of ΣΔM.

## 2 Linear input

We initially consider the possibility that the sigma delta modulator, due to its non-linear structure, may be capable of entering a chaotic mode of operation with a linear input. The work presented in [7] discusses a set of differential equations constructed to represent ΣΔM. The Jacobian of these equations is utilised [8] to show that the system is not chaotic, with a linear input.

Figure 2 presents the results of applying the Lyapunov exponent extraction algorithm [5] to time series derived from the output of a sigma delta modulator with a sinusoidal input. The exponents calculated are compared to those calculated from the original sine wave, and from a direct quantisation of the sine wave. By *direct quantisation*, we simply mean a software implementation of choosing the nearest quantisation level to the input at each sampling instant. In each case, the data was quantised to 4096 levels (i.e. 12 bit quantisation). Three Lyapunov exponents were calculated for each data set, although, of course, a

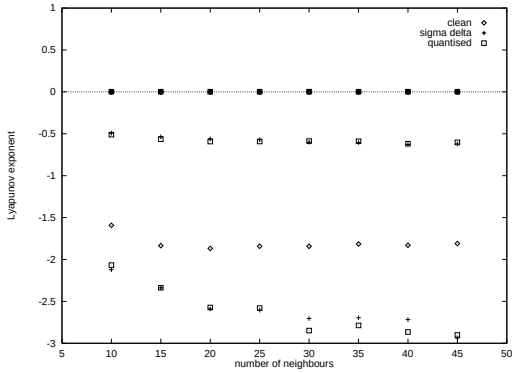


Figure 2: *Lyapunov exponents of sine wave time series for varying number of neighbours, for clean data, sigma delta modulated and direct quantised.*

clean sine wave does not have this many exponents. However, it is clear from the results that no posistive exponents are introduced by sigma delta modulation. Indeed, it can be seen that ΣΔM has the same effect on the Lyapunov exponents of the system as direct quantisation. Hence the modulator is not in a chaotic mode.

# 3 Chaotic input

The Lyapunov exponents commonly attributed [6] to the Lorenz system are $+1.37$, 0 and $-22.37$. These values indicate that the system is chaotic, in that positive and negative exponents are derived from the presence of both expansion and contraction in the system's phase space, and that the system is a flow, from the occurence of a zero exponent

Figure 3 shows the Lyapunov exponents calculated using the extraction algorithm, for both sigma

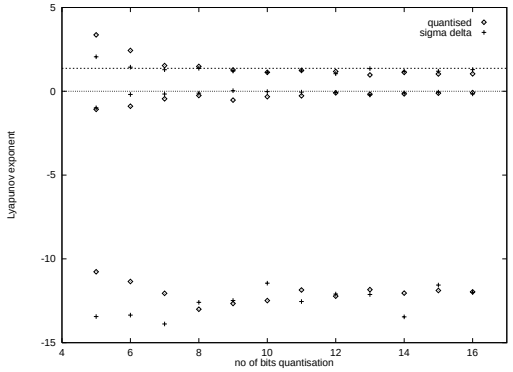


Figure 3: *Lyapunov exponents of Lorenz data after $\Sigma\Delta M$ and direct quantisation.*

delta modulated and directly quantised Lorenz time series. In both cases a range of quantisation levels have been employed, from 5-bit quantisation (32 quantisation levels) to 16-bit quantisation (65536 levels).

The accepted value of the positive exponents is marked ($+1.37$), and it can be seen that in both cases, above about 8-bit quantisation, good approximations of this value and the zero exponent are achieved. The amplitude of the negative exponent is consistently under-estimated, however. This is due to the extraction algorithm's method of dealing with noise on the signal, involving a global singular value decomposition process, and is common to all such algorithms known to the authors. This does not impede the comparison of time series with the same amount of noise, or, in this case, quantised to the same precision, however.

It is apparent that sigma delta modulation does not increase the chaotic content of the Lorenz time series Its over-all affect on the Lyapunov spectrum, and therefore, the predictability of the signal is not appreciably or consistently different to that of direct quantisation.

# 4 Tone suppression

It has been suggested that, in order to afford suppression of tones produced by $\Sigma\Delta$M, the modulator should purposefully be designed in what is labelled a 'chaotic' mode [1, 9]. This is achieved by moving one or more of the poles outside the unit circle; i.e. causing the integrator to become unstable by virtue of its leakage factor. This appears to be similar to the work in [10], whereby an adaptive ARMA predictor is constructed with an unstable pole, which is then stabilised by a non-linear element in a feedback loop. This similarity implies that, whilst the tone suppression architecture may be capable of chaotic modes of operation, and it certainly exhibits some phenomena of a chaotic system, it may not enter those modes during normal operation.

Figure 4 shows the Lyapunov exponents of the Lorenz time series after modulation by such a tone-suppressing architecture. The results are compared to those derived from conventional sigma delta modulation. In both cases, a 12 bit device was implemented, and the results are presented for a range of svd window sizes in the calculation [5]. Again it can be seen that the modulator, even in this 'chaotic' configuration, has not affected the Lyapunov exponents in comparison to the conventional configuration, and therefore does not adversely affect the predictability of the modulated signal by making it more chaotic.

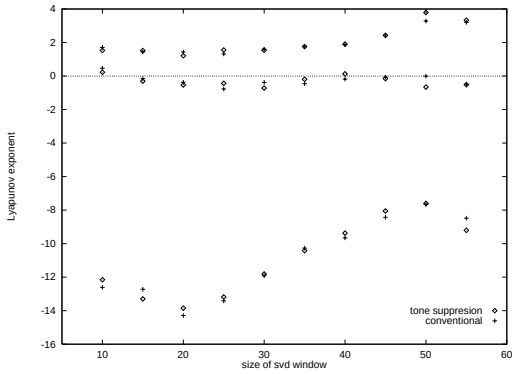


Figure 4: *Lyapunov exponents of Lorenz data after tone suppressed and conventional* $\Sigma\Delta M$.

# 5 Conclusions

It has been shown that there is little to choose between sigma delta modulation and direct quantisation when it comes to the effects on measuring a chaotic signal. Indeed the results are sufficiently similar to state, in a qualitative sense at least, that sigma delta modulation does not adversely affect the measurement of chaos. This finding, coupled with the other advantages of using sigma delta modulation where possible, increases the desirability of such an approach. Furthermore, the tone suppression architecture has been shown to have no additional detrimental effect on chaotic signals.

# References

[1] O.Feely. Nonlinear dynamics of chaotic double-loop sigma-delta modulation. In *IEEE ISCAS vol 6*, pages 101–106, 94.

[2] S.C.Pinault and P.V.Lopresti. On the behaviour of the double-loop sigma delta modulator. *IEEE Trans Circuits and Systems*, 40(8):467–479, Aug 93.

[3] S.Hein and A.Zakhor. On the stability of sigma delta modulators. *IEEE Trans Signal Processing*, 41(7), Jul 93.

[4] S.Rangan and B.Leung. Quantisation noise spectrum of double-loop sigma-delta converter with sinusoidal input. *IEEE Trans Circuits and Systems*, 41(2):168–173, Feb 94.

[5] M.Banbrook, G.Ushaw, and S.McLaughlin. Lyapunov exponents from a time series: a noise robust extraction algorithm. *to be submitted*, 95.

[6] A.G.Darbyshire and D.S.Broomhead. The calculationof liapunov exponents from time series data. *Submitted to Physica D*, 95.

[7] D.T.Hughes, G.Ushaw, S.McLaughlin, B.Mulgrew, and D.S.Broomhead. The search for chaotic output from a sigma delta modulator: an archetypal retarded nonlinear system. In *SPIE Proc Chaos in Communications*, Jul 93.

[8] A. Wolf, J.B. Swift, H.L. Swinney, and J.A. Vastano. Determining lyapunov exponents froma time series. *PHYSICA D*, 16:285–317, 1965.

[9] S.Hein. Exploiting chaos to suppress spurious tones in general double-loop sigma delta converters. *IEEE Trans Circuits and Systems II*, 40(10):651–659, Oct 93.

[10] M.Jaidane-Saidane and O.Macchi. Quasi-periodic self-stabilisation of adaptive arma predictors. *Int Jnl Adaptive Control and Signal Processing*, 2:1–31, 88.